

Institute für Geowissenschaften, Universität Potsdam

**INVESTIGATIONS ON SEDIMENTOLOGY AND EARLY  
DIAGENESIS IN SHALLOW-WATER WARM-TEMPERATE TO  
TROPICAL MIOCENE CARBONATES: A CASE STUDY FROM  
NORTHERN SARDINIA, ITALY**

Dissertation

Zur Erlangerung des akademischen Grades  
Doktor der Naturwissenschaften  
(Dr. rer. nat.)  
In der Wissenschaftsdiziplin Geologie

Eingericht an der  
Mathematisch-Naturwissenschaftlichen Fakultät  
Der Universität Potsdam

Von  
Gabriela Helena Marcano Romero

Published online at the  
Institutional Repository of the University of Potsdam:  
<http://opus.kobv.de/ubp/volltexte/2009/2920/>  
<urn:nbn:de:kobv:517-opus-29207>  
[<http://nbn-resolving.de/urn:nbn:de:kobv:517-opus-29207>]

## -ABSTRACT-

This study investigated the warm-temperate to tropical shallow-water Miocene carbonates of the Perfugas basin (Anglona area), northern Sardinia, Italy (Central Mediterranean). The aim of this study was to identify and document the existence and significance of early diagenesis in this carbonate system, especially the diagenetic history, which reflects the diagenetic potential in terms of skeletal mineralogy. The motivation behind the present study was to investigate the role that early cementation has over facies stabilization linked to differences in biotic associations in shallow-water settings. Principal to this was to unravel the amount, kind and distribution of early cements in this type of carbonates, in order to complement previous studies, and hence acquire a more global perspective on non-tropical carbonate settings.

The shallow-buried Sedini Limestone Unit was investigated for variations on early diagenetic features, as well as for the type of biotic association, and oxygen and carbon stable isotope stratigraphy. Results showed, that particularly at the Perfugas basin (< 15 km<sup>2</sup>), which evolves in time from a ramp into a steep-flanked platform, shallow-water facies are characterized by a “transitional” type of biotic association. The biotic assemblages change gradually over time from a heterozoan-rich into a photozoan-rich depositional system. This transition implies a change in the depositional environmental control factors such as temperature. It is considered that sedimentation took place under warm-temperate waters, which shifted to more warmer or tropical waters through time. Moreover, it was noticed that along with these changes, marine early syn-depositional cements (high-Mg calcite), with particular fabrics (e.g. fibrous), gradually contributed to the early lithification of rocks, favoring a steepening of the platform relief. The major controls for the shift of the depositional geometry was triggered by the change of the type of biotic associations (carbonate factory), related with the shift towards warmer conditions, and the development of early marine cementation.

The identification of the amount and distribution of different cement phases, porosities and early diagenetic features, within facies and stratigraphy, showed that diagenesis is differential along depth, and within the depositional setting. High-Mg calcite cements (micrite, fibrous and syntaxial inclusion-rich) are early syn-depositional, facies-related (shallow-water), predominant at the platform phase, and marine in origin. Low-Mg calcite cements (bladed, syntaxial inclusion-poor and blocky) are early to late post-depositional, non-facies related (shallow- to deep-water) and shallow-burial marine in origin. However, a particular difference exists when looking at the amount and distribution of low-Mg calcite bladed cements. They become richer in shallow-water facies at the platform phase, suggesting that the enrichment of bladed cementation is linked to the appearance of metastable grains (e.g. aragonite).

In both depositional profiles, the development of secondary porosity is the product of fabric-selective dissolution of grains (aragonite, high-Mg calcite) and/or cements (syntaxial inclusion-rich). However, stratigraphy and stable isotopes (oxygen and carbon), indicate that the molds found at shallower facies located beneath, and close to stratigraphic boundaries, have been produced by the infiltration of meteoric-derived water, which caused recrystallization without calcite cementation. Away from these stratigraphic locations, shallow- and deep-water facies show molds, and recrystallization, as well as low-Mg calcite cementation, interpreted as occurring during burial of these sediments by marine waters. The main cement source is suggested to be aragonite.

Our results indicate that the Sedini Limestone Unit was transformed in three different diagenetic environments (marine, meteoric and shallow-burial marine); however, the degree of transformation in each diagenetic environment differs in the heterozoan-dominated ramp from the photozoan-dominated platform. It is suggested that the sediments from the ramp follow a diagenetic pathway similar to their heterozoan counterparts (i.e. lack of marine cementation, and loss of primary porosity by compaction), and the sediments from the platform follow a diagenetic pathway similar to their photozoan counterparts (i.e. marine cementation occluding primary porosity). However, in this carbonate setting, cements are Mg-calcite, no meteoric cementation

was produced, and secondary porosity at shallow-water facies of the platform phase is mostly open and preserved.

Despite the temporal and transitional change in biotic associations, ramp and platform facies (shallow- to deep-water facies) showed an oxygen isotope record overprinted by diagenesis. Oxygen primary marine signatures were not found. It is believed that burial diagenesis (recrystallization and low-Mg calcite cementation) was the main reason. This was unexpected at the ramp, since heterozoan-rich carbonates can hold isotope values close to primary marine signals due to their low-Mg calcite original composition.

Ramp and platform facies (shallow- to deep-water facies) showed a carbon isotope record that was less affected by diagenesis. However, only at deep-water facies, did the carbon record show positive values comparable with carbon primary marine signals. The positive carbon values were noticed with major frequency at the platform deep-water facies. Moreover, these values usually showed a covariant trend with the oxygen isotope record; even that the latter did not hold positive values.

The main conclusion of this work is that carbonates, deposited under warm-temperate to tropical conditions, have a unique facies, diagenesis and chemostratigraphic expression, which is different from their cool-water heterozoan or warm-water photozoan counterparts, reflecting the "transitional" nature of biotic association.

## -ZUSAMMENFASSUNG-

Diese Arbeit befasst sich mit den warmen bis tropischen miozänen Flachwasserkarbonaten des Perfugas Beckens (Region Anglona) im nördlichen Sardinien, Italien. Ziel dieser Arbeit war es, die Existenz und Signifikanz der frühen Diagenese in diesem Karbonatsystem zu identifizieren und zu dokumentieren. Die Geschichte der Verfestigung reflektiert dabei das diagenetische Potential, welches von der Mineralogie der Grundgerüste ehemaliger Lebewesen abhängig ist. Die Motivation bestand darin, die frühe Zementation der Karbonate zu beschreiben, da sie eine wesentliche Rolle bei der Faziesstabilisierung spielt wenn diese durch unterschiedliche biotische Verbindungen im Flachwasser aufgebaut wurde. Der Fokus dieser Studie liegt bei der Trennung von Menge, Art und Verteilung der frühen Zemente in Karbonaten. Frühere Arbeiten wurden ergänzt und zusammen gefasst, um eine globale Übersicht bezüglich nicht tropischer karbonatischer Milieus zu erlangen.

Die flach abgelagerte Einheit der Sedini Karbonate wurde unter multiplen Gesichtspunkten z.B. früher diagenetischer Strukturen, biotischer Gesellschaften sowie durch Messungen stabiler Isotope an Sauerstoff und Kohlenstoff untersucht. Die Ergebnisse zeigen, dass das Perfugas Becken ( $< 15 \text{ km}^2$ ), welches sich von einer Rampe zu einem, von steilen Flanken begrenzten, Plateau entwickelte und sich durch eine Flachwasserfazies auszeichnet, die auf eine "Übergangsart" der biotischen Gemeinschaft hinweist. Diese Gemeinschaft veränderte sich allmählich von einem heterozöischen zu einem photozöischen Ablagerungssystem. Diese Verschiebung impliziert einen Wechsel der Faktoren, wie der Temperatur, die das Ablagerungsmilieu beeinflussen. Es wird angenommen, dass die Sedimentation in warmen Gewässern stattfand, welche sich bis hin zu tropischen Temperaturen kontinuierlich erwärmten. Es ist bekannt, dass sich parallel zu diesen marinen Veränderungen frühe Mg- reiche kalzitische Zemente bildeten, die ein ausgeprägtes z.T. faseriges Gefüge zeigen. Diese unterstützen die frühe Verfestigung der Kalke und ermöglichen eine Verteilung des Reliefs der Plattform. Die hauptsächlichen Faktoren, die eine Verschiebung der Ablagerungsumgebung hervorriefen, wurden durch die Veränderung der biotischen Gesellschaft und durch die Entwicklung früher Zemente aufgezeichnet, die wiederum mit der Erwärmung des Habitats zusammenhängen.

Die Identifizierung der Menge und Verteilung der verschiedenen Zementphasen, der Porosität und der frühen diagenetischen Elemente in Fazies und Stratigraphie zeigen, dass die Verfestigung mit zunehmender Tiefe und innerhalb des Ablagerungsareals variiert. Mg- reiche kalzitische Zemente (mikritisch, faserig, syntaxial einschlussreich) wurden im frühen, marinen Stadium während der Ablagerung gebildet. Mg- arme kalzitische Zemente (blättrig, syntaxial einschlussarm, blockig) entstanden nach der Ablagerung im flachen bis tiefen marinen Wasser z.T. unter überlagernden Einheiten. Ein offensichtlicher Unterschied existiert bei Menge und Verteilung von Mg-armen, blättrigen Zementen. Sie werden in der Flachwasserfazies innerhalb der Plattformphase häufiger, was mit dem Auftreten metastabiler aragonitischer Körner zusammen fällt.

In beiden Ablagerungsprofilen ist die Entwicklung der Sekundärporosität das Produkt einer gefügeabhängigen Auflösung der Körner (aragonit, Mg-reiche Kalzite) und/oder der Zemente (syntaxial einschlussreich). Stratigraphie und stabile Isotope (Sauerstoff, Kohlenstoff) zeigen jedoch, dass sich Abdrücke in der Flachwasserfazies finden lassen, die sich zwischen und in der Nähe der stratigraphischen Grenze befinden. Die Abdrücke entstanden durch Infiltration von meteorischen Wässern, was zu Rekristallisation ohne kalzitische Verfestigung führte. Fernab dieser stratigraphischen Lokalitäten, zeigen Flach- und Tiefwasserfazies Abdrücke, Rekristallisationen und Mg-arme kalzitische Zemente die offensichtlich durch Überlagerung dieser Sedimente in marinen Gewässern entstanden sind. Als Hauptzementkomponent wird Aragonit angenommen.

Unsere Ergebnisse zeigen, dass die Sedini Kalksteineinheit in drei verschiedene diagenetische Umgebungen umstrukturiert wurde (marin, meteorisch, flach überlagert). Der Grad der Umwandlung in den einzelnen diagenetischen Umgebungen unterscheidet sich von der heterozöisch dominierten Rampe zur photozöisch dominierten Plattform. Es wird angenommen,

dass die Sedimente der Rampe einem diagenitischen Pfad folgen, der ähnlich des heterozoischen Gegenstücks verläuft (z.B. Fehlen der marinen Zementation, Verlust primärer Porosität durch Kompaktion). Die Plattformsedimente folgen einer diagenetischen Abfolge ähnlich ihrer photozoischen Pendanten (z.B. marine Zementation welche die primäre Porosität). In diesem Karbonatfeld sind die Zemente Mg-reich und nicht meteorische verfestigt. Eine sekundäre Porosität der Flachwasserfazien in der Plattformphase ist offen und gut erhalten.

Trotz der temporären und vorübergehenden Wechsel in den biotischen Vergesellschaftungen, in den Flachwasserfazien von Rampe und Plattform wie in den Tiefwasserfazien der Rampen, sind Signale in den Sauerstoffisotopen erkennbar, wenn diese auch durch von der Diagenese überdeckt. In diesen Fazien wurden keine primären, marinen Sauerstoffisotopen gefunden. Es wird angenommen, dass die erfolgte überdeckte Diagenese (rekristallisation, Mg-arme kalzitische Zementation) der Hauptgrund dieser fehlenden Isotopensignale darstellen. Dies war an der Rampe unerwartet, da heterozoen-reiche Karbonate primäre, marine Isotopenwerte speichern können, welches aufgrund ihrer Mg-armen Zusammensetzung ermöglicht wird.

Das Kohlenstoffisotopensignal der unterscheidlichen Fazien von Rampe und Plattform, zeigten sich weniger von der Diagenese betroffen. Nur in den Tiefwasserfazien zeigte das Kohlenstoffsignal positive Werte, vergleichbar mit primären, marinen Signalen. Die positiven Kohlenstoffwerte wurden an den Plattfortmtiefenwasserfazien mit größter Häufigkeit registriert. Diese Werte zeigten in der Regel einen kovarianten Trend mit dem Sauerstoffisotopensignal, sogar wenn letzterer keine positiven Werte enthielt.

Die Schlussfolgerung aus dieser Arbeit ist, dass Karbonate welche unter warmen bis tropischen Verhältnissen abgelagert wurden, eine einmalige Faziesgenese und chemische Stratigraphie aufweisen. Diese ist unterschiedlich zu ihren heterozoischen Kaltwasser oder ihren photozoischen Gegenstücken aus wärmeren Wässern. Dies wiederum reflektiert gut das "transitionale" Wesen einer biotischen Gesellschaft.

## TABLE OF CONTENTS

Abstract	Page
Zusammenfassung	
Table of Contents	
Acknowledgements	
<b>1. Chapter 1: Introduction.....</b>	<b>10</b>
1.1 Background and aim of this study.....	10
1.1.1 Examples of the facies evolution related to major biotic changes at present and in the geological record.....	12
1.1.2 Diagenesis.....	13
1.1.3 Geochemical signature (stable oxygen and carbon isotope).....	14
1.2 Organization of this thesis.....	15
<b>2. Chapter 2: The Geological Setting.....</b>	<b>17</b>
2.1 The Western Mediterranean basin and the Oligo-Miocene Sardinian rift.....	17
2.1.1 The Oligo-Miocene Sardinian rift.....	17
2.2 The Perfugas Basin and Stratigraphy .....	19
<b>3. Chapter 3: The Sedini Limestone Unit.....</b>	<b>21</b>
3.1 The Sedini Limestone Unit at the study area.....	21
3.2 Stratigraphy and basin geometry.....	21
3.3 Transects and stratigraphic sections.....	24
<b>4. Chapter 4: A Miocene warm-temperate to tropical shallow-water carbonate setting (northern Sardinia, Italy): considerations on early diagenesis and facies stabilization.....</b>	<b>26</b>
4.1 Abstract.....	26
4.2 Introduction.....	26
4.3 Geological setting.....	27
4.4 Methods.....	29
4.4.1 Field work.....	29
4.4.2 Laboratory analysis.....	29
4.5 Results.....	31
4.5.1 Lithofacies description.....	31
4.5.2 Petrography of early diagenetic features.....	38
4.5.3 Summary of sediment composition and cement types.....	40
4.6 Interpretation and discussion.....	41
4.6.1 Paleoenvironments.....	41
4.6.2 Significance of the biogenic association.....	44
4.6.3 Early Diagenesis.....	44
4.6.4 Early Diagenesis and Facies Stabilization.....	45
4.6.5 Implications of this study.....	46
4.7 Conclusions.....	46
<b>5. Chapter 5: Relationships of early diagenesis, facies and stratigraphy of a warm-temperate to tropical Miocene carbonate setting (northern Sardinia, Italy).....</b>	<b>47</b>

5.1 Abstract.....	47
5.2 Introduction.....	47
5.3 Geological setting.....	48
5.4 The Sedini Limestone Unit.....	49
5.4.1 Lithologies and rock composition.....	50
5.4.2 Paleoenvironments.....	52
5.5 Analytical methods.....	53
5.6 Petrography.....	54
5.6.1 Syn- and early post- depositional events.....	54
5.6.2 Late post- depositional events.....	56
5.7 Geochemistry.....	58
5.7.1 Stable isotopes.....	58
5.7.2 Major and trace elements.....	60
5.8 Distribution of calcite cements and dissolution features with respect to facies and stratigraphy.....	61
5.9 Discussion.....	62
5.9.1 Origin of calcite cements.....	62
5.9.2 Origin of dissolution features.....	65
5.9.3 Source for calcite cementation.....	66
5.9.4 Significance of stable isotope values.....	67
5.9.5 Significance of calcite cementation.....	67
5.9.6 Mineralogical stabilization.....	68
5.9.7 Diagenetic history.....	68
5.9.8 Diagenesis and facies-stratigraphic context.....	69
5.9.9 Prediction of reservoir quality.....	71
5.10 Conclusions.....	72
<b>6. Chapter 6: Oxygen and carbon stable isotope stratigraphy of a shallow-water Miocene carbonate setting (northern Sardinia, Italy): response characteristics to diagenesis and climate.....</b>	<b>73</b>
6.1 Abstract.....	73
6.2 Introduction.....	73
6.3 Geological setting.....	74
6.4 The Sedini Limestone Unit.....	75
6.4.1 Stratigraphic and sedimentological setting.....	76
6.4.2 Diagenesis.....	78
6.5 Methods.....	79
6.6 Results.....	81
6.6.1 Stable isotopes.....	81
6.7 Discussion.....	81
6.7.1 Diagenetic overprint.....	82
6.7.2 Primary marine signatures.....	84
6.7.3 Lessons learned.....	88
6.8 Conclusions.....	88
<b>7. Chapter 7: Conclusions and references.....</b>	<b>89</b>
APPENDIX	



## **Acknowledgments**

I would like to thank my advisor, Prof. Dr. Maria Mutti, for the support, guidance and scientific tutoring she provided to me over the years. Without her enthusiasm, my first months here in Germany would have been very difficult to deal with.

Especially, I would like to thank Merle Hagen, with whom the sharing of joy, whether physical, emotional or intellectual, made possible this project's completion. I thank her for the discussions, support and motivation during the field seasons. I guess that the wonders of Sardinia enabled the meeting of two different lines of thought. Thank you very much!

I am greatly indebted to Prof. Dr. Manfred Strecker for his support, optimism and valuable advice, which helped me to overcome many difficulties during my studies.

I also owe gratitude to Prof. Dr. Christian Betzler from Hamburg University, for his valuable scientific comments, support and guidance throughout the investigation.

I would like to thank the Deutsche Forschungsgemeinschaft (DFG) for the valuable and continuous financial support offered during my PhD studies (grants Mu-1680/6-1, Be-1272/12). I also owe gratitude to the University of Potsdam for providing me of a special grant in order to finish my last months of studies ("Kurzzeitstipendium zum Abschluss der Promotion").

I would like to express my gratitude to the academic and technical staff at the Department of Geosciences, Potsdam University. I thank Christine Fischer and Antje Musiol for all their exemplary and essential laboratory work. I also give many thanks to my colleagues, Andrea Knoerich, Uwe Baaske and Arndt Peterhaensel, for offering valuable advice. I gratefully acknowledge their scientific remarks and discussions about carbonate sedimentology.

The people outside the university who I thank for helping me with technical procedures during this study include Ms. Oona Apelt, for her support at the EM; and Dr. Birgit Plessen, for her valuable support with the IRMS at the GeoForschungsZentrum Potsdam. I am in debt to the Department of Geosciences at Sassari University, especially Prof. Giacomo Oggiano, for his valuable scientific comments. I thank Prof. Lucia Simone and Prof. Gabriele Carannante from the Department of Geosciences at Napoli University, for their valuable scientific comments on my work and their support during the first field season in Sardinia. Many thanks also go out to students of Hamburg University, J. Christian Albertsen, Birgit Nagel and Hans Gienapp, for their nice maps and the interesting moments that we shared at the field. Thanks to Marion Hager and Johanna Mayer of Potsdam University for their help with the porosity and permeability measurements.

Many thanks to my friends, officemates and colleagues Katrin Rehak, Astrid Riemann, Annette Junginger, and Franziska Wilke, for their multiple conversations in English and German. Thank you for letting me learn a little bit more about your culture and your beautiful lives.

I owe an enormous debt of gratitude to my colleague and friend Giovanna Della Porta, for invaluable comments on my thesis, support and friendship. Thank you a lot!!!

Many thanks to my colleague and friend Sara Tomás for beautiful moments in my last time writing my thesis!!!!...and for the "Sardinian Team": Martin Homann, Michael Rumpf, Max Zitzmann and Sascha Serno.

I owe an enormous debt of gratitude to my colleagues and friends, Jessica Zamagni and Paolo Ballato, with whom I've shared many, many moments of emotional ups and downs. Thank you for sharing with me your knowledge, valuable comments, corrections, support and, most importantly, your joyful life, home and family. Without them it would have been very difficult to deal with my thesis and my life here in Germany! ¡Besos y Muchas Gracias!.

I owe an enormous debt of gratitude to my best and dearest friend, Rositsa Miteva: "Our friendship was born with a spark in which both were secretly charged...and cut across the accidents of place and time." Thank you a lot for everything!

I cannot express strongly enough my appreciation to my friends Elsy Pereira, Petia Vlahovska and Monica Vásquez. I believe that each friend represents a world in us, a world possibly not born until they arrive; and only by this meeting is a new world born.

I owe enormous and heartfelt appreciation to my dearest friend, Humberto Carvajal, who helped me to gain a deep appreciation of the beauty of life. Without his encouragement and faith, this thesis might have remained just another dream.

I deeply thank my sister, Diana, who shared with me the scent of the stars. You have been the only one who has touched my heart. Thank you for smiling even in the dark and sharing unconditional love. I cannot express strongly enough the love and appreciation I have for my parents. During my whole life, including my studies here in Germany, each of them provided me with “proof of love.” I love you both!

# - CHAPTER 1 - INTRODUCTION

## 1.1 Background and aim of this study

The biota comprising shallow-water carbonates are excellent indicators of environmental conditions, and thus provide important information on past climate change (Miller et al. 1991, Miller et al. 1998). For example, global cooling trends during the Miocene period left fundamental imprints in a wide range of biota and facies associations. These imprints help us to understand important changes in shallow-water environments in tropical regions, as well as in regions located in neighboring climatic threshold areas (John 2003, John 2005).

Based on carbonate-producing biotic assemblages, shallow-water carbonate environments have been grouped into two major groups (James 1997): the “photozoan assemblage” or light-dependant biota, which is characterized by green algae, zooxanthellate corals, and ooids; and the “heterozoan assemblage” or non-light dependant biota, which is characterized by coralline algae, bryozoans, molluscs, and foraminifers, together with echinoids and azooxanthellate corals. The first group is typical of tropical waters warmer than 22°C, whereas the second group is characteristic of cool-water environments with temperatures of less than 18°C (Fig. 1.1).

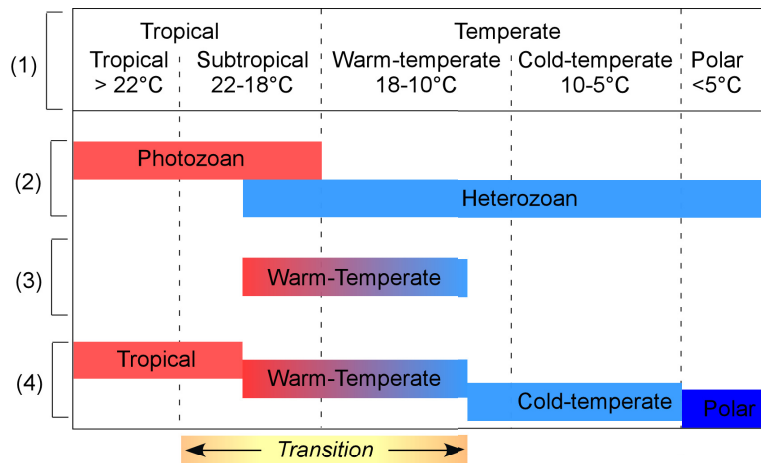


Figure 1.1. (1) Terminologies used for carbonate sediments of different climatic zones (modified from Mutti and Hallock 2003, and Schlager 2005). (2) Terminology based on biotic associations and proposed by James (1997). (3, 4) Terminology based on temperature of the waters and proposed by (3) Betzler et al. (1997) and (4) Halfar (2004).

Carbonate environments in neighboring climatic threshold areas, such as temperate (warm-temperate) to tropical (subtropical) waters (~ 22° to ~ 18°C) (Fig. 1.1), are usually characterized by an “intermediate” or “transitional” type of carbonate system. Carbonate-producing biota is mainly heterozoan in nature, but with a variable amount of light-dependant or photozoan biota (e.g., heterozoan-photozoan transition, Halfar et al. 2004).

Carbonate accumulation is primarily determined by factors such as ocean circulation (e.g., Collins et al. 1997, James et al. 1999), nutrient content and sea-water temperature (e.g., James et al. 1997, Mutti and Hallock 2003), effects of continental runoff (uplift/weathering) (e.g., John et al. 2003), and climatic changes (e.g., Brachert et al. 1996).

The spatial distribution of shallow-water carbonates, and related biota, is considered to be controlled by two main limiting parameters (James 1997, Mutti and Hallock 2003): sea-water

temperature and sea-water nutrient content (Fig. 1.2). In those environments where sea-water temperature is high and the water is nutrient depleted, the photozoan association dominates. Conversely, in cool, nutrient-rich waters, the heterozoan association develops. Thus, temperature and nutrient content lead to a spatial distribution of biotic associations that are strongly dependent on latitude and the latitudinal arrangement of principal climatic zones (Mutti and Hallock 2003) (Figs. 1.2 and 1.3).

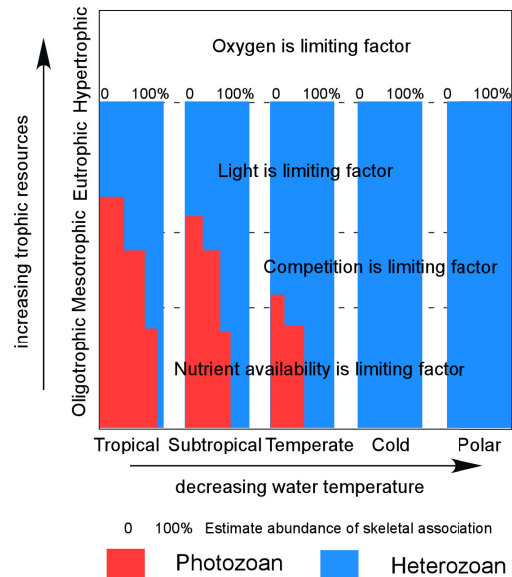


Figure 1.2. Distribution of heterozoan and photozoan biotic associations related to sea-water temperature and nutrient content (modified from Mutti and Hallock 2003).

In regions located in neighboring climatic threshold areas, such as temperate (warm-temperate) to tropical (subtropical) waters ( $\sim 22^\circ$  to  $\sim 18^\circ\text{C}$ ) (Figs. 1.1, 1.2), the heterozoan association can be found with variable contribution of the photozoan biota (areas within  $\sim 10^\circ$  north and south of  $30^\circ$  of latitude), and thus are potential recorders of changes that reflect variability in environmental conditions (Fig. 1.3).

In addition to the biota distribution in these environments, the sedimentological character of the carbonate deposits, their degree of diagenesis, and their stable oxygen and carbon isotopic signatures are important characteristics that help to characterize past and present carbonate depositional environments.

Although many advances have been made in our understanding of carbonate depositional environments in marginal tropical settings and in the transition to temperate regions (e.g., Less 1975, Esteban 1996, James 1997, James et al. 2005), these systems are still poorly understood, and many unanswered questions remain. Indeed, there is currently a debate about the relationship between basin depositional geometry and early diagenesis, as well as the response of the biotic associations to local environmental or global climate changes. Some of the major controversies and specific questions in this debate are:

- 1) How are the facies and sediment configured? Does a relationship exist between facies stabilization and early diagenesis?
- 2) Is there a systematic relationship between the biotic transition, original mineralogy and calcite cementation? If yes, what is the diagenetic history of these rocks? Does a differential

amount of depositional aragonite result in a higher amount of cementation? In which diagenetic environments does most cementation occur?

3) Can we trace global climate events, or is this potential paleoclimate signature weakened or masked by local environmental factors? To what extent are these signatures preserved in diagenetically overprinted, shallow-water carbonate rocks?

The motivation for this work is derived from these questions, and they will guide the testing of the following research hypotheses: (1) Early diagenesis and the resulting diagenetic history are clearly distinguished from non-tropical carbonates; and, (2) Shallow-water carbonate facies, containing a transitional biotic association, are sensitive recorders, not only of environmental change, but also of global climate change.

Before addressing these issues, a short background (facies, diagenesis, and chemostratigraphy) from some examples of recent and past shallow-water depositional environments, deposited in neighboring climatic threshold areas, is provided. This background will give a basis for comparison of the data deduced from the geological record analyzed in this study.

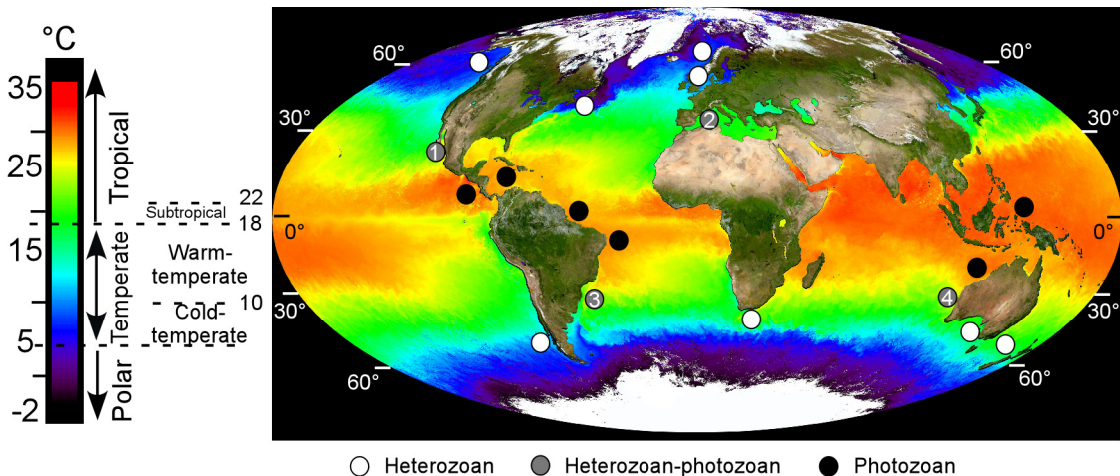


Figure 1.3. Global distribution of heterozoan and photozoan carbonates (modified from James 1997). Photozoan carbonates are found at 0°C to 30°C N-S (black circles). Heterozoan carbonates are found at 30°C N-S towards the poles (white circles). Areas where heterozoan-photozoan carbonates are found (grey circles) are based on recent examples: (1) Halfar et al. (2004), (2) Fornós and Ahr (2006), (3) Carannante et al. (1988), and (4) James et al. (1999). This image can be downloaded at [http://visibleearth.nasa.gov/view\\_set.php?sensorID=6](http://visibleearth.nasa.gov/view_set.php?sensorID=6), and refers to sea surface temperature that was produced using the MODIS (Moderate Resolution Imaging Spectroradiometer).

### 1.1.1 Examples of the facies evolution related to major biotic changes at present, and in the geologic record:

*Southwestern Australia: A recent depositional environment.*

Recent shallow-water environments in southwestern Australia (22° S–32° S) represent an example of a transitional carbonate setting. Nutrients, paleotopography and ocean circulation are the main controlling factors in this area (Collins et al. 1997, James et al. 1999). Here, biotic changes occur by latitudinal change along with platform morphology. Along the same shelf (from south to north in latitude), a transition from open shelf to reef platform to ramp occurs in relation with sediment composition. Shelf sediments are characterized by sea grasses growing on hard-

ground sand pockets containing the largest number of living larger benthic foraminifers, in association with living zooxanthellate corals (low diversity and abundance), together with bryozoans, molluscs and small benthic foraminifers. Platform top sediments are characterized by coral framestones and sand sheets composed of coral and coralline red algae debris. Ramp sediments are characterized by a fringing reef at the inner ramp; meanwhile, the euphotic mid-ramp area is foraminifer-dominated sand (mainly *Amphistegina* and *Heterostegina* genera).

#### *Examples from Miocene depositional environments.*

Lower and Middle Miocene carbonate facies from the Latium-Abruzzi carbonate ramp (central Italy) record an example of a transitional biotic association in the Central Mediterranean. At shallow-water facies, scattered coral colonies (*Porites*) occur with coarse-grained sediments rich in larger benthic foraminifers (e.g., *Heterostegina*, *Amphistegina*, and *Operculina*), red algae and molluscs. Studying the facies architecture, Brandano et al. (2002) suggested that the appearance and disappearance of coral build-ups in contrast with the contemporaneous bloom of suspension-feeders (e.g., bryozoans) is the result of trophic changes within the water column.

Upper Miocene carbonates from southern Spain show a turnover of depositional modes from ramp to rimmed platforms. Carbonate deposits show intervals rich in corals, intercalated with non-reefal carbonate rocks formed on ramps in near-shore environments. Brachert et al. (1996) suggested that these changes have been caused by variations in temperature related to glacial-interglacial cycles.

#### **1.1.2 Diagenesis:**

The subdivision of shallow-water carbonates into photozoan or heterozoan associations, not only implies a different biogenetic composition, but also reflects their diagenetic potential in terms of grain original mineralogy. Photozoan associations are characterized mostly by metastable aragonite and high-Mg calcite grains (> 4 mole % MgCO<sub>3</sub>); meanwhile, heterozoan associations predominantly consist of low-Mg calcite grains (< 4 mole % MgCO<sub>3</sub>). This strongly contributes to the contrasting diagenetic evolution of each biotic association. There is a wide literature describing in detail the general diagenetic evolution of photozoan carbonates, including, among many others, Bathurst (1975), James and Choquette (1990a, 1990b), Tucker and Wright (1990), and Moore (2001). On the contrary, limited attention has been paid to the diagenetic processes and pathways in the heterozoan carbonates. Consequently, their diagenetic evolution continues to be poorly understood, beside the increasing interest in these systems (James and Bone 1989, James and Bone 1991, Hood and Nelson 1996, James, 1997, Kyser et al. 1998, Dodd and Nelson 1998, Knoerich and Mutti 2003, Knoerich and Mutti 2006).

As previously described, shallow-water carbonates deposited in regions located in neighboring climatic threshold areas, such as tropical areas (subtropical) to temperate areas (warm-temperate) (latitudinal belt +/- 10° degrees north and south of 30° degrees latitude), are contrasting settings (James et al. 2005, Knoerich and Mutti 2006), and their diagenetic evolution helps for comparison. A general overview of sediment alteration in the different diagenetic environments shows the following features:

- *Marine diagenetic environment.* This diagenetic environment is located on the sea floor and the area just below it (tens of cm within the sediment) (Tucker and Wright 1990). In this diagenetic environment, the diagenetic potential of the carbonate rocks depends on the saturation state of the seawater with respect to carbonate minerals. From the tropics towards the poles, shallow seawater becomes progressively undersaturated with respect to CaCO<sub>3</sub>. Thus, either: (a) marine cementation occurs, then environmental, paleoceanographic or sea level changes might have contributed to enhance the CaCO<sub>3</sub> saturation state of seawater

(Nelson and James 2000); or (b) marine cementation does not occur, then grains are more liable to suffer reworking, bioerosion, abrasion and dissolution of the metastable mineral phase aragonite (Smith and Nelson 2003).

- *Meteoric diagenetic environment.* This diagenetic environment occurs when carbonate rocks are in contact with rainfall-derived waters. The amount of metastable aragonite and high-Mg calcite within the sediment determines the diagenetic potential of the carbonate rocks in this environment. During meteoric diagenesis, aragonite and high-Mg calcite are dissolved or stabilized into low-Mg calcite. Thus, either: (a) aragonite and/or high-Mg calcite grains are dissolved, then saturation with respect to low-Mg calcite can occur, and low-Mg calcite cements might precipitate (e.g., syntaxial inclusion-poor cement) (This has been observed when rocks are close to erosive surfaces or in shallower shelf areas [Knoerich and Mutti 2003]); or (b) aragonite and high-Mg calcite grains are stabilized (or perhaps dissolved) without evident cementation, then original grain fabrics are retained and their geochemical signature is modified, as it has been observed in carbonate sands exposed to chemically inactive meteoric phreatic lenses (Melim et al. 2002).

- *Burial diagenetic environment.* This diagenetic environment is known to occur below the zone affected by surface processes at tens to hundred meters of depth, down to several thousands of meters, before the zone where metamorphism starts to act (Tucker and Wright 1990). With subsidence and increasing overburden, sediments are subject to chemical compaction by pressure-solution (stylolitization), which contributes to a high fluid saturation state with respect to  $\text{CaCO}_3$ . If sediments contain organic matter, then  $\text{CO}_2$  gases are released by maturation processes, leading to undersaturation of the pore fluid, and to dissolution (Moore 2001). That is, if sediments are buried deep enough to reach the threshold between pressure-solution and cementation, then these rocks will produce extensive low-Mg calcite precipitation. It is usually considered that carbonate rocks rich in heterozoan grains are modified in this diagenetic environment (Nelson et al. 1988, Nicolaidis and Wallace 1997).

### 1.1.3 Geochemical signature (stable oxygen and carbon isotopes):

Stable oxygen and carbon isotope stratigraphy has rarely been applied to shallow-water carbonates. In most cases, this is primarily due to the diagenetic effects that change the original geochemical signals and, secondly, because of the wide variability of the isotopic composition due to rapid changes of facies and their discontinuous nature. Shallow-water carbonate settings reflect their sensitivity to many controlling factors, such as climate and sea-level changes (Miller et al. 1998). Therefore, deep-sea sediments are used for paleoceanography and paleoclimatology reconstructions, in order to reach a more comprehensive understanding of global climatic change. There are few known attempts to correlate time-equivalent deep-sea records with shallow-water signals, but there are even fewer interpretations of geochemical signatures from shallow-water temperate (warm-temperate) to tropical carbonate settings with a transitional biotic association. The few examples from Neogene shallow-water sediments show the following features:

- 1) From heterozoan carbonate slope sediments (Marion Plateau, NE Australia), major variations in mean ocean  $\delta^{13}\text{C}$  and  $\delta^{18}\text{O}$  have been identified (John et al. 2005). Miocene global climatic and glacio-eustatic events were distinguished. By comparing periods of globally cooler climate or  $\delta^{18}\text{O}$  events (Mi events) (Miller 1991), global cycles of productivity or  $\delta^{13}\text{C}$  events (CM events), mass accumulation rates with time-equivalent carbonate sediments, and relative controls on the evolution of a Miocene subtropical carbonate system, were identified. The correlation of these data with platform sediments is still a matter of debate.

2) From Quaternary to Neogene platform and periplatform carbonate sediments (Great Bahamas Bank), the diagenesis and origin of cement phases were better addressed (Melim et al. 2002). By comparing sediment composition, diagenesis and  $\delta^{13}\text{C}$  and  $\delta^{18}\text{O}$  shifts, the diagenetic evolution and cement (calcite and dolomite) origin was better established. Melim et al. (2002) determined that at periods of sea-level lowstands, meteoric cementation does not necessarily occur. Moreover, early diagenetic features produced at the shallow-marine burial domain could “mimic” its effect, and would have, as a result, depleted stable isotope shifts only produced by a chemically inactive meteoric phreatic lens. The product of meteoric diagenesis within these types of rocks leaves a geochemical signature, rather than a low-Mg calcite cementation.

In summary, models describing carbonate settings located in tropical (subtropical) to temperate (warm-temperate) regions, reveal their sensitivity to local environmental up to global changes. To complement the existing record, this work attempts to address and integrate stratigraphic and diagenetic models developed from shallow-water carbonate settings in regions located in neighboring climatic threshold areas, such as subtropical to temperate regions (latitudinal belt  $\pm 10^\circ$  degrees north and south of  $30^\circ$  degrees latitude). This requires the integration of facies and sedimentological descriptions that need to be put into a stratigraphic framework. Moreover, to reach a better understanding of the dynamics of carbonate accumulation and transformation (diagenesis), it is essential to track a carbonate system generated during a period in which important global climatic changes have occurred. In light of all of these aspects, Miocene subtropical to temperate Mediterranean basins are ideally suited for such a study, because the corresponding shallow-water deposits share these components. Accordingly, the present study can be considered the first step towards a more extensive comprehension of the shallow-water record.

## 1.2 Organization of this thesis

In order to address the research questions and test the outlined hypotheses, the results have been grouped into three separate chapters, each individually structured as papers. In chapter 4, biotic assemblages and the early diagenetic features are described, in chapter 5, a detailed diagenetic study framed into facies and stratigraphy is presented. In chapter 6, the stable oxygen and carbon isotope stratigraphy is presented. The following is a detailed summary of this thesis:

**Chapter 1. General Introduction** provides background on biotic assemblages, sediment, facies, diagenesis and stable oxygen and carbon isotopes. The aims and general location of the study area, as well as the organization of the thesis, are presented.

**Chapter 2. Geological Setting** briefly introduces the study area in terms of regional geological context and the stratigraphy of the rocks studied in this work.

**Chapter 3. The Sedini Limestone Unit** presents the geology of the specific Miocene carbonate strata at the study area. Acquisition of the data was based on several months of field campaigns in conjunction with our partners at Hamburg University. The field data supporting the results of this thesis have been collected in an area where previous studies were limited. Extended information presented in Chapter 3 has been accepted for an IAS special publication, and the authors are Benisek, Marcano, Betzler, and Mutti.

**Chapter 4. A Miocene warm-temperate to tropical shallow-water carbonate setting (northern Sardinia, Italy): considerations on early diagenesis and facies stabilization.** In this chapter, the link between the gradual transition of two depositional settings with different biotic associations and early diagenesis is analyzed. Field and petrographic analyses led to the



identification of a heterozoan-dominated ramp that evolves into a photozoan-dominated platform. The deposition took place under warm-temperate to tropical waters. It is suggested that the change in geometry is not only a consequence of the change through time of the carbonate factory, but also because of the increment of early lithification by marine cementation. This paper is in preparation, and the authors are Marcano, Benisek, Mutti, and Betzler.

**Chapter 5. Relationships of early diagenesis, facies and stratigraphy of a warm-temperate to tropical Miocene carbonate setting (northern Sardinia, Italy).** In this chapter, the diagenetic evolution in terms of stages of cementation, origin and source of cements and controls over its occurrence, are presented. Petrographic and chemical analysis allowed the identification of three diagenetic environments of transformation in both depositional settings (ramp and platform). It was established that shallow-water rocks of the heterozoan-dominated ramp followed a diagenetic pathway similar to their non-tropical counterparts, while the photozoan-dominated platform followed a diagenetic pathway similar to its tropical counterparts. This paper is in preparation for submission to the JSR (Journal of Sedimentary Research), and the authors are Marcano, Mutti, Benisek, and Betzler.

**Chapter 6. Oxygen and carbon stable isotope stratigraphy of a shallow-water Miocene carbonate setting (northern Sardinia, Italy): response characteristics to diagenesis and climate.** Here, the oxygen and carbon isotope results from shallower to deeper water facies are presented. The geochemical data are used to obtain an integrated chemostratigraphic framework. These data are compared to overall diagenesis and stratigraphy. Results reveal that the oxygen record is highly biased by the burial diagenetic trend of the rocks. The carbon records partially modified primary marine signals. This paper is in preparation, and the authors are Marcano, Mutti, Benisek, and Betzler.

**Chapter 7. Conclusions and References.** The main findings of this work are summarized here. It includes the preliminary conclusions on the results of Chapters 4, 5 and 6, as well as all references cited throughout the thesis and supportive literature.

## - CHAPTER 2 - THE GEOLOGICAL SETTING

This chapter briefly summarizes the overall regional geological setting of the Western Mediterranean basin, the Oligo-Miocene Sardinian rift and the geological and stratigraphic framework of the Perfugas basin, which includes the study area of this research.

### 2.1 The Western Mediterranean basin and the Oligo-Miocene Sardinian rift

The complexity of the structural trends and evolution of the Mediterranean regions resulted in the interaction of the Eurasian plate with the African, Arabian, and Anatolian plates (Dercourt et al. 2000) (Fig. 2.1). This process was driven by the differential spreading along the Atlantic ridge, which led to the closure of the Tethys Ocean, and eventually to the Alpine orogenesis (Dercourt et al. 2000).

During Oligocene-Miocene times, a complex rift system affected the southern margin of the European plate. One of the arms evolved toward a small oceanic basin, or the Western Mediterranean Basin, while others, such as the Gulf of Valencia and the Sardinian rift, aborted and remained at the rift stage (Cherchi and Montadert 1982). The Sardinian rift was the easternmost part of the NE-SW trending post-collisional, extensional system (Monaghan 2001).

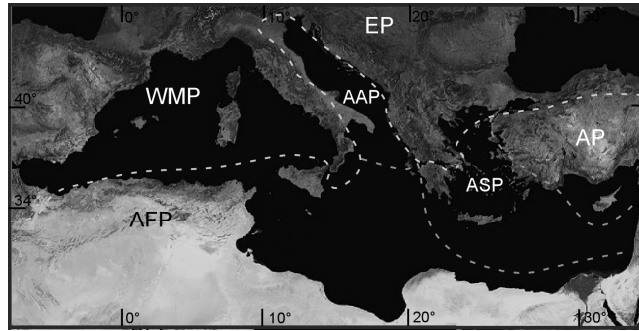


Figure 2.1. The Mediterranean basin and tectonic plates. WMP: Western Mediterranean Plate. AFP: African Plate. EP: Eurasian Plate. AP: Anatolian Plate. AAP: Apulia Adria Plate. ASP: Aegean Sea Plate. Satelital map modified from: <http://search.nasa.gov/search/search.jsp?nasalinclude=satellital+images>. Dashed lines indicate relative plate boundaries.

The Sardinian rift forms part of the continental Corsica-Sardinia block that split apart from Europe in a southeastward lateral drift and anticlockwise rotation (Monaghan 2001). The separation of the Corsica-Sardinian block was coeval with the NW-dipping subduction of the Neo-Tethyan oceanic crust beneath the microplate (Monaghan 2001). As a result, the Corsica-Sardinian block created a volcanic arc in its eastern side. Therefore, the Western Mediterranean basin is considered as a back-arc basin, while the Oligo-Miocene Sardinian rift is considered as an aborted intra-arc basin on the fore-arc side of the back-arc basin.

#### 2.1.1 The Oligo-Miocene Sardinian rift

The Sardinian Oligocene-Miocene rift is a 55-km wide, 220-km long, roughly N-S, elongated depression (Fig. 2.2), filled with more than 1000 m of littoral to epibathyal sediments, represented by siliciclastic, mixed siliciclastic and carbonatic deposits, as well as primary and reworked pyroclastic products (Cherchi and Montadert 1982, Assorgia et al. 1997, Faccenna et al. 2002). Along the rift, many basins recorded the nature, timing and sedimentary-infill of the rifting. These depocenters formed during different extension phases, and formed usually as half-grabens.

Most of the pre-rift basement rocks are constituted of Paleozoic metamorphic rocks (Figs. 2.2 and 2.3) deformed during the Hercynian orogeny, upper Carboniferous-Permian granitoids, and Mesozoic platform carbonate deposits (Faccenna et al. 2002). These pre-rift basement rocks

were cross-cut by E-NE- and N-S-oriented faults, with mainly strike-slip and normal motion, respectively (Figs. 2.2 and 2.3).

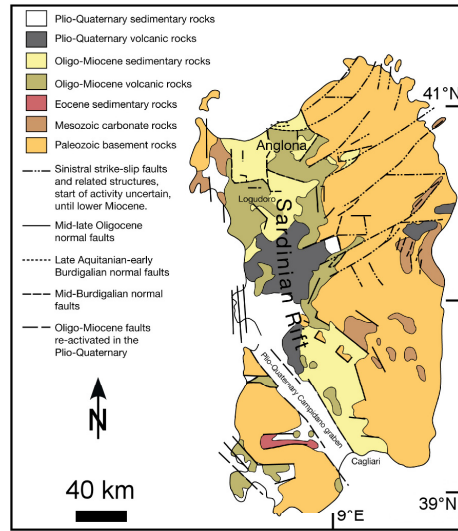


Figure 2.2. The Oligo-Miocene Sardinian Rift. The geological features are represented. At the Anglona area (northern Sardinia), Oligo-Miocene sedimentary rocks were deposited in a half-graben basin. Related movements were produced by late Aquitanian-early Burdigalian normal faults (second period of rifting or third tectonic phase (Monaghan 2001)). Map is modified from Sowerbutts (2000) and Monaghan (2001).

Data constraining the tectonic evolution and sedimentary infill of the Oligo-Miocene rift are found widely in the literature (Cherchi and Montadert 1982, Thomas and Gennesseaux 1986, Assorgia et al. 1997, Sowerbutts 2000, Monaghan 2001). Whilst all the detailed models were appropriate to a part of the Oligocene-Miocene Sardinian rift, they showed that along the rift, from south to north, different tectonic phases, volcanism and sedimentary infill occurred within specific timescales. The following summarized the main features included in the tectonic-sedimentary evolution of the Oligo-Miocene Sardinian rift: Monaghan (2001), with special emphasis on Thomas and Gennesseaux (1986) and Sowerbutts (2000) because of their analysis at northern areas of the Sardinian rift. The features are compared and represented in Figure 2.4.

Rifting started during the late Oligocene times, coeval with the first sedimentary continental deposits and an eruption of the first volcanic-arc rocks (Thomas and Gennesseaux 1986, Monaghan 2001). The “proto-rift” consisted of grabens oriented from SW to NW Sardinia as E-W, NW-SE, and N-S, respectively. Sedimentary synrift infill consisted of continental deposits, preferentially near the foot of faults (Usanna Fm., Thomas and Gennesseaux 1986). Monaghan (2001) suggested that passive-infill of the existing fault topography (Marmilla Fm., Thomas and Gennesseaux 1986) lasted until early Miocene times (Phase 1).

During early Miocene times (Aquitanian), a period of distension and rotation of Sardinia started (opening of the Western Mediterranean basin) and is marked by ignimbrites (ignimbrites  $\tau_1$  of Thomas and Gennesseaux 1986; Phase 2-lower ignimbrites, Monaghan 2001).

During early Burdigalian times, volcanism came to an end (ignimbrites  $\tau_2$  of Thomas and Gennesseaux 1986; Tergu Fm., Sowerbutts 2000; upper ignimbrites, Monaghan 2001) followed by a second period of rifting (Phase 3, Monaghan 2001). Extension occurred on E-W to NE-SW and NW-SE to N-S trending, high-angle, planar faults with throws of hundreds of meters. In northern Sardinia, half-graben basins formed with N-S to NNW-SSE and E-W trending normal faults (Monaghan 2001). Thomas and Gennesseaux (1986) identified synrift deposits as lacustrine limestones mixed with volcanic debris (basal part of the Perfugas Fm., Sowerbutts 2000) resting unconformably upon the  $\tau_2$  ignimbrites.

Following the extensional phase, during middle to late Burdigalian times, a marine transgression occurred (Phase 4, Monaghan 2001). These deposits filled the fault topography created during the previous extensional phase. A “basal conglomerate” marked the Brudigalian

transgression (Perfugas Fm., Sowerbutts 2000). Shallow- to deep- marine deposits overlapped and infilled the complex fault topography created by the second period of rifting (The Sedini Limestone Unit, Thomas and Gennessaux 1986). The typical thickness of these deposits ranged from 40 to < 200 m in northern areas of Sardinia.

During Langhian to Tortonian times, local vertical movements and deepening of the Western Mediterranean basin occurred (Thomas and Gennessaux 1986). Thermal subsidence took place (Monaghan 2001). Sedimentary infill was characterized by marls locally preserved in northern regions of Sardinia. Thomas and Gennessaux (1986) interpreted an erosional surface above the previous sediments as being related to the well-known Messinian event; however, evidence was local and random in northern areas like the Castelsardo basin.

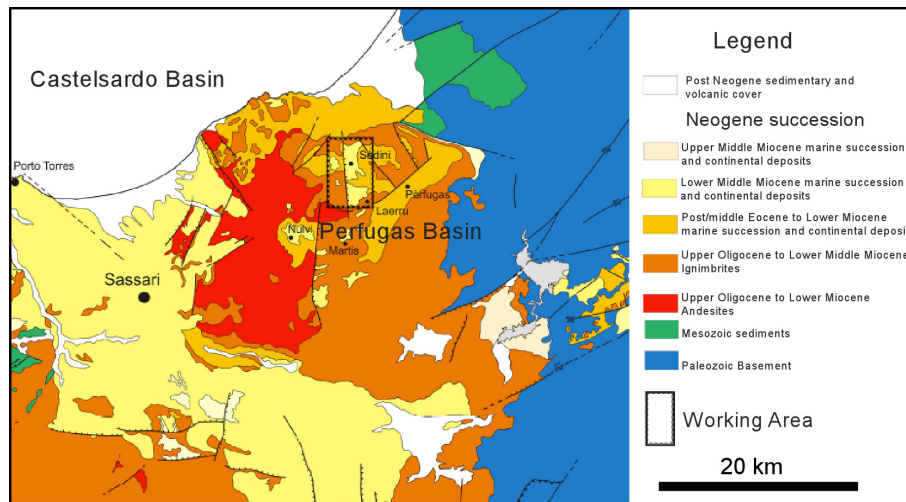


Figure 2.3. Schematic geological map of the Anglona area. The box indicating the “working area,” corresponds to a part of the Perfugas basin. The area of study is located at the south of the Castelsardo basin and its limited to the west and east by high areas of volcanic rocks (Upper Oligocene to Lower Middle Miocene Ignimbrites, Phase 3 of Monaghan 2001, Figure 2.4). Map is modified from Carmigiani et al. 2000.

A last marine sedimentary cycle consisted of Pliocene marly and sandy clay deposits cropping out only in a few localities in Sardinia. This cycle was evident in the southern areas of Sardinia and related to the formation of the NNW narrow and deep Campidano graben (Phase 5, Monaghan 2001) (Fig. 2.2).

## 2.2 The Perfugas Basin and Stratigraphy

The Perfugas Basin, located in the Anglona area (Fig. 2.2) in northwestern Sardinia, south of the Castelsardo basin, is limited to the east and west by high areas of volcanic rocks (Fig. 2.3). This basin was part of a number of intra-arc basins which formed during the Oligo-Miocene multiphase extension in the northern part of Sardinia (Phase 3, Monaghan 2001). As previously mentioned, the Perfugas basin includes the area of study of this research; therefore, the following comments about stratigraphy were made upon two studies that compiled the most complete revised lithostratigraphic scheme produced until now. Comparison of both was sketched in Figure 2.4, and compared with the tectonic and sedimentary events described previously for the geological evolution of the Oligo-Miocene Sardinian rift.

Thomas and Genesseaux (1986) gave the first comments on the Oligo-Miocene deposits onshore and offshore in northern Sardinia. Furthermore, they compared the formational and lithologic deposits with southern Corsica and the different tectonic regimes. That led to a broader and better understanding of the tectonics and sedimentary infills during the major transgressive event (Burdigalian) that occurred after the previous extensional phase. They defined the “Sedini Limestone Unit” as a formational unit that compiled the main characteristics of the marine deposits during Burdigalian times, which were easily correlated with the carbonate succession at the Perfugas basin.

Sowerbutts (2000) gave the first detailed stratigraphic characterization for all Oligo-Miocene deposits for northern Sardinian basins. The compilation was made by extensive field work among Miocene half-graben basins at the Anglona area. They defined formational names for the last volcanic episode (Tergu Fm.), synrift volcanoclastics and post-rift clastic deposits (Perlugas Fm.), and marine deposits (Laerru Fm.). However, the marine deposits were divided into four members with compiled characteristics observed from the different basins of the Anglona area. Unfortunately, all lithostratigraphic members could not be found in a single basin. Therefore, the identification and interpretation of the whole Laerru Fm. is substantially reduced at the Perlugas basin.

For the purpose of this research, the “Sedini Limestone Unit” was considered as a formational name for the marine deposits, and for the volcanic, volcanoclastic and lacustrine deposits; the Tergu Fm. and Perlugas Fm. are considered, respectively.

Age	Tectonic events		Stratigraphy	
	Monaghan (2001)	Thomas and Gennesseaux (1986)	Sowerbutts (2000)	Thomas and Gennesseaux (1986)
PLEISTOCENE PLIOCENE	Phase 5 Extension	Deepening of the WMB		Basinal sediments/Evaporites
Messinian		End of graben filling sediments. Evaporites (Castelsardo Basin)		
MIOCENE	Tortonian	Local tectonic movements Deepening of the WMB	Laerru Fm.	Sandy marls and Marls
	Serravalian			
	Langhian	Marine Transgression Rifting Stage/ Volcanic activity	Perlugas Fm.	Sedini Limestone Unit
	Burdigalian			BC
	Aquitanian	Phase 2 Volcanism/ Opening of the WMB	Drifting Stage Rotation of Sardinia	τ2 Ignimbrites
OLIGOCENE	Chattian	Rifting Stage Infilling of the graben by continental deposits	Tergu Fm.	Ussana Fm.

Figure 2.4. Different tectonic and stratigraphic schemes for the Oligo-Miocene deposits in northern Sardinia. This study refers to the stratigraphic scheme of Thomas and Gennesseaux (1986) for the marine carbonates, and Sowerbutts (2000) for the clastic and volcanic deposits. WMB: Western Mediterranean Basin. LD: Lacustrine deposits. BC: Basal Conglomerates. PH3: Phase 3 post rotation; end of volcanism.

## - CHAPTER 3 - THE SEDINI LIMESTONE UNIT

The purpose of this chapter is to report briefly on the local geology of the study area, and on the field characteristics of the Sedini Limestone Unit. This information has been developed in conjunction with our partners at Hamburg University. The stratigraphic architecture, and extended information, is submitted and accepted for an IAS (International Association of Sedimentology) special publication, and the authorship is as follows: Benisek, M.F.; Marcano, G.; Betzler, C.; and Mutti, M.

### 3. 1 The Sedini Limestone Unit at the study area

At the Perfugas basin, in areas between the Sedini and Laerru villages (Fig. 3.1), the Sedini Limestone Unit outcrops along high cliffs (< 60 m high), road cuts and quarries (south of the study area and close to Laerru village). The level of exposure is excellent. The extension and quality of the outcrops means that the approach taken was to subdivide the study area into transects based on geographical location, access to the outcrops and geological characteristics (facies, stratigraphy). Eight transects compiling the main geological characteristics of the Sedini Limestone Unit were chosen (Fig 3.1): (A) Casa Trigu, (B) Northern Ispilunca Valley, (C) Sa Rocca Manna, (D) Tanca Manna, (E) Marls, (F) Sedini South, (G) Southern Ispilunca Valley, and (H) Grotta Su Coloru (appendix 3.6). This thesis is based on the information studied from transects "A" to "E". Transects "F" to "H" have been studied in detail by Benisek (Hamburg University). The southern stratigraphic section included in transect "F" (and named in this thesis as Sedini south) is used to complement the work presented in this thesis.

In order to compile the complete geological characteristics of the Sedini Limestone Unit, mapping was performed, as well as the acquisition of large photomosaics (appendix), which helped as synthetic seismic lines. In addition, stratigraphic sections and sampling were developed.

Mapping covered an aerial extension of ~ < 15 km<sup>2</sup> (Fig. 3.1). Fieldwork utilized the Istituto Geografico Militare 1:10.000, 1: 25.000 and 1: 50.000 topographic maps. Information was complemented by satellite images ([www.nasa.gov](http://www.nasa.gov)), and with a DEM (digital elevation model) produced with PETREL (Fig. 3.1 and appendix). Large photomosaics (appendix) were taken to analyze and document sediment geometries, and for the spatial correlation of the units.

In this thesis, a total of 14 stratigraphic sections (summarizing ~ 520 m of vertical section) were described in several localities (Figures 3.1 and 3.2). Stratigraphic sections are (from north to south): Transect A- Casa Trigu (sections: S2a, S2b and S2c); Transect B- Northern Ispilunca valley (sections: S3, S5, S6, S7, and S8); Transect C- Sa Rocca Manna (sections: VT7, VT2, and C1); Tanca Manna (D); Sedini south (F); and Marls (E). In these stratigraphic sections, samples were taken at a spacing of 0.2-2 m, depending on the variability of lithologic changes, biotic content and diagenetic features.

### 3. 2 Stratigraphy and basin geometry

At the study area, the Sedini Limestone Unit is considered an example of a fault-block carbonate platform with a complex stratigraphic architecture. By the recognition of sedimentological features and facies arrangement, Benisek et al. (in press.) have suggested that the Sedini Limestone Unit is represented by two depositional sequences (Fig. 3.3). They have considered a change in the depositional geometry from a ramp to a steep-flanked platform. Furthermore, they identified several sediment packages (subsequences/units) separated by erosional contacts. The lower sequence 1, comprises two informal units: S1a and S1b. The upper

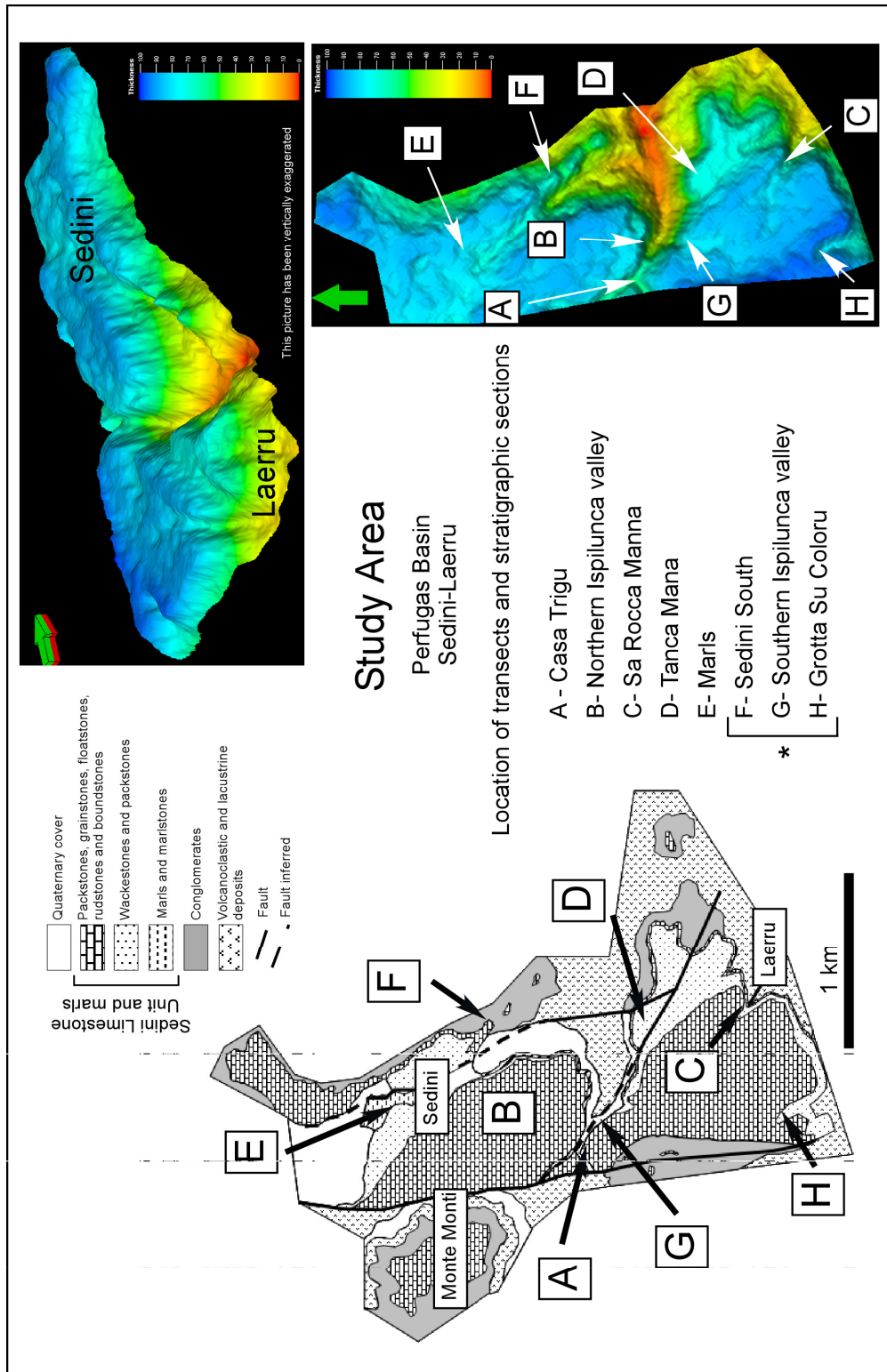


Figure 3.1. The geological map of the Sedini Limestone Unit and marls at the area between the Sedini and Laerru villages (Perfugas basin). The location of the transects studied in this thesis and in Benisek et al. (in press) (asterisk) are shown. This data was performed in collaboration with our partners from Hamburg University.

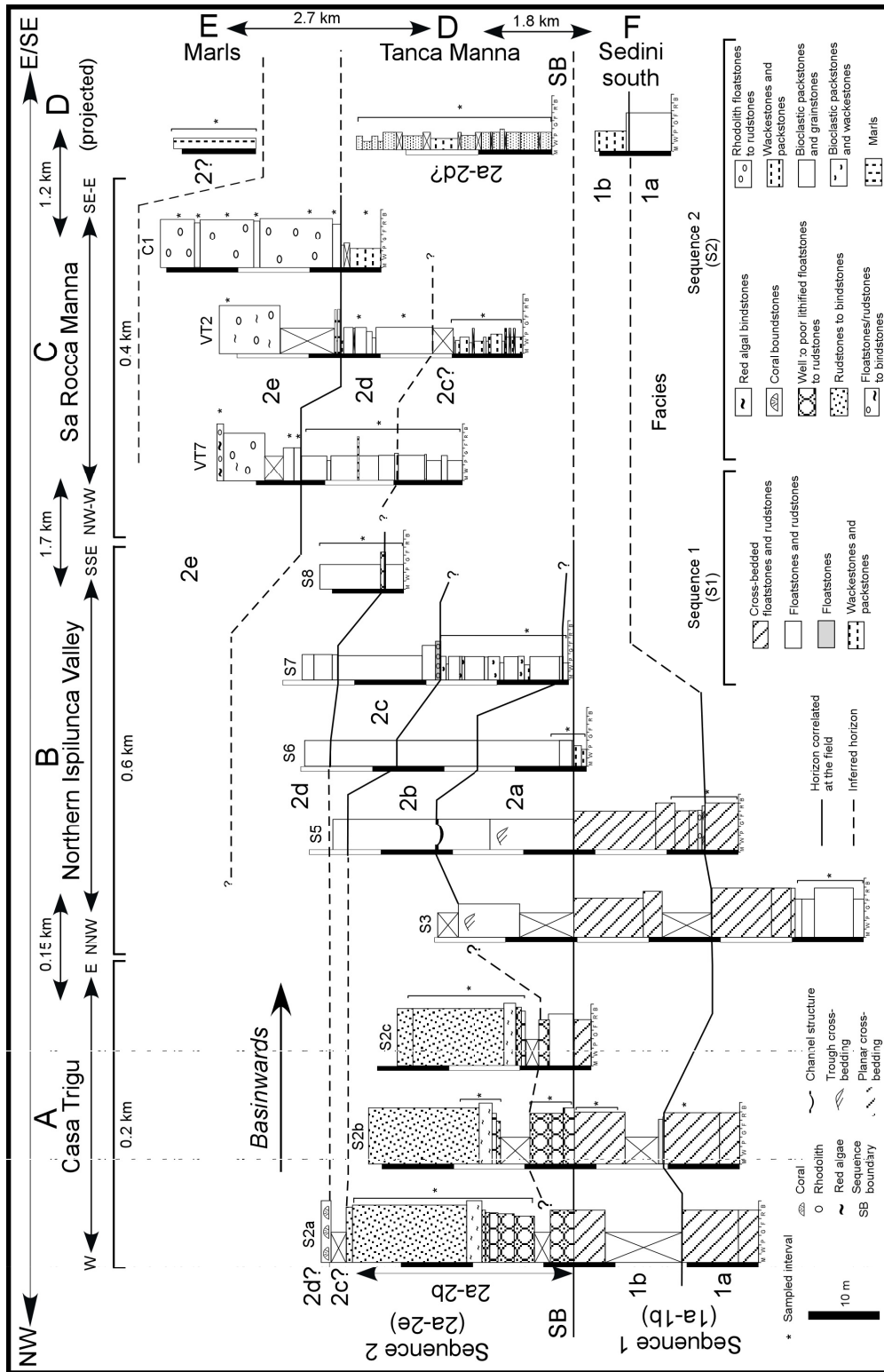


Figure 3.2. Correlation of the stratigraphic sections measured in the different areas showing the distribution of different lithofacies and other sedimentary attributes. The correlation was established by means of physical tracing of the beds in the field as well as with photopanoramas.



sequence 2, comprises six informal units: S2a to S2f (in this thesis it is studied S2a to S2e because of their wide exposure and recognition in the field). In addition, a marly unit was recognized and considered the last and youngest sediment package. The sequences and the informal units were traced in each transect (appendix 3.4 and 3.6) studied in this thesis, and marked in the stratigraphic correlation presented in Figure 3.2. Benisek considered that the change in basin geometry through time corresponds to the change of the carbonate factory. Sequence 1 is dominated by coralline red algae with bryozoans, bivalves, echinoids, barnacles, and large benthic foraminifers (among others; extended information in Chapter 4); meanwhile, sequence 2 (the last units S2d and S2e) is rich in reef-building zooxanthellate corals (extended information in Chapter 4). The ramp is represented by beaches, longshore bars (submarine) and outer-ramp deposits. The steep-flanked platform contains coral reef framestones forming a reef flat, rhodolithic slope deposits and deeper-water outer platform deposits.

In chapter 4, details on the sedimentology, biotic association and related paleoenvironments will be discussed, from transects A to F.

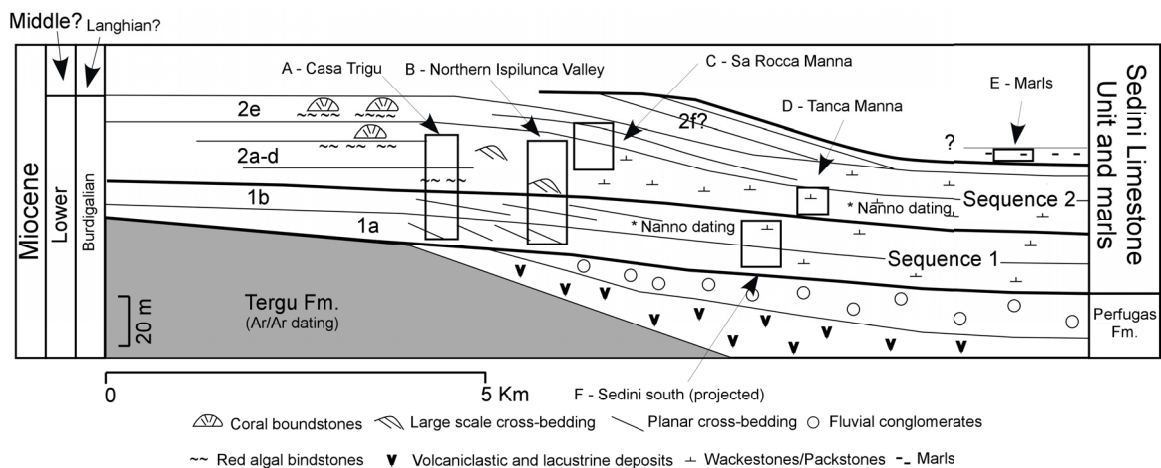


Figure 3.3. Schematic cross section illustrating the geometric relationships among the stratigraphic units identified within the "Sedini Limestone Unit" (modified from Benisek et al., in press.). The relative location of vertical stratigraphic profiles A, B & C shown here correspond to the Casa Trigu, Northern Ispilunca Valley, and Sa Rocca Manna transects, respectively. D and E correspond to the Tanca Manna and Marls sections. Vertical stratigraphic profile F, is part of the Sedini south transect described in Benisek et al. (in press). Ar/Ar dating is proposed in Sowerbutts (2000). Nannoplankton dating was performed by Benisek et al. (in press.)

### 3. 3 Transects and stratigraphic sections

Figure 3.2 shows a stratigraphic correlation with the main lithologic and stratigraphic features described in transects A to F. Figure 3.2 is used in chapter 4, 5 and 6, as a reference. The information related to transect H and G is only referenced in Figure 3.1, and can be found in Benisek et al. (in press). In this chapter I do not intend to describe and interpret the geological features of transects A to F, because they are analyzed in chapter 4. Here, we refer the reader only to the main features recognized in each transect, and to stratigraphic sections and their relationship with the stratigraphy proposed by Benisek et al. (in press). In appendices 3.2 to 3.6. the photomosaics studied in this thesis are depicted.

Transect "A"-Casa Trigu (appendix 3.2) is roughly oriented W-E, and is approximately 0.2 km long. The transect is partially accessible; however, limitations are steep slopes, high density of vegetation and high level of meteorization. Three sections were measured: S2a, S2b and S2c. It contains the lower and middle part of the Sedini Limestone Unit. The two sequences and informal units proposed by Benisek et al. (in press) were identified. The lower sequence is characterized by units S1a and S1b. Unit S1a is represented by planar cross-bedded rudstones. The unit S1b is represented by floatstones and planar cross-bedded rudstones. The upper sequence is characterized by units S2a to S2d (?). Units S2a and S2b are represented by well to

poor lithified floatstones to rudstones, red algal bindstones, and rudstones to bindstones. Unit S2c is covered and does not outcrop (appendix 3.4). Unit S2d is localized, and characterized by coral boundstones.

Transect "B"-Northern Ispilunca valley (appendix 3.3) is closely oriented NNW-SSE, and is approximately 0.6 km long. The transect is partially accessible; however, limitations are the overall steep slopes. Five sections were measured: S3, S5, S6, S7, and S8. It contains the lower and middle part of the Sedini Limestone Unit. The two sequences and informal units proposed by Benisek et al. (in press) were identified. The lower sequence is characterized by units S1a and S1b. Unit S1a is represented by floatstones and rudstones, and planar cross-bedded rudstones. The unit S1b is represented by floatstones and planar cross-bedded rudstones. The upper sequence is characterized by units S2a to S2d. Unit S2a is represented by bioclastic packstones and grainstones. Unit S2b is represented by bioclastic packstones and grainstones, and bioclastic packstones and wackestones. Units S2c and S2d are represented by bioclastic packstones and grainstones; and localized rhodolith floatstones (S2c), and well to poor lithified floatstones to rudstones (S2d).

Transect "C"-Sa Rocca Manna (appendix 3.4) is oriented NW-W to SE-E, and is approximately 0.4 km long. The transect is completely accessible and shows excellent exposures of the lithologies involved. Three sections were measured: VT7, VT2, and C1. It contains the upper part of the Sedini Limestone Unit. The upper sequence 2, and informal units S2c, S2d, S2e, and S2f proposed by Benisek et al. (in press) were identified. However, S2f is not studied in this thesis because of lack of accessibility and a high degree of meteorization. Units S2c and S2d are represented by bioclastic packstones and grainstones, floatstones/rudstones to bindstones, and wackestones and packstones. Unit S2e is represented by floatstones to rudstones, showing a differential degree of lithification, floatstones/rudstones to bindstones, and rhodolith floatstones to rudstones with clinoformal geometry.

Section "D"-Tanca Manna (appendix 3.5) is approximately 28-29 meters high and is partially accessible; however, limitations are the overall steep slopes. It contains the upper sequence 2 of the Sedini Limestone Unit and is represented by wackestones and packstones. A high degree of bioturbation is present. Section "E"-Marls (appendix 3.5) is approximately 12 meters high and is totally accessible because of its exposure as a road cut in northern areas of the Sedini village. It contains the upper sequence 2 of the Sedini Limestone Unit and is only represented by grey marlstones. Section "F"-Sedini South (appendix 3.5) is approximately 12-14 meters high and is partially accessible. It contains the lower sequence 1 (units S1a-S1b) of the Sedini Limestone Unit. Unit S1a is represented by floatstones and rudstones. Unit S1b is represented by floatstones, and wackestones and packstones.

**- CHAPTER 4 -**  
**A MIOCENE WARM-TEMPERATE TO TROPICAL SHALLOW-WATER  
CARBONATE SETTING (NORTHERN SARDINIA, ITALY): CONSIDERATIONS  
ON EARLY DIAGENESIS AND FACIES STABILIZATION**

This chapter discusses the biotic differences in the Sedini Limestone Unit and its relationship with the change of depositional geometry and early diagenesis. The data are the product of the merging of field and laboratory analyses. This chapter is structured for consideration as a manuscript for publication.

#### **4.1 Abstract**

Latitude, temperature, nutrients and ocean chemistry are important controlling factors on the occurrence of carbonate biota assemblages and their distribution. A number of studies have focused on the role of different biotic assemblages (photozoan and heterozoan) in determining the depositional architecture of carbonate systems. However, there is little known about the role that differential early diagenesis associated with photozoan versus heterozoan assemblages might play on depositional architecture.

In northern Sardinia, Miocene shallow-water limestones of the "Sedini Limestone Unit" comprise both heterozoan and photozoan assemblages. These carbonates offer an ideal opportunity to demonstrate the importance and the impact of early diagenesis in stabilizing depositional facies and therefore in affecting depositional geometries.

Two depositional sequences separated by a major unconformity have been recognized and mapped. The lower sequence documents a ramp geometry and is characterized by limestones containing bryozoans, bivalves, red algae, and echinoids with large benthic foraminifers (*Amphistegina* and *Heterostegina*) and barnacles. Reworked corals have also been observed. Early diagenetic features are rare. At mid-ramp facies, thin and scarce micritic envelopes, fibrous and syntaxial cements occur, but these are scarce overall. The upper sequence documents a platform geometry. Here, corals (*in situ*), rhodolites, molluscs, and small and large benthic foraminifers exist. In the lower part, mid-platform submarine dunes, stabilized by red algal bindstones, occur; in contrast, in the upper part, coral boundstones at the platform top have led to a marked slope break with clinoformal geometry (up to 27°). Early diagenetic features are abundant and diversified. Early cemented intervals show a facies-dependant character. Marine cements such as micritic cements are recognized in shallower platform facies (red algal bindstones), whereas fibrous cements are rich in (shallow) mid-platform facies.

The temporal and gradual change from a heterozoan-dominated into a photozoan-dominated carbonate setting and the differential distribution of early cements support the observed change in depositional geometry. While in sequence 1, early marine cements are too scarce to stabilize the substrate, the amount and distribution of early lithification observed in sequence 2 allows sediment stabilization and the development of a steep prograding slope.

#### **4.2 Introduction**

Studies based on modern carbonates have analysed the distribution of skeletal-grain associations related to changes in environmental parameters (e.g., Lees and Buller 1972; Carannante et al. 1988; Nelson 1988; James 1997). Carbonate-producing biota are commonly divided into heterozoan assemblages (non-light dependant biota, including bryozoans, echinoids, and foraminifers, among others, with variable coralline red algae content) and photozoan assemblages (light dependant biota, which include green algae, hermatypic corals and non-skeletal grains) (James 1997). Controls over their distribution are widely discussed in the literature (Lees and Buller 1972; Lees 1975; Carannante et al. 1988; Hallock et al. 1988; Nelson 1988; Mutti and Hallock 2003; Halfar et al. 2004) in reference to temperature, nutrient, salinity, water depth, and terrigenous supply, among other factors.

Occurrences of photozoan assemblages are related to warm water and tropical low-latitude areas. On the other hand, heterozoan assemblages occur in cooler waters, at

intermediate and higher latitudes (e.g., temperate to polar latitudes). However, where specific environmental parameters dominate (i.e. nutrient-rich waters), heterozoan association can also occur in tropical areas (James 1997). Many studies have addressed this (Carannante et al. 1988; Hallock et al. 1988; Halfar et al. 2004; Wilson and Vecsei 2005), pointing out the differentiation of carbonates deposited in cool water from those produced in warmer water with an elevated nutrient supply (both representing a heterozoan association; James 1997).

Because the two carbonate assemblages tend to grade into one another somewhat transitionally rather than sharply, mixed assemblages have often been described (Carannante et al. 1988; James and Bone 1991; Betzler et al. 1997; Collins et al. 1997; Shubber et al. 1997; James et al. 1999; Halfar et al. 2000; Lukasik et al. 2000; Brachert et al. 2001; Halfar and Ingle 2003; Halfar 2004).

Furthermore, examples from Spain (Brachert et al. 2001) and the south-western Australian coast (James et al. 1999) have revealed that a transition in biotic assemblages coincides with the evolution of the depositional system geometry of a “cool-water” ramp to a “tropical” type platform (Brachert et al. 1996; James et al. 1999; Brachert et al. 2001). Moreover, it has been observed that where photozoan components occur (aragonitic and high-Mg calcite grains), early cementation is involved, contributing to the gradational transformation of the depositional geometry (James et al., 1999). There is also a growing awareness that calcite cementation is not restricted to the deep-burial diagenetic environment, but also takes place early in the marine diagenetic environment (Nelson and James 2001) or meters below the surface in the shallow-burial marine diagenetic environment (Knoerich and Mutti 2003). However, the identification of the transition in biotic assemblages and facies with early diagenesis (e.g., type of cements) is largely absent in the literature.

Miocene carbonate deposits in northern Sardinia comprise spectacular outcrops which display lateral and vertical variations of biotic assemblages in terms of heterozoan-photozoan associations, providing a natural laboratory to test whether or not early diagenesis contributes to the gradational change of the depositional geometry and early lithification of the rocks. This chapter focuses on the carbonate facies and its early diagenesis related to the 50-60 m laterally extensive Miocene limestones of the “Sedini Limestone Unit” (Thomas and Gennesseaux 1986) exposed in the Perfugas basin (northern Sardinia), between the villages of Sedini and Laerru (Figs. 4.1 and 4.2). Here, we show that lateral and vertical variation in biotic associations and their facies assemblages also produce important differences in early cementation.

### **4.3 Geological Setting**

The Perfugas basin is located in the Anglona area in northwestern Sardinia, south of the Castelsardo basin and is limited to the east and west by high areas of volcanic rocks (Fig. 4.1). This basin is part of a number of intra-arc sub-basins which formed during the Oligo-Miocene multiphase extension and transtension in the northern part of Sardinia. This was caused by oceanic spreading and the formation of the western Mediterranean back-arc basin (Cherchi and Montadert 1982) and its subsequent Corsica-Sardinia microplate rotation (Sowerbutts and Underhill 1998; Sowerbutts 2000). Oceanic spreading in the western Mediterranean back-arc basin and the majority of Corsica-Sardinia microplate rotation occurred between 24-18 Ma (latest Aquitanian - early Burdigalian) (Sowerbutts 2000; Monaghan 2001). From Oligocene times to the present day, the arc-trench system and surrounding zones of compressional deformation migrated progressively outwards as Neotethyan oceanic crust, which was consumed at a subduction zone (Sowerbutts 2000). The Tyrrhenian Sea on the fore-arc side of the Sardinian Rift system began to open in late Miocene times (Sowerbutts 2000). Paleogeographic reconstruction locates the northernmost area of Sardinia between ~ 32°-35° during early Burdigalian times, moving due to an anticlockwise rotation towards ~ 35-38° in early Langhian times (Dercourt et al. 2000), then localizing the Perfugas basin in between the subtropical to temperate latitudinal areas.

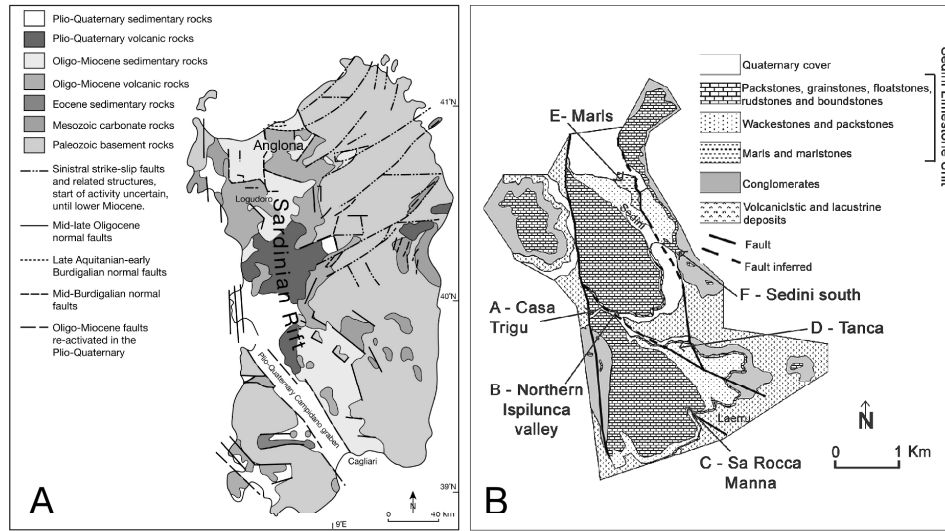


Figure 4.1. (A). Geological map of Sardinia, showing the distribution of the Rift and the location of the study area in the Anglona area (modified from Sowerbutts 2000). (B). Detailed geological map of the study area, located in the Perfugas basin, a half-graben with a Neogene sedimentary infill, located between the Sedinì and Laerru villages. The map illustrates the distribution of different lithological units present in the area (modified after Benisek et al., in press, Albertsen 2005, Giennapp 2005, and Nagel 2005), as well as the different carbonate lithologies occurring within the “Sedinì Limestone Unit” that have been defined in this study. The locations of vertical stratigraphic profiles and transects analyzed in this study are also indicated.

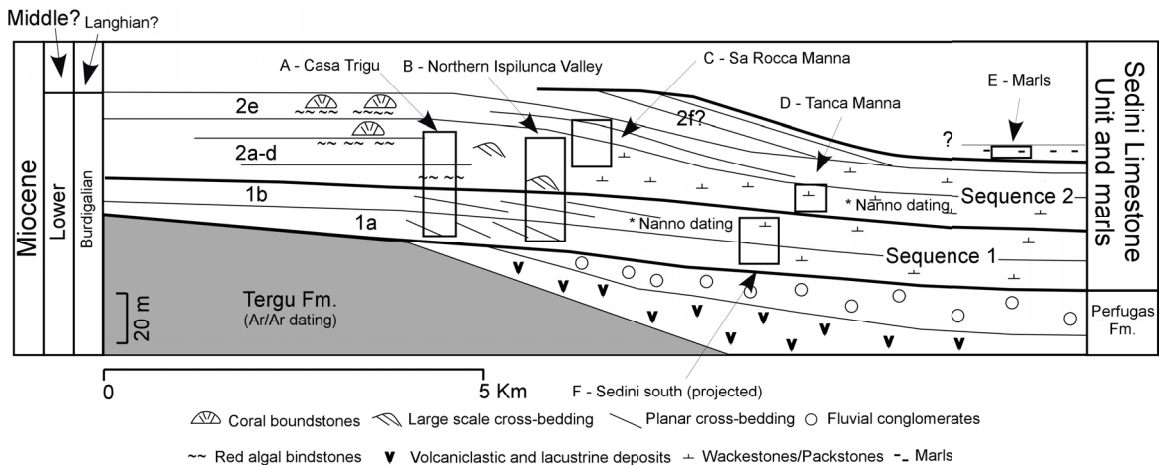


Figure 4.2. Schematic cross section illustrating the geometric relationships among the stratigraphic units identified within the “Sedinì Limestone Unit” (modified from Benisek et al., in press). Vertical stratigraphic profiles A, B & C shown here correspond to the Casa Trigu, Northern Ispilunca Valley, and Sa Rocca Manna transects respectively. D and E correspond to the Tanca Manna and Marls sections. Vertical stratigraphic profile F is part of the Sedinì south transect described in Benisek et al., in press.

A number of previous studies have provided information on the structural and tectonic evolution of the Oligo-Miocene Sardinian rift and on the biostratigraphy and lithological characterization of its infilling (Cherchi and Montadert 1982, Thomas and Gennesseaux 1986, Martini et al. 1992, Assorgia et al. 1997, Sowerbutts and Underhill 1998, Sowerbutts 2000, Monaghan 2001). Arnaud et al. (1992), Sowerbutts (2000), and Monaghan (2001) have specifically focused on the Perfugas basin (Anglona area), and have investigated the Oligo-Miocene structural configuration, lithological mapping, biostratigraphy, Ar/Ar dating, volcanism and sedimentation. More recently, Benisek et al. (in press) have defined facies associations, depositional environments and stratigraphic architecture (Chapter 3).

Sediments outcropping in the Perfugas basin comprise Miocene siliciclastics and carbonates (Figs. 4.1, 4.2), recording the syn-rift phase and post-rift sedimentation (third tectonic phase of N-S to NNW-SSE-faulting and sedimentation by marine transgression; Sowerbutts 2000, Chapter 2 this thesis). Sedimentary succession is exposed above a Burdigalian volcanic marker ignimbrite ( $\tau_2$ ; Sowerbutts 2000) overlain by the Perfugas Fm. (Sowerbutts 2000), which is characterized by volcanoclastics and lacustrine deposits. Siliciclastic sediments refer to a fluvial to an alluvial environment. Marine carbonates overlie the siliciclastics denominated the “Sedini Limestone Unit” (Thomas and Gennesseaux 1986).

Our study focuses on the marine carbonates of the “Sedini Limestone Unit”, a 50-60 m thick succession exposed along high cliffs between the Sedini and Laerru villages (Figs. 4.1, 4.2 and 4.3). Benisek et al. (in press) consider the carbonate unit as an example of a fault-block carbonate platform due to the complexity of its stratigraphic architecture. They have distinguished two depositional sequences (sequence 1 and sequence 2) separated by an erosional unconformity (SB) and informal units, which record an evolution of a ramp to a platform depositional setting along with a change of the carbonate factory.

#### **4.4 Methods**

This study is based on extensive field work and laboratory analysis (optical petrography). Field work was conducted in order to generate geological maps and for the acquisition of photopanoramas, detailed stratigraphic sections, and samples. Laboratory analyses, based on detailed optical petrography, were performed in order to determine and interpret litho- and bio-facies previously identified at the field, as well as the different early diagenetic features.

##### *4.4.1 Field Work*

A total of 14 stratigraphic sections (summarizing ~ 520 m of vertical section) were described in several localities in the area between the villages of Sedini and Laerru (Fig. 4.2). Outcrops are located along the study area exposed as 50-60 m high cliffs (Figs. 4.1, 4.2, 4.3 and 4.4). Stratigraphic sections from three main transects (from north to south) and three single stratigraphic sections were examined and described in detail (Figs. 4.3 and 4.4): 1) the Casa Trigu transect (sections: S2a, S2b & S2c); 2) the Northern Ispilunca valley transect (sections: S3, S5, S6, S7, S8); and 3) the Sa Rocca Manna transect (sections: VT7, VT2, C1), the Tanca Manna section (D), Sedini south (F) and Marls (E). The spatial relationships among these three areas are visible on the geological map (Fig. 4.1B), the stratigraphic architecture of the deposits based on Benisek et al. (in press) in Fig. 4.2; and the field overview panorama in Fig. 4.3. Sections E and F are not visible on the photopanorama overview, due to the difficulty of obtaining a good exposure of the sections.

Excellent outcrop conditions allow a detail correlation of closely spaced measured cliff sections, resulting in a nearly continuous physical correlation of the units and facies along the extent of outcrop exposure (Fig. 4.3). Large photomosaics (appendix) were taken to analyze and document sediment geometries and for the spatial correlation of the units (Fig. 4.3). Samples were taken at a spacing of 0.2-2 m, depending on the variability of lithological changes, biotic content and diagenetic features.

##### *4.4.2 Laboratory Analysis*

The descriptions of compositional and diagenetic characteristics are based on transmitted-light microscopy on ~ 350 thin sections. Thin sections were analyzed following standard petrographic procedures and were stained with alizarin red S and potassium ferricyanide (Dickson 1965), in order to distinguish calcite and dolomite. Visual estimations of skeletal grains and cements were obtained by comparison with estimation charts for sedimentary

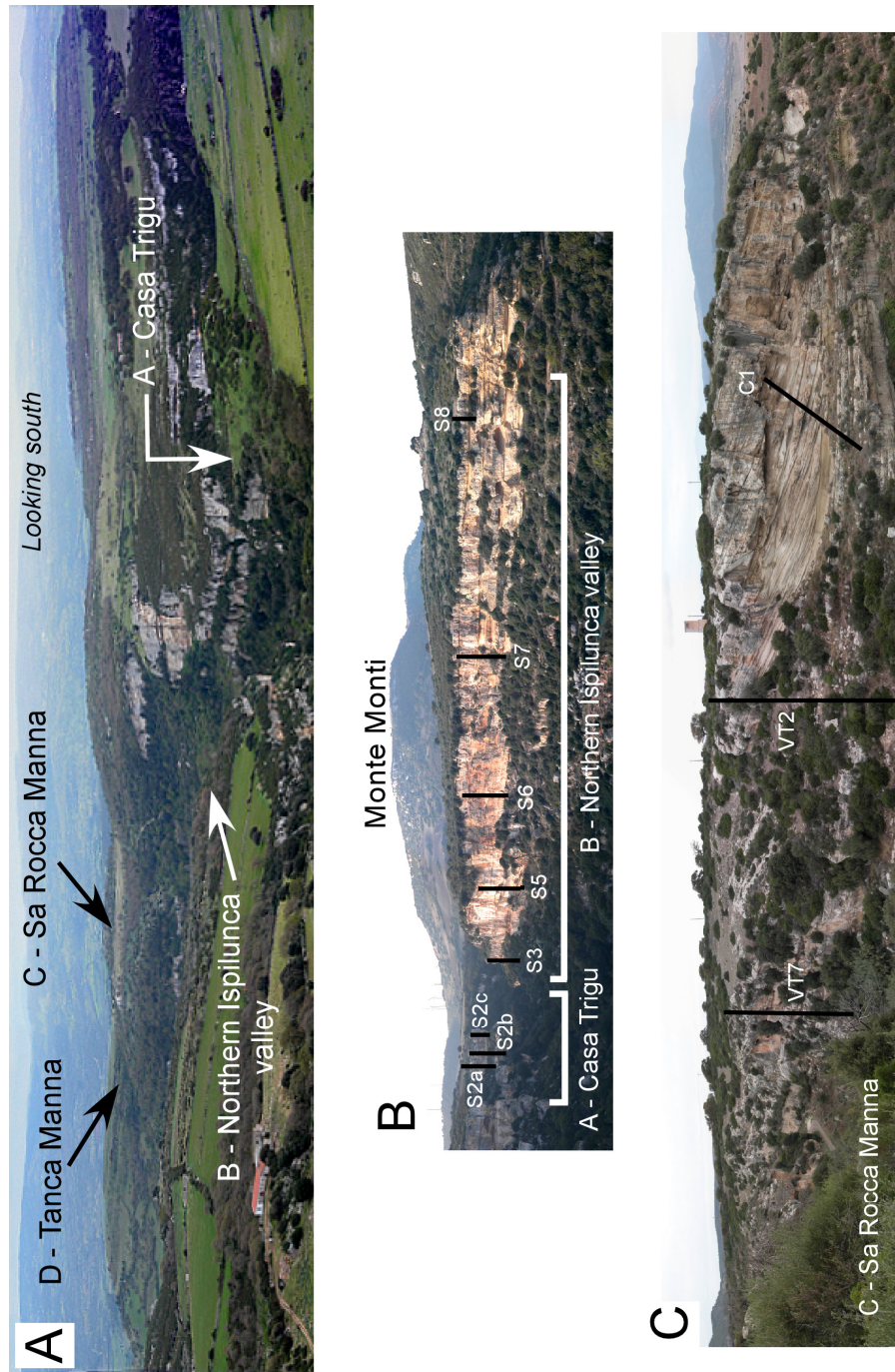


Figure 4.3. (A). Panorama showing an overview of the depositional units observed in the area. The picture is taken from Monte Monti, looking south. The contact of the carbonates (the Sedini Limestone Unit) with the underlying volcanics (Tergu Fm.) is visible to the west (and right). Within the Sedini Limestone Unit, the transition from shallow marine limestones and coral reefs to outer platform deposits is visible from west to east. (B). Panoramic view of the Casa Trigu and Northern Ispilunca valley transects, looking north. Monte Monti is visible in the back. Sequence 1 is poorly outcropping, generally covered, and is only visible in northern areas. In contrast, sequence 2 exposes a thick succession, as is shown in the photopanorama (C). Panoramic view of Sa Rocca Manna. Note the well exposed clinoforms. Stratigraphic sections and their lateral correlation in (B) and (C) are based on physical tracing of the stratal units. See Figure 4.4 for their details, and Table 4.1 and 4.2 (appendix) for a detailed description of the facies.

rocks (Baccelle and Bosellini 2001 in: Flügel 2004). Qualitative estimations have been defined to indicate the following percentages: absent (less than 1%), rare (1-5%), common (5-10%), present (10-20%), and abundant (more than 20%).

## 4.5 Results

The “Sedini Limestone Unit” has been divided in two depositional sequences (Benisek et al., in press): the lower (sequence 1) and the upper (sequence 2). In addition, within each sequence, informal subsequences or units reflecting different litho- and bio-facies characteristics were identified. Two informal units were identified in sequence 1: S1a and S1b. Five informal units were identified in sequence 2: S2a to S2e. A unit 2f (not studied in this thesis) and a unit (S2?, Fig. 4.2) composed by marls, were identified. The marly unit occurs stratigraphically above unit S2e-f, as indicated by regional, spatial geometrical relationships. However, its basal contact is not exposed. Benisek et al. (in press) discuss in detail the stratigraphic architecture of the two sequences and their internal characteristics (depositional facies, sedimentology, and carbonate factory). Here, we provide only a description in terms of the lithofacies and sediment composition (biota and cements) which constitute the framework for interpreting the significance of biogenic association, paleoenvironments and early diagenetic features. This information is briefly summarized in Table 4.1 and Table 4.2 (appendix), along with the diagenetic characteristics.

Figures 4.5, 4.6, and 4.7 show the vertical and horizontal biotic distribution and cements identified within the sequences and lithofacies. The figures show sections from Casa Trigu (Fig. 4.5), Northern Ispilunca valley (Fig. 4.6), and Sa Rocca Manna (Fig. 4.7). The stratigraphic sections were constructed as composite sections (vertical consecutive segments) in order to summarize the main components and differences within each sequence and informal units. The composite section called “Casa Trigu” was based on S2a-S2b-S2c; however, unit S1a (cross-bedded strata) and the floatstone above the contact S1a/S1b data include section S3 and S5 from the Northern Ispilunca valley transect. The Northern Ispilunca composite section gathers data from S6 to S8. For the composite section representing the Sa Rocca Manna composite section, data are compiled from VT2 (base) and C1 (top).

### 4.5.1 Lithofacies Description

**Sequence 1.** The lower sequence or sequence 1, outcrops at Casa Trigu and Northern Ispilunca valley transects (Fig. 4.3 for location, Fig. 4.4 for the detailed transects). Benisek et al. (in press) have recognized this sequence at southern areas of Sedini town (Fig. 4-1B, section Sedini south), and also at Grotta Su Coloru and Southern Ispilunca valley (Fig. 4-1B).

This sequence is characterized overall by a bryozoan-coralline red algae- bivalves-echinoid skeletal assemblage, with large benthic foraminifer (*Amphistegina* and *Heterostegina*) barnacles and corals as subordinate components. In this sequence, four lithofacies (Table 4.1 in the appendix and Fig. 4.4) were identified (accordingly with Benisek et al., in press), and their distribution within units S1a and S1b is as follows.

At Northern Ispilunca valley, the succession starts at unit S1a with echinoid-bivalve floatstones and rudstones, deposited in beds of less than 2 m thickness (Fig. 4.4). Serpulids and some bioturbation are observed. This facies is overlain by skeletal floatstones and rudstones which occur in large scale planar cross-beds (Fig. 4-8A). Two sets are observed, one in each unit, having 4-8 m of set thickness. They outcrop in the Casa Trigu transect and the Northern Ispilunca valley. Fore-set shapes are straight where top-set boundaries are irregular and discordant. Localized in the Northern Ispilunca valley, the top-set boundaries can show wave action (trough-cross bedding, details in Benisek et al., in press). Each set can be traced laterally for at least 200 m. Progradation of these planar cross-stratified bodies is towards the east (Benisek et al., in press). Fragments of nodular bryozoans (encrusting), coralline red algae (*Lithothamnion?*), molluscs (calcitic bivalves), echinoids (plates) and barnacles characterize these rocks. Larger benthic foraminifers (*Amphistegina* and *Heterostegina*) are present and the latter becomes dominant in the upper set (unit S1b, Fig. 4.5). Biotic grains are fragmented and reworked. Sorting is poor. Occasionally, some skeletal grains (especially barnacles) show iron oxide coating.



Between the two sets of planar cross-bedded floatstones to rudstones (lower part of unit S1b), massive beds of floatstones occur. The thickness of the strata varies from 0.5 to 1.5 m. Encrusting biota such as nodular bryozoans, and encrusting foraminifera with coralline red algae (*Lithothamnion* ?), characterize the floatstones at the Casa Trigu transect, whereas rhodolites characterize the floatstones at the Northern Ispilunca transect. At the Casa Trigu transect, a large amount of early cements (e.g., micrite) is observed at the floatstones (lower part of S1b, Fig. 4.4), and large benthic foraminifera (*Amphistegina* and *Heterostegina*) are relatively well preserved and become abundantly important. A low abundance of planktic foraminifera (globigeriniids) occurs. At Northern Ispilunca valley, rhodolites are composed by *Lithothamnion*?, and their cores are usually affected by borings. The floatstones randomly contain glauconite and iron oxides. To the E to SE direction (Northern Ispilunca valley and Sedini south), cross-bedded floatstones and rudstones of the upper set (unit S1b) grade into wackestones and packstones. Planktic foraminifera, in combination with highly reworked molluscs (calcite bivalves) and echinoid fragments, characterize these rocks.

**Sequence 2.** The upper sequence, or sequence 2, is exposed at the Casa Trigu, Northern Ispilunca valley, and Sa Rocca Manna transects (Fig. 4.3 for location, Fig. 4.4 for the detailed transects). At sections D and E, only fine-grained facies are exposed. In section F, marls are characteristic, which are only found at the northern areas of the Sedini village (Fig. 4-1B).

Overall, this sequence is characterized by the appearance of in-situ corals, rhodolites, small and larger benthic foraminifera (*Amphistegina* and *Heterostegina*), and molluscs. Additionally, coralline red algae, bryozoans, barnacles, and serpulids can also occur.

In this sequence, nine lithofacies were identified (Table 4.2 in the appendix and Fig. 4.4) (accordingly with Benisek et al., in press). A sixth unit (S2?, Fig. 4.2), characterized by deep-water marls, is briefly mentioned here (section E, Fig. 4.3). The distribution of the lithofacies within units is as follows.

At the base of the sequence (units S2a-S2b), in the northern areas such as in Casa Trigu, thin beds (< 2 m) of floatstones to rudstones occur. Coralline red algae (*Lithothamnion*?), nodular bryozoans (encrusting), molluscs (calcite bivalves) and reworked corals (undetermined) are the dominant biota. Differences in early lithification are observed. Calcite cements such as micritic, fibrous, syntaxial and blocky cements have been identified. Beds have a lateral continuity to the east (in the direction of the Northern Ispilunca transect) and to the south (in the direction of the Sa Rocca Manna transect). Upsection, at Casa Trigu, the floatstones and rudstones are followed by a < 2 m yellow red algal bindstone. They occur localized and its aerial extension is limited to Casa Trigu and Northern Ispilunca valley (observed at the field). Coralline red algae are the dominant biota; their growth forms vary from encrusting to layered. Among the taxa are *Lithothamnion*, *Lithophyllum*, and *Neogoniolithon* (Benisek et al., in press); however, *Lithothamnion*? constitute the major contributor. In addition, corals (undetermined), echinoid spines (3-4 cm long), and articulated bivalves (oysters, *Spondylus*) occur. In addition, nodular bryozoans (encrusting) and barnacles are also found. The vertical development of these bindstones starts with horizontal oriented crusts, lying directly on the floatstones previously described. Upsection, the abundance and extension of these crusts increase along with the articulated bivalves and size of the echinoderm spines. Coralline algae encrust corals which usually appear towards the top of the bindstone. Isolated branches of *Lithothamnion*? occur within the layering. Upsection, these bindstones turn into a rudstone-bindstone up to 10 m thick. The biota is dominated by coralline red algae and occur as reworked grains (branches and detritus) and isolated encrustations (*Lithothamnion*?). In addition, a mix of reworked neritic biota (bryozoans, large benthic foraminifera and reworked corals) is observed.

The previous lithofacies, within units S2a and S2b, grades towards the east into cross-bedded to massive and moderately to good sorted bioclastic wackestones, packstones and grainstones. In Northern Ispilunca valley, units S2c and S2d are characterized by this lithofacies; however, due to the physically restricted outcrop exposure, detailed description was not possible. In Sa Rocca Manna, unit S2d is characterized by this lithofacies; good outcrop exposure allowed its description.

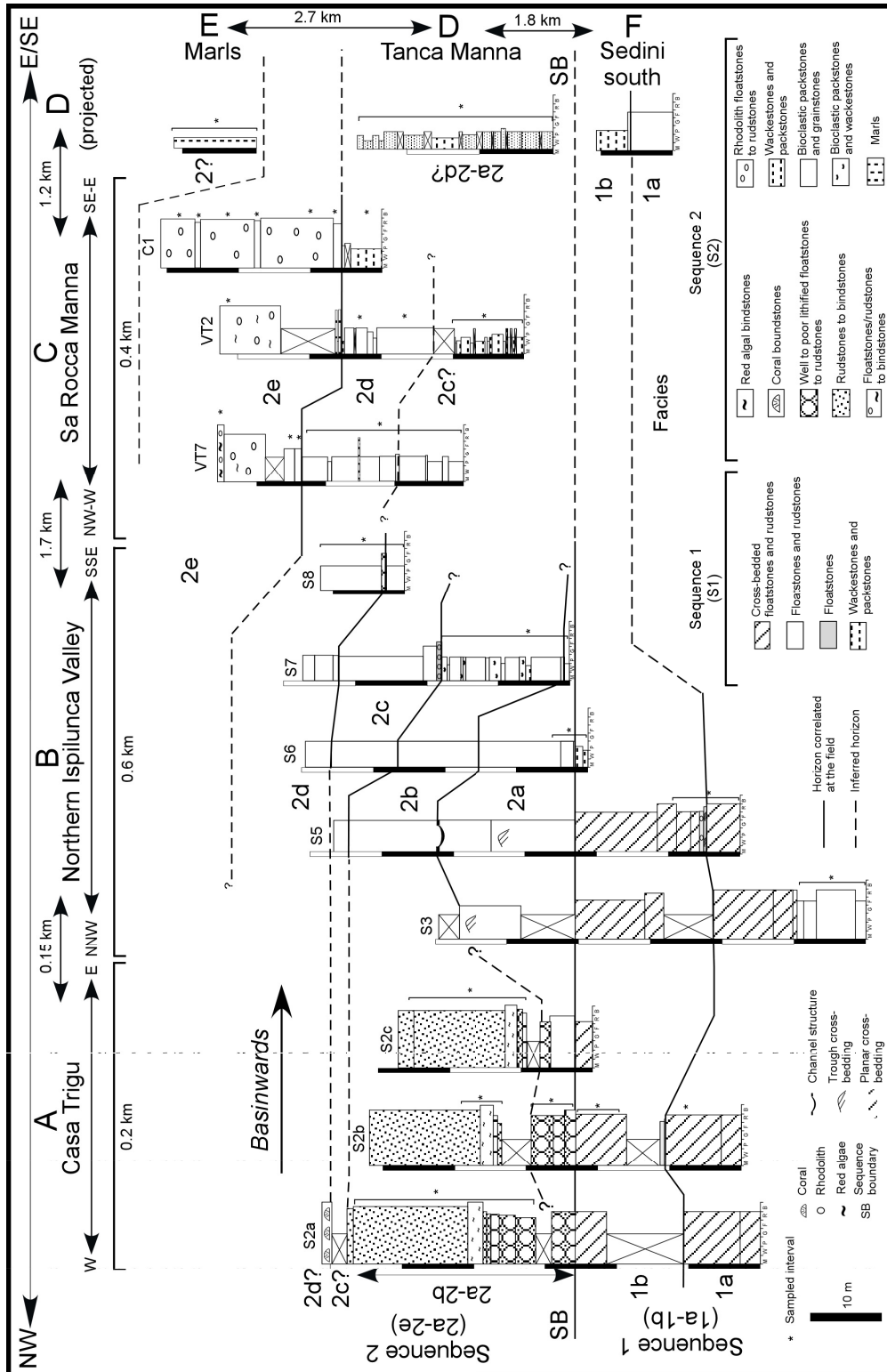


Figure 4.4. Correlation of the stratigraphic sections measured in the different areas showing the distribution of different lithofacies and other sedimentary attributes. The correlation was established by means of physically tracing the beds in the field as well as with photopanoramas.

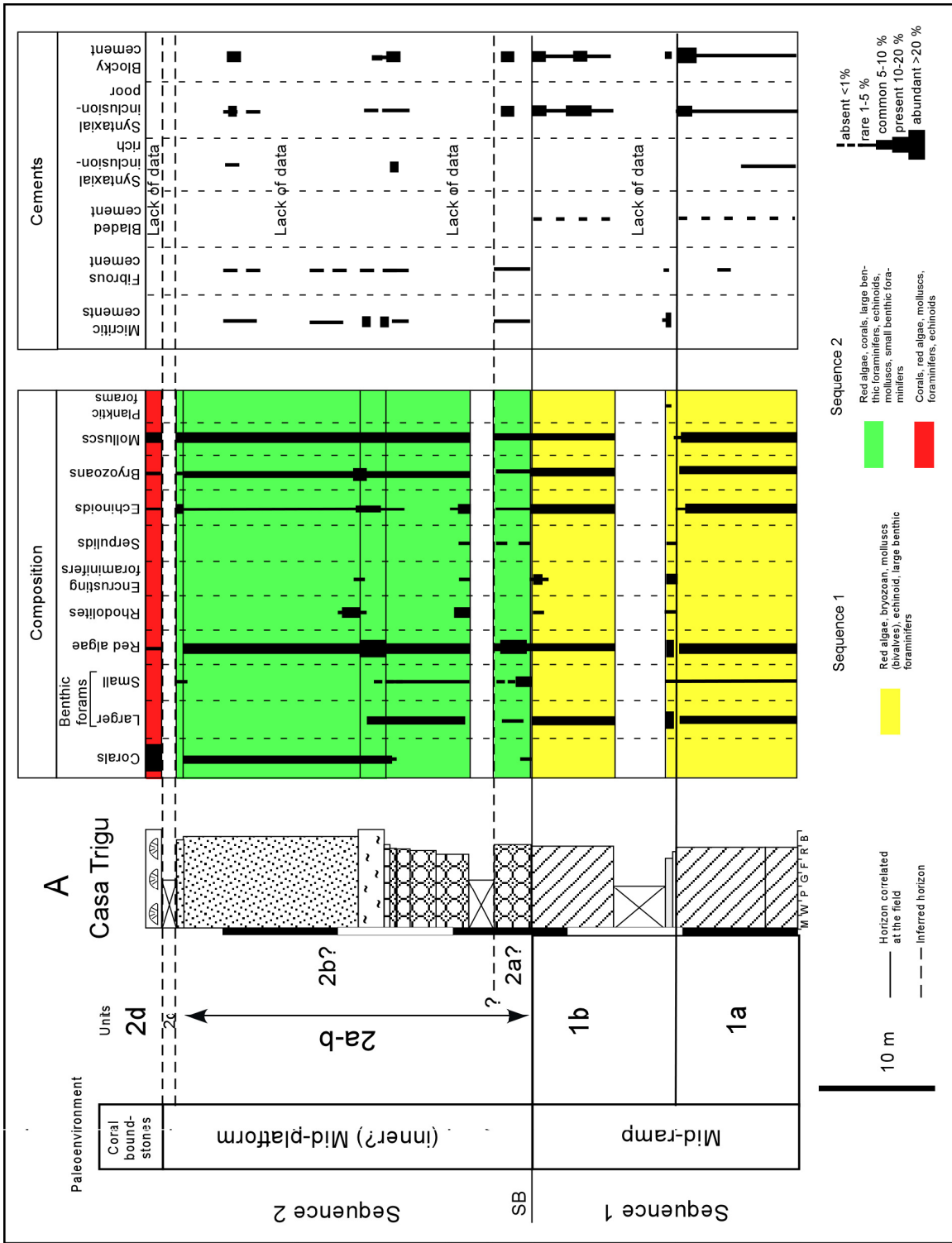


Fig. 4. 5. Relative abundances of biota and early cements of facies plotted in a composite section, based on field data and petrographic analysis at the Casa Trigu transect. Here, the two sequences can be observed bounded by a sequence boundary (SB). The lower sequence shows a bryozoan-bivalve-red algae-echinoid character where larger benthic foraminifers and some reworked corals have been recognized. Early cements are scarce. In contrast, the upper sequence contains more corals (in situ and reworked) and early cements.

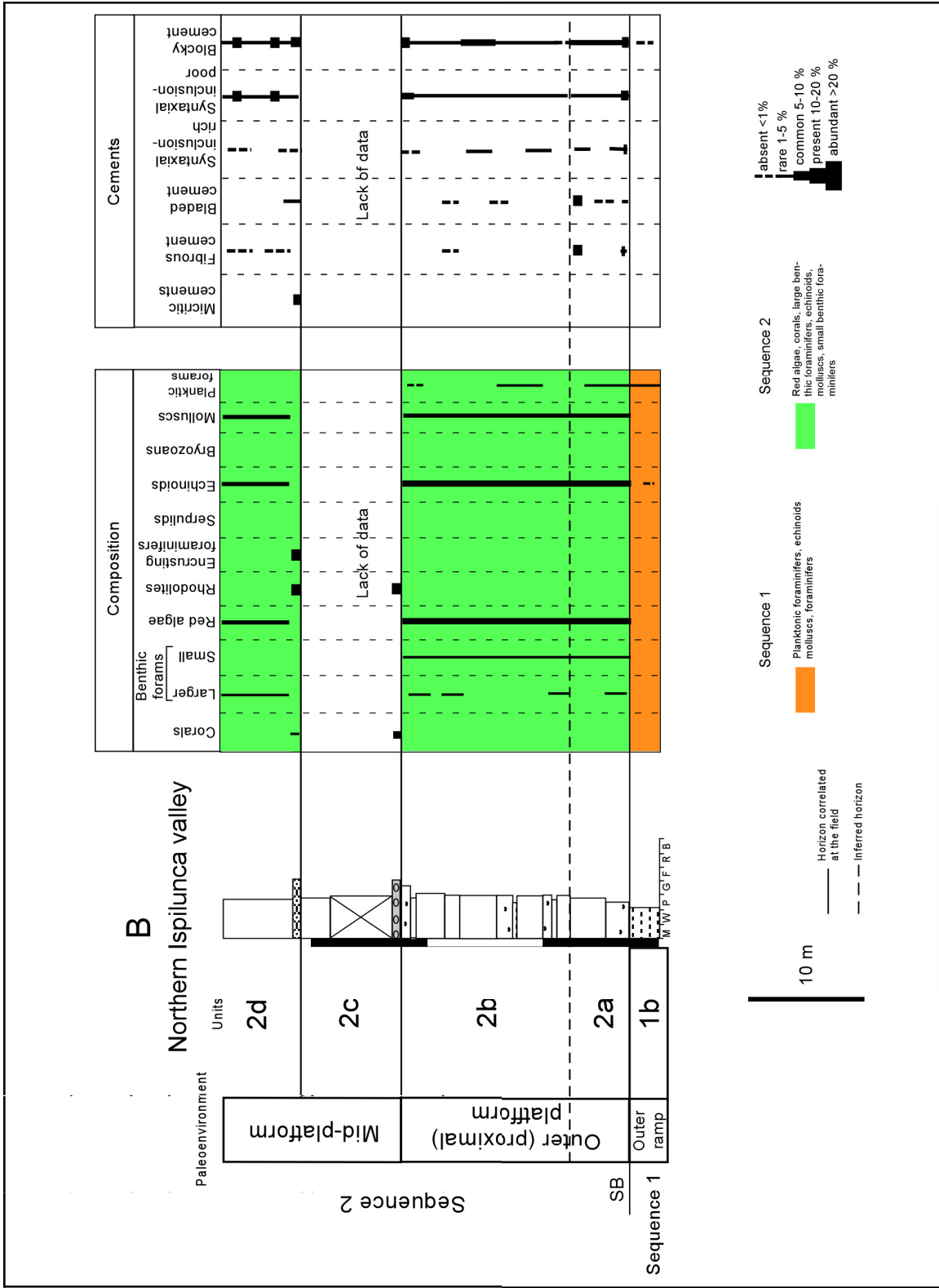


Figure 4.6. Relative abundance of biota and early cements plotted in a composite section of the Northern Ispilunca valley transect. The compiled stratigraphic section includes sections S6 to S8, and strata from sequence 1 and 2.

Bioclasts are represented by a mixture of molluscs (calcitic bivalves and aragonitic gastropods), large benthic foraminifers (*Amphistegina* and *Heterostegina*), coralline red algae (undetermined), and echinoids (plates). Grainstones and packstones can contain small benthic foraminifers (textulariids). Bryozoans are observed; however, they are scarce and usually highly reworked. Traces of highly reworked corals are found. Distally, at Sa Rocca Manna, scarce planktic foraminifers are locally observed. Packstones are mostly characterized by coralline red algae and echinoids, whereas grainstones are rich in molluscs and large benthic foraminifers. This lithofacies usually has micritic envelopes, moldic porosity, and different phases of calcitic cements. Thickness along the Northern Ispilunca valley and Sa Rocca Manna varies from decimetres to < 30 m of thickness, respectively (Fig. 4.4). At the base of unit S2a, bioclastic packstones and grainstones can show localized small trough-cross stratification. At unit S2c and S2d, floatstones with rhodolites, encrusting foraminifers and coralline red algae are found. Reworked corals are only observed in S2d (Fig. 4.5). However, their expression is vertically restricted and spatially localized at the Northern Ispilunca valley transect (S7-S8).

Basinwards, bioclastic packstones and grainstones interfinger with yellow/white moderately-sorted bioclastic wackestones and packstones. Exposure is restricted and localized to Northern Ispilunca valley and at unit S2b. Bioclasts are represented by a mixture of molluscs (calcitic bivalves), coralline red algae (undetermined), echinoids (plates), and small benthic foraminifers (textulariids). Open-water biota, such as planktic foraminifers, are identified.

To the east and south, bioclastic wackestones, packstones and grainstones grade into fine-grained brown/yellow good sorted wackestones and packstones. Spatially, they occur from the Northern Ispilunca valley transect (S7) to the north and northeast of Sedini town (Fig. 4-1B), and from Northern Ispilunca valley (S7) to the south (tens to hundred meters) of the Sa Rocca Manna transect (VT2, C1) and the Tanca Manna section (Fig. 4.4). They are considered within units S2a to S2d. This fine-grained lithofacies is characterized by planar beds, of which some bioturbation has obscured their boundaries and internal stratification. Thickness gradually increases from 10 to 30 m at Northern Ispilunca valley towards the east (Fig. 4-1B, Sedini town) and south-southeast (Fig. 4.4, Sa Rocca Manna and Tanca Manna). Two types of packstones and wackestones were identified: (1) wackestones and packstones containing a mix of neritic and open water biota. Neritic biota is characterized by small benthic foraminifers (textulariids and low abundance of miliolids), molluscs, coralline red algae (highly fragmented), echinoderms (highly fragmented), thin bivalve shells (pectinids), and serpulids. Open-water biota is characterized by traces of planktic foraminifers (Globigeriniids). This type outcrops at Northern Ispilunca valley (sections S6 to S7) and Sa Rocca Manna (base of VT2); (2) wackestones and packstones containing open water biota such as planktic foraminifers (Globigeriniids) and traces of highly reworked very-fine-sand size detritus of echinoderms. This type outcrops at the Tanca Manna section. In both types, the matrix can contain glauconite and phosphate (Table 2).

At the top of sequence 2 (unit S2d?), at the Casa Trigu transect, a thin (< 1 m), massive bed of coral boundstone occurs (Fig. 4.4). Corals show massive growth forms and low taxa diversity. A secondary framework is constructed mainly of encrusting coralline-red algae, bryozoans, and molluscs. In our study, coral boundstones only occur locally; however, they can be traced laterally in direction towards the east (Fig. 4-8B) and the Sa Rocca Manna outcrop (Benisek et al., in press).

At the Sa Rocca Manna transect, overlying the bioclastic grainstones and packstones of unit S2d (Fig. 4.4, sections VT7 and VT2), unit S2e is characterized by float/rudstones to bindstones and floatstones and rudstones. The thickness of float/rudstones to bindstones does not exceed 1 m. Floatstones and rudstones are up to 28 m thick and show basinward-dipping clinobeds (< 27°) (Fig. 4-8C). Float/rudstones to bindstones are predominantly constituted by coralline red algae together with nodular bryozoans (encrusting), encrusting foraminifers (acervuliids), and molluscs (bivalves). Highly reworked coarse-grained large benthic foraminifers, echinoids, red algae, bryozoans and corals can be observed. Floatstones and rudstones are characterized by rhodolites, which have a sphaeroidal to ellipsoidal shape with a coarse-grained bioclastic nucleus (bryozoans or bivalves). Rhodolith (Fig. 4-8D) size ranges from a few cm to 10 cm across. Rhodolith layers are characterized by coralline red algae, encrusting foraminifers (undetermined),

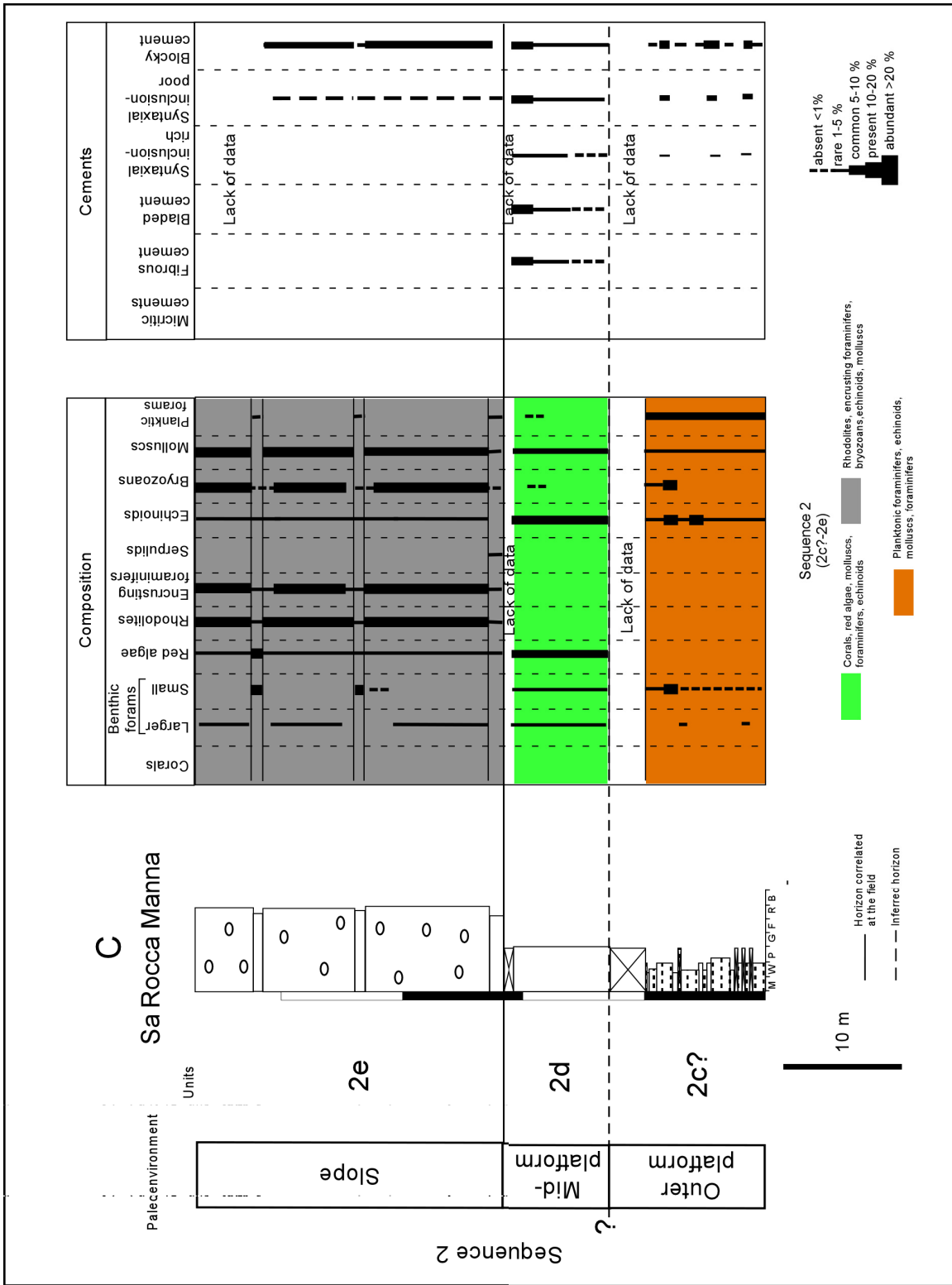


Figure 4.7. The relative abundance of biota and early cements plotted in a composite section of the Sa Rocca Manna transect. The compiled stratigraphic section includes sections VT2 and C1, and shows the mid, slope and outer platform facies of sequence 2. Note the dominance of rhodolites, encrusting foraminifers, and bryozoans in the slope facies. Early cements are only observed at mid-platform facies, in contrast with outer platform and slope facies.

and nodular bryozoans (encrusting). A high diversity of red algae taxa can be observed. In this work, no grow-forms or biotic components of the rhodolites have been studied.

In E direction, at the northern area of Sedini Town (Fig. 4.1), a < 15 m thick marly stratigraphic section occurs (S2?). No basal contact with unit S2e-f or any other unit is observed. Biota is poorly preserved and scarce. However, random fish remains can be preserved, as well as planktic foraminifers.

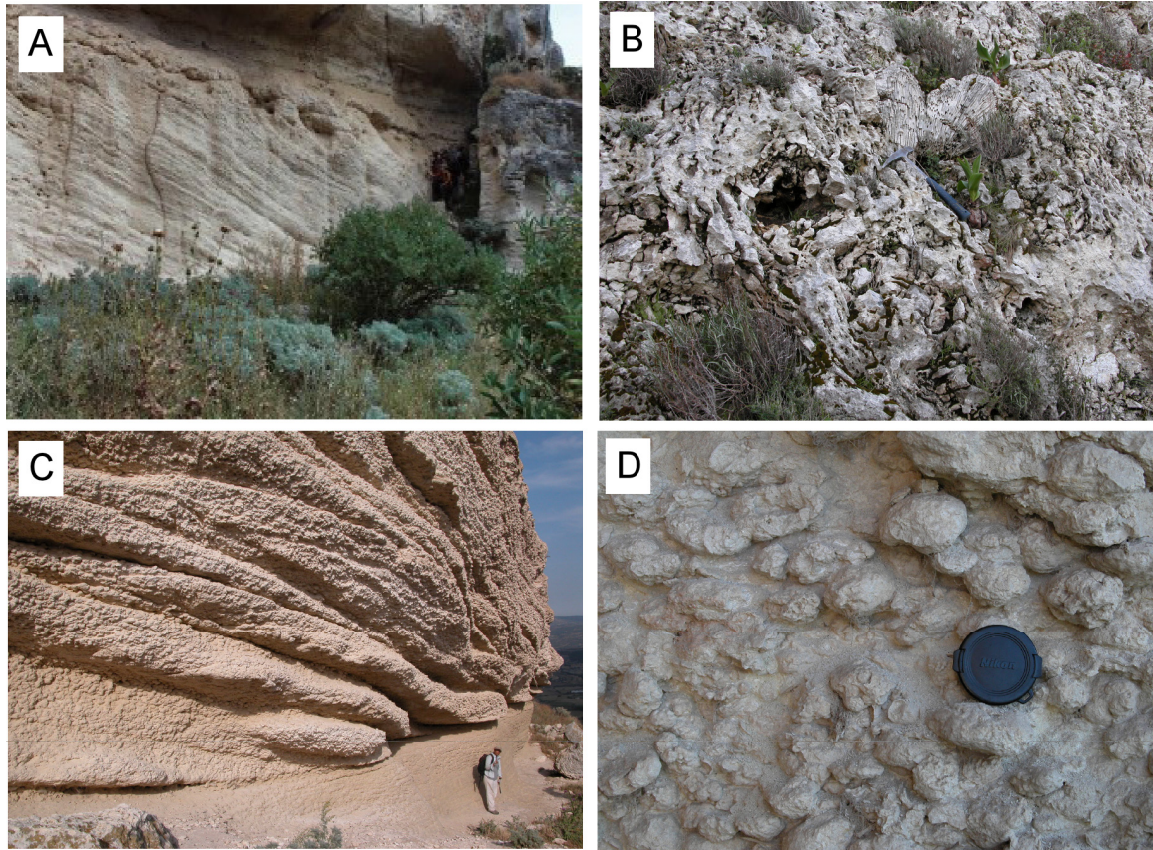


Figure 4. 8. (A) Northern Ispilunca valley transect: planar cross-bedded strata at Sequence 1. Lithology is represented by floatstones to rudstones containing reworked skeletal grains. (B) Ispilunca valley: coral boundstones at Sequence 2. In general, they occur at the uppermost informal units S2d and S2e. (C) Sa Rocca Manna transect: rhodolith floatstones to rudstones with clinoformal geometry. They occur at Sequence 2, informal unit S2e. (D) Sa Rocca Manna transect: detail of the rhodolites. Note the ellipsoidal to discoidal forms.

#### 4.5.2 Petrography of early diagenetic features.

In this study, diagenetic features are identified as syn- and early-depositional and post-depositional. The main criterion is their direct relationship with the substrate and pre-dating compaction. Therefore, in order to interpret and discuss the relationship of early diagenesis and facies stabilization, attention is given to syn- and early-depositional diagenetic features (micritic envelopes, micritic cements, fibrous and syntaxial inclusion-rich). The post-depositional features identified are related to calcite cementation (bladed, syntaxial and blocky calcite cements), creation of secondary porosity and compactional features; however, its interpretation goes beyond the scope of this contribution and will be discussed in Chapter 5.

**Micritic Envelopes (me).** Micrite envelopes occur as fine to thick rims defining the shape of micritized bioclasts (Fig. 5.8, Chapter 5). They occur in both sequences, although with different characteristics. In sequence 1, micritic envelopes are only observed at cross-bedded floatstones to rudstones, where envelopes are thin and almost absent on every grain.

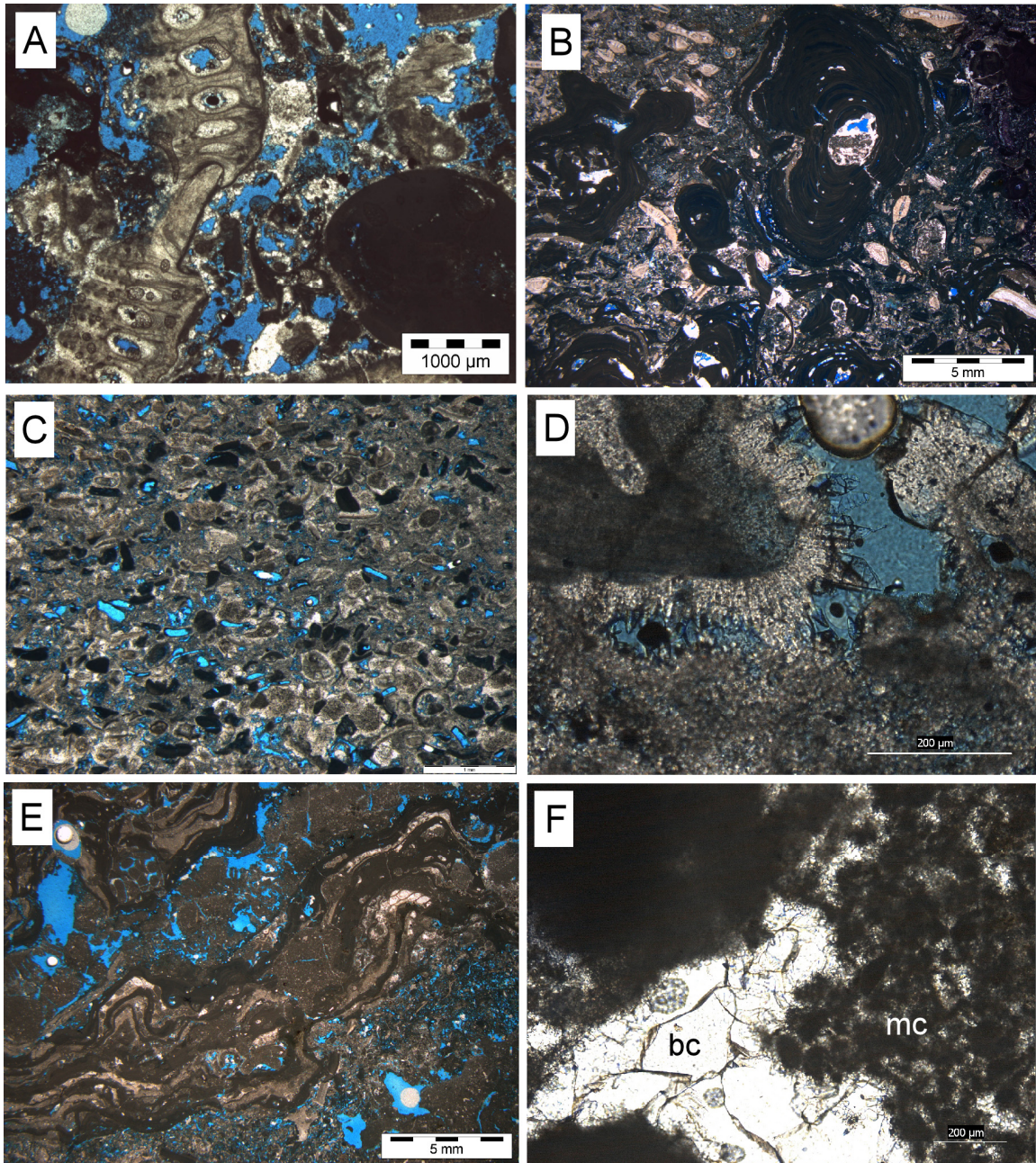


Figure 4.9. Biota and early cements. (A) Sequence 1. Rudstone (planar cross-bedded strata). Biota is mainly reworked skeletal red algae, bivalves, echinoids and barnacles. Cements are scarce. (B) Sequence 1. Floatstone located in unit S1b above the contact S1a-S1b. Biota is represented by rhodolites, reworked bioclasts and large benthic foraminifers. Cements are micritic and blocky. (C) Sequence 2. Bioclastic packstone to grainstones from the informal unit S2d. Biota is represented by echinoids, molluscs (dissolved), red algae, bivalves and large benthic foraminifers. Cements are fibrous, bladed, syntaxial and blocky. (D) Sequence 2. Detail of cements at the bioclastic packstone to grainstone represented in (C). (E) Sequence 2. Red algal bindstone. Biota are encrusting red algae, foraminifers, bryozoans. Cements are micritic; however, detrital micrite can be present. (F) Detail of micrite (peloidal) and blocky calcite cement in (E).

In sequence 2, micritic envelopes are found in bioclastic packstones and grainstones, where envelopes are thick and on nearly every grain. Micritic envelopes are also present, however, in deeper water facies (platform), but the rims are thinner and many grains lack them.

**Micritic Cements (mc).** Micrite cements mostly occur in sequence 2, where they show homogeneous, clotted and micropeloidal fabrics. Micritic cements are pore-fill and localized to



specific lithofacies (red algal bindstones and floatstones). Micritic cements (peloidal and clotted) can be observed filling geopetal structures and together with blocky calcite cements (Fig. 4.9). In sequence 1, micritic cements show homogeneous and micropeloidal fabrics and occur only at floatstones above the boundary of S1a with S1b (Casa Trigu).

**Fibrous Cements (fc).** This cement is characterized by inclusion-rich crystals generally less than ~ 50  $\mu\text{m}$  thick, with weak extinction and poorly defined crystal boundaries (Fig. 4.9). This cement is found as an isopachous calcite cement. Crystals are equidimensional and grow normal to the substrate. This cement occurs as thin isopachous cement in sequence 1 and as thick and continuous in sequence 2. In sequence 1, fibrous cements are only found and rarely in floatstones and rudstones. In sequence 2, fibrous cements are abundant and found in bioclastic packstones and grainstones, and at floatstones and rudstones. Fibrous cements are observed in samples where micritic cement occurs; however, their spatial relationship is not observed. Where syntaxial inclusion-rich overgrowths are also present, they were formed during the precipitation of the isopachous fibrous cement.

**Syntaxial Inclusion-Rich Cement (sc1).** Syntaxial cements grow in optical continuity over echinoderms (Fig. 4.9), and the presence or absence of inclusions allows for the recognition of two phases: a first, inclusion-rich phase (sc1), described here, and a later inclusion-poor phase (sc2), described in Chapter 5 as post-depositional events. The inclusion-rich syntaxial cement forms rims ranging from ~ 30 to < 100  $\mu\text{m}$  in width. The presence of inclusion allows for the recognition of the former presence of crystals perpendicular to the substrate, with prismatic terminations. This cement occurs in both sequences; however, it is apparent in minor proportions with respect to other types of cements.

#### 4.5.3 Summary of sediment composition and cement types

##### Sequence 1.

*Biota.* Field and petrographic observations indicate that the shallower water sediments of sequence 1, distributed in units S1a and S1b, at Casa Trigu, the Northern Ispilunca valley transect and the Sediní south section are represented by (Figs. 4.5 and 4.6): coralline red algae (*Lithothamnion?*) (10-15 %), bryozoans (nodular and robust) (5-10 %), molluscs (mostly calcitic bivalves) (5-10 %), echinoderms (plates) (10 %), and large benthic foraminifers (*Amphistegina* and *Heterostegina*) (~10 %). Minor components are: small benthic foraminifers (highly reworked and undetermined) (< 5 %), serpulids (< 5 %), rhodolites (localized, < 5-10 %), encrusting foraminifers (< 5 %). Deeper water sediments in general contain echinoids (< 5%), planktic foraminifers (< 5 %) and molluscs (calcitic bivalves) (< 5%).

*Cement types and distribution.* On average, sequence 1 contains about < 10 vol. % cement (Fig. 4.5 and 4.6). The dominant cement phases are syntaxial inclusion-poor, precipitated around echinoderm fragments and blocky calcite cement as pore-fill cement. These cement types are predominantly abundant in the cross-bedded floatstones and rudstones. Syntaxial inclusion-rich is also observed; however, it is generally dissolved. Traces of fibrous cements are overall scarce with the exception of floatstones above the contact of units S1a and S1b, where micrite as cement has also been observed. Bladed cement is scarce and does not constitute an important phase of cementation.

##### Sequence 2.-

*Biota.* Field and petrographic observations indicate that shallower water sediments of sequence 2, distributed in units S2a to S2b, at the Casa Trigu transect, are represented by (Fig. 4.5): coralline red algae (*Lithophyllum?*, *Lithothamnion?*, only identified in this work) (10-20 %), corals (low diversity) (< 10 %), large benthic foraminifers (*Amphistegina* and *Heterostegina*) (< 10 %), molluscs (bivalves and gastropods) (10-15 %), echinoderms (spines and plates) (5-10 %), small benthic foraminifers (5-10 %), and bryozoans (nodular and branching) (< 10 %). Minor

components are: serpulids (< 5 %), rhodolites (localized, < 10 %), encrusting foraminifers (< 5 %). Deeper water sediments contain, in general, echinoids (< 5%) and planktic foraminifers (5-10 %).

Field work allows for the identification of corals (low diversity) in unit S2d at the Casa Trigu transect (Fig. 4.5). Petrographic observations indicate that the shallower water sediments of sequence 2 distributed in unit S2c and S2d at the Northern Ispilunca valley and Sa Rocca Manna transect are represented by (Figs. 4.6 & 4.7): coralline red algae (*Lithothamnion?*) (10-15 %), molluscs (bivalves and gastropods) (10-15 %), echinoderms (plates) (5-10 %), small benthic foraminifers (undetermined) (5-10 %), and large benthic foraminifers (*Amphistegina* and *Heterostegina*) (< 10 %). Minor components are: rhodolites (localized, < 10 %), encrusting foraminifers (acervuliinids) (< 10 %), bryozoans (nodular) (< 5 %), and planktic foraminifers (< 1 %). Reworked corals were identified and represent values of < 5 %. Deeper water sediments contain, in general echinoids, (< 5%) and planktonic foraminifers (< 5 %).

Petrographic observations indicate that the sediments of sequence 2 distributed in unit S2e at Sa Rocca Manna are represented by (Fig. 4.7): rhodolites (10-20 %), encrusting foraminifers (acervuliinids) (< 10 %), encrusting bryozoans (nodular) (< 10 %), molluscs (calcitic bivalves) (< 10 %), and echinoderms (plates) (5-10 %). Minor components are: small (highly reworked and unidentified) and large benthic foraminifers (highly reworked) (*Amphistegina*) (5-10 %), serpulids (< 1 %), and planktic foraminifers (< 1 %).

**Cement types and distribution.** Sequence 2 contains on average about < 20 % vol. of cement (Figs. 4.6 and 4.7). Micrite is usually observed at shallow-water limestones when red algae-rich facies are involved. Fibrous and bladed cements are common in bioclastic grainstones, packstones and wackestones. Syntaxial inclusion-rich is overall present in all facies with the exception of its scarcity in deeper water facies. Syntaxial inclusion-poor and blocky calcite cements occur everywhere and no differences are observed.

## 4.6 Interpretation and discussion

### 4.6.1 Paleoenvironments

Sequence 1 was deposited on a ramp and facies distribution, in combination with the biotic association, led to the identification of a (shallow) mid-ramp as well as outer- (proximal) ramp deposits. The arrangement of the depositional facies at the ramp is based on hydrodynamic conditions (Burchette and Wright 1992), and the distribution of the biotic association in terms of light penetration-depth (Pomar 2001).

In accordance with Benisek et al. (in press), sequence 2 records the turnover of geometry into a “platform-like” setting. The change in geometry is gradual during earlier stages (units S2a-S2d), and becomes clearly marked at the latest stages of platform growth (unit S2d to S2e). Benisek et al. have suggested that paleoenvironments within sequence 2 are comparable with patterns of deposition within a platform (e.g., Burchett and Wright 1998). Therefore, in units S2a to S2d, facies distribution, in combination with the biotic association, led to the identification of (inner?-shallow) mid- and outer-platform deposits; meanwhile, in unit S2e, a platform top, margin, and slope have been identified.

Figure 4.10 (A, B and C) shows a 2D model of the aerial distribution of facies within the sequences, including the relationship of the lithofacies and sediment composition identified and proposed in this study.

**Sequence 1.** In sequence 1 (units S1a and S1b), (shallow) mid-ramp deposits are characterized by bioclastic floatstones and rudstones, which show characteristics consistent with submarine bars.

Planar cross-bedded stratification shows the involvement of currents; the presence of highly reworked bioclasts is indicative of high-energy conditions. This suggests that the submarine bars were deposited at or below the fair-weather wave-base. On the other hand, wave action at the top of the bars (contact S1a/S1b) indicates that they developed close to high-energy areas of the inner-ramp, most probably at the fair-weather wave base (local trough cross-bedding, Northern Ispilunca valley). The presence of red algae (*Lithothamnion?*) with large

benthic foraminifers (*Amphistegina* and *Heterostegina*) places the deposition of the bars at the mesophotic zone (Pomar 2001). Floatstones at the top of the bars (above the limit S1a/S1b), showing shallow-water benthic and open-water planktic biota (Fig. 4.5), indicate a rapid deepening of the depositional system. However, red algae (encrusting and rhodolites), bryozoans (nodular and branching) and large benthic foraminifers (*Amphistegina* and *Heterostegina*) indicate that the deposition took place under photic conditions, more probably within the mesophotic zone of the mid-ramp (Brandano and Corda 2002).

These submarine bars can be compared with the shallow-water mid-ramp bars reported by Brachert et al. (1998) in the Miocene deposits in Southern Spain. Both examples share sedimentological and biogenic characteristics. Brachert et al. (1998) have estimated depositional water-depths of 20-25 meters.

In sequence 1, outer-ramp deposits are characterized by wackestones and packstones, which are consistent with sediments deposited below the storm wave base.

**Sequence 2.** At sequence 2, (inner? and shallow) mid-platform deposits from units S2a to S2d are characterized by red algal bindstones, floatstones, rudstones, rudstones to bindstones, and bioclastic wackestones, packstones and grainstones (units S2a to S2d).

Red algal bindstones are characterized by encrusting biota and epibenthic communities which show some degree of reworking. The occurrence of large benthic foraminifers and corals suggests that these bioconstructions were growing in the photic zone. The preservation of large echinoderm spines in association with articulated bivalves (oysters, *Spondylus*) suggests in situ carbonate production and accumulation. Substrate stability is supported by the combination of nodular bryozoans (Bone and James 1993) and coralline red algae such as *Lithothamnion?* (Rasser and Piller 2004). The intercalation with floatstones and rudstones showing differential degrees of early cementation acts as substrate reinforcement for these bindstones. The transition upsection into a rudstone to bindstone facies indicate a change in hydrodynamic energy close to the carbonate production. However, the biotic association of the red algal floatstones to rudstones indicate deposition under photic conditions, and the absence of open-water biota constrains their deposition at shallow-water settings.

The morphologic characteristic of trapping and binding of the red algae encrustations, the low degree of fragmentation of bioclasts, the lack of wave related structures, and the deposition under photic conditions, all indicate that the red algal bindstones, floatstones, rudstones and rudstones to bindstones were deposited under moderate hydrodynamic conditions, most probably below wave base in an (inner?) shallow mid-platform setting. The appearance of *Spondylus* points to a water depth most likely not exceeding 50 m. The relationship of *Lithothamnion?*, *Lithophyllum*, and *Neogoniolithon* (Benisek, et al., in press) indicates water depth for deposition above 60-70 m. Therefore, it is considered to be a deposition at < 70 m of water depth, which is comparable with Miocene or present-day Mediterranean environments (Betzler 1997; Rasser 2000). Normally, these are found below the normal wave base, at shallow circalittoral depths of 20 to 100 m (Carannante et al. 1988).

Bioclastic packstones and grainstones at units S2a-S2d are interpreted as submarine dunes deposited in a mid-platform depositional environment. Time-equivalent bioclastic wackestones and packstones, which have a low percentage of open-water biota, most probably represent a more distal basinwards lithofacies. Cross-bedded stratification indicates current action, most probably developed at shallower areas of a mid-platform depositional setting. Based on the abundance and taxa of coralline red algae, the scarcity of corals, and other shallow-water biota (larger benthic foraminifers), it is presumed that the deposition of this lithofacies took place within the photic zone at few tens to several tens of meters. Large benthic foraminifers like *Amphistegina* and *Heterostegina* live (nowadays) in shallow water to near the limit of penetration depth. They can thrive over a wide bathymetric range, but become abundant between 40 and 70 m of water depth (Hottinger 1997). Therefore, it is considered that these submarine dunes were deposited in a mid-platform with mesophotic conditions at water depths shallower than 70 m.

At unit S2e, rhodolith floatstones and rudstones are interpreted as slope deposits. The change of float/rudstones to bindstones into the rhodolithic rudstones to floatstones with cliniform geometry marks the transition. The steepened slope (27°) most probably indicates increased sedimentation and accumulation. The short horizontal distance (Fig. 4.4), where float/rudstones

to bindstones changes into rhodolithic rudstones to floatstones, probably indicates production *in situ*. High-energy conditions are thought to be responsible for the presence of coarse-grained bioclasts among the rhodolites which act as nuclei.

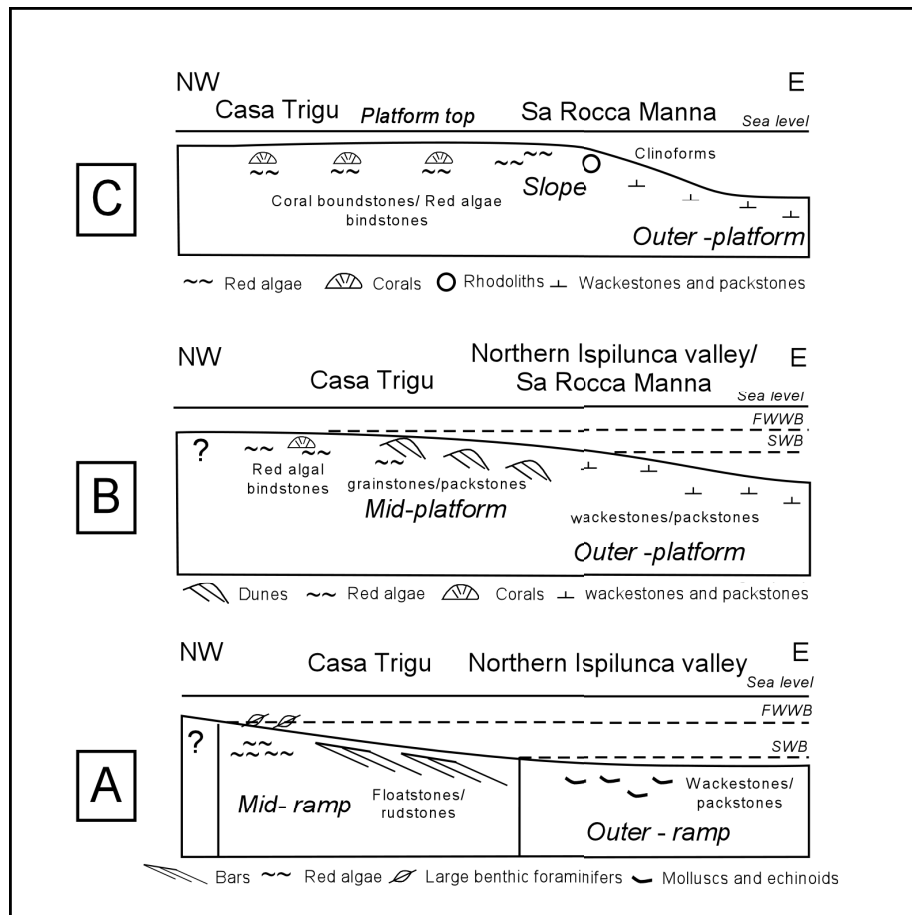


Figure. 4.10. Schematic 2D paleoenvironmental reconstruction. Three orientations are provided (A, B and C), where different distributions of facies and lithology are exposed. This sketch is based on the outcropping facies at the Casa Trigu, Northern Ispilunca valley, and Sa Rocca Manna transects. Figure 10-A is based on sequence 1. Figure 10-B is based on sequence 2 and units S2a to S2d. Figure 10-C is based on sequence 2, units S2d?-S2e.

Red algae can grow from shallow water to the deepest photic environments in temperate regions (Pérès and Picard 1964; Boscence 1985; Bourrouilh-Le January and Hottinger 1988). For depositional settings where rhodolites are the important components, 20 to 160 m of depositional depth is considered depending on water turbidity (Boscence 1985; Fornos and Ahr 1997). However, the lack and high diversity of other photo-dependant organisms (e.g., large benthic foraminifers) and the dominance of a benthic photo-independent association indicate a deposition in the deepest part of the photic zone. If 70 m is the deepest bathymetric range for larger benthic foraminifers to live, and < 160 is the lower limit of the photic zone where red algae grow, then slope deposits might have occurred between +/- 70m to < 160 m. Further analyses, such as a taxonomic identification of the coralline red algae, are necessary to close the gap of the bathymetry of the lower photic zone (e.g., deposition < 70 m).

Outer platform deposits are characterized by packstones and wackestones. They occur below the storm wave-base, where no winnowing of the micrite occurred, and where some bioturbation was preserved. This depositional setting is characterized by low-energy imported and exported neritic carbonate grains mixed with open-water carbonate sedimentation. Judging from the depositional topography exposed in the outcrops (section thickness < 50-60 m), this lithofacies (excluding compactional adjustments) was deposited at < 100 m. Based on the

abundance and type of biotic association, the outer platform can be divided into three parts: a proximal, characterized by mollusc-echinoid-benthonic and planktonic foraminifera packstones and wackestones; an intermediate with echinoid-planktonic foraminifera (showing bioturbation) packstones and wackestones; and a distal represented by marls.

#### 4.6.2 Significance of the Biogenic Association

The terms “photozoan association” and “heterozoan association” (James 1997) have been widely used to classify benthic carbonate particles in terms of their light dependency and trophic requirements. The introduction of this terminology has suppressed previous classifications such as *Chlorozoan*, *Chloralgal* and *Foramol* associations (Lees and Buller 1972, Less 1975, Carannante et al. 1988, Simone and Carannante 1988).

A domain in between photozoan and heterozoan has been identified by several authors (e.g. Halfar et al. 2004); in this domain, environmental controlling factors like temperature and/or nutrients (among others) play an important role. In shallow-water carbonate settings, heterozoan and photozoan biota do not occur abruptly, but rather gradationally, and usually occur as a transition. For example, Carannante et al. (1988) compared regions in the Mediterranean (Italy and Spain) and the Brazilian shelf, recognizing a transitional zonation in terms of biotic association. Lukasik et al. (2000) and Collins et al. (1997) documented carbonates with intermediate or transitional carbonate associations. Halfar et al. (2004), based on field data combined with data compilation, pointed out the occurrence of a heterozoan-photozoan transition, which can be characterized by sediments containing photozoan components between ~ 1 and ~ 20 %. They suggested that the presence of such assemblages could reflect warmer water conditions and higher nutrient contents, rather than cool-water or low-nutrient conditions (Halfar et al. 2004).

The biogenic associations found at the “Sedini Limestone Unit” suggest the following:

1) The different lithofacies identified consist of heterozoan associations (James 1997) but with an important (and variable) contribution of photozoan components (e.g., corals and large benthic foraminifers). A gradual and temporal change from a heterozoan-richer (sequence 1) into a photozoan-richer (sequence 2) depositional setting is documented. However, it should be noted that in sequence 2 (S2e), a lateral change, along with the bathymetric profile from a shallower water photozoan-dominated setting (corals) into deeper water heterozoan-dominated setting, occurs (rhodolith clinofolds).

2) Large foraminifera of the genera *Heterostegina* and *Amphistegina* suggest deposition under warm-temperate conditions. They are principally restricted to oligotrophic, shallow-water photic zones (< 70 m depth) in the subtropics and tropics (Hottinger 1997, Langer and Hottinger 2000, Gourley and Gallagher 2004). Large foraminifera, especially *Amphistegina*, are known (Betzler et al. 1997) to have a relatively low temperature tolerance limit of around 20°; this suggests that warm-temperate conditions (~ 10 to 22°C) prevailed during the deposition of these rocks.

3) The affiliation of *Lithophyllum* to the family of Lithophylloidae underlines the temperate character at the time of deposition (Braga and Aguirre 2001).

4) In both sequences, the existence of corals (reworked or *in situ*) supports the warmer character at the time of deposition. Limestones containing corals or other photozoan assemblages (tropical-type) are poorly documented in Lower-Middle Miocene deposits of the central Mediterranean areas (Mutti et al. 1999). Moreover, the impact of environmental conditions (e.g., nutrient excess) on the distribution and appearance of corals in subtropical to temperate regions has been a matter of discussion in the last decade (Mutti et al. 1999, Brandano and Corda 2002). However, Mediterranean coral associations during Miocene times indicate minimum sea surface water temperatures of ~18 to 21°C (Brachert et al. 1996; Betzler et al. 1998), which is consistent with the subtropical warm-temperate character at the time of deposition. To determine the causes and controls of coral development in our study area, a taxonomic, morphologic, and distribution study of the coral assemblages is needed. Nevertheless, these studies are beyond the scope of this contribution.

#### 4.6.3 Early Diagenesis

**Micritic Envelopes.** Micritization by endolithic algae, fungi and/or bacteria is considered a diagenetic process affecting grains at the seafloor interface. The continuity of the process over time leads to the formation of micritic envelopes around bioclasts (Bathurst 1975).

In tropical regions, micritic envelopes can occur as thick rims in shallow-water facies and thin rims in deeper-water facies. Within the photic zone, endolithic algae affect grains, especially at depths less than 50 m. Below the photic zone, grains are bored by fungi producing smaller borings and are usually indistinguishable under normal petrography (1-2 m $\mu$  diameter). In non-tropical regions, as in the warm-temperate province, micritic rims occur in shallow-water carbonate settings; however, they are of minor importance and the data available are not abundant enough to estimate temperature associations (Betzler et al. 1997).

In our case, thin and scarce micritic envelopes occur in shallower water facies in sequence 1 compared to the thicker ones in sequence 2. The gradual change of a warm-temperate to a warmer condition at the time of deposition of these limestones could have influenced the degree of micritization. However, further considerations are necessary to understand this occurrence.

**Micritic Cements.** Petrographically, micritic cements resemble marine calcite cements precipitated at the seafloor (James and Choquette 1990). Mineralogically, micritic cements are usually associated with original high-Mg calcite (Macintyre 1985, James and Choquette 1990a).

Micritic cementation is widely recognized in the shallow- and deep-water facies of tropical marine carbonate settings (Bathurst 1975, Harris et al. 1985, James and Choquette 1990a, Tucker and Wright 1990). In non-tropical settings, seafloor cementation by micrite is usually related to condensed intervals (Hood and Nelson, 1996; James et al. 1999, Nelson and James 2000, Mutti and Bernoulli 2003) or coralline red algal facies (Carannante and Simone, 1996), and the diversity of microfabrics has been reported (Kyser et al. 1998, Pedley and Grasso 2006). Its origin is widely discussed and usually attributed to bacterial processes (Reid 1983; Chafetz 1986, Reid 1987) and the decomposition of organic matter (Mutti and Bernoulli 2003).

In our case, micritic cements are localized in both sequences at red-algal rich lithofacies. The lack of paragenetic evidence with other calcitic cements reduces the interpretation of its origin. However, an explanation as to why they are exclusively confined to this lithofacies is not currently available.

**Fibrous and Syntaxial-Rich Cements.** Their petrographic characteristics are compatible with those of marine calcite cements precipitated at or just below the sea floor (Tucker and Wright 1990). Usually, their original mineralogy is high-Mg calcite, which is common for this cement type (James and Choquette 1990a). Petrographic data suggest that fibrous and syntaxial inclusion-rich cements precipitated early (syn-depositional), most probably from marine-derived waters.

Similar cements have been described in heterozoan settings. For example, in cool-water carbonates from New Zealand and South Australia, fibrous cements are localized at specific facies (e.g., cross-bedded sand bodies) or specific stratigraphic positions (e.g., unconformities). Their amounts have been related to high initial permeabilities in concurrence with high-energy conditions (Wilson and Evans 2002) and prolonged exposure time at the sediment-water interface (Ehrenberg 2004a 2004b). In Oligo-Miocene heterozoan carbonates from the Central Mediterranean (Knoerich and Mutti 2006), echinoderms show multiple growth stages of calcite syntaxial cements, in which the first and early one is interpreted as early marine in origin.

#### *4.6.4 Early Diagenesis and Facies Stabilization*

The differential distribution of early diagenetic features could have contributed to sustaining differential depositional slopes and facies types. It is noted that early marine diagenesis (micritic envelopes, micritic and fibrous cements) is related to specific facies (shallower water). Furthermore, it occurs in different proportions and distributions (Figs. 4.5, 4.6, and 4.7). Thus, important observations with respect to early diagenesis and facies stabilization are:

- (1) The amount of marine cements and their distribution within shallower water facies contrasts from sequence to sequence. Shallower water facies showing early lithification by marine cements coincide with the turnover of geometry and biotic change. Therefore, the gradual and temporal change of a heterozoan-dominated setting into a more photozoan-dominated setting goes along with the change of the early diagenetic pattern of cementation.
- (2) Early lithification by marine cements at shallower water facies was major during the latest episodes of platform growth (e.g. S2d, Fig. 4.7). The increase in volume of marine cements coincides with the warmer character at the time of deposition.
- (3) Marine cementation at shallower water facies (mid-ramp) from the earlier episode of ramp growth is localized and usually restricted at some strata (Sequence 1, Fig. 4.5). Therefore, likewise heterozoan carbonates, marine cementation at the ramp-phase is localized and does not contribute extensively to the stabilization of the sediments.

#### 4.6.5 Implications of this study

Usually, heterozoan carbonates are dominated by Mg-calcite mineralogy, unlike their warm-water, photozoan carbonate counterparts, which are richer in high-Mg calcite and aragonite. This difference is important because it means that heterozoan carbonates have low diagenetic potential (i.e., they are not subject to early lithification by marine cementation and dissolution-precipitation processes and, as a result, are more likely to display the effects of extensive mechanical compaction). This conjecture appears to be true for most of heterozoan-dominated Miocene settings described until now (e.g., Nelson 1988, James and Bone 1989), although that early cementation (marine) may be important (but localized) in shallow-water facies (Knoerich and Mutti 2006).

This study, however, indicates that a gradual and temporal change in the biotic association from a heterozoan-dominated into a photozoan-dominated carbonate setting goes along with the gradual increment of early marine cementation and with the change of the depositional profile. Therefore, this work shows an example where early lithification can occur and that it is not an uncommon feature in carbonate settings outside the tropical latitudinal region.

#### 4.7 Conclusions

- (1) Based on extensive field work and laboratory analysis from the "Sedini Limestone Unit", it is evident that our case study documents the transition of a heterozoan-dominated into a photozoan-dominated carbonate setting, with a change of the depositional profile from a ramp to a platform.
- (2) Looking at the significance of the biotic association, it is considered that the deposition initially occurred under warm-temperate conditions and evolved over time into more tropical conditions. This is considered as the major environmental control over the deposition of these sediments.
- (3) It is recognized that early diagenesis is differential according to depth (vertical) and depositional profile (sequences). When shallower water facies are dominantly composed with a heterozoan association and deposited during warm-temperate conditions, early diagenetic features generated in the marine diagenetic environment is represented by scarce marine cementations and thin or absent micritic envelopes. On the contrary, when shallower water facies turn into a more photozoan association and are deposited under more tropical conditions, early diagenetic features are characterized by major volumes of marine cements and thicker micritic envelopes. This is striking when expecting only one pattern of diagenesis for these types of carbonate depositional settings.
- (4) It is suggested that, along with the change of the biotic association, and the early and marine diagenesis of these rocks (syn- and early depositional cements), early lithification contributes gradually to the early stabilization of the facies, as well as for the steepening of the platform relief.

**- CHAPTER 5 -**  
**RELATIONSHIPS OF EARLY DIAGENESIS, FACIES AND STRATIGRAPHY**  
**OF A WARM-TEMPERATE TO TROPICAL MIOCENE CARBONATE SETTING**  
**(NORTHERN SARDINIA, ITALY)**

This chapter shows the diagenetic history of the Sedini Limestone Unit at the Perfugas basin. The data for analysis were obtained by optical petrography (transmitted light, cathodoluminescence), geochemical analysis (major and trace elements, oxygen- and carbon-stable isotopes), facies and stratigraphy. This chapter is structured as a manuscript for consideration as a publication for the Journal of Sedimentary Research (JSR).

### **5.1 Abstract**

The major source for calcite cementation in heterozoan carbonate settings is usually assumed to be provided by pressure-solution of calcitic grains in the burial diagenetic environment. The reason for this is the low share that aragonite grains have during their early dissolution for subsequent early lithification of these rocks. This chapter presents a study on the diagenetic evolution of an Early to Middle Miocene shallow-water heterozoan carbonate setting with a variable amount of photozoan (aragonite) components that indicate that early calcite cementation can occur and, in fact, it is widely distributed. The combined stratigraphic setting, petrographic analysis (optical and cathodoluminescence), and geochemical (stable isotope and trace element) approaches, allowed us to distinguish the different early diagenetic transformations. The occurrence and comparison of the different cement phases among facies, together with their stratigraphic occurrence, enabled us to determine the timing of early lithification and origin of the source for calcite cementation.

The rocks involved in this study correspond to a ramp dominated by heterozoan, with lesser photozoan components, which later evolved into a platform-like depositional setting, enriched in photozoan components. Different cement phases can be distinguished and related to a primary mineralogy: syn- and early post-depositional high-Mg calcite cements (micrite, fibrous, syntaxial inclusion-rich), early post-depositional low-Mg calcite cements (bladed), and late post-depositional low-Mg calcite cements (syntaxial inclusion-poor, blocky). Comparing early vs. late generation of cements with their stratigraphic location, reveals that early post-depositional calcite cements are more related to aragonite-richer facies, and are found at a specific stratigraphic location; in contrast, late post-depositional low-Mg calcite cements are widely distributed and can occur mostly everywhere. Geochemical analyses indicate that calcite cements precipitated from marine-derived waters. The merging of these data allows us to determine that the main diagenetic realms for cementation are the marine and the shallow-burial marine diagenetic environments. It is suggested that aragonite is a common source of  $\text{CaCO}_3$  for the low-Mg calcite cements. From analyzing the facies and stratigraphic distribution of fabric-selective dissolution features (bioclasts and syntaxial inclusion-rich cements), it is suggested that early dissolution occurred by the infiltration of fresh-waters close to, and beneath stratigraphic boundaries. We suggest that the amount of early cementation depends greatly on the original skeletal mineralogy (e.g., aragonite) and its distribution. The gradual transition from heterozoan-rich into photozoan-rich depositional settings coincides with increasing marine cementation and bladed calcite cementation, as well as warmer temperatures at the time of deposition. The diagenetic pathway of this carbonate setting indicates that the main carbonate lithification occurred early, rather than only during sediment burial; as observed in similar time-equivalent Miocene carbonate settings.

### **5.2 Introduction**

The diagenetic evolution of heterozoan carbonate settings has been the subject of many studies during the past decades (James and Bone 1989, James and Bone 1992, Hood and Nelson 1996, Nelson and James 2000, Knoerich and Mutti 2003). Most of these studies identified the burial domain as the main environment for cement precipitation (Nicolaidis 1995). Pressure-solution during burial is considered as the major  $\text{CaCO}_3$  source, because heterozoan settings



contain very small amounts of aragonite, which, in tropical, photozoan settings, dissolves early, providing CaCO<sub>3</sub> as a source of cements. However, more recent studies have shown that cementation can occur early, directly from marine pore-waters, while aragonite dissolution can occur during marine and shallow-burial diagenesis (Brachert and Dullo 2000, Nelson and James 2000, Knoerich and Mutti 2006). These findings suggest the existence of a range of options for different diagenetic pathways. It is not clear, however, which factors control these differences in early lithification. Among others, some of the possible factors are the composition of the biotic assemblages (e.g., the amount of depositional aragonite), the depositional facies, and the specific location with respect to sequence/unit boundaries.

Tracing the diagenetic evolution of a heterozoan carbonate setting with a variable amount of aragonite components and different depositional facies, might be a start for a better understanding of its overall diagenetic transformation, and the nature of subsequent cementation. Comparison of early versus late generations of calcite cements could provide clues, by linking the origin of the source of CaCO<sub>3</sub> to the timing of its occurrence.

In this paper, we present the diagenetic evolution of an Early to Middle Miocene shallow-water heterozoan-photozoan carbonate setting. The “Sedini Limestone Unit” (Thomas and Gennesseaux 1986), the focus of this study, is located in northern Sardinia (Central Mediterranean) at the Perfugas basin, Anglona area (Fig. 5-1A). Benisek et al. (in press) (Chapter 3 and 4, this Thesis) have characterized this setting as a ramp dominated by heterozoan, with less photozoan components, which evolved into a platform-like depositional setting, enriched in photozoan components. These strata were never deeply buried and show differential degrees of cementation, dissolution and recrystallization.

From the above reasons, this setting provides a unique opportunity to test the following hypotheses: 1) Does a differential amount of depositional aragonite result in a variable amount of cementation?; and 2) In which diagenetic environments do most of the cementation occur?

To answer these questions, we selected stratigraphic profiles cross-cutting the “Sedini Limestone Unit” from shallow- to deep-water settings (Figs. 5-1B, 5.2 and 5.3) in order to cover the extension of the whole basin (approx. 15 Km<sup>2</sup>), and for comparison between the carbonate strata of the two depositional sequences involved.

### 5.3 Geological setting

During Oligocene to Miocene times, Sardinia was affected by a NW-SE rift system. The Perfugas basin (Anglona area; Sowerbutts 2000) forms part of an intra-arc basin located in northern Sardinia (Fig. 5.1). Paleogeographic reconstructions locate the northernmost area of Sardinia between ~32°-35° of latitude during early Burdigalian times, moving with an anticlockwise-rotation towards ~35-38° of latitude in the early Langhian times (Dercourt et al. 2000).

Previous studies have provided information on the structural and tectonic evolution of the Oligo-Miocene Sardinian rift on a regional scale, and have investigated the biostratigraphic and lithological history of the basin infills (Cherchi and Montadert 1982, Thomas and Gennesseaux 1986, Martini et al. 1992, Assorgia et al. 1997, Sowerbutts and Underhill 1998, Sowerbutts 2000, Monaghan 2001). Arnaud et al. (1992), Sowerbutts (2000), and Monaghan (2001), have specifically focused on the structural configuration, lithological mapping, biostratigraphy, Ar/Ar dating, volcanism and sedimentation in the Perfugas basin. More recently, Benisek et al. (in press) (and this Thesis, Chapters 3-4) have described the facies, sedimentology, sequence stratigraphy, and basin architecture.

In the Perfugas basin, located between the Sedini and Laerru villages (Fig. 5-1B), a Burdigalian volcanic marker ignimbrite ( $\mu$ 2/Tergu platform) (Sowerbutts 2000) denotes the base of the sedimentary succession. It is overlain by volcanoclastics, lacustrine deposits and fluvial conglomerates (Perfugas Formation) (Sowerbutts 2000). A 50-60 m thick marine carbonate and marlstone succession, the “Sedini Limestone Unit” (Thomas and Gennesseaux 1986) (Fig. 5.2), overlies the previous sedimentary rocks. The age of deposition ranges between Burdigalian, as indicated by Ar/Ar dating (Sowerbutts 2000), to lower Langhian, as indicated by nannoplankton biostratigraphic data (Benisek et al. in press) (Fig. 5.2).

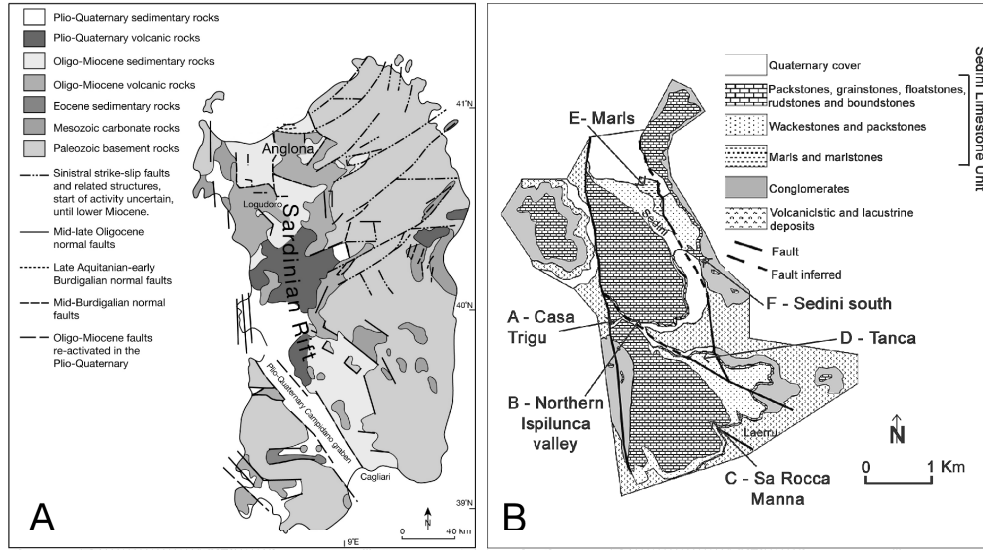


Figure 5.1. (A). Geological map of Sardinia, showing the distribution of the Rift and the location of the study area in the Anglona area (modified from Sowerbutts 2000). (B). Detailed geological map of the study area, located in the Perfugas basin, a half-graben with a Neogene sedimentary infill, located between the Sedini and Laerru villages. The map illustrates the distribution of different lithological units present in the area (modified after Benisek et al., in press., Albertsen 2005, Giennapp 2005, and Nagel 2005), as well as the different carbonate lithologies occurring within the “Sedini Limestone Unit” that have been defined in this study. The location of vertical stratigraphic profiles and transects analyzed in this study are also indicated.

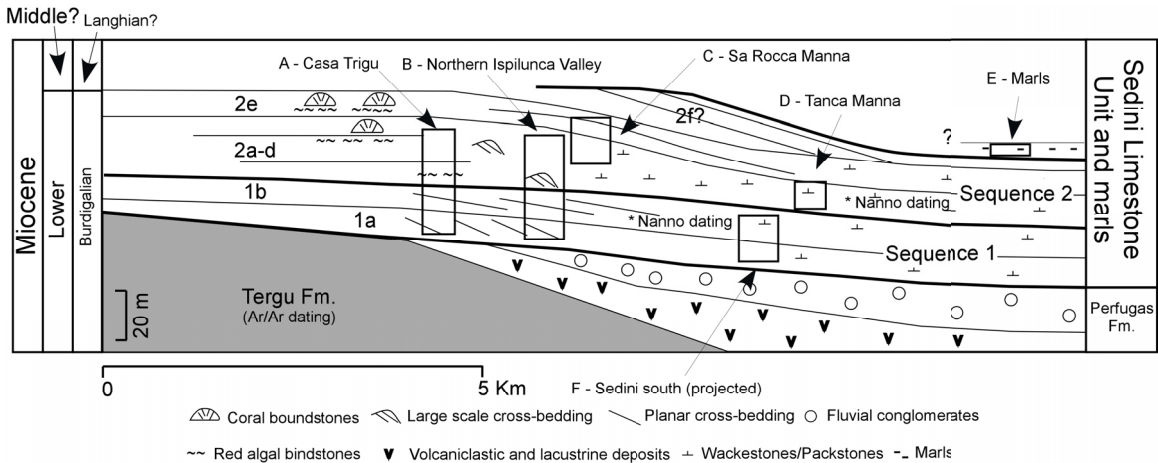


Figure 5.2. Schematic cross-section illustrating the geometric relationships among the stratigraphic units identified within the “Sedini Limestone Unit” (Modified from Benisek et al., in press.). Vertical stratigraphic profiles A, B & C shown here correspond to the Casa Trigu, Northern Ispilunca Valley, and Sa Rocca Manna transects, respectively. D and E correspond to the Tanca Manna and Marls sections. Vertical stratigraphic profile F, is part of the Sedini south transect described in Benisek et al. (in press).

#### 5.4 The Sedini Limestone Unit

The “Sedini Limestone Unit” (Thomas and Gennesseaux 1986) (Figs. 5.2 and 5.3) is the focus of this study, and was described in the field and mapped in six main locations (Transects Casa Trigu, Northern Ispilunca valley, and Sa Rocca Manna, and sections D, E & F) (Figs. 5.2 and 5.3), where stratigraphic sections were logged, sampled and described in detail. Thin sections of the samples were qualitatively analyzed for rock composition and diagenetic features. Field study and petrographic analysis allowed us to recognize different lithofacies. The data are

integrated with the facies and stratigraphic model of Benisek et al. (in press), which divides the carbonate unit into two main depositional sequences: sequence 1 and sequence 2 (Fig. 5.2). By the recognition of several erosional surfaces, Benisek et al. (in press) have recognized two subsequences, or informal units, within sequence 1: S1a and S1b; and five subsequences, or informal units within sequence 2: S2a to S2e. A unit, s2f, was identified but not studied in his thesis, because of lack of exposure in the field. A unit composed only by marlstones (S2?), has also been interpreted by Benisek et al. (in press), as the youngest sedimentary unit. Furthermore, a total of thirteen carbonate lithofacies have been distinguished: four in sequence 1 and nine in sequence 2. A cross-section correlation at the scale of the basin is presented in Figure 5.3 to illustrate the spatial relationships among lithofacies within both sequences and units. The section below summarizes lithologies, rock composition and paleoenvironments of the depositional sequences, with the purpose of providing the background for the diagenetic observations.

#### 5.4.1 Lithologies and Rock Composition

**Sequence 1.** This sequence is characterized by a ramp-like geometry (Benisek et al. in press), and is dominated by heterozoan, with subordinate photozoan components. The biogenic components include coralline red algae, bryozoans, echinoids, molluscs (bivalves) and barnacles, with larger benthic foraminifers and reworked corals as minor components. The occurrence of *Amphistegina* and *Heterostegina*, typical for warm-temperate conditions (Betzler et al. 1997), confirms the paleogeographic reconstructions that locate the area in the subtropical to temperate belt.

In this sequence, four lithofacies were identified (according to Benisek et al. in press), and their distribution within units S1a and S1b is as follows. The lowermost unit (S1a) consists of massive and cross-bedded floatstones and rudstones lithofacies (Fig. 5.3). Predominantly, they are composed of coralline red algae, bivalves, bryozoans, echinoids and large benthic foraminifers with minor barnacles. Sediment particles are reworked. Planar cross-bedded stratification indicates current action. Towards the east, at the top of unit S1a (base of S1b), rudstones show trough cross-bedded stratification (Northern Ispilunca valley), which indicates wave action. Upsection, a floatstone lithofacies is found (S1b). The floatstone lithofacies is characterized by a high amount of early cements. At Casa Trigu, encrusting coralline red algae, bryozoans, large benthic foraminifers and some scarce planktonic foraminifers exist. At the Northern Ispilunca valley, the floatstone is characterized by rhodolites, coralline red algae and barnacles. Upsection, unit S2b consists of cross-bedded floatstones and rudstones. Sediments show similar reworking and composition as those previously described in unit S2a. To the SSE-E, unit S1b grades into packstones and wackestones lithofacies (Northern Ispilunca and Sedin south), predominantly consisting of echinoid and bivalve fragments together with coralline red algae, barnacles and bryozoans with minor serpulids.

**Sequence 2.** This sequence records a turnover of a ramp into a platform-like geometry (Benisek et al. in press). In general, this sequence is characterized by heterozoan, with subordinate photozoan components; however, it progressively turns into a photozoan-dominated carbonate depositional setting. The biogenic components include in-situ corals, rhodolites, small and large benthic foraminifers (*Amphistegina* and *Heterostegina*) and molluscs. Additionally, coralline red algae, bryozoans, barnacles, and serpulids can also occur. The occurrence at the top of the sequence of well developed coral frameworks with different species, indicates that deposition occurred into a warmer-water (tropical) environment.

In this sequence, nine lithofacies were identified (Fig. 5.3) (according to Benisek et al. in press). A sixth unit (S2?, Fig. 5.2), characterized by deep-water marls, was only considered for the isotope correlation, and is briefly mentioned here (section E, Fig. 5.3). The distribution of the lithofacies within units is as follows.

Units S2a-2b consist of red algal bindstones, rudstones to bindstones, well to poor lithified floatstones to rudstones, bioclastic packstones and grainstones, bioclastic wackestones and packstones, and planar packstones and wackestones. At Casa Trigu, at the base of the section, floatstones and rudstones show different degrees of early cementation (see below for

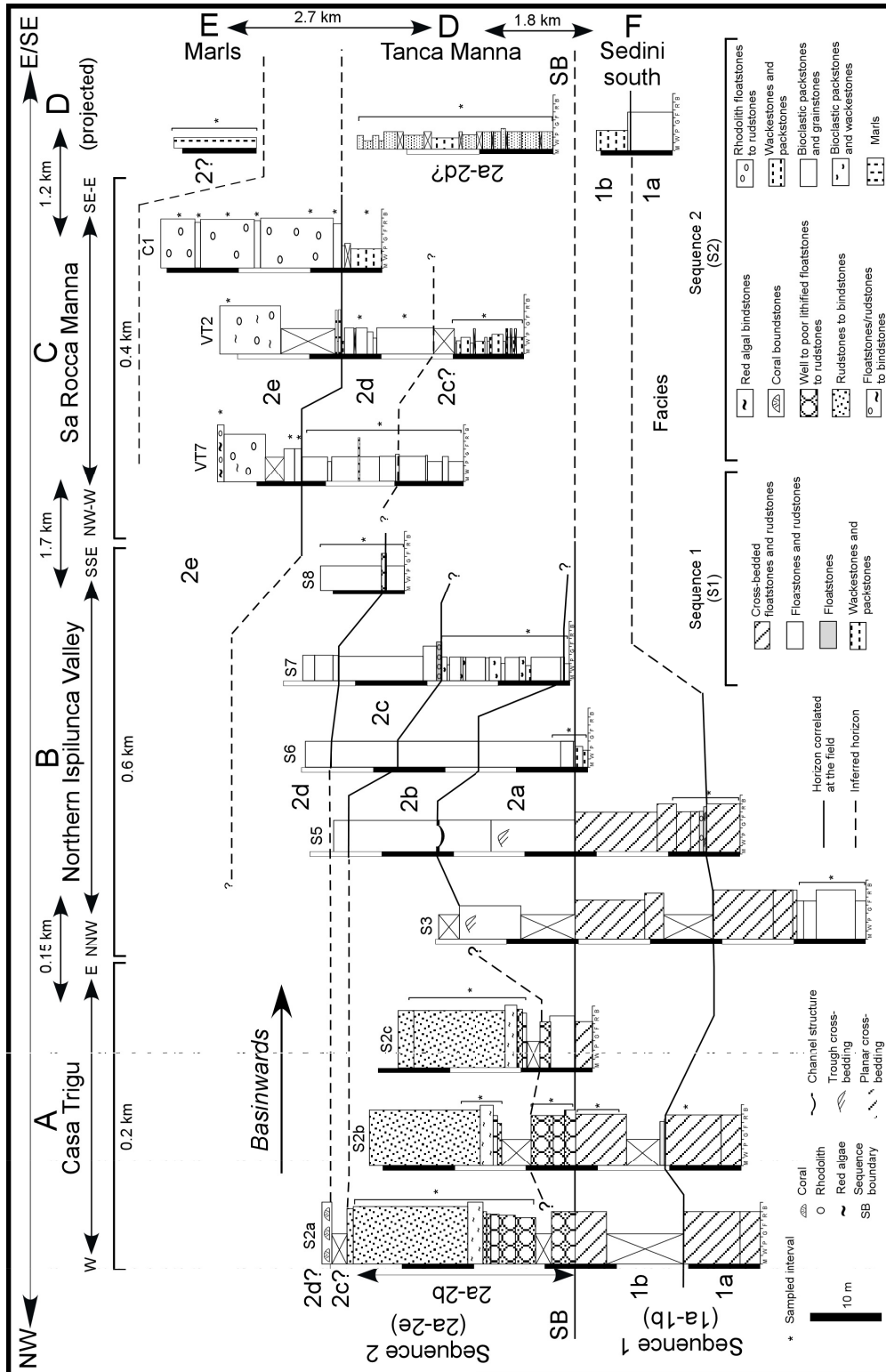


Figure 5.3. Correlation of the stratigraphic sections measured in the different areas showing the distribution of different lithofacies and other sedimentary attributes. The correlation was established by means of physical tracing of the beds in the field, as well as with photopanoramas.

further explanation)(Fig. 5.3). They mainly consist of red algae, large benthic foraminifers, echinoids, bryozoans, molluscs and minor rhodolites. They are followed by red algal bindstones lithofacies. At the top, rudstones to bindstones, rich in coralline red algae, molluscs, echinoids and coral fragments are found. To the E and SSE, these rocks grade into bioclastic grainstones, packstones and wackestones lithofacies. These rocks are rich in small benthic foraminifers, molluscs, coralline red algae, and echinoids. Large benthic foraminifers (*Heterostegina* and *Amphistegina*) can occur. At the Northern Ispilunca valley (Fig. 5.3), bioclastic grainstones to packstones lithofacies with scours (channels) and small-scale trough cross-bedded stratification have been observed (sections S3 to S5). To the E and SSE (section S7), these rocks grade into finer-grained bioclastic packstones and wackestones lithofacies. Planktonic foraminifera start to appear. They show clear storm action.

At the Northern Ispilunca valley and Sa Rocca Manna Transect, units S2c-2d consist mainly of well sorted bioclastic wackestones, packstones and grainstones, and planar packstones and wackestones lithofacies. Locally, rhodolith floatstones are observed. At the top of the Casa Trigu transect (section S2a), thin (< 3 m) coral framestones within S2d? are observed. Bioclastic packstones and grainstones are rich in echinoid fragments, molluscs, and coralline red algae. Coral fragments are minor. Packstones are rich in echinoid fragments and red algal fragments; whereas grainstones intervals contain biomolds of molluscs preserved by thick micrite envelopes. To the E (Sa Rocca Manna, and Tanca Manna?), this interval grades into finer-grained planar wackestones and packstones lithofacies. Some bioturbation is found. Lime mud and planktonic foraminifera are the main rock constituents.

Unit S2e consists of the following lithofacies: floatstones/rudstones to bindstones, and rudstones and floatstones. At the Sa Rocca Manna transect, red algal bindstones to rhodolith floatstones/rudstones are found NW of the outcrop. Predominantly, the biotic constituents are coralline red algae together with bryozoans, encrusting foraminifers and molluscs (bivalves). Highly reworked large benthic foraminifers, echinoids, red algae and bryozoans can be observed. Downdip (SE direction), rocks grade into rhodolith floatstones and rudstones. They show clinoformal geometries. The rhodolites have a sphaeroidal to ellipsoidal shape, with a bioclastic nucleus, and their size ranges from a few cm to 10 cm across. Rhodolith layers are characterized by coralline red algae, encrusting foraminifers, and bryozoans.

#### 5.4.2 Paleoenvironments

Sequence 1 records a ramp and facies distribution in combination with the biotic association which allows for the identification of (shallow) mid- and outer- (proximal) ramp deposits.

According to Benisek et al. (in press), sequence 2 records the turnover of geometry into a "platform-like" setting. The change in geometry is gradual during earlier stages (units S2a-S2d), and becomes clearly marked at the latest stages of platform growth (units S2d to S2e). They have suggested that paleoenvironments within sequence 2 are comparable with patterns of deposition within a platform (e.g., Burchett and Wright 1998). Therefore, in units S2a to S2d, facies distribution, in combination with the biotic association, allowed for the identification of (inner?) mid- and outer-platform deposits; meanwhile, in unit S2e, a platform top-margin-slope is identified.

**Sequence 1.** Cross-bedded floatstone to rudstone deposits in units S1a and S1b show characteristics consistent with longshore bars (submarine). They occurred at, or below the fair-weather wave-base in the mid-ramp. Wave action at the top of the bars, and subsequent deposition of floatstones (S1b at Casa Trigu and Northern Ispilunca valley) have been considered as a rapid wave-base lowering, resulting in a deepening of the system; indicated by red algae floatstones (Benisek et al. in press). The bar system is restored after, as indicated by the subsequent cross-bedded floatstones to rudstones (S1b). Packstones and wackestones are considered as sediments deposited in deeper waters. They occurred at the outer (proximal) ramp below the storm wave-base, where no winnowing of the micrite occurred, and where bioturbation was preserved.

**Sequence 2.** In Units S2a-2b, red algal bindstones are interpreted to have formed in an (inner ?) to mid-platform setting. Benisek et al. (in press) have suggested water depths between 20 and 40 m by the recognition of *Lithophyllum* sp., *Mesophyllum* sp., and *Neogoniolithon* sp. Floatstones to rudstones containing reworked large benthic foraminifers (*Amphistegina* and *Heterostegina*), red algae, benthic foraminifers and molluscs, together with encrusting biota, such as coralline red algae and bryozoans, indicate deposition under moderate-energy. The presence of light-dependant large benthic foraminifers locate the deposition of these sediments within the photic zone, most probably at < 70 m of water-depth (Brandano et al. 2001). The lateral change to bioclastic wackestones, packstones and grainstones indicates a shift in the environmental conditions. The recognition of reworked bioclasts, signs of current action (cross-bedding), and the decrease of large benthic foraminifers indicate deepening of the depositional system, most probably below the fair-weather wave-base at the mid-platform. Paleoenvironmentally, these bioclastic rocks are considered as submarine dune deposits developed at a mid-platform depositional setting. Benisek et al. (in press) have proposed that the red algal bindstones locally stabilize these sediments. The correlation downdip with sediments showing scour structures (channels) were most probably induced by storms. The appearance of finer-grained wackestones and packstones suggests deposition below the storm wave-base, probably as outer (proximal) platform deposits.

In Units S2c?-2d, bioclastic wackestones, packstones and grainstones are considered as submarine dunes. Paleoenvironmental conditions are similar to those interpreted in units S2a-2b. Packstones and wackestones indicate a decrease in hydrodynamic conditions, suggesting their deposition under quieter environmental conditions. Their deposition is similar to those described in S2a-2b as outer (proximal) platform deposits.

Occurrence of coral boundstones at S2d is considered as a change of the carbonate factory (Benisek et al. in press). For this reason, the “platform-like” geometry is clearly marked at this latest stage of platform growth. However, the turnover in geometry could also be enhanced by the gradual increase in slope by the accentuation of the depositional dip of prograding submarine dunes, which acts as a quasi-stationary high-energy barrier, or incipient platform margin (*sensu* Schlager 2005). In unit S2e, rhodolith floatstones/rudstones to red algal bindstones are considered as the platform top (edge), and rhodolith floatstones to rudstones with clinoformal geometry are considered as slope deposits.

The marls are interpreted as deep-water sediments. Benisek et al. (in press) have considered these rocks as the youngest deposits within the Sedin Limestone Unit. We suggest deposition in an outer-platform (distal) depositional setting.

## 5.5 Analytical Methods

Sampling of the stratigraphic section for petrographic and geochemical analyses was done at a vertical spacing ranging from 0.3 to 2.0 m, depending on the accessibility to the outcrop. Standard petrographic analyses were carried out with a transmitted light petrographic microscope in 40 thin sections from sequence 1, and in 140 thin sections from sequence 2. All were previously stained with alizarin red S and potassium ferricyanide (Dickson 1965) in order to allow differentiation of calcite and dolomite. Visual semi-quantitative estimations of cement percentages were obtained by typical visual comparison charts for sedimentary rocks (Flügel 2004).

Selected samples were examined under cathodoluminescence (CL) at the Institute of Geosciences, University of Potsdam. Operating conditions were set at an acceleration voltage for the electron beam of 18-20 Ke V, and the beam current was set to 280-310 mA.

Five thin sections from sequence 1 and eight thin sections from sequence 2 were highly polished and coated with carbon for electron microprobe analysis, performed using a JEOL Hyperprobe JXA-8500F at the GeoforschungZentrum of Potsdam (GFZ). Conditions were 15 kV accelerating potential; 10 nA beam current; 20 seconds counting time on peaks; and a 10 micron beam raster. Detection limits were 230 ppm Fe, 220 ppm Mn, 90 ppm Mg, 120 ppm Ca and 145 ppm Sr.

Bulk-rock oxygen and carbon isotope analyses were performed on powdered material obtained by normal drilling procedures. Oxygen and carbon isotope analyses of fabric-specific

calcite cement were performed using powdered material obtained by drilling approx. 300  $\mu\text{m}$  thick slides under the binocular microscope. Analyses were performed at the Geoforschung Zentrum of Potsdam (GFZ), with a DELTA <sup>plus</sup> XL Finnigan MAT 253. Data are reported in per mil versus Vienna Pee Dee Belemnite ( $^0/_{00}$  PDB).

Bulk rock samples were selected in order to perform porosity ( $\phi$ ) and permeability (K mD) analyses. To obtain porosity ( $\phi$ ) values; plugs (2.5 cm with x 2.5 cm height x 2.5 cm diameter) were cut in order to measure density by a helium “Pycnometer” combined with an “Envelope Density Analyzer” for porosity determinations. To obtain permeability values, bulk rock samples were cut in order to obtain a selective smooth and horizontal surface. Nitrogen injection under 18-20 bar of confined pressure was performed, and the data obtained are reported as Klinkenberg-corrected millidarcy values (K mD).

## 5.6 Petrography

Optical and cathodoluminescence petrographical analyses have revealed different generations of cement precipitation, dissolution events and compactional features (Figs. 5.6 and 5.8). These features occur in both sequences, but they are characterized by variations in abundance, spatial distribution and geochemical composition. The diagenetic features are described below in the paragenetic order of occurrence, separately for each sequence, and are summarized in Figure 5.4. A semi-quantitative distribution of the observed cements percentages according to their stratigraphic position is shown in Figure 5.5. In addition, types of dissolution, porosity and permeability values are shown and related to each depositional sequence.

Major and trace element composition (Ca, Mg, Sr, Mn, and Fe) of the different cement types was determined by measurement of single points, as well as transects, in order to document variations within single cement zones. The mean, minimum, maximum, and standard deviation, as well as the number of measurements of the trace elements are displayed in Table 5.1 for sequence 1, and in Table 5.2 for sequence 2, and can be found in the appendix. Profiles of Fe, Mn, and Sr obtained in the different cement types are plotted in Figure 5.7.

### 5.6.1 Syn- and Early Post-depositional Events

**Micritic Envelopes (me).** Micrite envelopes occur as fine to thick rims defining the shape of micritized bioclasts (Fig. 5.8). They occur in both sequences, although with different characteristics. In sequence 1, micritic envelopes are only observed at cross-bedded floatstones to rudstones, where envelopes are thin and almost absent on every grain. In sequence 2, micritic envelopes are found in bioclastic packstones and grainstones, where envelopes are thick and on nearly every grain. Micritic envelopes are also present, however, in deeper-water facies, but the rims are thinner and many grains lack them.

**Micritic Cements (mc).** Micrite cements mostly occur in sequence 2, where they show homogeneous, clotted and micropeloidal fabrics. Micritic cements are pore-fill and localized to specific lithofacies (red algal bindstones and floatstones). Micritic cements (peloidal and clotted) can be observed filling geopetal structures, and together with blocky calcite cements (Fig. 5.6). In sequence 1, micritic cements show homogeneous and micropeloidal fabrics and occur only above the boundary of S1a with S1b (Casa Trigu). All of the micritic cements at both sequences have been recrystallized; based on the bright-patchy red appearance under cathodoluminescence (see discussion below on Recrystallization), which is clearly distinguished from other cements and bioclasts (Fig. 5.6). Trace element analyses reveal the following mean values: (Fe=328, Mn=102, Mg=3571, Sr=29) in sequence 1, and the following for sequence 2 (Fe=737, Mn=83, Mg=3024, Sr=459).

**Fibrous Cements (fc).** This cement is characterized by inclusion-rich crystals generally less than 50  $\mu\text{m}$  thick, with weak extinction and poorly defined crystal boundaries (Fig. 5.6). This cement is found as an isopachous calcite cement. Crystals are equidimensional and they grow normal to the substrate. Under cathodoluminescence, crystals show a dull patchy orange/red luminescence, which indicates recrystallization (see discussion below on Recrystallization). This

cement occurs as thin isopachous cement at sequence 1 and as thick and continuous in sequence 2. In sequence 1, only fibrous cements are found and they are found rarely in floatstones and rudstones. In sequence 2, fibrous cements are abundant and found in bioclastic packstones and grainstones, and in floatstones and rudstones. Fibrous cements are observed in samples where micritic cement occurs, however, their spatial relationship is not observed. Where syntaxial-inclusion rich overgrowths are also present, they formed during the precipitation of the isopachous fibrous cement. Trace element analyses reveal the following mean values: (Fe=37, Mn=37, Mg=2668, Sr=393) in sequence 1, and the following for sequence 2 (Fe=93, Mn=0, Mg=2554, Sr=478).

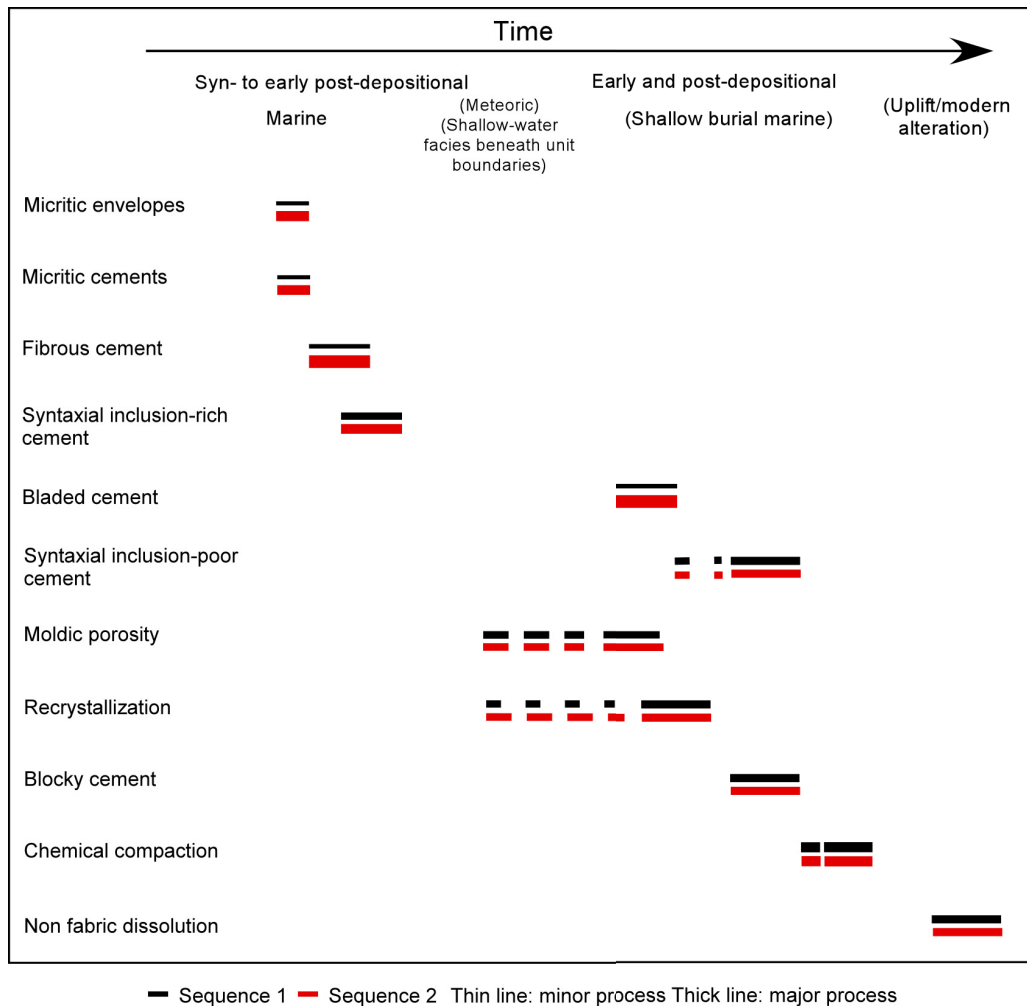


Figure 5.4. Paragenetic sequence.

**Syntaxial Inclusion-Rich Cements (sc1).** Syntaxial cements grow in optical continuity over echinoderms (Fig. 5.6), and the presence or absence of inclusions allows us to recognize two phases, a first, the inclusion-rich phase (sc1), described here, and a later inclusion-poor phase (sc2), described in the post-depositional events. The inclusion-rich syntaxial cement forms rims ranging from 30 to < 100  $\mu\text{m}$  in width. The presence of inclusion allows us to recognize the former presence of crystals perpendicular to the substrate, with prismatic terminations. Cathodoluminescence reveals a patchy pattern (Fig. 5.6), which indicates recrystallization (see discussion below on Recrystallization). The inclusion-rich syntaxial cement phase can be partially or totally dissolved (Fig. 5.8). This cement occurs in both sequences, however, in minor proportions with respect to other types of cements. Trace element analyses reveal the following



mean values for the inclusion-rich-phase in sequence 1 (Fe=259, Mn=31, Mg=975, Sr=200), and the following for sequence 2 (Fe=120, Mn=37, Mg=1699, Sr=309).

**Bladed Cements (blc).** This cement consists of inclusion-poor, bladed crystals of 30-80  $\mu\text{m}$  long. Bladed cements are found overgrowing the crystals of the fibrous cement (Fig. 5.6) and as irregular linings on primary and secondary porosity. Sometimes, the boundary between the fibrous and the bladed cements is difficult to distinguish by optical petrography. Crystals are non-equidimensional. The morphology of individual crystals is bladed; but granular to irregular forms also occur. Under cathodoluminescence, the crystals show well defined luminescence with a change from bright to dull patterns, overgrowing the patchy pattern observed in the fibrous crystals (Fig. 5.6). Bladed cements rarely occlude the porosity. In addition, seldom is there even complete overgrowth of all the isopachous fibrous cement. However, bladed crystals are better developed when primary and secondary porosity (molds, enhanced) are optically better connected (network). Where syntaxial inclusion-poor overgrowths are also present, they are clearly related to echinoderms, and they formed after the precipitation of the bladed cements (Fig. 5.8). This cement occurs at grain-supported lithofacies in both sequences, but with clear dominance in sequence 2 (S2d). Trace element analyses reveal the following mean values: (Fe=155, Mn=19, Mg=1183, Sr=324) in sequence 1, and the following for sequence 2 (Fe=131, Mn=11, Mg=2516, Sr=556).

**Moldic Porosity.** The selective dissolution of specific skeletal grains (aragonite and high-Mg calcite) and cements (syntaxial inclusion-rich), observed in both sequences, have as a result moldic porosity. In sequence 1, molds of aragonitic biota occur in both shallow and deeper water facies. Molds in shallow-water facies remained open, as there is no evidence of post filling cementation, whereas in deeper-water they are filled by blocky calcite. In sequence 1, moldic porosity is affected by mechanical compaction, indicating they remained open throughout the burial history. In sequence 1, there is, locally, the occurrence of pores that are bigger than the normal average interparticle porosity of the facies (arrows in Fig. 5.8). These are typically found in the cross-bedded floatstones and rudstones lithofacies. These "larger" pores could indicate the development of enhanced porosity by selective dissolution of a previous component, likely aragonitic, but not affecting the surrounding framework, composed of calcitic grains (Fig. 5.8). In sequence 2, molds produced from the selective dissolution of aragonitic biota also occur in both shallow and deeper water facies. Bladed and blocky calcite can occur as post-filling calcite cements, but they are not exclusive. In most of the cases, the infilling took place before mechanical compaction (Fig. 5.8). In both sequences, the selective dissolution of high-Mg calcite grains are only observed at shallow-water lithofacies located close to sequence/unit boundaries.

### *5.6.2 Late Post-depositional Events*

**Syntaxial Inclusion-Poor Cements (sc2).** These cements are found in optical continuity with the substrate (echinoderms), or growing around the syntaxial inclusion-rich phase, postdating it (Fig. 5.6). Syntaxial inclusion-poor cements consist of inclusion-poor crystals, with an average length of crystal size of 50 to 200  $\mu\text{m}$ . Under cathodoluminescence, the crystals show a well marked zonation from dark/dull to bright (Fig. 5.6). Where bladed cements are also present, they usually formed before the precipitation of the syntaxial inclusion-poor cement (Fig. 5.8). Syntaxial inclusion-poor cements can fill intergranular pores (Fig. 5.8). This cement can occur almost everywhere (Fig. 5.5). The following are the mean values for the inclusion-poor phase in sequence 1: (Fe=115, Mn=74, Mg=1107, Sr=265), and the following for sequence 2 (Fe=174, Mn=59, Mg=3095, Sr=316).

**Recrystallization.** Under cathodoluminescence, recrystallization of micritic, fibrous and syntaxial inclusion-rich cements are attested by the patchy appearance and lack of clear zonation of the crystals. Skeletal components show similar optical attributes, and ghosts of microstructures are poorly observed. The bladed, syntaxial inclusion-poor, and blocky calcite cements, that precipitated as pore-fill cement, show clear zonings and no evidence of alteration (Fig. 5.6), which

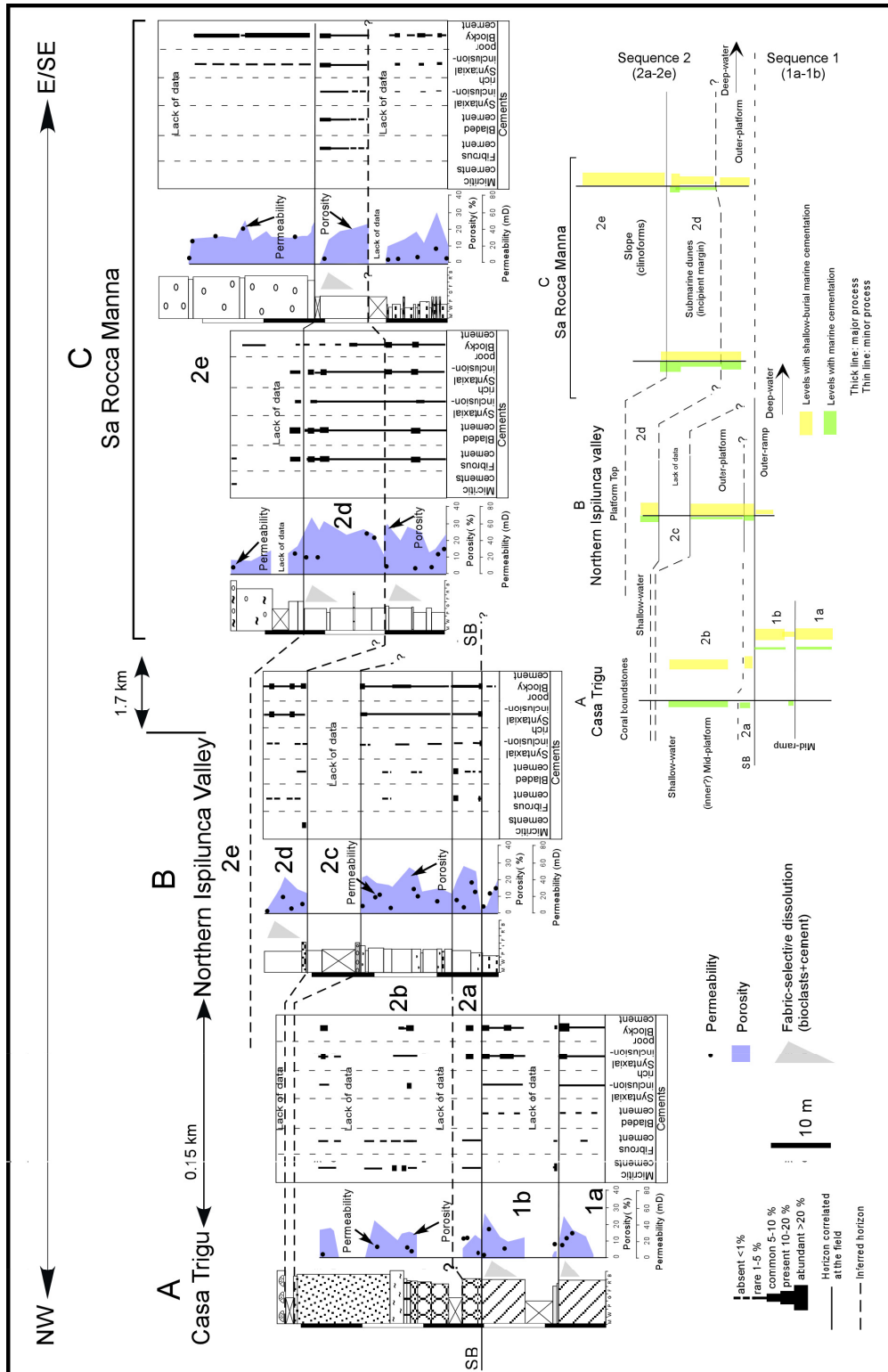


Figure 5.5. Stratigraphic distribution and facies relationship of types of cements, dissolution features, porosity and permeability values. Legend captions are the same as Figure 5.3. Each composite section is enlarged at the appendix.

testifies that recrystallization most probably occurred before, or during the precipitation of those cements.

**Blocky Calcite (bc).** Blocky calcite cement is characterized by clear and inclusion-poor crystals ranging from >50 to 300  $\mu\text{m}$ . Crystals are clear, having equant to anhedral morphologies. It occurs as pore-filling cement in both primary and secondary pores (Fig. 5.6). Blocky calcite cement is coeval with the dissolution of skeletal grains (aragonite) because of its presence in filling moldic porosity (Fig. 5.8). Under cathodoluminescence, crystals show a clear sequence, starting with a first phase characterized by dull to bright orange zonation, followed by a dull zone, and finally by a non-luminescent zone (Fig. 5.6). Not all zones are present in all pores, but their relative order is always the same. This cement is found in almost every facies at both sequences (Fig. 5.5), with the only difference being that the last non-luminescent zone is almost absent in sequence 1. The following are the mean values for the two different phases in sequence 1 (bright orange: Fe=152, Mn=62, Mg=6785, Sr=397; dull: Fe=995, Mn= 170, Mg= 5525 , Sr=743), and the following are for the three phases observed in sequence 2 (bright orange: Fe=421, Mn=99, Mg=4982, Sr=480; dull: Fe=4494, Mg=216; Mg=5184 , Sr= 1185; non-luminescent: Fe=1759, Mn= 102, Mg= 3556, Sr=421).

**Compaction.** Compaction occurs in two different ways: (1) as mechanical compaction, which is found as grain reorganization, minor fractures (in skeletal-rich sediments), and grain deformation (mud-rich sediments); and (2) as chemical compaction, which is found as incipient sutured contacts (Fig. 5.8) ( Nicolaidis and Wallace 1998). Mechanical and chemical compaction is observed in both sequences; however, they differ in intensity. In sequence 1, mechanical compaction is commonly evident by the displacement of moldic porosity and grain reorganization. On the contrary, in sequence 2, mechanical compaction is only evident by grain reorganization, and the intensity was highly reduced by the amount of calcite cements (see below for further explanation). In both sequences, chemical compaction is mild and poorly developed (Fig. 5.8). Obvious stylolites or sutured contacts are absent. Moreover, calcite cementation or dissolution related to chemical compactional features is clearly absent.

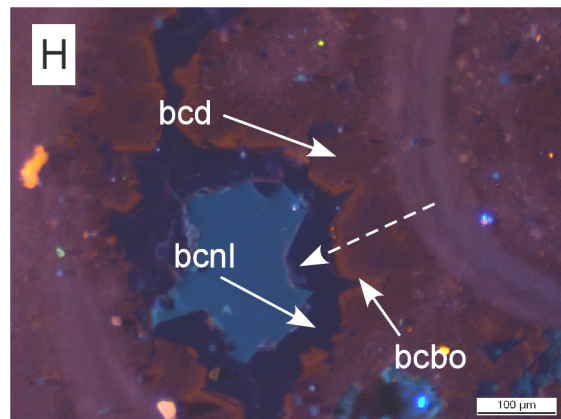
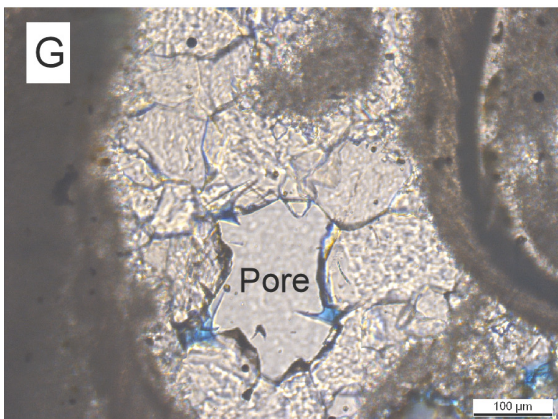
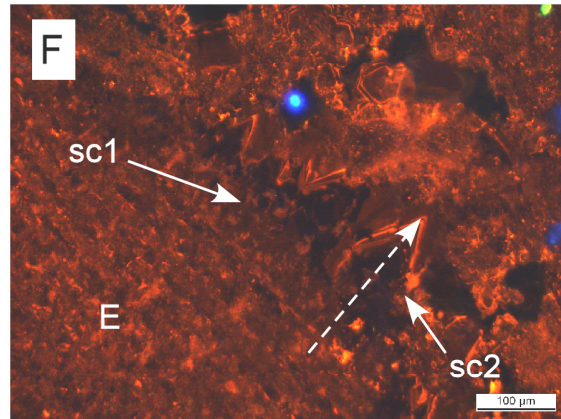
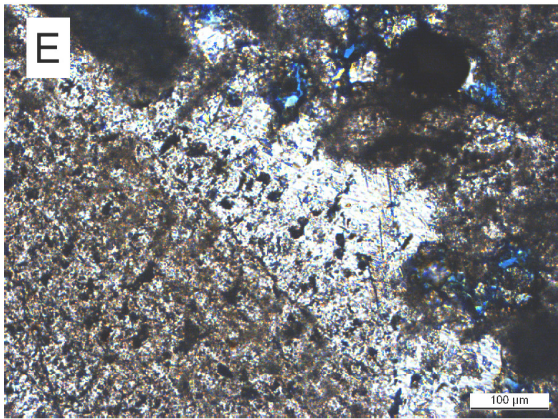
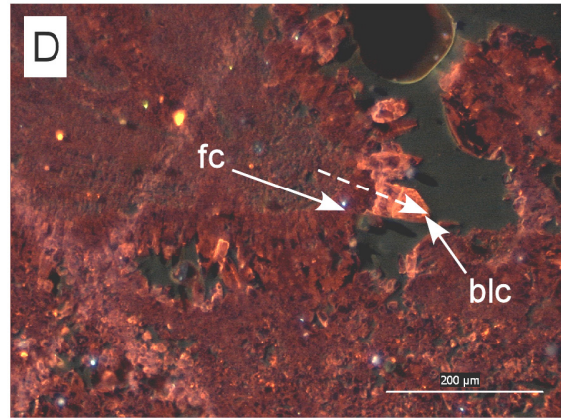
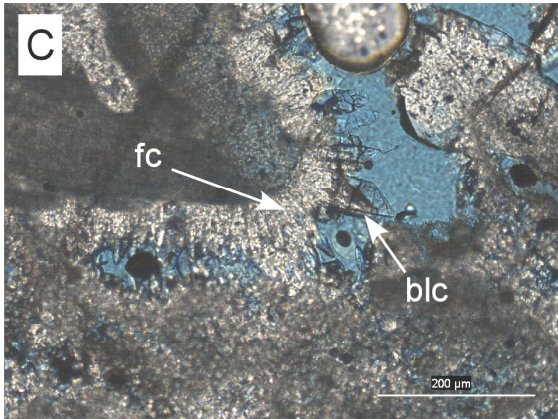
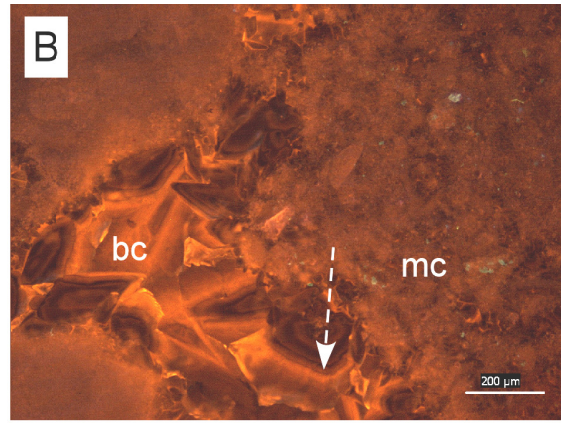
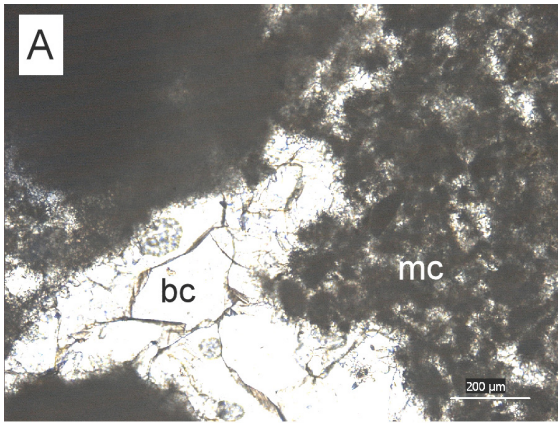
**Non-selective Dissolution.** Locally, non-selective dissolution is observed at sequence 2, related to recent uplift.

## 5.7 Geochemistry

### 5.7.1 Stable Isotopes

Bulk-rock samples have been measured with the purpose of identifying the influence of diagenetic and stratigraphic variability. Figure 5.9 shows bulk-rock oxygen/carbon data plotted against stratigraphic vertical profiles, from: (A) "Casa Trigu Transect" (sections S2b/S2c, and base of S3 and S5, see Fig. 5.3), (B) Northern Ispilunca valley Transect (sections S6 to S8, Fig. 5.3), (C) Sa Rocca Manna Transect (VT7 and VT2/C1, Fig. 5.3), (D) Tanca Manna section (see Fig. 3), (E) Marls (see Figs. 1B and 2), and (F) Sedini south (see Figs. 5.1-B and 5.2). The Northern Ispilunca valley and Sa Rocca Manna are constructed as vertically consecutive segments from the individual profiles. These data provide an overview of the isotopic variability across the different stratigraphic intervals, units and depositional facies described in the area. These data are also displayed in a cross-plot graphic (Fig. 5.10), where they are "keyed" according to the depositional facies, as well as to the unit and depositional sequence they belong to.

In addition to bulk samples, when cement width was large enough, powder samples have been collected from single cement phases as well. Due to the general small dimensions of cement phases, only samples from blocky calcite could be measured. The data from the blocky cements obtained from both depositional sequences are also plotted in Figure 5.10.



**Bulk-rock.**  $\delta^{18}\text{O}$  stable isotopic values range from -5,54 ‰ to -1,13 ‰ in sequence 1, and from -5,80 ‰ to -1,13 ‰ in sequence 2.  $\delta^{13}\text{C}$  stable isotopic values range from -3,40 ‰ to 1,25 ‰ in sequence 1, and from -3,30 ‰ to 2,06 ‰ in sequence 2.

The shallower-water facies (vertical profiles A, B and C) generally show, along the vertical trend, a larger internal variability in amplitudes (up to 4 ‰), whereas the deeper water facies (e.g., profile D) show a narrower range of amplitude variability (1 to 2 ‰). The previous results can also be applied when comparing the shallower-water facies of sequence 1 with sequence 2 showing the latter as having more internal variability. Within the shallower-water facies, it can be observed that within each sequence and units, both  $\delta^{18}\text{O}$  and  $\delta^{13}\text{C}$  values tend to become lighter upsection, and the sequence/unit boundaries mark the transition to renewed heavier values. Within the deeper-water facies, it can be observed that values remain constantly heavier than their age-equivalent shallower-water counterparts, and no strong “off-set” of values upsection is marked.

The cross-plot shows the bulk isotopic composition plotted according to depositional facies (ramp, platform) with the purpose of highlighting facies-specific isotopic variability. Isotope values can be clearly identified and tied to a specific depositional facies. In both sequences, deeper water facies show heavier isotopic values than shallower water facies. A tendency into lighter carbon values is observed in shallower-water samples obtained from strata below, and close to sequence/unit boundaries. Deeper-water facies do not show these tendencies, and usually the values remain in the same isotopic field.

**Blocky Cement.** Stable isotopic values for the blocky cement vary between -6,38 ‰ to -2,86 ‰ for  $\delta^{18}\text{O}$ , and -2,02 ‰ to 0,03 ‰ for  $\delta^{13}\text{C}$ . Values are represented in a cross-plot diagram (Fig. 5.10) showing that in both sequences all the isotope values from blocky cements are clustered in one isotope area. Differences or tendencies among sequences are not observed.

### 5.7.2 Major and Trace Elements

Major and trace elements at the different cement phases have been measured with the purpose of identifying environments of precipitation, alteration, and source(s) of  $\text{CaCO}_3$ . Tables 5.1 and 5.2 show the results from sequence 1 and sequence 2, respectively (appendix). Figure 5.7 shows how the trace elements vary among the different calcite cement phases.

Overall, cements have low Mg concentrations. For syn/early post-depositional cements, micrite and fibrous show relative enrichments compared to syntaxial inclusion-rich and bladed cements. Subsequently, at late/post-depositional cements, syntaxial inclusion-poor and blocky cement Mg values turn enriched, even though their values are low. Sr values show, in general, an enrichment trend, from a minimum of 297-479 ppm in syn/early post-depositional cements to a maximum of 421- 1185 ppm in late/post-depositional cements. Within all cements, Fe and Mn have low concentrations. However, Fe values turn richest in late/post-depositional blocky cements within sequence 2. Mn values are very low, but show their richest values in late/post-depositional syntaxial inclusion-poor cements.

It is important to notice that the Sr and Fe trends are more evident in sequence 2 than in sequence 1.

---

Previous page: Figure 5.6. Diagenetic features. A) Floatstone showing syn-depositional early micritic cement (mc) and late post-depositional blocky cement (bc). B) Same as (A) but in CL. Note the clear crystal zonation of the blocky cement in contrast with the patchy luminescence of the micrite. The straight dashed line indicates the measured trace element transect expressed in Fig. 5.7A. C) Bioclastic packstone-grainstone with fibrous (fc), and bladed (blc) cement. D) Same as (C) but in CL. Clear patchy luminescence of the fibrous cement. Bladed crystals post-date fibrous cementation. The straight dashed line indicates the measured trace element transect expressed in Fig. 5.7B. E) Syntaxial inclusion-rich (sc1) and inclusion-poor (sc2) cement. F) Same as (E) but in CL. Note the bright-orange/dull zoning within the sc2 (arrow). The straight dashed line indicates the measured trace element transect expressed in Fig. 5.7C. G) Bioclastic packstone with blocky cement (bc). H) Same as (G) but in CL. Three zoning phases are shown. Bright-orange (bcbo), dull (bcd), and non-luminescent (bcnl). The straight dashed line indicates the measured trace element transect expressed in Fig. 5.7D

## 5.8 Distribution of calcite cements and dissolution features with respect to facies and stratigraphy

Type, amount and distribution of early cementation and dissolution features can be related to different lithofacies and stratigraphic position. They are shown in Figure 5.5, and are based on semi-quantitative (qualitative) estimations by optical and cathodoluminescence petrography.

Differences in the amount and distribution of calcite cements between sequence 1 and sequence 2 reveal the following important observations: (1) Micritic cements occur in sequence 2 in shallow-water red algal bindstones, whereas in sequence 1 they are only localized to floatstones rich in red algae. Micritic cements are absent in their deeper-water facies counterparts; (2) Fibrous cements are rare and unimportant in sequence 1, they only occur as traces in floatstones above the boundary S1a/S1b, whereas in sequence 2 they are abundant and occur widely in bioclastic wackestones, packstones and grainstones (e.g. S2d); (3) Bladed cements occur in both sequences in grain-supported lithofacies; however, this cement type occurs extensively in sequence 2; (4) Syntaxial inclusion-rich cement in sequence 1 was present throughout all grain-supported lithofacies, but is currently only preserved at the base of Unit S1a. In the other locations, it has been removed by fabric-selective dissolution. In sequence 2, syntaxial inclusion-rich cements are found overall at shallow-water facies, but also at deeper-water facies, where they are found as traces; and (5) Syntaxial inclusion-poor and blocky cements occur, overall, in all facies and both sequences; therefore, no major differences are recorded concerning these two types of cements.

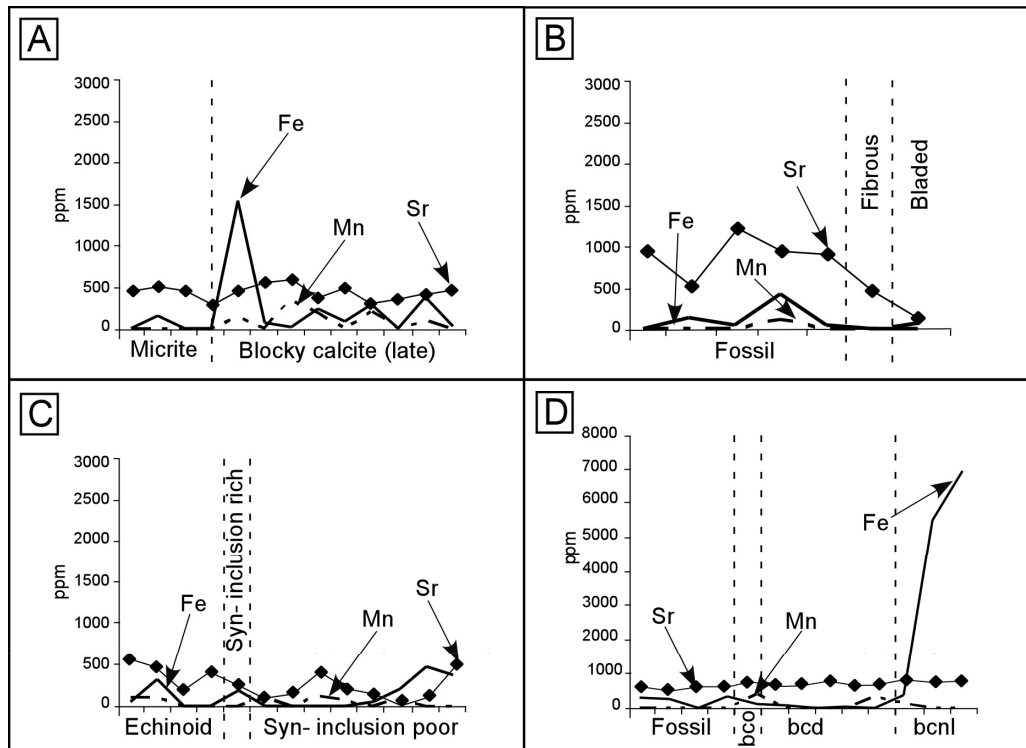


Figure 5.7. Trace element transects. A) Trace element transect of micrite and blocky cement. The dashed line shown in Figures 5.6-B is the path of the microprobe transect. Profiles of Fe, Mn, and Sr are plotted alongside. B) Trace element transect of fibrous and bladed cement. The dashed line shown in Figures 5-6D is the path of the microprobe transect. Profiles of Fe, Mn, and Sr are plotted alongside. C) Trace element transect of syntaxial cement. The dashed line shown in Figures 5-6F is the path of the microprobe transect. Profiles of Fe, Mn, and Sr are plotted alongside. D) Trace element transect of blocky cement. The cement pattern shows clear zonation from low luminescent to non-luminescent. The dashed line shown in Figures 5.6-H is the path of the microprobe transect. Profiles of Fe, Mn and Sr are plotted alongside, with cement zones labeled as, on photo (5.6-H): bcbo = blocky calcite bright-orange; bcd = blocky calcite dull; bcnl = blocky calcite non-luminescent.

Differences in the distribution of dissolution features between sequence 1 and sequence 2 are observed. The most important observation is that fabric selective dissolution of bioclasts and high-Mg calcite cement (syntaxial inclusion-rich cement) occur in shallow-water facies, and in both sequences; however, it is also found within the uppermost layers and below sequence/unit boundaries. On the contrary, deeper-water facies only show traces of fabric selective-dissolution of bioclasts, without following any particular stratigraphic distribution.

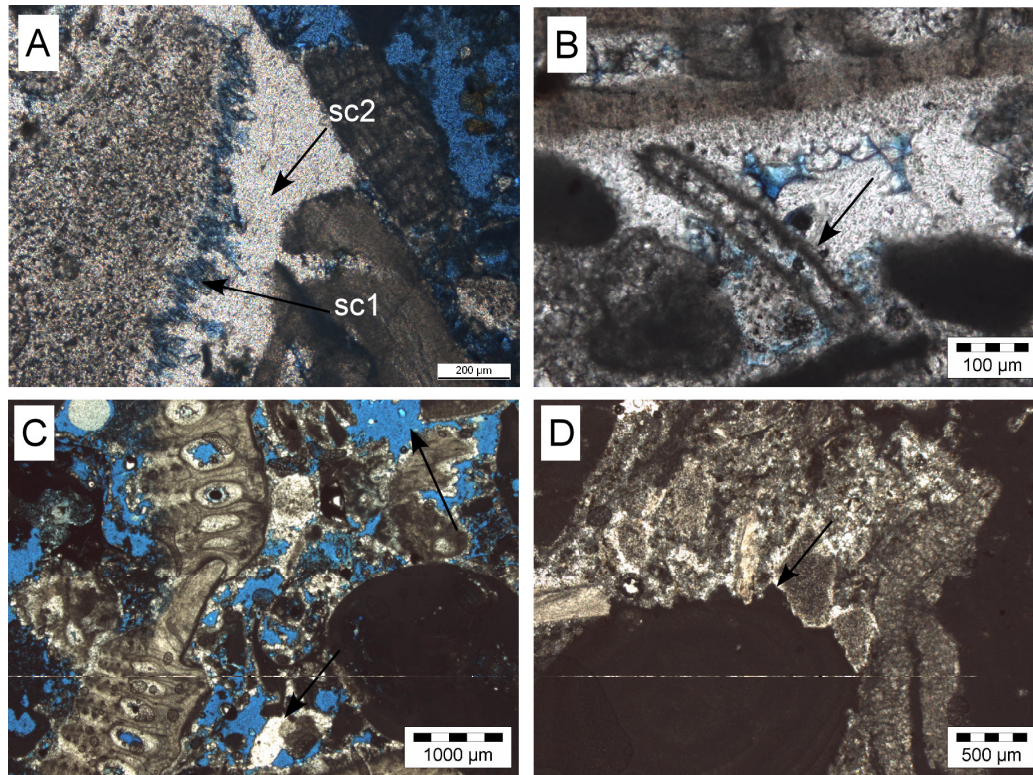


Figure 5.8. Diagenetic features. A) Skeletal rudstone showing selective dissolution of syntaxial inclusion-rich cement (arrow). Syntaxial inclusion-poor cement fills intergranular porosity (sc2) and post-date bladed cements. B) Bioclastic packstone-grainstone with micritic envelopes (me). Fibrous cements are pore-lining and pre-date pore-filling blocky calcite cements. C) Skeletal rudstone with “enhanced” porosity (arrows). D) Skeletal rudstone-floatstone showing mild evidence of chemical compaction (arrow).

## 5.9 Discussion

### 5.9.1 Origin of Calcite Cements

**Micritic Envelopes.** Micritization caused by endolithic algae, fungi and/or bacteria is considered to be a diagenetic process affecting grains at the seafloor interface. The continuity of the process over time leads to the formation of micritic envelopes around bioclasts (Bathurst 1975).

In tropical regions, micritic envelopes can occur as thick rims in shallow-water facies and thin rims in deep-water facies. Within the photic zone, endolithic algae particularly affect grains at depths less than 50 m. Below the photic zone, fungi produce small bores in grains that are usually invisible under normal petrography (1-2  $\mu\text{m}$  diameter). In non-tropical regions, as in the warm-temperate province, micritic rims do not occur with enough frequency to estimate temperature associations (Betzler et al. 1997).

In our case, differential micritization within the sediments is evidenced by the thin and scarce micritic envelopes recorded in shallow-water facies in sequence 1, compared to the thicker ones found in sequence 2. Clearly, the gradual change from warm-temperate to warmer conditions when these limestones were deposited has influenced the micritizations. However,

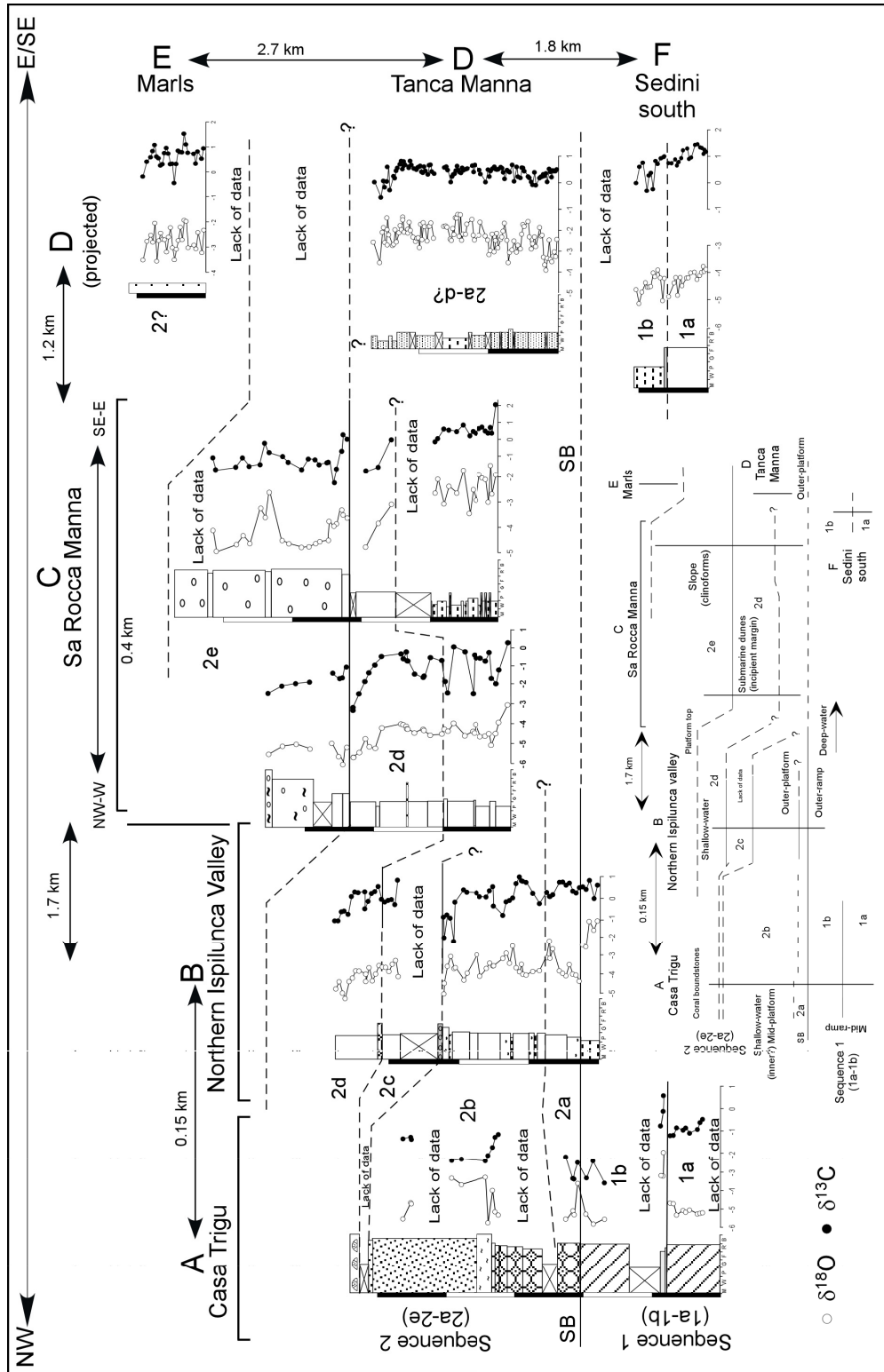


Figure 5.9. Measurements of the stable isotopic composition of bulk samples, plotted against stratigraphic position. Legend captions are the same as Figure 5.3.



temperature alone cannot explain the variability in micritization and further considerations are necessary to understand its occurrence.

**Micritic Cements.** Micritic cements are syn-depositional and, in both sequences, were localized within cavities or geopetal structures to red algal-rich lithofacies (Figs. 5.4 and 5.5). Micrite has been described as internal sediment or cement in other heterozoan carbonate settings, and has been attributed to an early, syn-depositional origin (Hood and Nelson 1996, Simone and Carannante 1985, Nelson and James 2000). Reid (1983) believes that biological processes, such as the degradation of organic matter, can explain its occurrence. In Miocene heterozoan carbonates from the Italian Apennines, micritic cements have also been found to be localized to red algal-rich lithofacies (Simone and Carannante 1985). However, an explanation as to why they are exclusively confined to such lithofacies is not currently available.

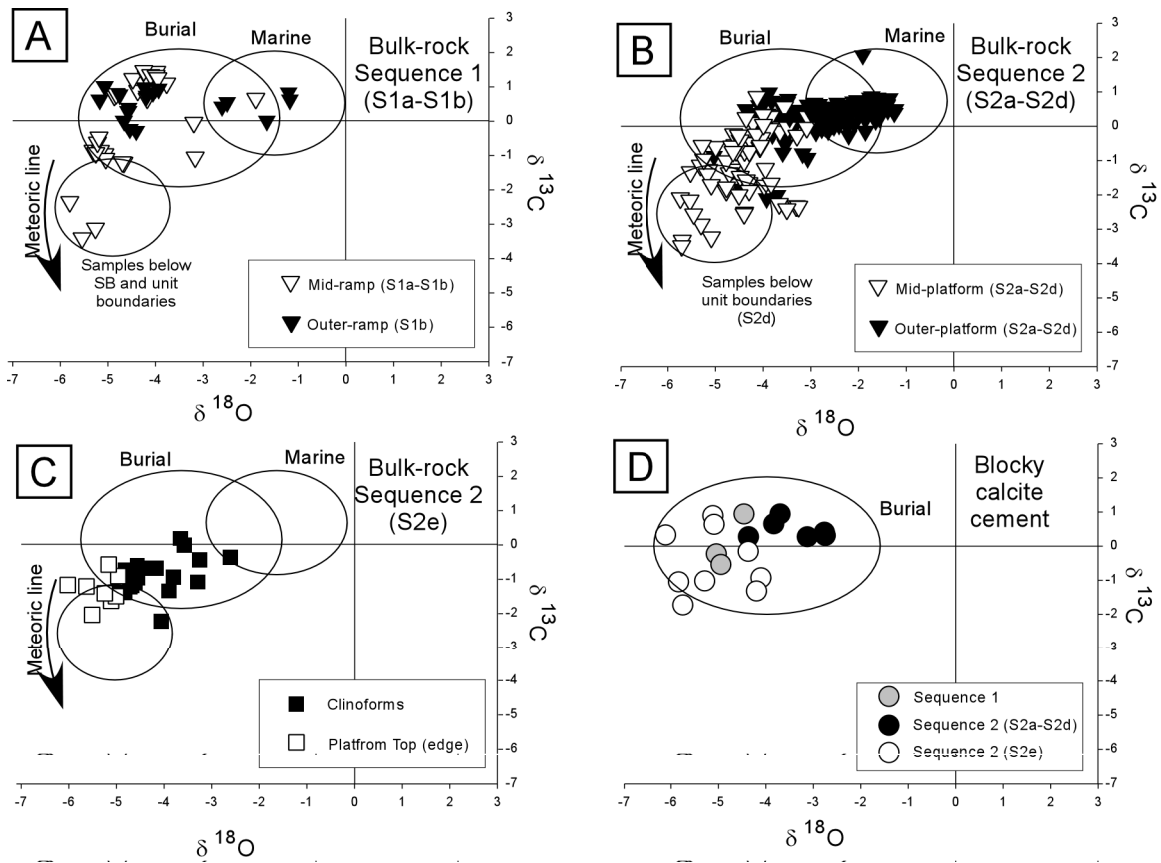


Figure 5.10. Cross-plot of oxygen and carbon isotopic values ( $\delta^{18}\text{O}$ ,  $\delta^{13}\text{C}$ ) of the bulk rock samples and blocky cement. A) Sequence 1 (S1a-S1b) values, B) Sequence 2 (S2a-d) values, C) Sequence 2 (S2e) values, D) Values from blocky calcite cements of: sequence 1, sequence 2 - S2a-d, and sequence 2 - S2e.

**Fibrous and Syntaxial Inclusion-Rich Cements.** The petrographic characteristics of the fibrous and syntaxial inclusion-rich cements are comparable to those of marine calcite cements precipitated at, or just below, the sea floor (Tucker and Wright 1990). Their patchy appearance under CL indicates recrystallization, suggesting an original mineralogy as high-Mg calcite, as is common for this cement type (James and Choquette 1990a). Petrographic and geochemical data suggest that fibrous and syntaxial inclusion-rich cements precipitated early in marine-derived waters and their later alteration was most probably due to the involvement of meteoric or marine-derived waters.

Similar cements have been described in other heterozoan settings. For example, in cool-water carbonates from New Zealand and South Australia, fibrous cements are localized at specific facies (e.g., cross-bedded sand bodies) or specific stratigraphic positions (e.g.

unconformities). Their amounts have been related to their high initial permeability, caused by high-energy conditions (Wilson and Evans 2002) and prolonged exposure time at the sediment-water interface (Ehrenberg 2004a 2004b). In Oligo-Miocene heterozoan carbonates from the Central Mediterranean (Knoerich and Mutti 2006), echinoderms show multiple growth stages for calcite syntaxial cements, with the earliest stage believed to be early marine in origin.

**Bladed Cements.** Bladed cements are believed to be early post-depositional in origin because of 1) their occurrence in primary and secondary pores; 2) their paragenetic relationship in comparison to fibrous cements (Fig. 5.6); and, 3) their pre-dating relationship with syntaxial inclusion-poor and blocky cements (Fig. 5.8). Petrographically, bladed cements show crystal morphologies that resemble those precipitated in marine and shallow-burial marine diagenetic environment (Bathurst 1975, Tucker and Wright 1990). Their clear CL zonations indicate that their precipitation also post-dated the diagenetic events responsible for the recrystallization of the previous phases. This would suggest that cementation most probably occurred in the shallow-burial marine diagenetic environment.

Alternatively, it could be argued that bladed cements precipitated from meteoric fluids rather than marine-derived waters (Bathurst 1975, Tucker and Wright 1990). Melim et al. (2001) have pointed out that diagenesis in a shallow-burial marine diagenetic environment follows a path similar to fresh-water diagenesis due to the similarities between the morphologies of calcite cements. However, there are several reasons for rejecting the possibility of a fresh-water origin for bladed cements. Firstly, bladed cements are found in coarse-grained shallow-water facies with bulk-rock stable isotope composition (Figs. 5.5 and 5.9) within the marine burial domain (Nelson and Smith 1996). Secondly, bladed cements have low Mn values and this is uncharacteristic of fluids with meteoric origins (Morse and Mackenzie 1990). Thirdly, meteoric evidence, such as dissolution cavities and a paragenetic connection to other meteoric cements, is absent.

Therefore, bladed cements are interpreted to be shallow-burial (at meters of sediment load?) in origin and precipitated from marine-derived waters.

**Syntaxial Inclusion-Poor and Blocky Calcite Cements.** As previously discussed, the paragenetic relationships are indicative of a late post-depositional origin for these cements. Syntaxial inclusion-poor and blocky calcite cements show clear crystal zonations under cathodoluminescence (Fig. 5.5) and have a low-Mg calcite composition (Table 5.1 and Table 5.2, appendix). Petrographically, their crystal fabric indicates either a meteoric or a burial origin (Morse and Mackenzie 1990, Tucker and Wright 1990).

Syntaxial inclusion-poor and blocky cements occur almost everywhere in the studied sections and show no preferential distribution with respect to any specific stratigraphic surfaces. There is not evidence of any special spatial association with intervals where fabric-selective dissolution occurs. These features would suggest that both cements are more likely to be marine-burial than meteoric. The isotope-stable composition of the blocky calcite cements (both sequences: Fig. 5.10) is characteristic of burial marine cements (Nelson and Smith 1996). Trace elements reveal that Fe values are always higher than Mn values and these values increase systematically from the syntaxial inclusion-poor to blocky cements (including the three calcite zonations). This suggests that both cements are compatible with marine-derived waters (James and Choquette 1991a).

In summary, this data suggests that post-depositional cements precipitated in a marine-burial diagenetic environment.

### *5.9.2 Origin of Dissolution Features*

Examination of petrographic relationships, together with the distribution of secondary porosity (fabric-selective dissolution: Fig. 5.5) among depositional facies enables the accurate inference of the origins of the dissolution features.

Dissolution affects single bioclasts and syntaxial inclusion-rich cements. Within the carbonate succession, fabric-selective dissolution occurs in shallow-water facies beneath the boundaries of the sequence/unit zones. The dissolution appears to have occurred early on in post-depositional history as they are post-dated by the precipitation of post-depositional cements

(e.g. bladed or blocky calcite cements: Fig. 5.8). Within sequence 2, the correlation between fabric-selective dissolution and stratigraphic boundaries is not as clear as in sequence 1 because of the lack of precise correlative boundaries and stratigraphic contacts (Fig. 5.3); however, the correlation clearly occurs under the boundary between units S2d and S2e.

Since fabric-selective dissolution is apparent within intervals where the stable isotopes are lighter (shallower-water facies) (Figs. 5.5 and 5.9), it is reasonable to assume that the incursion of fresh-water promoted the dissolution of mineralogically unstable skeletal fractions (e.g. aragonite) and cements such as syntaxial inclusion-rich (high-Mg calcite). The solutions were most probably depleted with respect to aragonite, but in thermodynamic equilibrium with respect to Mg-calcite favoring a slow dissolution rate of aragonite (Schroeder 1969, Walter and Morse 1985, Walter 1985). This is especially important when the carbonate system is exposed to Mg<sup>2+</sup> depleted meteorically derived waters (fresh-waters); as such exposure allows the incongruent dissolution of high-Mg calcite and aragonite.

However, away from the stratigraphic boundaries and at deeper-water facies where rocks are further from fresh-waters and less susceptible to its effects, the dissolution of metastable grains (i.e. aragonite) is recorded, it is likely that this has been produced by the degradation of organic matter at shallow-burial depths in marine-waters (More 2001).

The recognition and distribution of fabric-selective dissolution features in shallower-facies suggests that moldic porosity is a diagenetic feature that is controlled by both the original skeletal mineralogy and the influence of meteoric fresh-waters. However, the relative timing of the dissolution event in relation to the basin evolution is complex. The turnover of geometry into a “platform-like” at the S2d-S2e boundary, along with the settlement of a platform top and the progradation of the carbonate system (Benisek et al., in press) most probably led the infiltration of fresh-waters into an exposed shallow-water depositional realm. However, this does not explain how the carbonate system evolved over time and with respect to the rate of sea-level changes.

Details of the dynamics of the prograding system and resulting geometry are beyond the scope of this contribution.

### 5.9.3 Source of Calcite Cementation

Recent studies in shallow-buried non-tropical and heterozoan-rich carbonate settings have hypothesized that the early dissolution of aragonite grains can be the source of CaCO<sub>3</sub> for early calcite cementation (Brachert and Dullo 2000, Cherns and Wright 2000, Nelson and James 2000, Wright et al. 2003, James et al. 2005). In general, dissolution of aragonite skeletons begins early at the uppermost interface of the seafloor where oxidizing conditions can occur (a few centimeters of sediment load). However, evidence is limited (Nelson and James 2000) and most probably not preserved in the geological record (James et al. 2005). In addition, geochemical data supporting an aragonite source is biased by recrystallization and the low rock/fluid interaction (Knoerich and Mutti 2006).

Aragonite, released during dissolution, originally incorporated more Sr<sup>2+</sup> than does magnesium calcite (Walter 1985). The amount of Sr<sup>2+</sup> found in low-Mg calcite cements can therefore be used to determine whether the dissolved aragonite was a source for calcite cementation (Melim et al. 2002, Knoerich and Mutti 2006). Only if these values are high enough, then aragonite can be the source. However, this is dependent on the rock-water interaction. For example, in relatively open systems of low rock-water interaction, Sr<sup>2+</sup> is lost via water flow, whereas in effectively closed systems with high rock-water interaction, Sr<sup>2+</sup> values will be preserved (Morse and Mackenzie 1990).

In our case, calcite cementation was found to occur in at least two different diagenetic environments (marine and shallow-burial marine). Micritic, fibrous and syntaxial inclusion-rich cements pre-date moldic porosity so must have precipitated directly from marine waters in the marine diagenetic environment. However, late post-depositional cements, precipitated in a shallow-burial marine diagenetic environment, post-date the fabric-selective dissolution of skeletal grains (i.e. aragonite) and their Sr<sup>2+</sup> values become progressively higher over time than the earlier marine cementation. Sr<sup>2+</sup> values in the late post-depositional cements from sequence 2 showed higher Sr<sup>2+</sup> values than those in sequence 1, suggesting that aragonite was most probably a major source for low-Mg calcite cementation. The source for post-depositional

cements in sequence 1 is still not clear, even though  $\text{Sr}^{2+}$  values in bladed to blocky calcite cements show numerical an increment. The possible options are: 1) dissolution of early cements, 2) opening of the geochemical system, and, 3) lateral and vertical migration of fluids.

#### 5.9.4 Significance of the Stable Isotope Values

Shallow-water facies show bulk isotopic composition that reflects values from different sources (a mixture of diagenesis and skeletal particles). In contrast, deeper-water facies that are primarily composed of Mg-calcite skeletal particles, probably record primary marine signatures (see Chapter 6) that are heavier and not strongly biased by diagenesis at its shallower time-equivalent facies.

The vertical pattern among shallower-water facies (Fig. 5.9) clearly shows a differentiation by depth of diagenesis associated with a zone of meteoric alteration and a zone of shallow-burial marine diagenesis. The lighter and covariant  $\delta^{13}\text{C}$  and  $\delta^{18}\text{O}$  values found upsection and beneath the sequence/unit boundaries (S1a, S1b, S2d; Fig. 5.9) show a pattern comparable to those limestones influenced by the percolation of fresh-waters (Allan and Matthews 1982, Moore 2001). This supports the notion of localized meteoric alteration (Longman 1988). Downsection, values are heavier, suggesting a transition into a shallow-burial marine diagenetic domain. This differentiation indicates that rocks were locally altered by a meteoric influence, despite the lack of substantial evidence for meteoric cementation (previously discussed). Therefore, at these stratigraphic levels, the  $\delta^{13}\text{C}$  and  $\delta^{18}\text{O}$  values are the result of fabric-selective dissolution and the mineralogical stabilization of the sediments. This is particularly important because fresh-waters are overprinting these rocks with a geochemical signal rather than with petrographic evidence such as meteoric cementation.

The isotopic record of shallow-water facies varies much vertically, indicating that these rocks were diagenetically resettled and that noise is the sum of the variations in the original skeletal mineralogy and the type of diagenetic transformation. Comparing both sequences reveals that sequence 2 turns progressively into a coral and coralline red algae-dominated setting over time (Benisek et al., in press; Chapters 3 and 4 of this thesis). In addition, sequence 2 shows volumetrically more early syn-depositional marine cementation than sequence 1. This point out that the variability of the  $\delta^{18}\text{O}$  and  $\delta^{13}\text{C}$  compositional values are resettled principally by the type of calcite cementation (i.e. lighter or heavier values of  $\delta^{18}\text{O}$  by temperature-related fractionation) and, probably, by the changes in the biotic associations (see Chapter 6).

The  $\delta^{18}\text{O}$ - $\delta^{13}\text{C}$  cross-plot shows that samples from each paleoenvironment tend to occupy unique areas of the isotope diagram. In both sequences, the  $\delta^{18}\text{O}$  and  $\delta^{13}\text{C}$  compositional range is broadly similar to that observed in their non-tropical counterparts (Nelson and Smith 1996), where the  $\delta^{13}\text{C}$  values (c. +2 to -3) are mostly inherited from their calcitic mineralogy; meanwhile, the  $\delta^{18}\text{O}$  values (c. -1 to -5) reflect their main burial diagenetic trend. A difference between the two is that the  $\delta^{18}\text{O}$ - $\delta^{13}\text{C}$  values from the studied shallow-water facies showed lighter values resulting from the effects of meteoric alteration. Therefore, the grouping of samples from deeper-water facies suggests that their primary isotope values have not been significantly resettled (see Chapter 6). In fact, the shallow-water facies suggest that isotope compositions were biased by their susceptibility to diagenetic changes and, therefore, the negative shift in  $\delta^{18}\text{O}$  is a response to diagenetic transformation of sediment into limestone, mainly by the precipitation of carbonate cements into pore spaces.

By analyzing the isotope data of the blocky cements together with the bulk-rock isotope data from which they were derived (both sequences), it can be inferred that the main diagenetic trend for shallow- and deep-water facies involves progressive burial; however, with the superimposed effects of meteoric alteration that were only apparent in samples from shallower-water deposits.

#### 5.9.5 Significance of Calcite Cementation

Cementation began in the marine diagenetic environment and continued in the shallow-burial marine diagenetic environment. However, an important issue must be taken into account

when evaluating the calcite cementation of both sequences. The contrast in the amount and distribution of marine cementation needs to be considered. With the exception of the bladed cementation, post-depositional calcite cements were widely distributed and show no particular pattern among facies and stratigraphy.

In the shallow-water facies of sequence 2, marine cements made up a significant portion of the total rock volume (e.g., S2d). In contrast, these cements were local in sequence 1 and were usually traces (Fig. 5.5). This difference suggests that marine cementation played a major role in the early lithification of the rocks in sequence 2 as opposed to those in sequence 1 (see Chapter 4). As a result, the shallow-water facies in sequence 1 were more susceptible to mechanical compaction when they were overlaid by a few meters of sediment load. Therefore, the initial porosities were modified and reduced rather than preserved by early lithification (Fig. 5.5). In consequence, the shallow-water facies in both sequences would have followed different diagenetic pathways when they entered the shallow-burial marine diagenetic domain.

Looking at the stratigraphic distribution of marine cementation and bladed cements, it is apparent that they become progressively representative in the shallow-water facies in sequence 2. Moreover, they also become volumetrically important when the geometric transition is definitively evident (S2d/S2e). This contrast is compatible with the change from a warm-temperate to a warmer type of deposition and with the change of depositional geometry (see Chapter 4).

#### *5.9.6 Mineralogical Stabilization*

The bulk-rock stable isotope composition for shallow-water samples plotted against the stratigraphic profiles indicate that those samples close to sequence/unit boundaries began their stabilization into low-Mg calcite during early diagenesis by fresh-waters.

The burial history of the Sedin Limestone Unit is considered to have been continuous and gradual since the Middle to Late Miocene. However, post-depositional tectonic activity is not discarded to have disturbed the burial history of these rocks (Sowerbutts 2000). Based on outcrop thicknesses, stratigraphic patterns and depositional facies, samples from sequence 1 appear to have been buried to a depth of 60 m +/- 20 m (uncompacted values) over approximately 15 to 16 m.y. (underestimated estimates), which suggests an average burial rate of 1-2 cm per 1000 years. Sequence 2, however, are believed to have been buried +/- 20 meters less than the sequence 1 with uncertainty about the real thickness of the youngest marls deposited (Fig. 5.3). Therefore, depending upon climate and the availability of fresh-water, the transformation of aragonite and high-Mg calcite to low-Mg calcite is completed in approximately 10400 k.y. in modern environments (Budd 1988, Budd and Land 1990). Assuming that it took the maximum of 500 k.y. to stabilize calcite-dominated limestone (heterozoan-rich) with random amounts of metastable bioclasts, then all grains in meteoric zone of alteration would have been stabilized within the first < 5 m of burial. Although these calculations are crude, they suggest that the Sedin Limestone Unit (both depositional sequences) deposits would have been converted to low-Mg calcite whilst near the surface.

#### *5.9.7 Diagenetic History*

This case study provides two depositional sequences that have undergone transformations in marine and shallow-burial marine diagenetic environments with localized meteoric alterations. It is important to clarify that not all depositional facies were exposed to all diagenetic environments. Their diagenetic evolution (paragenesis: Figure 5.4) show pathways of diagenetic transformation where differential early cementation (and dissolution) (previously discussed) are denoted. In addition, no single sample in this study contained all of the diagenetic features listed in Figure 5.4.

Before considering the evolution over time, it is useful to “set the stage” by briefly considering the types of rocks involved in the diagenetic history. We will not attempt to cover all lithofacies, but will concentrate on how the involvement of the differential amount of skeletal fraction (aragonite, Mg- calcite) and cements with different original mineralogy affected the diagenetic pathway of these rocks. Two schematic representations of the successive stages of

cementation and dissolution in the marine, meteoric and shallow-burial marine diagenetic environments are shown in Figure 5.11. The two scenarios are based on a combination of stratigraphic and petrographic observations with geochemical analyses. Both scenarios are based on shallow-water and grain-supported lithologies. The first is composed mainly of Mg-calcitic grains (heterozoan-dominated) with low and variable amounts of aragonite grains. This represents the scenario for the sequence 1. The second is based on a grain-supported rock composed of Mg-calcitic grains (heterozoan-dominated) with larger amounts of aragonite grains (photozoan-enriched), representing the scenario for sequence 2 (e.g. unit S2d).

**Marine Diagenesis.** In both sequences, the diagenetic evolution began with the formation of micritic envelopes and the precipitation of high-Mg calcite fibrous and syntaxial inclusion-rich cements directly from marine waters. Marine diagenesis was major in sequence 2, as evidenced by a significant number of micritic envelopes and thicker isopachous fibrous cements. Consequently, in sequence 2 (S2d), marine cementation contributed to the early lithification (Fig. 5.11).

**Meteoric Alteration.** Following the marine diagenesis, rocks from shallower waters were altered by the influence of meteoric waters (although only those close to stratigraphic boundaries). Pores were filled by fresh-waters. Fabric selective-dissolution took place. Secondary porosity (moldic) was produced without being subsequently filled by post-depositional meteoric cementation. It is assumed that, in sequence 2 (S2d), a higher value of moldic porosity was created by the greater number of metastable grains (Fig. 5.5). Recrystallization most probably began at this diagenetic stage, converting the rocks into low-Mg calcite.

**Shallow-Burial Marine Diagenesis.** When the rocks were overlaid by a few meters of sediment load, their pore-networks were modified by mechanical compaction. With the lack of marine calcite cementation, mechanical compaction was more effective in sequence 1. Low-Mg calcite cementation started by the precipitation of bladed cements. A significant amount of low-Mg calcite bladed cementation was recorded in sequence 2. As the process of burial continued, syntaxial inclusion-poor and blocky cements were formed. The source for cementation was most probably aragonite (at least in sequence 2). Burial depths were not enough to produce strong cementation by pressure-dissolution. Mild chemical compaction caused sutured contacts between grains (particularly in sequence 1).

#### *5.9.8 Diagenesis and the Facies-Stratigraphic Context*

It was noticed that the shallow-water facies in each sequence recorded the effects of diagenesis differently in the marine, meteoric and shallow-burial marine diagenetic environments. The consequences of this were: (1) the impact that marine calcite cementation has on the early lithification, (2) the differential amount of fabric-selective dissolution by meteoric alteration for the creation of secondary porosity, (3) the amount and distribution of post-depositional calcite cements and the source of cementation; and, (4) the lack (or rarity) of the previous three features. Furthermore, it would seem that the marine (fibrous) and bladed cementation increased as the transformation of the ramp-to-platform profile is established.

In order to visualize the diagenetic differences with respect to the facies and the stratigraphic context, a figure was sketched (Fig. 5.12).

In Figure 5.12 three “diagenetic facies” (A, B and C) are proposed: two for shallow-water facies from each sequence (A and B), and one for deep-water facies in general (C). Diagenesis A is proposed for sequence 1 and diagenesis B and C for both sequences. Each diagenetic facies is defined on the dominant diagenetic environment of transformation, and is distinguished as follows: (1) “Diagenesis A” is characterized by shallow-burial marine diagenesis with localized marine diagenesis, (2) “Diagenesis B” is characterized by marine and shallow-burial marine diagenesis, and, (3) “Diagenesis C” is characterized by shallow-burial marine diagenesis. Zones where meteoric alteration was identified are placed graphically in Figure 5.12. These were supported by the stable isotope composition analysis and fabric-selective dissolution (Figs. 5.5 and 5.9).

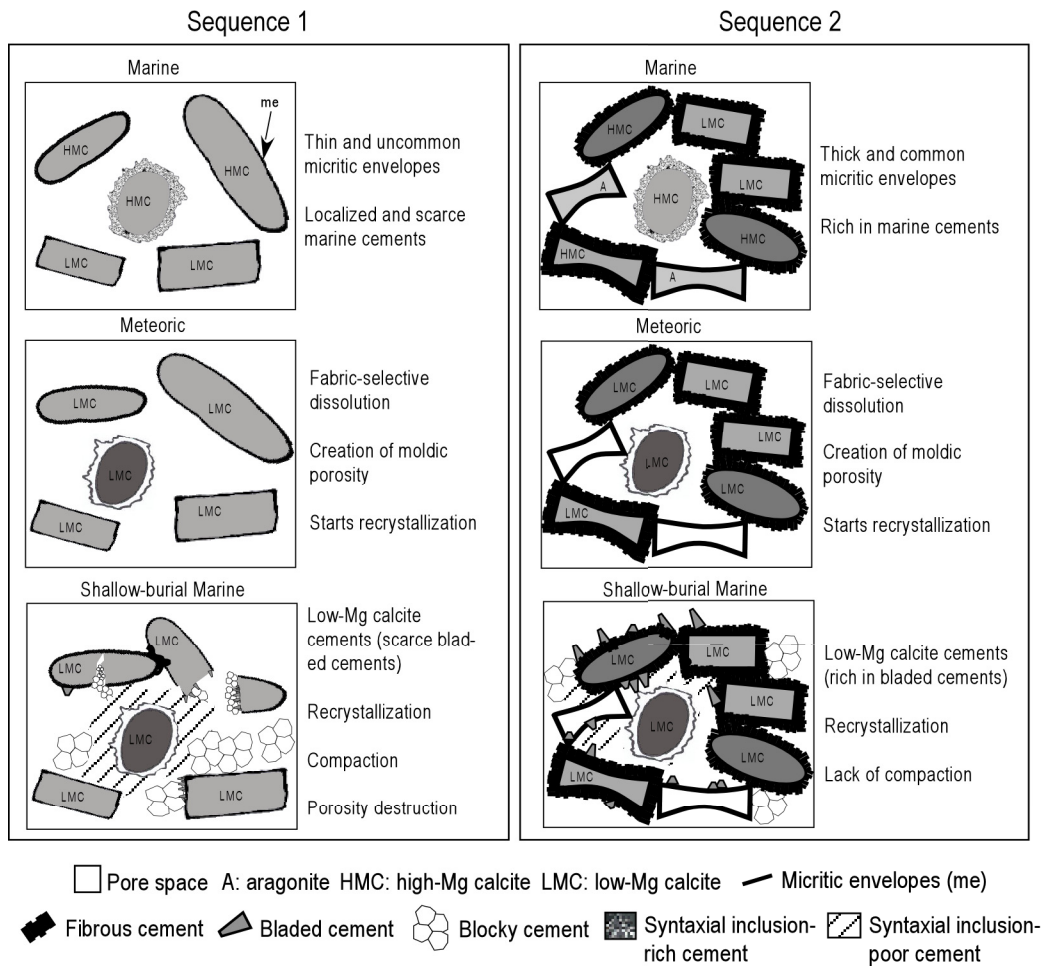


Figure 5.11. Paragenetic history of grain-supported shallower-water lithologies in sequence one and sequence two.

Figure 5.12 illustrates the following in shallow-water facies: (1) The shift from a warm-temperate to warmer (tropical) conditions at the time of deposition was accompanied by the incrementation of marine calcite cementation; and, (2) The shift in the mineralogy of the biotic elements from heterozoan-rich (calcitic mineralogy) into photozoan-rich (metastable mineralogy) coincided with the incrementation of bladed cementation. These facts suggest that marine cementation could be a response of the initial saturation state of the marine waters to  $\text{CaCO}_3$ , or to prolonged exposure time (Ehrenberg 2004a 2004b) accompanied with high initial porous networks (Wilson and Evans 2002) at the sediment-water interface. Furthermore, high volumes of marine cementation occur when there are differences in hydrodynamic energy at the time of deposition (dunes, incipient platform margin) similar to those described in previous research (e.g., cross-bedded sand bodies, Nelson and James 2000). Although the source of  $\text{CaCO}_3$  for post-depositional calcite cementation in sequence 1 is not as clear as in sequence 2, and  $\text{Sr}^{+2}$  values have revealed aragonite as a possible source for the low-Mg calcite cementation, it should be noted that bladed cementation is volumetrically more important when facies are initially aragonite-richer. Therefore, bladed cementation could mark the contrast when deciphering the diagenetic history of shallow-buried transitional carbonates in order to determine the source for calcite cementation.

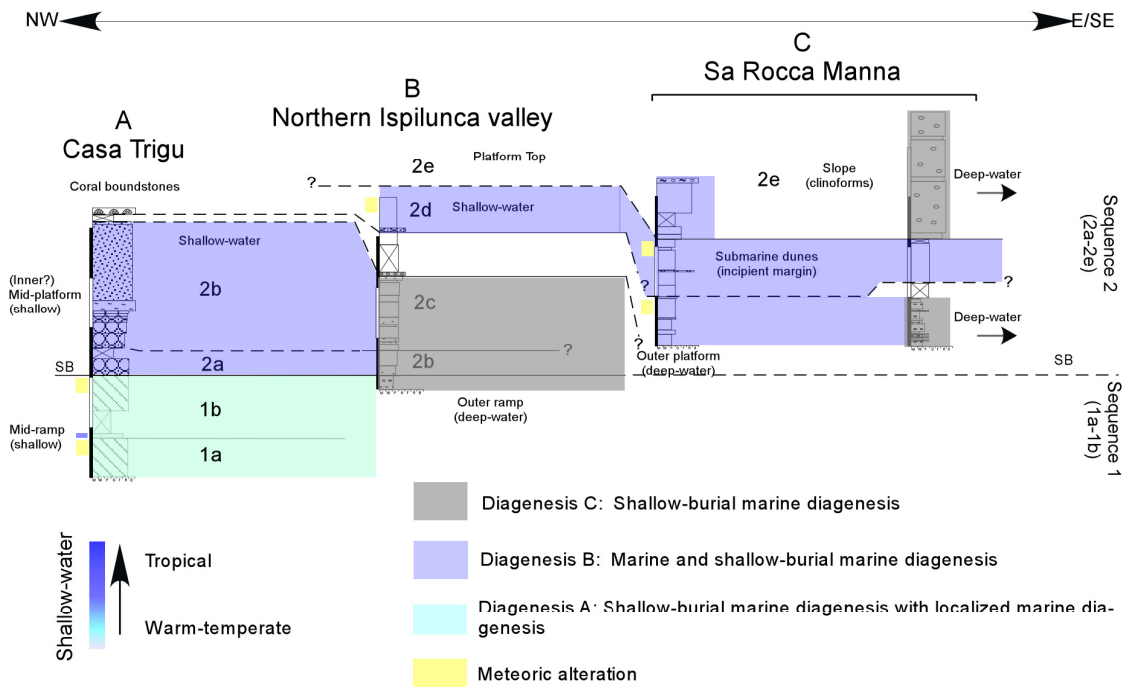


Figure 5.12. Diagenetic facies “A-B-C” placed in the stratigraphic context.

### 5.9.9 Prediction of Reservoir Quality

The lack of post-depositional dissolution, combined with pervasive, burial cementation make non-tropical (heterozoan) carbonates very unlikely targets for oil and gas exploration. In contrast, heterozoan carbonates containing variable amount of metastable grains (e.g. aragonite) possess the potential for hydrocarbon exploration.

High and variable porosities combined with low permeability values below sequence and unit boundaries indicate that the downward and downdip flow of the early subsurface fluids was highly restricted by the levels of early lithification (at least in sequence 2, S2d). In these types of carbonate settings, the genetically related porosity networks beneath sequence or unit boundaries were highly influenced by early fabric-selective dissolution (e.g. bioclasts originally composed of aragonite). Consequently, the prediction of flow paths will not be only controlled by the stratigraphy, but also by the original mineralogy of the skeletal fraction. It is assumed that the infiltration of fresh-waters at the same stratigraphic levels was responsible for the dissolution and marginward (or downward) transportation of dissolved minerals. These factors appear to have contributed to the modification and creation of effective porosity at levels where the opposite would be expected (Hopkins 1999).

The relationship of the stratigraphic context with the lithology (and skeletal mineralogy), facies distribution and diagenetic facies, constitutes a key finding for the evaluation of these type of carbonate settings for the identification and potential development of reservoir facies. In addition, the diagenetic facies and their changes over time according to the stratigraphic context, offer better predictability to the identification of potential reservoir facies and their quality when evaluating possible production strategies. From a wider perspective, when interpreting “Plays” it is necessary to define and identify potential traps that may restrict the secondary migration of hydrocarbons in a basin. In this study, the levels of meteoric alteration were not a potential cause of stratigraphic traps because of the ubiquitous meteoric calcite cementation. Therefore, special attention is required when evaluating transitional carbonates to reduce the risks in hydrocarbon exploration.



## 5.10 Conclusions

(1) This study illustrates the diagenetic pathway of a Miocene warm-temperate to tropical carbonate setting. The combined stratigraphic, petrographic and geochemical approach allowed us to determine early diagenetic transformations in the marine, meteoric and shallow-burial marine diagenetic environments.

(2) Cementation occurred in two stages, each related to a different diagenetic environment: (a) marine cementation (micrite, fibrous, and syntaxial inclusion-rich), originally high-Mg calcite, developed in the marine diagenetic environment; and, (b) post-depositional cementation (bladed, syntaxial inclusion-poor, and blocky), originally low-Mg calcite, developed in the shallow-burial marine diagenetic environment.

(3) Meteoric alteration was localized and specific to shallower facies beneath the sequence/unit stratigraphic boundaries. It is suggested that the original skeletal mineralogy is a major controlling factor for fabric-selective dissolution (moldic porosity) without meteoric calcite cementation. Recrystallization is believed to have occurred early and near to the surface.

(4) The identification of the stratigraphic distribution of calcite cements (in accordance with their paragenesis) and their dissolution features, and the use of the geochemical approach pointed to aragonite as the source for low-Mg calcite cementation (at least in sequence 2). However, below the sequence/unit boundaries, the dissolution of early marine precipitated high-Mg calcite cements (syntaxial inclusion-rich) and bioclasts were probably also contributing sources.

(5) The identification, in shallow-water facies, of diagenetic features within the stratigraphic context (Diagenetic facies A, B and C) showed that marine (fibrous) and bladed cementation become gradually more important as the system evolves over time and the depositional geometry changes. Thus, lithification occurs early and porosity-permeability evolution is significantly altered before entering the shallow-burial marine diagenetic environment. These observations are supported by the gradual change from a heterozoan into a photozoan-richer depositional setting.

(6) The main difference, other than scale, between this interpretation and those derived from previous diagenetic studies of Miocene non-tropical limestone is the implication of our findings that major carbonate lithification occurred early during marine and shallow-burial marine diagenesis, rather than only during the late sediment burial (deep-burial diagenesis). In addition, the study of the stratigraphic distribution of the diagenetic features using geochemical and petrographic data helps to reduce uncertainty when unraveling the source for calcite cementation.

(7) Outcrop-based analysis (such as this work) is a powerful tool for understanding the development of diagenetic patterns in these types of transitional carbonate systems. Moreover, this model produced improved resolution over seismic analysis and can help to reduce the risk of oil exploration when predicting unconformity related carbonate reservoirs.

**- CHAPTER 6 -**  
**OXYGEN AND CARBON STABLE ISOTOPE STRATIGRAPHY OF A  
SHALLOW-WATER MIOCENE CARBONATE SETTING (NORTHERN  
SARDINIA, ITALY): RESPONSE CHARACTERISTICS TO DIAGENESIS AND  
CLIMATE**

This chapter summarizes the oxygen and carbon stable isotope data and its significance with respect to diagenesis, facies (biotic association) and the overall stratigraphic context. Comparisons on a local and regional scale are considered with respect to climate changes recorded during Miocene times. This chapter is structured for consideration as a manuscript for publication.

### **6.1 Abstract**

The carbon and oxygen isotopic composition ( $\delta^{13}\text{C}$  and  $\delta^{18}\text{O}$ ) of bulk carbonates deposited in a warm-temperate to tropical Miocene carbonate setting, have been studied to ascertain whether changes in the isotope record are related to global changes over this time period, or whether such changes are entirely due to a diagenetic transformation of the primary marine values. Several transects cross cutting shallower to deeper water facies of the Sedinì Limestone Unit were investigated. The carbonate setting is characterized by two depositional sequences which record a turnover of the carbonate factory from a heterozoan-dominated ramp to a photozoan-dominated platform. In both depositional settings, all oxygen values are negative ( $\sim -6$  ‰ to  $-1$  ‰) and no positive values are recorded. On the other hand, carbon values from deeper water facies show positive values ( $> 0$  ‰ to  $\sim +2$  ‰) that are heavier than their shallower water counterparts ( $\sim -3$  ‰ to  $0$  ‰). Taking in account that the rocks have been strongly affected by marine burial diagenesis, with differential marine and meteoric alteration in shallower water environments, it is suggested that the overall oxygen record is the result of shallow-burial marine diagenesis. This was unexpected at the ramp, since heterozoan-rich carbonates can hold isotope values close to primary marine signals due to their low-Mg calcite original composition. The  $\delta^{13}\text{C}$  value of the sediment seems less affected by diagenetic processes. The appearance, and higher frequency, of positive carbon values at the deeper water platform deposits goes along with the turnover into a photozoan-dominated carbonate setting. However, the correlation of the carbon enrichments with their time-equivalent shallower water facies is not evident. These  $\delta^{13}\text{C}$  values usually showed a covariant trend with the oxygen isotope record, even in cases where the latter did not hold positive values.

### **6.2 Introduction**

The use of  $\delta^{13}\text{C}$  and  $\delta^{18}\text{O}$  stable isotope stratigraphy has generally been used in deep sea carbonate sediments for recognizing environmental changes on local, regional, and global levels. The data have served as the principal means of reconstructing global and regional climate change on a variety of geologic time-scales. Meanwhile  $\delta^{13}\text{C}$  data helps explain the global carbon cycle and its perturbations;  $\delta^{18}\text{O}$  data provides constraints on the evolution of deep sea temperature and continental ice volume.

The Miocene is a time interval characterized by significant changes in climate. The transition from relative global warmth of the late Oligocene to the Neogene "icehouse" took place with a series of stepwise changes, like brief periods of glaciations (e.g., Mi-events) (Miller et al. 1991, Wright and Miller 1992) tied to major temporal variation in the mean ocean  $\delta^{13}\text{C}$  (e.g., Monterrey Carbonate Excursion) (Vincent and Berger 1985). Those signals and variations have been recognized in the deep sea sedimentary benthic and pelagic record as well as in bulk-rock samples from Mediterranean regions (John et al. 2003).

Recognition that the  $\delta^{13}\text{C}$  and  $\delta^{18}\text{O}$  in deep-water sediments varies in response to global changes and their use for stratigraphic purposes led many authors (Immenhauser 2003, John et al. 2003) to search for such variations in their shallow-water counterparts. However, the type of

carbonate setting and biotic association (heterozoan vs. photozoan), original mineralogy (stable or not), and diagenesis are factors to consider when comparing deep-water sediments with their shallow-water counterparts. While deep-water sediments are composed of relatively stable low-Mg calcite, shallow-water carbonate settings can include high-Mg calcite and aragonite. Such differences impact the diagenetic history, which in the end can bias the stable isotope record.

In order to further clarify whether diagenesis, sediment composition, and climate can influence the  $\delta^{13}\text{C}$  and  $\delta^{18}\text{O}$  fluctuations from shallow marine settings, we have investigated several outcrop sections of a temperate to subtropical carbonate setting deposited during the Miocene, which has been affected by different styles of early diagenesis and degrees of calcite cementation. The rocks involved in this study, correspond to the "Sedini Limestone Unit" (Thomas and Gennesseaux 1986), a shallow-water carbonate depositional system located in northern Sardinia (Central Mediterranean) at the Perfugas basin, Anglona area (Fig. 6-1A). Benisek et al. (in press.) (and this work, Chapter 3 and 4) have characterized this setting as a ramp dominated by heterozoan components, which evolved into a platform-like depositional setting, enriched in photozoan components. For these reasons, this setting provides a unique opportunity to test if the superimposition of diagenetic effects erased  $\delta^{13}\text{C}$  and  $\delta^{18}\text{O}$  primary marine signals, and if so, to determine the reasons.

To answer these questions, we selected stratigraphic profiles cross-cutting the "Sedini Limestone Unit" from shallow to deeper water settings (Figs. 6-1B, 2 and 3) in order to cover the extension of the whole basin (approx. < 15 km<sup>2</sup>) and for comparison between the carbonate strata of the two depositional sequences involved.

### 6.3 Geological Setting

This chapter introduces data on the Perfugas basin (Fig. 6.1) (Anglona area; Sowerbutts 2000), an intra-arc basin (< 15 km<sup>2</sup>) established in northern Sardinia during Oligocene to Miocene times by the development of a NW-SE rift depositional system (Fig. 6.1).

The rift development was caused by oceanic spreading and the formation of the western Mediterranean back-arc basin (Cherchi and Montadert 1982) and its consequent Corsica-Sardinia microplate rotation (Sowerbutts and Underhill 1998, Sowerbutts 2000). Oceanic spreading in the western Mediterranean back-arc basin and the majority of the Corsica-Sardinia microplate rotation occurred between 24-18 ? Ma (latest Aquitanian to early Burdigalian) (Sowerbutts 2000, Monaghan 2001). From Oligocene times to the present day, the arc-trench system and surrounding zones of compressional deformation migrated progressively outwards as a Neotethyan oceanic crust, which was consumed in a subduction zone located on the eastern side of Sardinia (Sowerbutts 2000). The Tyrrhenian Sea on the fore-arc side of the Sardinian Rift system began to open from late Miocene times (Sowerbutts 2000).

Paleogeographic reconstruction locates the northernmost area of Sardinia between 32°-35° of N latitude during early Burdigalian times, moving due to an anticlockwise rotation towards 35°-38° of N latitude in early Langhian times (Dercourt et al. 2000).

At the Perfugas basin (Fig. 6.2), a Burdigalian volcanic marker ignimbrite ( $\tau$ 2/Tergu Formation) (Sowerbutts 2000) marks the base of the sedimentary succession and is overlain by volcanoclastics, lacustrine deposits and fluvial conglomerates (Perfugas Formation) (Sowerbutts 2000). The focus of this study, a 50-60 m thick shallow-water marine carbonate and marlstone succession, the "Sedini Limestone Unit" (Thomas and Gennesseaux 1986), overlies the previous sedimentary rocks. The age of deposition ranges between Burdigalian, as indicated by Ar/Ar dating in the ignimbrites (Sowerbutts 2000) to lower Langhian? as indicated by nanoplankton biostratigraphic data (Benisek et al. in prep).

Thomas and Gennesseaux (1986) considered that the carbonates from the Sedini Limestone Unit are Burdigalian in age, and were deposited during a passive infill by a major marine transgression. During the Langhian, local vertical movements and deepening of the Western Mediterranean basin occurred (Thomas and Gennesseaux 1986), accompanied by thermal subsidence (Monaghan 2001), which is reflected by marlstones and locally preserved in northern regions of Sardinia as in the Perfugas basin (Fig. 6-1B).

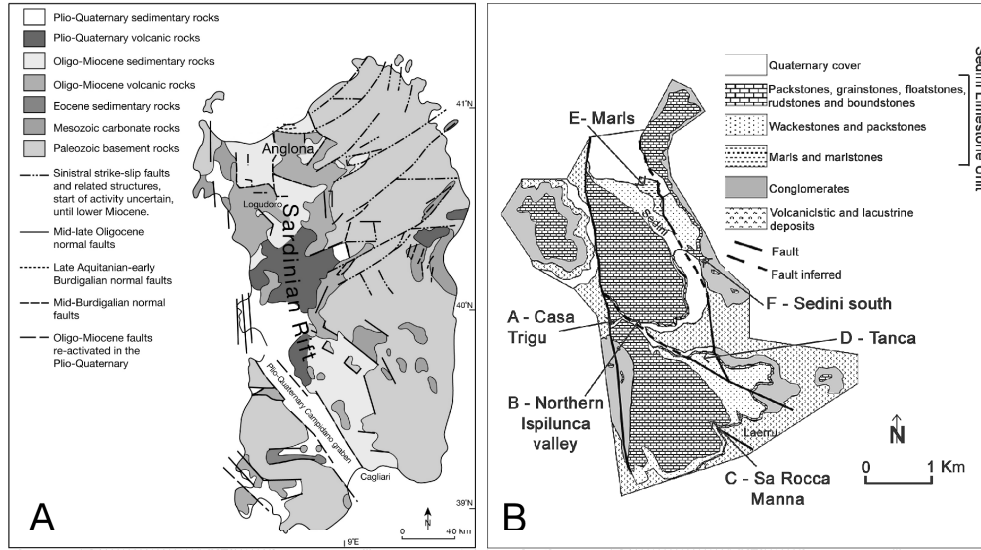


Figure 6.1. (A). Geological map of Sardinia, showing the distribution of the Rift and the location of the study area in the Anglona area (modified from Sowerbutts 2000). (B). Detailed geological map of the study area, located in the Perfugas basin, a half-graben with a Neogene sedimentary infill, located between the Sedini and Laerru villages. The map illustrates the distribution of different lithological units present in the area (modified after Benisek et al., in press., Albertsen 2005, Giennapp 2005, and Nagel 2005), as well as the different carbonate lithologies occurring within the “Sedini Limestone Unit” that have been defined in this study. The location of vertical stratigraphic profiles and transects analyzed in this study are also indicated.

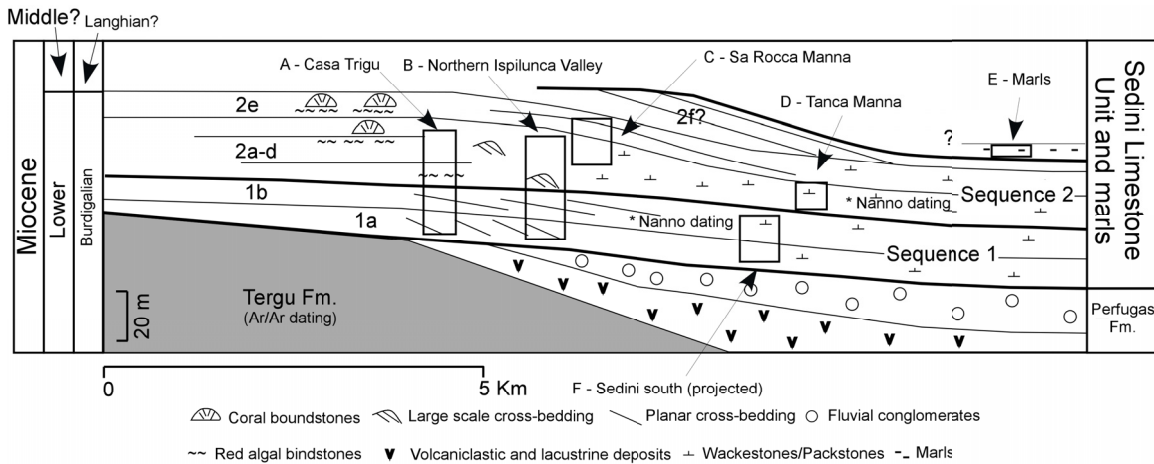


Figure 6.2. Schematic cross section illustrating the geometric relationships among the stratigraphic units identified within the “Sedini Limestone Unit” (Modified from Benisek et al., in press.). Vertical stratigraphic profiles A, B & C shown here correspond to Casa Trigu, Northern Ispilunca Valley, and Sa Rocca Manna transects respectively. D and E correspond to Tanca Manna and Marls sections. Vertical stratigraphic profile F is part of the Sedini south transect described in Benisek et al. in press.

#### 6.4 The Sedini Limestone Unit

The “Sedini Limestone Unit” was described at the field and mapped in six main locations (Transects Casa Trigu, Northern Ispilunca valley, Sa Rocca Manna, and sections D, E & F), where stratigraphic sections were logged, sampled and described in detail (Figs. 6-1B, 6.2 and 6.3). Field study and petrographic analysis enable us to recognize different sediment compositions, lithofacies and diagenetic features (Chapter 4 and 5). Figure 6.3 show the different lithofacies at the six main locations and their correlation within the stratigraphic context. For the diagenetic and isotopic analysis, composite sections from Casa Trigu, Northern Ispilunca valley and Sa Rocca Manna were used to identify, describe and interpret the main features.

#### 6.4.1 Stratigraphic and Sedimentological Setting

The data collected for this study was integrated with the stratigraphic model of Benisek et al. (in press.) which divides the Sedini Limestone Unit into two main depositional sequences: the lower, or sequence 1 and the upper, or sequence 2. By the recognition of several erosional contacts, they have recognized within the sequence 1 two informal units: S1a and S1b; and within the sequence 2, five informal units: S2a to S2e. A unit S2f and a marly unit (S2?), were identified by Benisek et al. (in press.) as the youngest and last sedimentary units.

Overall, the stratigraphic evolution of the Sedini Limestone Unit records the transition from a ramp to platform geometry. Benisek et al. (in press.) considered that the change is accompanied with the change of the carbonate factory (Chapter 3 and 4). It is considered a transition from a heterozoan-dominated into a photozoan-dominated carbonate setting. The biotic change is marked from the sequence 1 to sequence 2 respectively.

**Sequence 1.** Sediments in sequence 1 are dominated by a heterozoan association. Biota is rich in coralline red algae, bryozoans, molluscs (bivalves), echinoids and barnacles. Minor components (photozoan) are large benthic foraminifers and reworked corals. The occurrence of *Amphistegina* and *Heterostegina* indicates that these sediments formed under warm-temperate conditions (Betzler et al. 1997). Sedimentation took place on a shallow (inner?) mid-ramp to an outer (proximal) ramp setting. Mid-ramp facies comprise floatstones and rudstones, while deeper water facies of the outer (proximal) ramp facies comprise packstones and wackestones.

The lower unit S1a (Fig. 6.3) is characterized at the base by massive floatstones and rudstones followed upsection by cross-bedded floatstones and rudstones. Wave action at the top of the floatstones and rudstones strata (Northern Ispilunca valley) is observed. Following that, at the upper unit S1b, a floatstone layer occurs. This layer is characterized by encrusting red algae (Casa Trigu) at western outcrops and by rhodolites at eastern outcrops (Northern Ispilunca valley). Upsection, in unit S2b, cross-bedded floatstones and rudstones are found. They grade into packstones and wackestones in eastern direction where some bioturbation is observed.

Paleoenvironmentally (within the two units), cross-bedded floatstones to rudstones deposits are considered as longshore bars (submarine). They occurred at the (shallow) mid-ramp at or below the fair weather wave base. Wave action at the top of the bars (Northern Ispilunca valley) and subsequent deposition of a floatstone (S1b- Casa Trigu and Northern Ispilunca valley) have been considered by Benisek et al. (in press.) as a short wave-base lowering followed by a deepening of the depositional system. They have suggested that the reinstoration of the bar system is documented by the subsequent cross-bedded floatstone to rudstones (S1b). Packstones and wackestones deposits are considered as a deepening of the depositional system. They occurred at the outer-ramp below storm wave base, where no winnowing of the micrite occurred, and where some bioturbation was preserved.

**Sequence S2.** This sequence is characterized by a heterozoan to photozoan biotic association. The occurrence of a well developed coral framework with different species indicates that deposition occurred into a warmer-water environment. Overall, sedimentation took place in a platform. Five units were distinguished: S2a to S2e. Benisek et al. (in prep.) have considered a sixth unit (S2f) and deeper-water marly sediments (S2?), considered as the youngest carbonate strata outcropped at the study area.

Unit S2a-2b at Casa Trigu consists of well to poorly lithified floatstones to rudstones overlaid by red algal bindstones (Fig. 6.3). Basinwards (Northern Ispilunca valley), these rocks grade into bioclastic grainstones, packstones and wackestones. Paleoenvironmentally (within the two units), red algal bindstones are shallow-water (inner?) mid-platform deposits. By looking at coralline red algae taxa, Benisek et al. (in prep) have considered their deposition at water depths between 20 and 40 m. In general, these rocks are rich in small benthic foraminifers, molluscs, red algae, and echinoids. Large benthic foraminifers (*Amphistegina* and *Heterostegina*) and coral fragments (minor components) locate them into the photic zone of deposition. Bioclastic

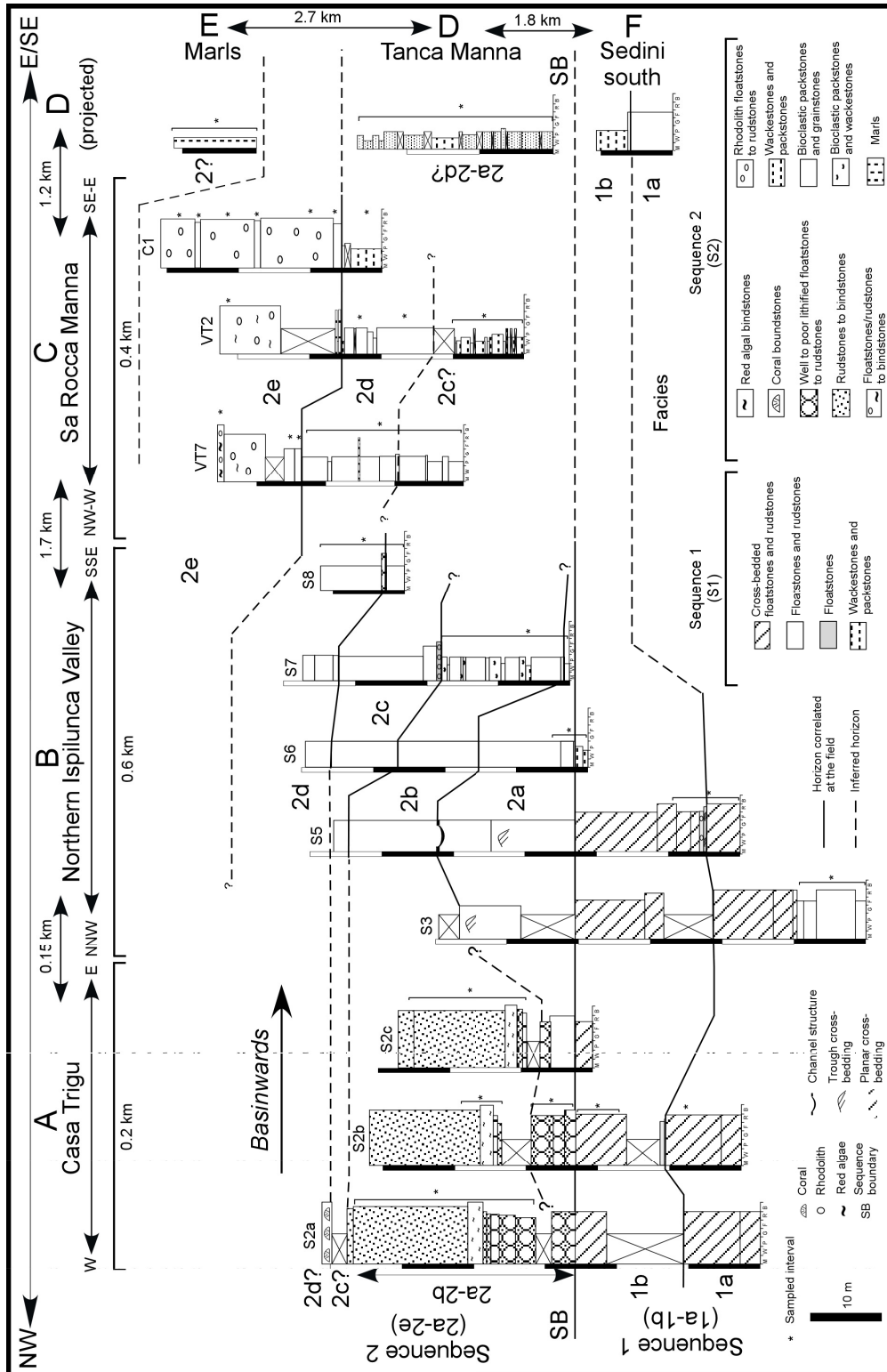


Figure 6.3. Correlation of the stratigraphic sections measured in the different areas, showing the distribution of different lithofacies and other sedimentary attributes. The correlation was established by means of physical tracing of the beds in the field as well as with photo panoramas.

grainstones, packstones and wackestones are considered as dune deposits (incipient platform margin). Those that show increase of lime mud matrix (wackestones and lime-supported packstones) were deposited in a deeper environment, most probably below storm wave-base as outer-platform deposits. Unit S2c-2d consists mainly of bioclastic wackestones and packstones, bioclastic packstones and grainstones, and packstones and wackestones with some bioturbation. In unit S2d coral boundstones occur locally at the top of the stratigraphic section located at Casa Trigu, meanwhile at Northern Ispilunca valley, rhodolith floatstones occur locally. Overall, sediment composition is characterized by reworked corals, red algae, molluscs, foraminifers (large and small) and echinoids. Bioturbated packstones and wackestones can contain planktonic foraminifers. Packstones are rich in echinoid fragments and red algal debris; while grainstones intervals contain biomolds of molluscs preserved by thick micritic envelopes. Paleoenvironmentally, bioclastic limestones are considered as dune deposits (incipient platform margin). Benisek et al. (in prep.) observed their spatial arrangement with respect to the red algal bindstones, and considered the last ones as sediment stabilizers. Bioturbated wackestones and packstones are considered as outer-platform deposits.

Unit S2e consists of rudstones/floatstones to bindstones, rudstones and floatstones. Rudstones/floatstones to bindstones are composed by coralline red algae, encrusting foraminifers, bryozoans, echinoids and mollusks and are considered as platform top (edge) deposits. Rudstones and floatstones are composed mainly by rhodolites and characterized by their clinoformal geometry. They are considered as slope deposits.

Unit S2? consists of marls. Expression of these rocks in the field is restricted to the north part of the study area (Fig. 1B). Lower stratigraphic contact with subunit S2e-f is not observed. These deposits are the youngest rocks of the Sedini Limestone Unit. They are considered as outer (distal) platform deposits.

#### 6.4.2 Diagenesis

The Sedini Limestone Unit is characterized by different generations of calcite cements, dissolution and compactional features. In Chapter 5, we described how both depositional sequences (ramp and platform) experienced alterations at the marine and shallow-burial marine diagenetic environments with localized meteoric alteration at shallower-water facies beneath and close to stratigraphic boundaries.

Marine diagenesis is characterized by the formation of micritic envelopes and precipitation of high-Mg calcite cements (micrite, fibrous and syntaxial inclusion-rich cements). Shallow-burial diagenesis is characterized by low-Mg calcite cementation (resulting in bladed, syntaxial inclusion-poor and blocky cements), compaction and recrystallization. Chemical analysis of trace elements suggested aragonite as a source of  $\text{CaCO}_3$  for low-Mg calcite cementation (at least in sequence 2). Meteoric alteration is only evident at shallower-water facies beneath stratigraphic boundaries and characterized by fabric-selective dissolution (bioclasts and high-Mg calcite syntaxial inclusion-rich cement) and recrystallization.

Based on the distribution of the different diagenetic features linked to facies, and the stratigraphy, Marcano et al. (in prep.) (Chapter 5) observed that at shallower-water facies the effect (and degree of alteration) of the marine (fibrous) and bladed cementation was substantially different in both sequences. Marine cementation was major at sequence 2 (platform) but not in sequence 1 (ramp). Bladed cements increased as the transformation of ramp-to-platform profile was established. Furthermore, Marcano et al (Chapter 5), observed that shallow-burial marine cementation by syntaxial inclusion-poor and blocky calcite cements were distributed overall; however, at shallower-water facies in sequence 1 (ramp) these constituted the major type of calcite cementation.

In deeper water, facies marine cementation was less than its shallower-water counterparts (both sequences) and the main domain for diagenetic transformation took place at the shallow-burial marine diagenetic environment (cementation and recrystallization).

Based on the previous, Marcano et al (in prep.) (Chapter 5) proposed different diagenetic facies (Diagenesis A, B and C) (Fig. 6.4) depending on the distribution and amount of the diagenetic features. As a result, they noticed that along with the shift from a warm-temperate to

warmer (tropical) conditions at the time of deposition, differences in the diagenetic pathway of shallow-water facies from both sequences also took place.

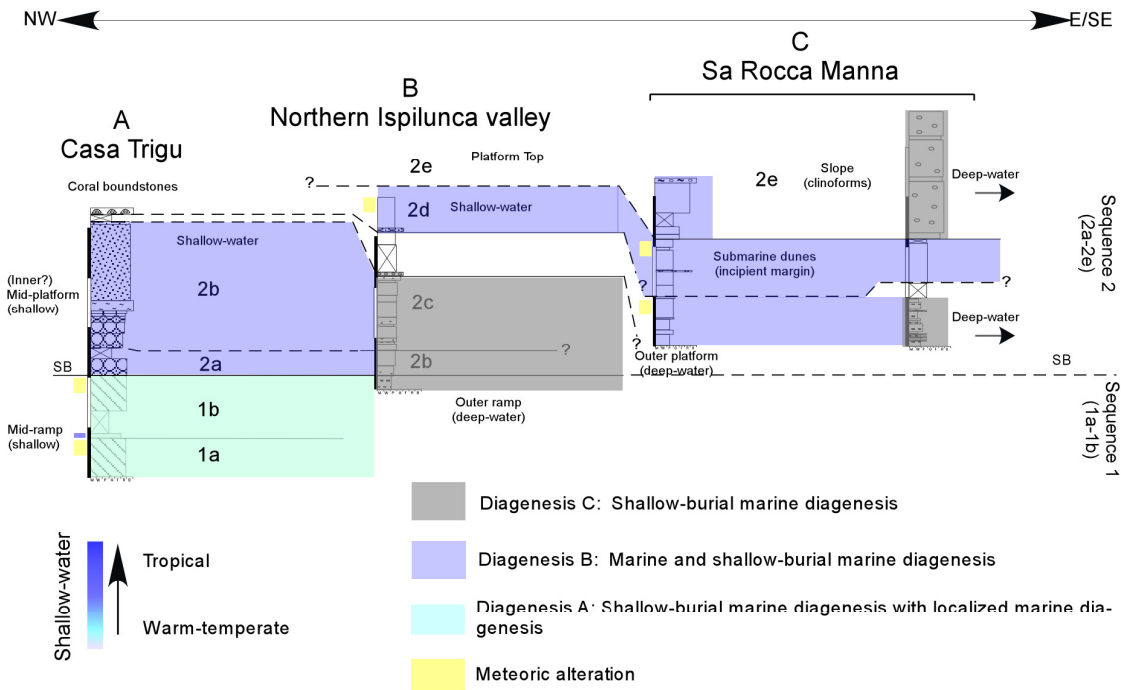


Figure 6.4. Schematic representation of the “Diagenetic facies” within the stratigraphic context.

Shallow-water facies from sequence 1, dominated by a heterozoan biotic association, were lithified later at the shallow-burial marine diagenetic domain. On the other hand, shallow-water facies from sequence 2, progressively dominated by a photozoan association through time, were lithified earlier by marine cements and bladed cementation.

These differences show the different diagenetic potential of the rocks. Shallow-water facies from sequence 1 show similar diagenetic pathway to their heterozoan counterparts (i.e., lack of marine cementation), while shallow-water facies from sequence 2 show similarities with their photozoan counterparts (i.e. early marine cementation); however, cements are only originally Mg-calcite and no meteoric cementation was produced.

## 6.5 Methods

### 6.5.1 Stratigraphic Sections and Sampling

The Sedini Limestone Unit was sampled for bulk-rock oxygen and carbon isotope analysis in shallow- and deep-water facies from both sequences (ramp and platform). Sampling was carried out in different locations and transects (Figs. 6-1B, 6.2 and 6.3): (A) Casa Trigu Transect, (B) Northern Ispilunca Valley Transect, (C) Sa Rocca Manna Transect, (D) Tanca Manna section, (E) Marls, and (F) Sedini south.

Locations (A), (B) and (C) were sampled with a resolution of 1 sample/ 0.5-2 m. Locations (D), (E) and (F) were sampled with a resolution of 1 sample/ 0.2-0.5 m.

Bulk-rock oxygen/carbon isotopic data plotted against stratigraphic vertical and composite profiles is shown in Figure 5. Section (A), Casa Trigu, corresponds to a composite section built from vertically consecutive segments of (Fig. 6.3): S5 (base of the profile belonging to unit S1a-S1b, samples named S3A and S5), S2b and S2c. Section (B) corresponds to a composite section built from vertically consecutive segments of (Fig. 6.3): S6, S7 and S8. Sections from transect (C), Sa Rocca Manna, correspond to the “VT7” section and a composite section built from vertically consecutive segments of (Fig. 6.3): VT2 (base) and C1 (top).



These data provide an overview of the isotopic variability across the different units and depositional facies. These data are displayed in a cross-plot graphic (Fig. 6.6), where they are “keyed” according to the depositional facies and depositional sequence they belong to.

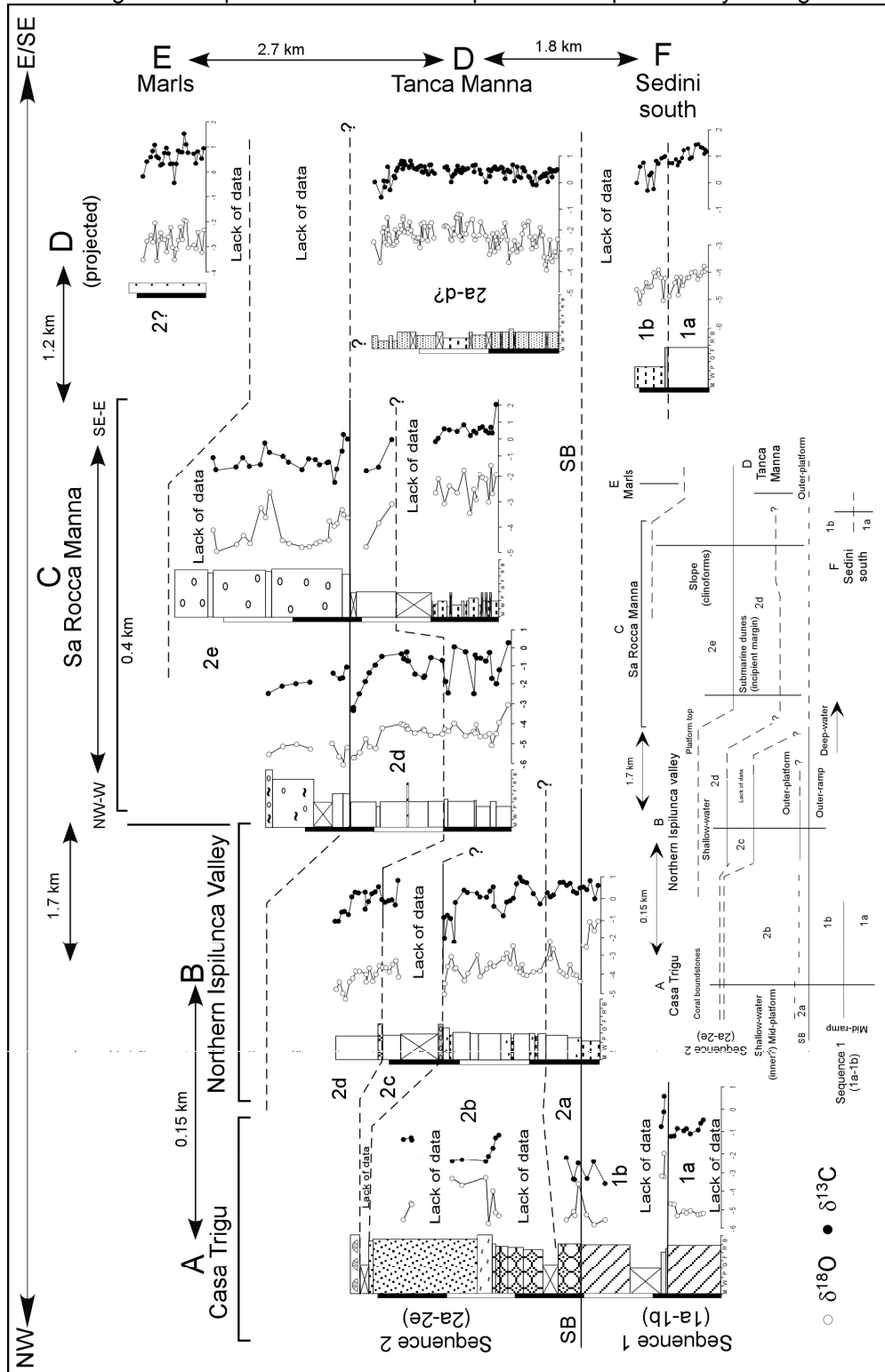


Figure 6.5. Stable isotopic composition measured on bulk samples, plotted against stratigraphic position. Legend captions are the same as Figure 6.3.

## 6.5.2 Analytical Procedures

Powdered material was obtained by normal drilling procedures from a bulk-rock sample. Stable oxygen and carbon isotopes were measured for 323 samples (Tables 6.1 to 6.7, appendix). About 0.2 to 0.3 mg of sample were loaded in a clean and pristine glass and analyzed at the GeoforschungZentrum Potsdam (GFZ), with a DELTA<sup>plus</sup> XL Finnigan MAT 253. Data are reported in per mil versus Vienna Pee Dee Belemnite ( $^0/_{00}$  PDB).

## 6.6 Results

### 6.6.1 Stable Isotopes

Stable isotopic values of bulk  $\delta^{18}\text{O}$  ranged from  $-5,54$   $^0/_{00}$  to  $-1,13$   $^0/_{00}$  for sequence 1 and from  $-5,80$   $^0/_{00}$  to  $-1,13$   $^0/_{00}$  for sequence 2. Stable isotopic values of bulk  $\delta^{13}\text{C}$  ranged from  $-3,40$   $^0/_{00}$  to  $1,25$   $^0/_{00}$  for sequence 1 and from  $-3,30$   $^0/_{00}$  to  $2,06$   $^0/_{00}$  for sequence 2.

**Oxygen and carbon vertical profiles.**  $\delta^{18}\text{O}$  and  $\delta^{13}\text{C}$  values plotted against the stratigraphic profiles show a gradational change towards negative values upsection in both sequence 1 and sequence 2. This tendency is clear in shallow-water facies (Fig. 6.5) rather than in deep-water facies.

The strong amplitude variability of the obtained values in shallower water sediments is related to a mixture of a diagenetic signal with facies variability (e.g. Casa Trigu, Northern Ispilunca valley and Sa Rocca Manna), and the frequency of that combination is less evident towards deeper water sediments (sections D, E and F).

Intervals showing a covariant oxygen and carbon change in amplitude towards heavier values are usually observed above stratigraphic contacts (SB and units). Samples showing positive ( $> 0$ ) and enriched carbon values are only observed at deep-water facies. Samples showing positive ( $> 0$ ) and enriched oxygen values are not observed.

Intervals showing a covariant oxygen and carbon change in amplitude towards lighter values are only observed below stratigraphic contacts (SB and units).

In general we observed that oxygen and carbon values show a higher degree of change in amplitude in sequence 2 than in sequence 1.

**Cross-plots.** In both sequences, samples from shallow-water facies are grouped in areas characterized by depleted oxygen values ranging from  $\sim -1$   $^0/_{00}$  to  $-6$   $^0/_{00}$ , and carbon values ranging from low positive (close to zero) to  $\sim -4$   $^0/_{00}$ . In general, shallow-water facies fall into the burial field of isotope alteration (Nelson and Smith 1996); however, samples close to stratigraphic boundaries or at the platform top (edge, S2e) follow the meteoric line of alteration (Meyers and Lohmann 1985).

Deep-water facies are grouped in areas characterized by depleted oxygen values ranging from  $\sim -1$   $^0/_{00}$  to  $\sim -4$   $^0/_{00}$ , and carbon values ranging from low negative  $\sim -3$   $^0/_{00}$  to positive and enriched values  $\sim + 2$   $^0/_{00}$ . In general, deep-water facies fall into the burial field of isotope alteration (Nelson and Smith 1996); however some samples fall into the interface between the burial and the marine field (grey area, Fig. 6.6). A few samples fall in the marine field with positive carbon but depleted oxygen values.

## 6.7 Discussion

From all sections analyzed (Figs. 6.5 and 6.6) an important observation is that, in general, bulk samples comprise carbonates from different sources. This implies a mixture of skeletal particles (e.g., biotic composition and mineralogy), diagenetic phases, and carbonate matrix (for finer grained rocks). Therefore, interpretation and discussion of the stable isotopic record is indispensable to account first the overprint of diagenesis. After discriminating the effect that diagenesis has had over the isotope record it is then possible to discuss the relationship between the original biotic composition and the preservation or loss of primary marine isotope values.

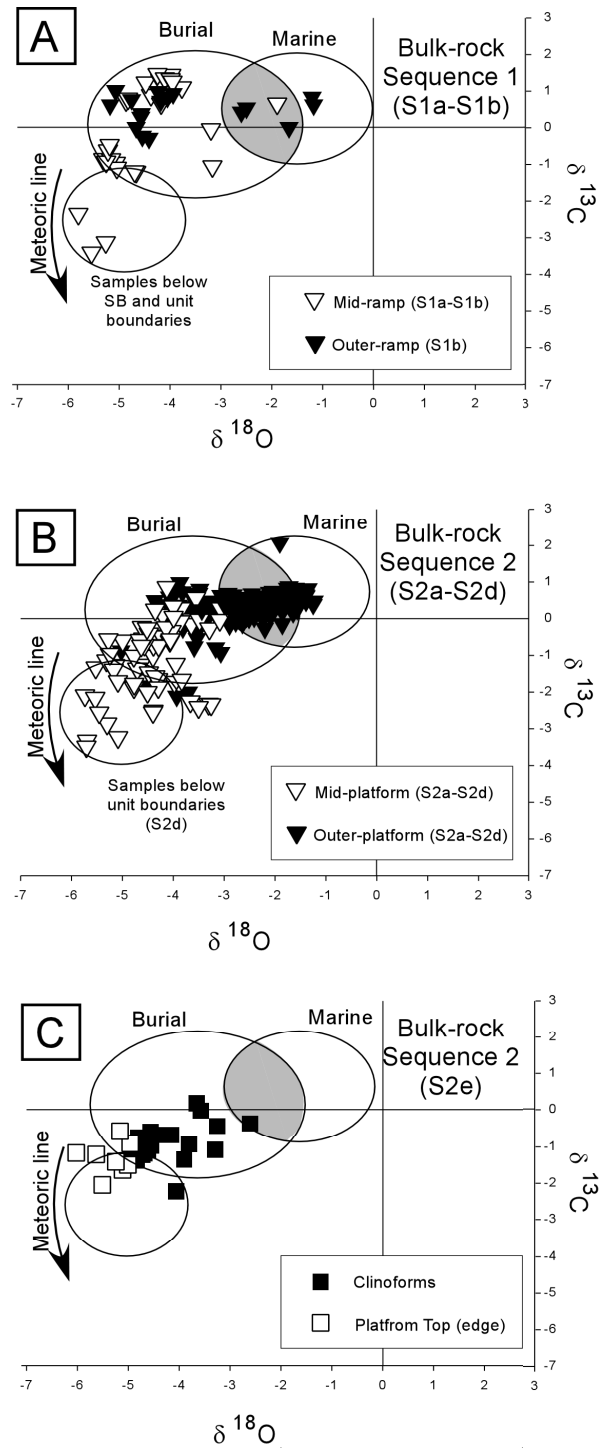


Figure 6.6. Cross-plot of oxygen and carbon isotopic values ( $\delta^{18}\text{O}$ ,  $\delta^{13}\text{C}$ ) of the bulk rock samples. A) sequence 1 (S1a-S1b) values, B) sequence 2 (S2a-d) values, C) sequence 2 (S2e) values.

### 6.7.1 Diagenetic Overprint

Isotope values can be attributed to two major groups: shallower water and deeper water facies. All samples were distributed in a cross-plot (Fig. 6.6) in order to observe tendencies with respect to diagenesis and facies. Isotope values were grouped in three different fields of

diagenetic transformation: marine, burial and meteoric. Field limits are based on Nelson and Smith 1996.

In order to discriminate and discuss the overprint of diagenesis, the oxygen and carbon values were filtered as follows. The exclusion of isotope values because of diagenetic alteration is based on comparison with parameters obtained from the cross-plot graphic. Values inside the burial and marine field with C values  $> -2 \text{ ‰}$  and O  $> -3 \text{ ‰}$  are considered for the evaluation. Those samples with O and C values  $< -2 \text{ ‰}$ , included in the meteoric field, are not used.

Therefore, the oxygen values for consideration [ $\delta^{18}\text{O}$  Bulk rock (f)] are calculated as follows:

$$\Delta o = [\delta^{18}\text{O Bulk rock (i)}] + \gamma \quad (1)$$

if  $\Delta o > 0$ , then:

$$[\delta^{18}\text{O Bulk rock (i)}] = [\delta^{18}\text{O Bulk rock (f)}]$$

Where,  $\gamma$  is  $-3 \text{ ‰}$  or lower limit of acceptance, and  $\Delta o$  is the standard deviation of [ $\delta^{18}\text{O}$  Bulk rock (i)] with respect to  $\gamma$ .

Similarly, the carbon values for consideration [ $\delta^{13}\text{C}$  Bulk rock (f)] are calculated as follows:

$$\Delta c = [\delta^{13}\text{C Bulk rock (i)}] + \lambda \quad (2)$$

if  $\Delta c > 0$ , then:

$$[\delta^{13}\text{C Bulk rock (i)}] = [\delta^{13}\text{C Bulk rock (f)}]$$

Where,  $\lambda$  is  $-2 \text{ ‰}$  or the lower limit of acceptance, and  $\Delta c$  is the standard deviation of [ $\delta^{13}\text{C}$  Bulk rock (i)] with respect to  $\lambda$ .

The values obtained from equations (1) and (2) are summarized in tables 6.1 to 6.7 (appendix). In Figure 6.7, the final oxygen and carbon values ([ $\delta^{18}\text{O}$  Bulk rock (f)] and [ $\delta^{13}\text{C}$  Bulk rock (f)]) are plotted against the stratigraphic profiles.

Figure 6.7 shows that the oxygen isotope values in all shallower water facies (both sequences) and in deeper water facies from sequence 1 were almost completely filtered out and excluded because their values reflect diagenetic rather than primary values. This suggests that most of the samples record altered oxygen marine values. Therefore the significance of primary oxygen marine values is highly reduced and only can be discussed in regards to the deeper water facies of sequence 2 (discussed below).

The carbon isotope record from both sequences has not been completely filtered out. Mostly excluded values are from shallower facies in the Casa Trigu section. Values from shallower to deeper water facies in the other stratigraphic sections remained almost intact and will be discussed later.

In general, shallower and deeper water environments were modified in different diagenetic environments (expressed by different phases of cementation, dissolution and recrystallization, Figure 6.4), which constitutes the main factor for the transformation of the oxygen isotope signature.

$\delta^{18}\text{O}$  primary values depend mainly on the temperature during precipitation and the isotopic composition of the fluid from which the carbonate precipitates (Morse and Mackenzie 1990). All samples in both sequences follow a burial diagenetic trend of alteration (Fig. 6.6) and show evidence of shallow-burial marine cementation (syntaxial inclusion-poor and blocky calcite cement, Chapter 5). Therefore, bulk-rock oxygen stable isotopes carry an isotopic signature significantly lighter in  $\delta^{18}\text{O}$  due to shallow-burial marine diagenesis, which modifies the primary, marine isotopic values.

It is surprising that in sequence 1 the oxygen values were almost all excluded. Considering that the carbonate sediments are dominated by a heterozoan association, it would be expected that oxygen values remain closer to the original marine values because of the lack of marine cementation and low-Mg calcite mineralogy (Mutti et al. 2006). However, this is not the case, and as previously mentioned, factors like recrystallization and burial cementation from the influence of external fluids control the oxygen isotope values. The same explanation could be also applied to the exclusion of the oxygen values in sequence 2; however, early diagenetic processes like marine cementation, recrystallization (localized meteoric and burial) and higher

amount of shallow-burial marine cementation (e.g. bladed) must have contributed to the loss of primary oxygen marine values mostly in the shallower water facies.

The oxygen values in deeper water environments from sequence 2 need a different explanation. Values are included at and within the burial to marine fields of diagenetic transformation in figure 6.6. However, they are negative. This suggests the action of two possible factors. First, the oxygen values are composed mainly by a stable mineralogy (low-Mg calcite); and second, their diagenetic transformation (e.g. alteration into low-Mg calcite) occurred in a closer geochemical system, which has a minimal influence (at least) on the  $\delta^{13}\text{C}$  (Swart 2000, Melim et al. 2001). The trend observed for the  $\delta^{18}\text{O}$  (figure 6.6) most probably represents the normal and uninterrupted burial of these sediments.

### 6.7.2 Primary Marine Signatures

After filtering the data with respect to diagenesis, some of the oxygen and carbon isotope values from both sequences remained valid. Oxygen values are exclusively related to deeper water facies. Carbon values are mostly found in shallower to deeper water facies of the platform, which are partially modified. Therefore, further analysis has to be made in order to determine whether primary marine values exist and their significance.

In order to distinguish if our data includes primary marine signatures linked to secular variations, values obtained from equation (1) and (2) or isotope values [ $\delta^{18}\text{O}$  Bulk rock (f) and  $\delta^{13}\text{C}$  Bulk rock (f)] from each stratigraphic section were filtered as follows. Values that show a variance of  $> 0,5 \text{ ‰}$  with respect to the average (named as:  $\sigma$  Value O and  $\sigma$  Value C, Table 6.1 to 6.8, appendix), and conversely those that show a major variance with respect to the minimum value ( $\Delta$  Value, Table 6.1 to 6.8, appendix), were considered for the interpretation.

The variance of  $> 0,5 \text{ ‰}$  with respect to the average is based on the fact that  $\delta^{18}\text{O}$  peaks previously identified in the literature as global variations (e.g. Mi events) usually show stepwise increments of  $0,5 \text{ ‰}$  to more than  $1 \text{ ‰}$  with respect to a reference curve (Miller et al. 1991, Wright and Miller 1992). Therefore, if we are looking for an oxygen-carbon covariant trend that reflects a secular change, then the  $\delta^{18}\text{O}$  values (at least) should show a variance of  $> 0,5 \text{ ‰}$  with respect to the main isotopic curve used in this study.

The resulting values, after filtering, are the absolute values of possible peak maxima, which can be compared with recorded events already described in the literature (e.g., Mi events and CM events). Table 6.8 (appendix) shows the results ( $\sigma$  Values and  $\Delta$  Values), and peak maxima, which are plotted in Figure 6.7 by a single gray band. Carbon and oxygen isotope values are evaluated as follows.

**Carbon values.** In our data set, the majority of carbon peaks are included in sequence 2, and usually confined to deep-water facies.

The carbon peaks in deep-water environments from both sequences can be found in tables 6.1 to 6.8 (appendix). Figure 6.8-A shows the carbon and oxygen record plotted against the original data from Tables 6.1 to 6.7 (appendix) and Figure 6.8-B shows the relevant peaks obtained from Tables 6.1 to 6.8 (appendix).

It is known that major temporal variations in mean ocean  $\delta^{13}\text{C}$  are related to the redistribution between two different carbon reservoirs (Vincent and Berger 1985): carbon deposited as organic carbon and inorganic carbon (calcium carbonate) in the ocean. During the late early (Burdigalian) to Middle Miocene (Langhian-Serravallian) a major maxima in mean ocean  $\delta^{13}\text{C}$  occurred, termed the Monterrey Carbon Isotope Excursion (Vincent and Berger 1985). The nature of this excursion has been attributed to the storage of large volumes of organic carbon in the Monterrey Formation of California, circum-North Pacific and the southeastern shelf of North America. It is postulated as the major contributor for global cooling through drawdown of atmospheric  $\text{CO}_2$  (Vincent and Berger 1985). In addition to the Monterrey hypothesis (OME) shorter-term carbon excursions during the Miocene have been recognized, named CM1 to CM7 (Woodruff and Savin 1989).

In Miocene examples from Mediterranean areas (Figure 6.8-C) the OME and shorter-term carbonate excursions have been recorded and identified from bulk-rock samples (Figure 6.8-C)

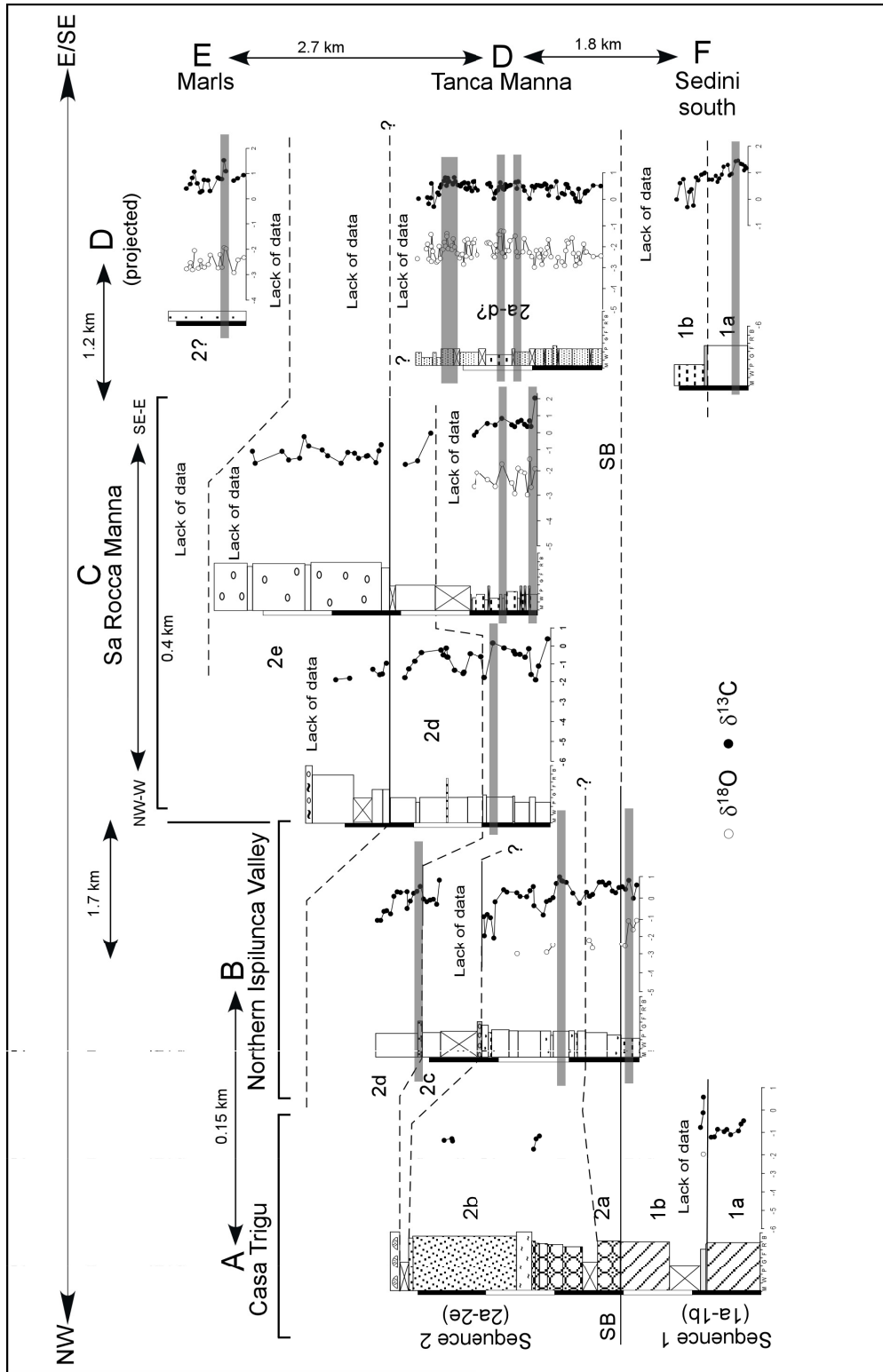


Figure 6.7. New oxygen and carbon stratigraphy after filtering the diagenetic overprint. Grey band indicate possible carbon peaks.

(John et al. 2003, Mutti et al. 2006). At least three peaks (CM1 to CM3) during Burdigalian to Langhian times are recognized. The OME occurred during the early Burdigalian. The CM1 peak

occurred during the late Burdigalian. The CM2 and CM3 occurred in the Langhian. CM2 and CM3 have been identified in marlstone units. However, the identification of the OME and the CM excursions matches with precise stratigraphic ages, sedimentation rates (e.g., John et al. 2003), and complete stratigraphic sections.

In our data, the presence of the OME and CM excursions can only be inferred and argued based on the appearances of major peaks, and variances with respect to the average ( $\sigma$  Value C, Table 6.1 to 6.8, appendix), and with respect to the minimum value ( $\Delta$  Value, Table 6.1 to 6.8, appendix). However, two important factors have to be taken in account: (1) in both sequences, the stratigraphic contacts among the deeper water facies are not exposed in the field (sections D, E and F), and (2) both sequences comprise rocks considered as Burdigalian in age. It is only the stratigraphic section named as “E-Marls” (Fig. 6.3), which could represent a major deepening of the basin and thus be labeled Langhian (?) in age. Therefore, comparing our values (Table 6.8, appendix, Figure 6.8-B) with data in the literature (Figure 6.8-C) the location of the OME could be at the base of the sequence 1 and the CM2?-CM3? Excursions could be at the base of the section E or Marls. The peak CM1 is difficult to infer because of the lack of stratigraphic contact between the deep-water D and F sections (Figure 6.8).

However, the existence of the OME and CM excursions in our carbon record is not final and can be argued as follows.

It is has been observed that in Mediterranean areas carbon maxima (OME, CM) occurred at times where reduced accumulation of neritic carbonates have been identified (e.g., sedimentation rates of  $\sim 1$  m/m.y. and  $< 10$  m/m.y. (John et al. 2003), in relation with drowning events, condensed or phosphate levels (Mutti et al 2006). In addition, these carbon maxima occur at times where carbonates reflect higher levels of trophic resources resulting in a world wide (high latitude) distribution of heterozoan carbonate settings rich in coralline algae (Halfar and Mutti 2005) and the lack of photo-dependent organisms (e.g., corals). In addition, these carbon peaks are found to be covariant with enriched oxygen peaks.

In our case, if OME is present in the carbon record from the heterozoan-dominated ramp, then carbon values should be covariant with positive tendencies in the oxygen record (e.g. John 2003), and associated with the exclusiveness of a heterozoan skeletal association, which, in the end, is not our case (Chapter 4). Therefore, the positive carbon values found at the deeper water facies at the base of the sequence 1 most probably reflect local changes in the carbon budget by the settlement of the carbonate system rather than a perturbation in the global carbon cycle.

Additionally, at the platform deep-water facies, carbon peaks are observed more frequently, and they usually show covariance with the oxygen record, even though the latter does not show positive values. However, if the age of the rocks is correct, those corresponding to Burdigalian in age (e.g., Units S2a-d, section D, Figure 6.7) could yield values related to the CM1 event (?); and those corresponding to Langhian (?) in age, represented exclusively by marls, could yield values related to the CM2 or CM3 event (Figure 6.8). The possibility of the previous will be discussed below.

**Oxygen values.** As previously mentioned, the oxygen stable isotopic record of shallower water environments has been completely resettled by diagenesis. Even values from deep-water facies in sequence 1 are completely biased, showing negative values (Figure 6.8-A). Only the values from deep-water facies from sequence 2 can be analyzed and discussed (Figure 6.8).

We note that, significant  $\delta^{18}\text{O}$  increases have been identified in the benthic foraminiferal records from the Miocene (Miller et al. 1991, Wright and Miller 1992) classified as Mi zones. Primary, these are related to the intensification of continental glaciation in Antarctica (Savin and Woodruff 1990) or to an increase in deep-water cooling (Prentice and Matthews 1988). These  $\delta^{18}\text{O}$  increases have been identified to be coeval with the variability of increased organic carbon burial (Vincent and Berger 1985), which is reflected as an enriched (positive peaks) and covariant isotope record.

During the Middle Miocene times (Langhian), a  $\delta^{18}\text{O}$  increment is observed and named as Mi2. For example, in bulk-rock samples (marls) from the Globigerina Limestone Formation at the Maltese Islands (Figure 6.8-C), the Mi2 peak records the first step of the Middle Miocene cooling in parallel with high fluxes of terrigenous material (John et al. 2003), suggesting long-term change in weathering, from warm arid to warm humid conditions.

**B**

Section/Sample	$\Delta$	Isotope	Peak value	Name of the event	Age
Marls/SM-3.0	1,97	Carbon	1,54	CM3? - CM2?	Base Langhian?
Tanca Mana/Q-24.4	2,55	Oxygen	-1,35	?	Burdigalian
Sedini South/S4ALDO-4.45	1,76	Carbon	1,47	OME?	Burdigalian

**C**

Location	Stratigraphy	Paleoenvironment	$\Delta$	Isotope	Peak value	Name of the event	Age	Reference
Maltese Islands	Globigerina Limestone Formation	Slope	0,5	Carbon	1,2	CM3	15.5	John et al. (2003)
			0,7	Carbon	0,9	CM2	15.8	
			1,5	Oxygen	1,5	Mi2	16.1	
			0,7	Carbon	0,5	CM1	16.4	
				Carbon	-0,2	OME	18	
Maiella (Abruzzi Italy)	Upper Bryozoan Ls.	Outer ramp	?	Carbon	1.6 +/- 0.3	OME	18	Mutti et al. (2006)

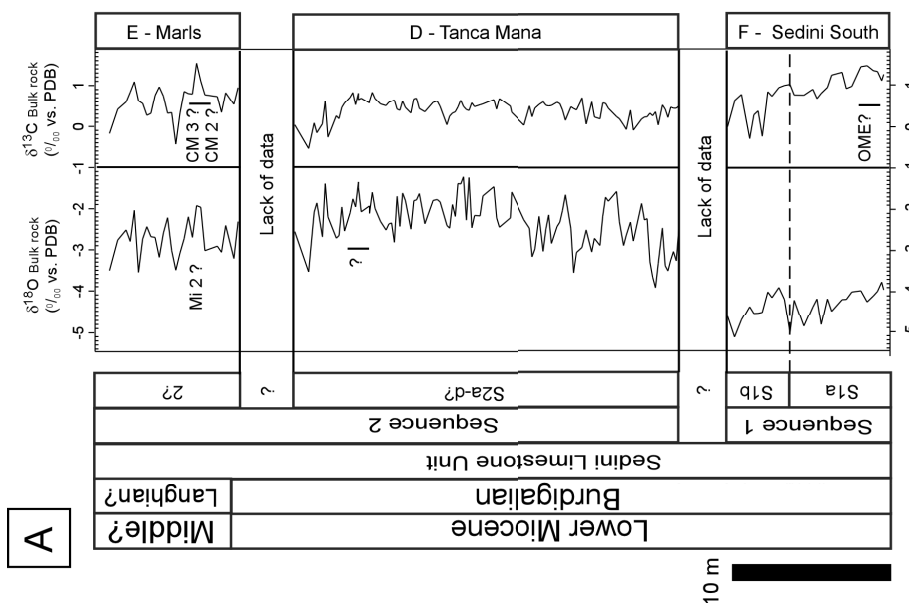


Figure 6.8. Deep-water stable isotope record. A- Study area showing vertical profiles of deep-water section: D, E, and F. B- Table showing possible events. C- Events measured in bulk rock samples from Miocene Mediterranean examples.

In our study area, the recognition of  $\delta^{18}\text{O}$  peaks is not only greatly reduced by diagenesis but also by the lack of the stratigraphic contact among the deep-water stratigraphic columns described in the area. Moreover, if the Mi peaks are coeval with carbon increases, our study can only address those at the Sa Rocca Manna transect (base), section D, and section E (Figure 6.7).

In units S2a-d, it is particularly noticed that the lateral change of facies towards deeper water environments (section D) show carbon and oxygen values that tend to be more covariant. However, carbon values are positive and oxygen values are negative.

We observed only one peak of oxygen and carbon that is covariant and shows a variance of  $> 0,5 \text{ ‰}$  with respect to the average. This peak is located at the marls or section E. If the Mi2 peak is considered to be found during Langhian times and in relation with marls, then the one observed in the section E could be in response to a global event. However, care must be taken because a detailed age determination is needed and the lower stratigraphic contact is not exposed.



### 6.7.3 Lessons Learned

Whole-rock isotopic data should be used with caution when studying isotopic signatures. Interpreting primary signals from shallow- and deep-water facies without a detail diagenetic analysis can lead to misinterpretations and erroneous chronostratigraphic significance. Key features that have to be recognized are the different biotic associations (heterozoan vs. photozoan), the original mineralogy and the depositional environment. In addition, a stratigraphic framework as a reference is essential. With this awareness, the significance of the stable isotope signature can be better assessed in light of a proper diagenetic history.

As mentioned during the discussion, O and C isotope excursions in marine carbonates are commonly interpreted as evidence of global perturbations (temperature and nutrient), which in turn is thought to be linked to global events such as sea-level fluctuations and/or climatic changes. If those excursions are identified in deep-water environments, along with strong age determinations in complete sections, then chronostratigraphic significance can be stated, and in certain instances traced into their shallow-water counterparts. If not, reasons such as diagenesis and/or a mix of carbonates having different mineralogies, and thus different isotopic signatures, can break down the correlation and the interpretation.

The previous statement is applicable to this work. With the exception of selected stratigraphic surfaces from shallow-water sections, which have been influenced by meteoric fluids (Chapter 5), the carbon and oxygen isotopic signatures from the ramp and platform sediments lie between the burial and marine diagenetic field (Figure 6.6). Early diagenesis has radically changed the O isotopic signature in both depositional sequences and no primary values (until now) can be properly interpreted. Surprisingly, the previous holds true independent of the change from a heterozoan-dominated ramp into a photozoan-dominated platform and in almost all depositional environments. We believe this to be a result of shallow-burial marine diagenesis (Figure 6.4) which changes the mineralogy (recrystallization and cementation) without significantly influencing the  $\delta^{13}\text{C}$  value of the sediment.

The reason for the changes in  $\delta^{13}\text{C}$  (peaks) with respect to time and sequences has to be further analysed. This is supported by the comparison between the data and time interval presented in this study and Miocene data from the Mediterranean (Figure 6.8-C, John et al. 2003). Possibilities are: (1) local environmental changes, (2) global perturbations marked as OME and CM (at least at the marls section).

## 6.8 Conclusions

(1) The oxygen and carbon stable isotope stratigraphy presented in this study records isotopic signatures which have been almost entirely resettled by diagenesis. Analyzing the influence of diagenesis along with original mineralogy and stratigraphy made it possible to argue influences of local environmental or global controls over the isotope record in deep-water facies. The basis is aided by the fact that the isotopic record is facies-dependent, which helped us to recognize and discriminate the causes of the isotopic changes.

(2) In general, this heterozoan-photozoan carbonate setting shows low preservation of primary marine signatures, and the main reason is the early diagenesis that resettled the oxygen bulk-rock signature. However, we notice that the carbon record has not been highly biased and the differential signatures along with their frequency are different from the ramp to the platform geometry.

(3) In order to clarify whether secular changes exist at the deep-water environments, we recommend a detailed age determination coupled with isotopes values obtained from the matrix fraction or calcitic biota such as benthonic or planktonic foraminifers. This would further clarify whether or not heterozoan-photozoan carbonate systems faithfully record global events typical for the Miocene and therefore can be used for stratigraphic purposes.

## - CHAPTER 7 - CONCLUSIONS

A main general question of this work was to determine how is the diagenesis of shallow-water warm-temperate to tropical carbonates, and how it impacts facies and the resulting chemostratigraphic signal. Special emphasis was put on the evaluation of types and amount of early cementation within a facies and stratigraphic framework. Three key questions were investigated:

- (1) How is the facies and sediment composed? Does early (marine) cementation exist? If yes, does it contribute to facies stabilization and the resulting basin geometry?
- (2) Is there a unique diagenetic pathway? When and where did cementation occur?
- (3) If the chemostratigraphic signal is resettled by diagenesis, then what are the reasons? Can we find primary marine global signals?

From chapter 4, field and detail petrographic analysis led to the determination of a carbonate setting characterized by a transitional type of biotic association (heterozoan/photozoan). It is apparent that along with the temporal and gradual change from a heterozoan-dominated into a photozoan-dominated carbonate setting, the depositional profile changes from a ramp into a steep-flanked platform. We argued that this transition indicates a change in the depositional environmental conditions, such as water temperature where it changes from warm-temperate to tropical. Moreover, marine cementation, which is only high-Mg calcite, becomes abundant in the latest stages of platform growth. It is suggested that early lithification gradually stabilizes the shallower facies at the platform stage, which contributes to the steepening of the depositional profile.

From chapter 5, detail petrographic and geochemical analyses (oxygen and carbon stable isotopes and trace elements) of the different cement phases linked to facies and stratigraphy allowed the determination of different diagenetic pathways and environments for transformation. The diagenetic history shows that these rocks evolved from a marine to a shallow-burial marine with localized meteoric alteration. At the marine environment, precipitation of high-Mg calcite micritic, fibrous, and syntaxial inclusion-rich cements occurred directly from marine waters. Shallower facies located close and beneath stratigraphic boundaries were affected by meteoric fluids, which led to fabric-selective dissolution (grains and syntaxial inclusion-rich cement) and recrystallization without low-Mg calcite cementation. At the shallow-burial marine environment, low-Mg calcite cementation occurred and temporarily in this order: bladed, syntaxial inclusion-poor and blocky calcite cements. It appears that dissolution of grains and recrystallization is also produced at the shallow-burial marine environment (shallow- to deep-water facies); however at strata away from the effect of the influence of meteoric fluids. Chemical compaction was mild without causing significant contribution of  $\text{CaCO}_3$  for calcite cementation. When rocks were exposed to current condition (uplift), locally non-fabric-selective dissolution was produced (at the platform facies).

The amount and distribution of cements and fabric-selective dissolution features showed that at the ramp (heterozoan-dominated setting), shallower facies lack marine cementation and porosity is reduced by compaction and late post-depositional low-Mg calcite cementation (syntaxial inclusion-poor and blocky cements). Conversely, at the platform (photozoan-dominated setting) shallower facies are rich in marine cements (occluding primary porosity) and secondary porosity is created. Furthermore, along with the change of depositional geometry we see the (temporarily) gradual increment of early late-postdepositional low-Mg calcite cementation

(bladed), which could probably be associated with the appearance of metastable grains (e.g., aragonite).

From chapter 6, the analysis and comparison of detailed geochemical analyses (oxygen and carbon stable isotopes), obtained from shallower to deeper water facies, with diagenesis and stratigraphy, indicate that shallow-burial marine diagenesis has strongly resettled the isotope values. However, the carbon isotopic record preserves positive values, which are usually observed in the platform depositional setting and are probably related to primary marine signals. These carbon values show the contrast that exists in the isotope record from the ramp to the platform; however, it is assumed that diagenesis has broken down the correlation of the positive values from the deeper water facies with respect to their shallower counterparts.

The result of this work clearly show that in carbonate settings characterized by a transitional type of biotic association (heterozoan/photozoan) and deposited under warm-temperate to tropical conditions, rocks do not follow a diagenetic pathway strictly similar to their photozoan nor heterozoan counterparts. It is actually different, and special attention should be paid when comparing them to the known non-tropical examples existent in the literature.

The results of this study hold an important implication for the oil industry. The evolution of pore networks is highly dependent on the original mineralogy of the components. These shallow-buried rocks show that the evolution of pore networks is controlled by mechanical compaction when rocks are heterozoan-dominated and by fabric-selective dissolution when photozoan-dominated. Usually, when rocks containing metastable mineralogies are modified by meteoric fluids, effective secondary porosity (connected) and low-Mg calcite cementation are developed. In this study, moldic pores are not connected (low permeability, Chapter 5) and low-Mg calcite cementation is developed later at the shallow-burial marine diagenetic environment.

## -REFERENCES AND LITERATURE-

ALBERTSEN, J.C, 2005, Kartierung des Miozäns bei Sedini and Fazies miozäner Karbonate bei Sedini/Nordsardinien: Diplomarbeit, Universität Hamburg, 86, p.

ALLAN, J. R., AND MATTHEWS, R.K., 1982, Isotope signatures associated with meteoric diagenesis: *Sedimentology*, v. 29, p. 797-817.

ARNAUD, M., MAGNÉ, J., MONLEAU, C., NÉGRETTI, B., AND OGGIANO, G, 1992, Nouvelle données sur le Miocène du Nord-Ouest de la Sardaigne (Italie): *C. R. Acad. Sc. Paris*, 315 II, no. 8, p. 965-970.

ASSORGIA, A., BARCA, S., AND SPANO, C. 1997, A synthesis on the Cenozoic stratigraphic, tectonic and volcanic evolution in Sardinia (Italy): *Buletino Della Società Geologica Italiana*, v. 116, p. 407-420.

BATHURST, R.G.C, 1975, Carbonate sediments and their diagenesis: Amsterdam, Elsevier, p. 658.

BENISEK, M-F., MARCANO, G., BETZLER, C., AND MUTTI, M., (Unpublished IAS Special Publication, in press.), Facies and stratigraphic architecture of a Miocene warm-temperate to tropical fault-block carbonate platform in Sardinia (Central Mediterranean Sea).

BETZLER, C., BRACHERT, T.C., AND NEBELSICK, J, 1997, The warm temperate carbonate province. A review of the facies, zonations, and delimitations: *Courier Forschungsinstitut Senckenberg*, v. 201, p. 83-99.

BONE, Y., AND JAMES, N.P., 1993, Bryozoans as carbonate sediment producers on the cool-water Lacedpede Shelf, southern Australia: *Sedimentary Geology*, v. 86, p. 247-271.

BOSENCE, D. W. AND H. M. PEDLEY, 1982, Sedimentology and palaeoecology of a Miocene coralline algal biostrome from the Maltese Islands: *Palaeogeography, Palaeoclimatology, Palaeoecology*, v. 38, p. 9-43.

BOSENCE, D. W. J., 1983, The occurrence and ecology of recent rhodoliths - a review, *in*: Peryt, T.M, eds. *Coated Grains*, Heidelberg, Springer-Verlag, p. 225-241.

BOURROUILH-LE JAN, F.G., AND HOTTINGER, L.C., 1988, Occurrence of rhodoliths in the tropical Pacific- a consequence of Mid-Miocene paleo-oceanographic change: *Sedimentary Geology*, v. 60, p. 355-367.

BRACHERT, T.C., AND DULLO, W.C.-, 2000, Shallow burial diagenesis of skeletal carbonates: selective loss of aragonite shell material (Miocene to Recent, Queensland Plateau and Queensland Trough, NE Australia)- implications for shallow cool-water carbonates: *Sedimentary Geology*, v. 136, p. 169-187.

BRACHERT, T.C., BETZLER, C., BRAGA, J.C., AND MARTIN, J.M., 1996, Record of climatic change in neritic carbonates: turnover in biogenic associations and depositional modes (Late Miocene, southern Spain): *Geologische Rundschau*, v. 85, p. 327-337.

BRACHERT, T.C., BETZLER, C., BRAGA, J.C., AND MARTIN, J.M., 1998, Micro-taphofacies of a warm-temperate carbonate ramp (upper Miocene, S-Spain): *Palaios*, v. 13, p. 459-475.

BRACHERT, T.C., HULTZSCH, N., KNOERICH, A.C., KRAUTWORST, U.M.R., AND STÜCKARD, O.M, 2001, Climatic signatures in shallow-water carbonates: high-resolution

stratigraphic markers in structurally controlled carbonate buildups (Late Miocene, southern Spain): *Palaeogeography, Palaeoclimatology, Palaeoecology*, v. 175, p. 211–237.

BRAGA, J. C., AND J. AGUIRRE, 1995, Taxonomy of fossil coralline algal species: Neogene Lithophylloideae (Rhodophyta, Corallinaceae) from southern Spain: Review of Palaeobotany and Palynology, v. 86, p. 265-285.

BRAGA, J. C., AND J. AGUIRRE, 2001, Coralline algal assemblages in upper Neogene reef and temperate carbonates in Southern Spain: *Palaeogeography, Palaeoclimatology, Palaeoecology* v. 175, p. 27-41.

BRAGA, J. C., AND J. M. MARTIN, 1996, Geometries of reef advance in response to relative sea-level changes in a Messinian (uppermost Miocene) fringing reef (Cariatiz reef, Sorbas Basin, SE Spain): *Sedimentary Geology*, v. 107, p. 61-81.

BRANDANO, M., AND CORDA, L., 2002, Nutrients, sea level and tectonics: constraints for the facies architecture of a Miocene carbonate ramp in central Italy: *Terra Nova*, v. 14, p. 257-262.

BUDD, D. A. 1988, Aragonite-to-calcite transformation during fresh-water diagenesis of carbonates: Insight from pore-water chemistry: *Geological Society of America Bulletin*, v. 100, p. 126-127.

BUDD, D. A., AND L. S. LAND 1990, Geochemical imprint of meteoric diagenesis in Holocene ooid sands, Schooner Cays, Bahamas: Correlation of calcite cement geochemistry with extant ground waters: *Journal of Sedimentary Petrology*, v. 60, p. 361-378.

BURCHETTE, T.P., AND WRIGHT, V.P., 1992, Carbonate ramp depositional systems: *Sedimentary Geology*, v. 79, p. 3-57.

CARANNANTE, G., ESTEBAN, M., MILLIMAN, J.D., AND SIMONE, L., 1988, Carbonate lithofacies as paleolatitude indicators: problems and limitations: *Sedimentary Geology*, v. 60, p. 333-346.

CARANNANTE, G. AND SIMONE, L., 1986, Rhodolith facies in the central-southern Apennines Mountains, Italy, *in*: Franseen, E.K., Esteban, M., Ward, W.C., Rouchy, J.-M eds. Models for carbonate stratigraphy from Miocene reef complexes of Mediterranean regions, Tulsa, Oklahoma, 5, p. 261-275.

CARMIGIANI, L., BARCA, S., OGGIANO, G., PERTUSATI, P.C., SALVADORI, I., CONTI, P., ELTRUDIS, A., FUNEDDA, A. AND PASCI, S., 2001, Memorie descrittive della carta geologica d'Italia Volume IX: Note illustrativa Della Carta Geologica della Sardegna in scala 1:200.000, *in*: Presidenza del Consiglio dei Ministri, Dipartimento per i Servizi Tecnici Nazionali, Servizio Geologico Nazionale, p. 283.

CHAFETZ, H.S., 1986, Marine peloids: a product of bacterially induced precipitation of calcite: *Journal of Sedimentary Petrology*, v. 56 (6), p. 812-817.

CHERCHI, A., AND MONTADERT, L. 1982, Oligo-Miocene rift of Sardinia and the early history of the Western Mediterranean Basin: *Nature*, 298: 736-739.

CHERNS, L., AND WRIGHT, V.P., 2000, Missing mollusks as evidence of large-scale, early skeletal aragonite dissolution in a Silurian sea: *Geology*, v. 28, p. 791-794.

COLLINS, L. B., FRANCE, R. E., ZHU, Z. R., AND WYRWOLL, K-H, 1997, Warm-water Platform and cool-water shelf carbonates of the Abrolhos shelf, southwest Australia, *in*: James, N.P. and Clarke, J.A.D. eds. Cool-water carbonates: Tulsa, Oklahoma, SEPM, 56, p. 23-36.

COLLINS, L. B., READ, J.F., HOGARTH, J.W., AND COFFEY, B.P., 2006, Facies, outcrop gamma ray and C-O isotopic signature of exposed Miocene subtropical continental shelf carbonates, North West Cape, Western Australia: *Sedimentary Geology*, v. 185, p. 1-19.

CORDA, L., AND M. BRANDANO, 2003, Aphotic zone carbonate production on a Miocene ramp, Central Apennines, Italy: *Sedimentary Geology*, v. 161, p. 55-70.

DICKSON, J.A.D., 1965, A modified staining technique for carbonates in thin section: *Nature*, v. 205, p. 587.

DERCOURT, J., M. GAETANI, VRIELYNCK, B., BARRIER, E., BIJU-DUVAL, B., BRUNET, M.F., CADET, J. P., CRASQUIN, S., AND SANDULESCU, M., 2000, Atlas Peri-Thethys, palaeogeographical maps, Paris, CCGM/CGMW, p. 1-269.

DODD, J. R., AND C. S. NELSON, 1998, Diagenetic comparisons between non-tropical Cenozoic limestones of New Zealand and tropical Mississippian Limestones from Indiana, USA: Is the non-tropical model better than the tropical model?: *Sedimentary Geology*, v. 121, p. 1-21.

EHRENBERG, S. N., PICKARD N. A. H., et al., 2002, Cement geochemistry of Photozoan carbonate strata (Upper Carboniferous - Lower Permian), Finmark carbonate platform, Barent Sea: *Journal of Sedimentary Research*, v. 72(1), p. 95-115.

EHRENBERG, S. N., 2004a, Porosity and permeability in Miocene carbonate platforms on the Marion Plateau, offshore NE Australia: Relationships to stratigraphy, facies and dolomitization, *in*: Braithwaite, C.J.R., Rozzi, G. and Darke, G., eds. The geometry and petrogenesis of dolomite hydrocarbon reservoirs: Geological Society (London) Special Publication, 235, p. 233-253.

EHRENBERG, S. N., 2004b, Factors controlling porosity in Upper Carboniferous-Lower Permian carbonate strata of the Barents Sea: *American Association of Petroleum Geologists*, v. 88 (12), p. 1653-1676.

ESTEBAN, M., 1996, An overview of Miocene reefs from the Mediterranean areas: general trends and facies models, *in*: Franseen, E.K., Esteban, M., Ward, W.C., and Rouchy, J.-M., eds. Models for carbonate stratigraphy from Miocene reef complexes of the Mediterranean region: Tulsa, Oklahoma, SEPM, 5, p. 3-55.

FACCENNA, C., SPERANZA, F., D'AJELLO CARACCILO, F., MATTEI, M. AND OGGIANO, G., 2002, Extensional tectonics on Sardinia (Italy): insights into arc-back-arc transitional regime: *Tectonophysics*, v. 356, p. 213- 232.

FUNEDDA, A., OGGIANO, G. AND PASCI, S., 2000, The Logudoro basin: a key area for the Tertiary tectono-sedimentary evolution of North Sardinia: *Bolletino della Società Geologica Italiana*, v. 119, p. 31-38.

FLÜGEL, E. 2004, *Microfacies of carbonate rocks*: Springer, p. 976.

FORNOS, J.J., AND AHR, W.M., 1997, Temperate carbonates on a modern, low-energy, isolated ramp: The Balearic Platform, Spain: *Journal of Sedimentary Research*, v. 67 (2), p. 364-373.

GIENAPP, H.P. 2005, Die miozänen Karbonate im Gebiet Nulvi, Region Anglona (N-Sardinien), Diplomarbeit, Universität Hamburg, 78 p.

- GRÖTSCH, J., BILLING, I., AND VAHRENKAMP, V., 1998, Carbon-isotope stratigraphy in shallow-water carbonates: implications for Cretaceous black-shale deposition, *Sedimentology*, v. 45, p. 623-634.
- HALFAR, J., GODINEZ-ORTA, L., AND INGLE JR., J. C., 2000, Microfacies analysis of Recent carbonate environments in the southern Gulf of California, Mexico: a model for warm-temperate to subtropical carbonate formation: *Palaios*, v. 15, p. 323-342.
- HALFAR, J., AND INGLE JR., J. C., 2003, Modern warm-temperate and subtropical shallow-water benthic foraminifera of the southern Gulf of California, Mexico: *Journal of Foraminiferal Research*, v. 33 (4), p. 309-329.
- HALFAR, J., GODINEZ-ORTA, L., MUTTI, M., VALDEZ-HOLGUIN, J. E., AND BORGES, J. M., 2004, Nutrient and temperature controls on modern carbonate production: an example from the Gulf of Mexico: *Geology*, v. 32, p. 213-216.
- HALLOCK, P., HINE, A.C., VARGO, G. A., ELROD, J. A., AND JAAP, W. C., 1988, Platforms of the Nicaraguan Rise: Examples of the sensitivity of carbonate sedimentation to excess trophic resources: *Geology*, v. 16, p. 1104-1107.
- HALLOCK, P., AND W. SCHLAGER, 1986, Nutrient excess and the demise of coral reefs and carbonate platforms: *Palaios*, v. 1, p. 389-398.
- HARRIS, P. M., KENDALL, C. G. ST. C., AND LERCHE, I., 1985, Carbonate cementation – A brief review, *in*: Schneidermann, N., and Harris, P, eds. *Carbonate Cements*: Tulsa, Oklahoma, SEPM., 36, p. 79-95.
- HOOD, S. D., AND NELSON, C.S., 1996, Cementation scenarios for New Zealand Cenozoic nontropical Limestones: *New Zealand Journal of Geology and Geophysics*, v. 39, p. 109-122.
- HOPKINS, J.C., 1999, Characterization of Reservoir Lithologies within Subunconformity Pools: Pekisko Formation, Medicine River Field, Alberta, Canada: *American Association of Petroleum Geologists*, v. 83-11, p. 1855-1870.
- HOTTINGER, L., 1997, Shallow benthic foraminiferal assemblages as signals for depth of their deposition and their limitations: *Bulletin of the Society of Geology of France*, v. 168 (4), p. 491-505.
- IMMENHAUSER, A., DELLA PORTA, G., KENTER, J. A. M., AND BAHAMONDE, J.R, 2003, An alternative model for positive shifts in shallow-marine carbonate  $\delta^{13}\text{C}$  and  $\delta^{18}\text{O}$ : *Sedimentology*, v. 50 (5), p. 953.
- JAMES, N. P., AND BONE, Y. 1989, Petrogenesis of Cenozoic, temperate water calcarenites, South Australia: a model for meteoric/shallow burial diagenesis of shallow water calcite sediments: *Journal of Sedimentary Petrology*, v. 59(2), p. 191-203.
- JAMES, N. P., AND CHOQUETTE, P.W. 1990a, Limestones-Sea Floor diagenetic environment, *in*: McIlreath, I.A., Morrow, D.W., eds. *Diagenesis*: Ottawa, Geological Association of Canada, p. 13-34.
- JAMES, N. P., AND CHOQUETTE, P.W. 1990b, Limestones-The burial diagenetic environment. *in*: McIlreath, I.A., Morrow, D.W., eds. *Diagenesis*: Ottawa, Geological Association of Canada, p. 75-111.
- JAMES, N. P., AND BONE, Y., 1991, Origin of a cool-water, Oligo-Miocene deep shelf limestone, Eucla Platform, southern Australia: *Sedimentology*, v. 38, p. 323-341.

JAMES, N. P., AND BONE, Y. 1992, Synsedimentary cemented calcarenite layers in Oligo-Miocene cool-water shelf limestones, Eucla platform, Southern Australia: *Journal of Sedimentary Petrology*, v. 62(5), p. 860-872.

JAMES, N. P., 1997, The cool-water carbonate depositional realm, *in*: James, N.P. and Clarke, J.A.D., eds. *Cool-water carbonates*: Tulsa, Oklahoma, SEPM., 56, p. 1-20.

JAMES, N.P., COLLINS, L.S., BONE, Y., AND HALLOCK, P., 1999, Subtropical carbonates in a temperate realm: modern sediments on the southwest Australian shelf: *Journal of Sedimentary Research*, v. 69 (6), p. 1297-1321.

JAMES, N.P., BONE, Y., AND KYSER , T.K., 2005, Where has all the aragonite gone? Mineralogy of Holocene neritic cool-water carbonates, southern Australia: *Journal of Sedimentary Research*, v. 75(3), p. 454-463.

JOHN, C. M., MUTTI, M., AND ADATTE, T., 2003, Mixed carbonate-siliciclastic record on the North African margin (Malta) - coupling of weathering processes and mid Miocene climate: *GSA Bulletin*, v. 115(2), p. 217-229.

JOHN, C. M., AND MUTTI, M., 2005, The response of Heterozoan carbonate systems to paleoceanographic, climatic and eustatic changes: perspective from slope sediments of the Marion Plateau (ODP Leg 194): *Journal of Sedimentary Research*, v. 75, p. 216-236.

KNOERICH, A.C., AND MUTTI, M. 2003. Controls of facies and sediment composition on the diagenetic pathway of shallow-water Heterozoan carbonates: the Oligocene of the Maltese Islands: *International Journal of Earth Science*, v. 92, p. 494-510.

KNOERICH, A.C., AND MUTTI, M. 2006, Missing aragonitic biota and the diagenetic evolution of heterozoan carbonates: a case study from the Oligo-Miocene of the central Mediterranean: *Journal of Sedimentary Research*, v. 76, p. 871-888.

KYSER, T.K., JAMES, N.P., AND BONE, Y., 1998, Alteration of Cenozoic cool-water carbonates to low-Mg calcite in marine waters, Gambier Embayment, South Australia: *Journal of Sedimentary Research*, v. 68, p. 947-955.

LANGER, M.R., AND HOTTINGER, L., 2000, Biogeography of selected "larger" foraminifera: *Micropaleontology*, v. 46 (1), p. 105-126.

LEES, A., AND BULLER, A.T., 1972, Modern Temperate-water and warm-water shelf carbonates contrasted: *Marine Geology*, v. 13, p. 67-73.

LEES, A., 1975, Possible influence of salinity and temperature on modern shelf carbonate sedimentation: *Marine Geology*, v. 19, p. 159-198.

LUKASIK, J. J., JAMES, N. P., MCGOWRAN, B., AND BONE, Y., 2000, An epeiric ramp: low-energy, cool-water carbonate facies in a Tertiary inland sea, Murray Basin, South Australia: *Sedimentology*, v. 47, p. 851-881.

LOHMANN, K.C., 1988, Geochemical patterns of meteoric diagenesis and their application to paleokarst, *in*: Choquette, P. W. and James, N.P., eds. *Paleokarst*: New York, Springer Verlag, p. 58-80.



- McCONNAUGHEY, T. A., BURDETT, J., WHELAN, J. F., AND PAULL, C., K., 1997, Carbon isotopes in biological carbonates: Respiration and photosynthesis: *Geochimica et Cosmochimica Acta*, v. 61 (3), p. 611-622.
- McINTYRE, I. G., 1985, Submarine cements-The peloidal question: *Carbonate Cements*. Tulsa, SEPM Special Publication, 36: 109-116.
- MARTINI, I.P., OGGIANO, G., AND MAZZEI, R., 1992, Siliciclastic-carbonate sequences of Miocene grabens of Northern Sardinia, western Mediterranean Sea: *Sedimentary Geology*, v. 76, p. 63-78.
- MELIM, L.A., SWART, P.K., AND MALIVIA, R. G, 2001, Meteoric and marine-burial diagenesis in the subsurface of Great Bahama Bank, *in*: Ginsburg, R.N., eds. *Subsurface geology of a prograding carbonate platform margin, Great Bahama Bank: results of the Bahamas Drilling Project*: Tulsa, SEPM, 70, p. 137-161.
- MELIM, L.A., WESTPHAL, H., SWART, P.K., EBERLI, G.P., AND MUNNECKE, A., 2002, Questioning carbonate diagenetic paradigms: evidence from the Neogene of the Bahamas: *Marine Geology*, v. 185, p. 27-53.
- MILLER, K. G., WRIGHT, J.D., AND FAIRBANKS, R.G., 1991, Unlocking the ice house: Oligocene-Miocene oxygen isotopes, eustasy, and margin erosion: *Journal of Geophysical Research*, v. 69, p. 6829-6848.
- MILLER, K. G., MOUNTAIN, G. S., BROWNING, J.V., KOMINZ, M., SUGARMAN, P. J., CHRISTIE-BLICK, N., KATZ, M. E., AND WRIGHT, J.D., 1998, Cenozoic global sea level, sequences, and the New Jersey transect: results from coastal plain and continental slope drilling: *Reviews of Geophysics*, v. 36, p. 569-601.
- MOORE, C.H., 2001, Carbonate reservoirs- porosity evolution and diagenesis in a sequence stratigraphic framework, *Developments in sedimentology*: Amsterdam, Elsevier, v. 55, p. 444.
- MONAGHAN, A., 2001, Coeval extension, sedimentation and volcanism along the Cainozoic rift system of Sardinia, *in*: Ziegler, P.A., Cavazza, A.H.F. eds. *Peri-Tethys Memoir 6: Peri-Tethyan rift/wrench basins and passive margins*, p. 707-734.
- MONLEAU, C., ARNAUD, M., MAGNÉ, J., NÉGRETTI, B., AND ROSSI, F., 1996, Précisions stratigraphiques et paléocéologiques sur le Miocène inférieur et moyen du Sud de la Corse et du Nord de la Sardaigne: *Géologie Méditerranéenne*, v. 23 (3-4), p. 235-241.
- MORSE, J. W., AND MACKENZIE, F. T., 1990, *Geochemistry of Sedimentary Carbonates*, Development in Sedimentology: Amsterdam, Elsevier, v. 48, p. 707.
- MUTTI, M., 1995, Porosity development and diagenesis in the Orfento Supersequence and its bounding unconformities (Upper Cretaceous, Montagna della Maiella, Italy), *in*: Budd, D.A., Saller, A.H., and Harris, P., eds. *Unconformities and porosity in carbonate strata*: Tulsa, Oklahoma, AAPG Memoir, 63, p. 141-158.
- MUTTI, M., BERNOULLI, D., SPEZZAFERRI, S., AND STILLE, P., 1999, Lower and middle Miocene carbonate facies in the central Mediterranean: the impact of paleoceanography on sequence stratigraphy, *in*: *Advances in carbonate sequence stratigraphy: application to reservoirs, outcrops and models*: Tulsa, SEPM, 63, p. 371-384.
- MUTTI, M., AND BERNOULLI, D., 2003, Early marine lithification and hardground development on a Miocene ramp (Maiella, Italy): Key surfaces to track changes in trophic resources in nontropical carbonate settings: *Journal of Sedimentary Research*, v. 73(2), p. 296-308.

MUTTI, M., AND HALLOCK, P., 2003, Carbonate systems along nutrient and temperature gradients: some sedimentological and geochemical constraints: *International Journal of Earth Sciences*, v. 92, p. 463-475.

MUTTI, M., JOHN, C.M., AND KNOERICH, A. C., 2006, Chemostratigraphy in Miocene heterozoan carbonate settings: applications, limitations and perspectives, *in*: Pedley, H.M, and Carannante, G., eds. *Cool-Water Carbonates: Depositional Systems and Palaeoenvironmental Controls: Special Publication*. London, Geological Society of London, 255, p. 307-322.

NAGEL, B. 2005, Kartierung der neogenen Schichtenfolge zwischen Sedini und Laerru, NW-Sardinien, Diplomarbeit, Universität Hamburg, 54 p.

NELSON, C.S., 1988, An Introductory perspective on non-tropical shelf carbonates: *Sedimentary Geology*, v. 60, p. 3-12.

NELSON, C. S., AND JAMES, N.P. 2000, Marine cements in mid-Tertiary cool-water shelf limestones of New Zealand and southern Australia: *Sedimentology*, v. 47, p. 609-629.

NELSON, C.S., AND SMITH, A. M. 1996, Stable oxygen and carbon isotope compositional fields for skeletal and diagenetic components in New Zealand Cenozoic nontropical carbonate sediments and limestones: a synthesis and review: *New Zealand Journal of Geology and Geophysics*, v. 39, p. 93-107.

NICOLAIDES, S., 1995, Cementation in Oligo-Miocene non-tropical shelf limestones, Otway Basin, Australia: *Sedimentary Geology*, v. 95, p. 97-121.

NICOLAIDES, S., AND WALLACE M. W. 1997, Pressure-dissolution and cementation in an Oligo-Miocene non-tropical limestone (Clifton Formation), Otway Basin, Australia. *in*: James, N.P. and Clarke, J.A.D., eds. *Cool-water carbonates: Tulsa, Oklahoma, SEPM.*, 56, p. 249-261.

PEDLEY, M., AND GRASSO, M., 2006, The response of cool-water carbonates to eustatic change in microtidal, Mediterranean Quaternary settings of Sicily, *in*: Pedley, H.M, and Carannante, G., eds. *Cool-Water Carbonates: Depositional Systems and Palaeoenvironmental Controls: Special Publication*. London, Geological Society of London, 255, p. 137-156.

PÉRÈS, J.M. AND PICARD, J., 1964, Nouveau manuel de bionomie benthic de la Mer Méditerranée: *Travaux Station Marine d'Endoume*, 47, 137 pp.

PRENTICE, M.L., AND MATHEWS, R.K., 1988, Cenozoic ice-volume history: development of a composite oxygen isotope record: *Geology*, v. 16, p. 963-966.

PIGRAM, C. J., DAVIES, P.J., AND CHAPRONIERE, G. C. H., 1993, Cement stratigraphy and the demise of the Early-Middle Miocene carbonate platform on the Marion Plateau, *Proceedings of the Ocean Drilling Program, Scientific Results*, v. 133, p. 499-512

POMAR, L., 2001, Ecological control of sedimentary accommodation: evolution from a carbonate ramp to rimmed shelf, Upper Miocene, Balearic Islands: *Palaeogeography, Palaeoclimatology, Palaeoecology*, v. 175, p. 249-272.

POMAR, L., BRANDANO, M., AND WESTPHAL, H., 2004, Environmental factors influencing skeletal grain sediment associations: a critical review of Miocene examples from the western Mediterranean: *Sedimentology*, v. 51, p. 627-651.

- RASSER, M., 2001, Paleocology and Taphonomy of *Polystrata alba* (Red Alga) from the Late Eocene Alpine Foreland: A New Tool for the Reconstruction of Sedimentary Environments: *Palaios*, v. 16, p. 601-607.
- RASSER, M.W. AND PILLER, W.E., 2004, Designation of *Phymatolithon* (Corallinaceae, Rhodophyta) in fossil material and its paleoclimatological indications: *Micropaleontology*, v. 46 (1), p. 89-95.
- READ, J.F., 1985, Carbonate Platform models: American Association of Petroleum Geologists, v. 69, p. 1-21.
- REID, R.P., 1987, Nonskeletal peloidal precipitates in upper Triassic reefs, Yukon Territory (Canada): *Journal of Sedimentary Petrology*, v. 57 (5), p. 893-900.
- REID, R.P., AND MACINTYRE, I.G., et al., 1990, Internal precipitation of microcrystalline carbonate: a fundamental problem for sedimentologists: *Sedimentary Geology*, v. 68, p. 163-170.
- REUNING, L., REIJMER, J.J.G., AND BETZLER, C., 2002, Sedimentation cycles and their diagenesis on the slope of a Miocene carbonate ramp (Bahamas, ODP Leg 166): *Marine Geology*, v. 185, p. 121-142.
- SAVIN, S.M., AND WOODRUFF, F., 1990, Isotopic evidence for temperature and productivity in the Tertiary oceans, Cambridge University Press.: New York, 241-259 p.
- SCHLAGER, W., 2005, Carbonate Sedimentology and Sequence Stratigraphy: Concepts in Sedimentology and Paleontology, *SEPM*, 8, p. 200.
- SCHROEDER, J., H., 1969, Experimental dissolution of calcium, magnesium, and strontium from recent biogenic carbonates: a model of diagenesis: *Journal of Sedimentary Petrology*, v. 39, p. 1057-1073.
- SHUBBER, B., BONE, Y., JAMES, N.P., AND MCGOWRAN, B., 1997, Warming-upward cycles in mid-Tertiary cool-water limestones, St. Vincent Basin, South Australia, *in*: James, N.P. and Clarke, J.A.D., eds. *Cool-water carbonates*: Tulsa, Oklahoma, *SEPM*, 56, p. 237-249.
- SIMONE, L., AND CARANNANTE, G., 1988, The fate of foramol ("temperate type") carbonate platforms: *Sedimentary Geology*, v. 60, p. 347-354.
- SIMONE, L., MURRU, M., AND VIGORITO, M., 2001, A syn-rift temperate-type carbonate margin: morphology and depositional geometries, *in*: 21st IAS-Meeting of Sedimentology, 1 page, Davos.
- SMITH, A. M. AND NELSON, C.S., 2003, Effects of early sea-floor processes on the taphonomy of temperate shelf skeletal carbonate deposits: *Earth-Science Reviews*, v. 63, p. 1-31.
- SOWERBUTTS, A. 2000, Sedimentation and volcanism linked to multiphase rifting in an Oligo-Miocene intra-arc basin, Anglona, Sardinia: *Geological Magazine*, v. 137, p. 395-418.
- SOWERBUTTS A. A., AND UNDERHILL J.R. 1998, Sedimentary response to intra-arc extension: controls on Oligo-Miocene deposition, Sarcidano sub-basin, Sardinia: *Journal of the Geological Society of London*, January Issue.
- SPERANZA, F., VILLA, I.M., SAGNOTTI, L., FLORINDO, F., CONSENTINO, D., CIPOLLARI, P., AND MATTEI, M., 2002, Age of the Corsica-Sardinia rotation and Liguro-Proccencal Basin spreading: new paleomagnetic and Ar/Ar evidence: *Tectonophysics*, v. 347, p. 231-251.

SUN, S. Q., AND ESTEBAN, M., 1994, Paleoclimatic Controls on Sedimentation, Diagenesis, and Reservoir Quality: Lessons from Miocene Carbonates: American Association of Petroleum Geology, v. 78 (4), p. 519-543.

SWART, P. K., AND EBERLI, G., 2005, The nature of the  $\delta^{13}\text{C}$  of periplatform sediments: Implications for stratigraphy and the global cycle: Sedimentary Geology, v. 175. p. 115-129.

THOMAS, B., AND GENNESEAUX, M. 1986, A two stage rifting in the basins of the Corsica-Sardinian straits: Marine Geology, v. 72, p. 225-239.

TUCKER, M.E., AND WRIGHT, V.P. 1990. Carbonate Sedimentology. Blackwell, Oxford, 482 p.

VINCENT, E. AND BERGER, W.H., 1985, Carbon dioxide and polar cooling in the Miocene: The Monterey hypothesis, *in*: Sundquist, E.T., and Broecker, W.S., eds. Natural variations Archean to present, American Geophysical Union, Geophysical Monographies.

WALTER, L., M., AND MORSE, J., W., 1985, The dissolution kinetics of shallow marine carbonates in seawater: A laboratory study: Geochimica et Cosmochimica Acta, v. 49, p. 1503-1513.

WALTER, L.M., 1985, Relative reactivity of skeletal carbonates during dissolution: implications for diagenesis: Carbonate Cements. Tulsa, SEPM Special Publication, 36: 3-16.

WILSON, M.E.J., AND EVANS, M.J. 2002, Sedimentology and diagenesis of tertiary carbonates on the Mangkalihat peninsula, Borneo: implications for subsurface reservoir quality: Marine and Petroleum Geology, v. 19, p. 873-900.

WILSON, M.E.J., AND VECSEI, A., 2005, The apparent paradox of abundant foramol facies in low latitudes: their environmental significance and effect on platform development: Earth-Science Reviews, v. 69, p. 133-168.

WRIGHT V.P., AND CHERNS, L., 2004, Are there "black holes" in carbonate deposystems?: Geologica Acta, v. 2, p. 285-290.

WRIGHT, J.D., MILLER, K.G., AND FAIRBANKS, R.G., 1992, Early and middle Miocene stable isotopes, implications for deepwater circulation and climate: Paleoceanography, v. 7, p. 357-389.

WRIGHT V.P., CHERNS, L., AND HODGES, P., 2003, Missing molluscs: field testing taphonomic loss in the Mesozoic through early large-scale aragonite dissolution: Geology, v. 31, p. 211-214.

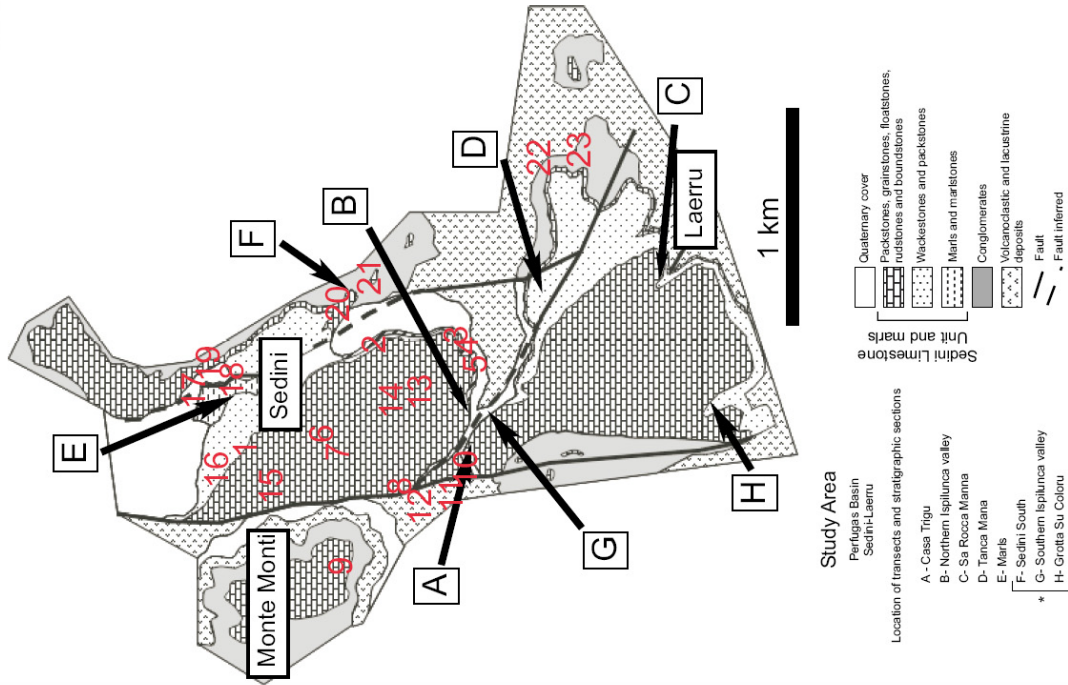
ZACHOS, J., PAGANI, M., SLOAN, L., THOMAS, E., AND BILLUPS, K., 2001, Trends, rhythms, and aberrations in global climate 65 Ma to present: Science, v. 292, p. 686-693.

ZACHOS, J. C., FLOWER, B.P., AND PAUL, H., 1997, Orbitally paced calimate oscillations across the Oligocene/Miocene boundary: Nature, v. 388, p. 567-570

APPENDIX  
CHAPTER 3

# APPENDIX 3.1

## DATA BASE and PETREL MODEL



Geological map of the study area.

With letters are marked the location of the stratigraphic sections and transect.

With numbers the location of the GPS measurements acquired at the field and used as synthetic points for the modelling.

These measurements were introduced in a data base for a first model in PETREL, which helped to recognize the geometry of the basin and centers of maximum infilling.

Most of the GPS measurements were taken at the sequence 2. Points 17, 18, 19 corresponds to the base of the marls. Points 20 to 23 corresponds to measurements at the conglomerates.

LOCATION	X	Y	Z (HEIGHT m)
1	32T0484379(82)	UTM 4522312 (15)	350
2	32T0484654 (55)	UTM 4521775 (77)	279-285
3	32T0484827	UTM 4521573	296-292
4	32T0484888 (90)	UTM 4521195	283-286
5	32T0484913 (14)	UTM 4520800 (01)	285
6	32T0484022	UTM 4522262	371
7	32T0483873 (74)	UTM 4522101 (99)	357
8	32T0483386 (89)	UTM 4521489	321
9	32T0482621	UTM 4521343	461
10	32T0483237	UTM 4520713	344
11	32T0483027 (28)	UTM 4521145	315
12	32T0483300 (01)	UTM 4521389 (88)	318
13	32T0484459 (60)	UTM 4521123 (24)	360
14	32T0484389	UTM 4521649 (50)	362
15	32T0483719 (18)	UTM 4522394 (95)	348
16	32T0483979 (78)	UTM 4522656	322
17	32T0484305	UTM 4522895	349
18	32T0484452	UTM 4522899	353
19	32T044819	UTM 4522110	355
20	32T0485832 (33)	UTM 4521748 (47)	197
21	32T0486325	UTM 4521420	191
22	32T0486655 (54)	UTM 4520739	128
23	32T0487417	UTM 4520444	124

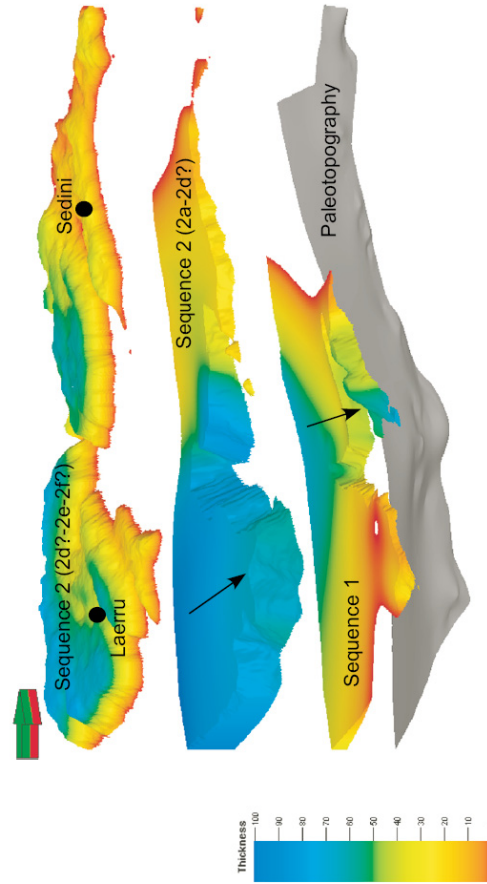
## APPENDIX 3.1

### DATA BASE and PETREL MODEL

TRANSECT	SECTION	X	Y	Z (HIGH m)	Surface 2d (TOP)	
CASA TRIGU	S2a	32T0483655	UTM 4520653	-314	SB	
		32T0483655	UTM 4520653	-260.000	Paleotopography 2d (TOP)	
	S3	No data	No data	-315.000	SB	
		No data	No data	-268.000	SB	
		No data	No data	-254.000	Paleotopography 2d (TOP)	
		32T0484130	UTM 4520638	-318.000	SB	
	S5	32T0484130	UTM 4520638	-264.500	Paleotopography 2d (TOP)	
		32T0484130	UTM 4520638	-324.000	SB	
	NORTHERN ISPILUNCA VALLEY	S6	32T0484235	UTM 4520655	-260.000	SB
			32T0484235	UTM 4520655	-260.000	Paleotopography 2d (TOP)
S7		32T0484322	UTM 4520623	-326.000	SB	
		32T0484322	UTM 4520623	-260.000	Paleotopography 2d (TOP)	
S8	C1	32T0484322	UTM 4520693	-330.000	SB	
		32T0484502	UTM 4520693	-255.000	Paleotopography S2d/S2e	
	32T0484502	UTM 4520693	-358	S2d/S2e		
	32T0485343	UTM 4518898	-356	S2d/S2e		
Sa Rocca Manna	C1	32T0485400	UTM 4518777	-325	S2d/S2e	
		32T0485521	UTM 4518776	-333	S2e	
		32T0485473	UTM 4518766	-317	S2e	

This table compiles the GPS measurements (X, Y, Z) introduced in PETREL of selected stratigraphic sections from the transect studied in this thesis. Not all surfaces were measured because of the lack of access or failure to find satellite connection. Each Z (high, meters) is negative because of using them as synthetic wells.

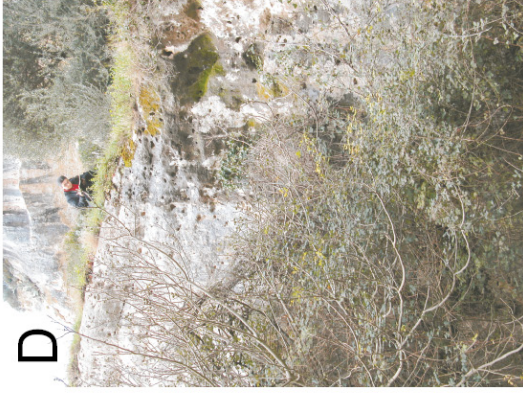
### MODEL



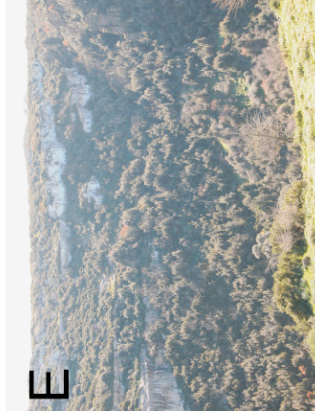
The model presented here was preliminary and constructed in order to visualize the direction of sediment infilling in both sequences. Both sequences show that major thickness was accumulated towards the E (black arrows). The initial surface of deposition, or named here as paleotopography, was constructed using GPS measurements acquire at the conglomerates (see geological map). However, most of the points (or GPS measurements) were synthetic (lack of data). The resulting paleotopography show an irregular surface. The sequence 1 show major sediment thickness towards the E, however, lack of points for interpolation (south and west) reduces the interpretation. Sequence 2 was constructed by the points measured in each stratigraphic section (tables). The interpretation of thickness variation of the upper part of the Sedini Limestone Unit is highly reduced by the lack of outcrops containing S2e. Therefore, the extension of the platform top (margin, slope) needs further revision. The model for this basin is part of a "work in progress" coordinated by Prof. Dr. Maria Mutti.

## APPENDIX 3.2

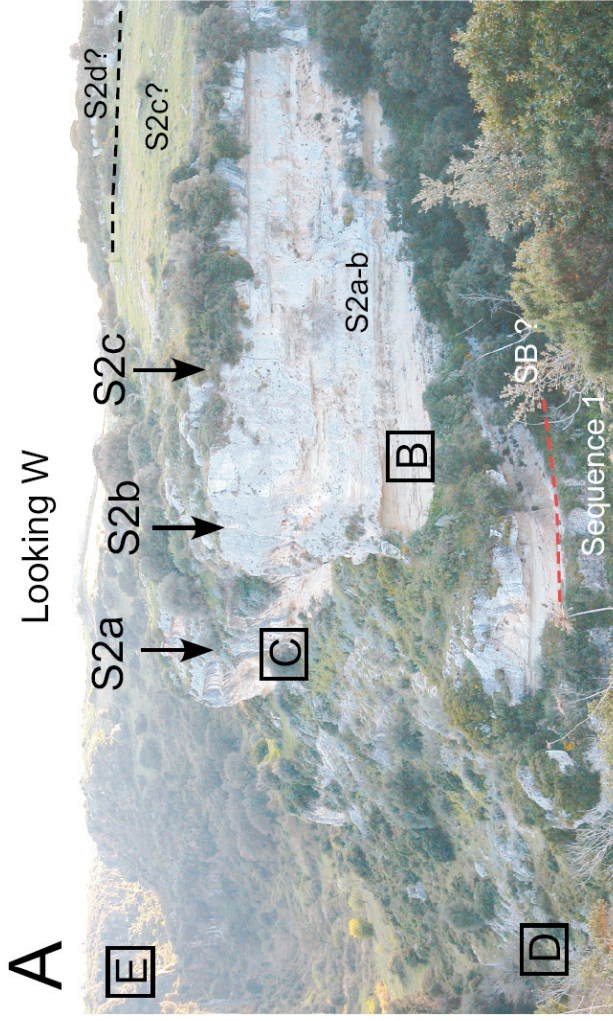
Transect "A"-Casa Trigu



D- This photo shows a detail of the lower Sequence 1 and the cross-bedded stratification.



E- This photo shows the contact of the volcanics and the Sedini Limestone Unit. The photo was taken from the Casa Trigu Transect and looking SW.



A- This figure show the location of the Transect "A" (Figure 3.1, 3.2, and 3.3) or Casa Trigu Transect. The spatial location of the stratigraphic sections are located (S2a, S2b and S2c).

C



B

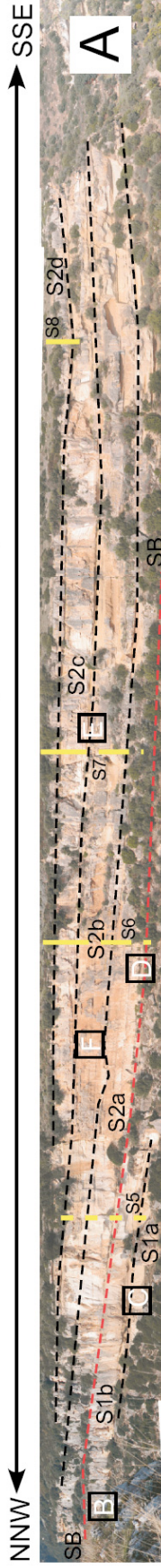


B and C- These two photographs shows the outcrop expression of the red algal bindstone found in sequence 2. In figure "A" is shown the location. The red algal boundstone is mostly characterized by layers of red algal encrustations, bivalves, and echinoid spines (< 7-10 cm long).

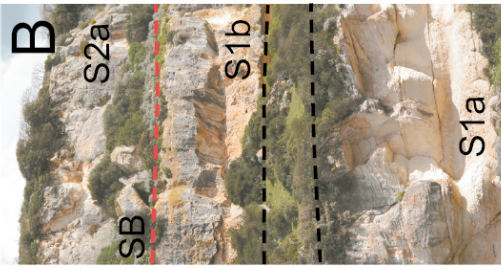


## APPENDIX 3.3

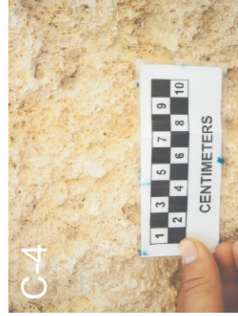
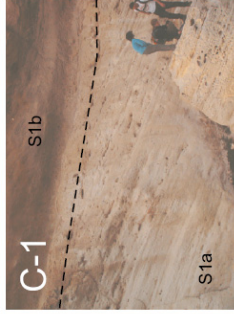
### Transect "B"-Northern Ispilunca valley



A- This figure show the Transect "B" (Figure 3.1, 3.2, and 3.3) or Northern Ispilunca valley Transect. The approx. location of the stratigraphic sections are located with a yellow vertical line (S5, S6, S7, S8).



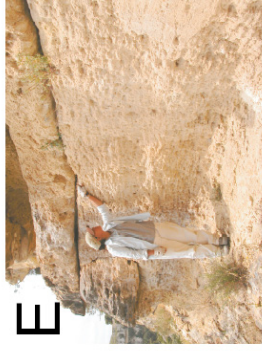
B- Location of section "S3". The lower and middle part of the Sediní Limestone Unit is shown. Sequence 1 corresponds to cross-bedded floatstones and rudstones (S1a-S1b). Sequence 2 is only represented by the unit S2a mostly characterized by bioclastic packstones and grainstones.



C C-1 & C-2 Location of the section "S5". The lower part of the Sediní Limestone Unit. Is shown the Sequence 1 (S1a-b), which corresponds to cross-bedded floatstones and rudstones. A Floatstone is observed at S1b. C-3 Detail of the top lap of the cross-bedding in unit S1a. C-4 Detail of the biotic constituents characterized by reworked red algae, bryozoans, echinoids, large benthic foraminifers, among others.



D- Detail of the limit between the sequences or Sequence Boundary. The photo was taken at the location of the section "S6".



E- Detail of the limit between unit S2b and S2c at the section "S7".

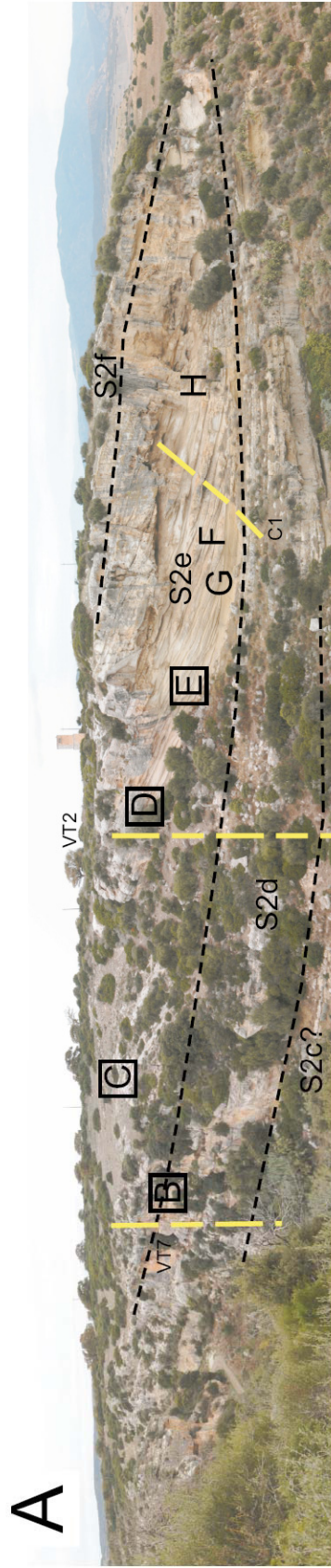


F- Detail of the contact between unit S2a and S2b.

### APPENDIX 3.4

Transect "C"-Sa Rocca Manna

NW-W ← → SE-E



A- This figure show the Transect "C" (Figure 3.1, 3.2, and 3.3) or Sa Rocca Manna Transect. The approx. location of the stratigraphic sections are located with a yellow vertical line VT7, VT2, C1).



B- Limit of Unit S2d and S2e. Section VT7.



C- Floatstones/rudstones to bindstones



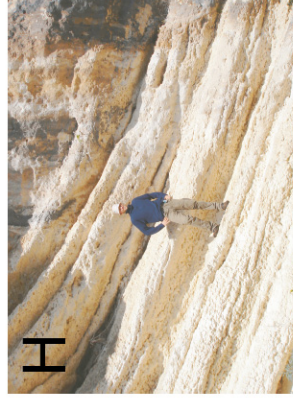
D- Floatstones/rudstones to bindstones



E- Detail of rodoliths in Unit S2e



F & H- Clinoformal geometry of the strata in Unit S2e

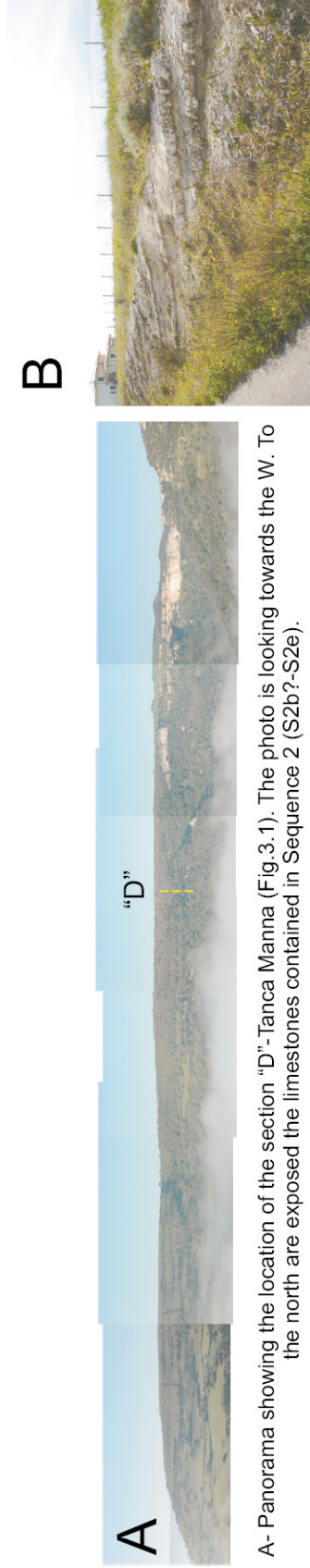


G- Detail of the stratification at the base of Unit S2e. Compaction has obscured primary structures.



## APPENDIX 3.5

### Section "D"- Tanca Manna, Section "E"- Marls & "F"- Sedini South



A- Panorama showing the location of the section "D"-Tanca Manna (Fig.3.1). The photo is looking towards the W. To the north are exposed the limestones contained in Sequence 2 (S2b?-S2e).

B- This figure show the location of the section "E" or Marls. The road cut is located in the Sedini village (Fig.3.1)



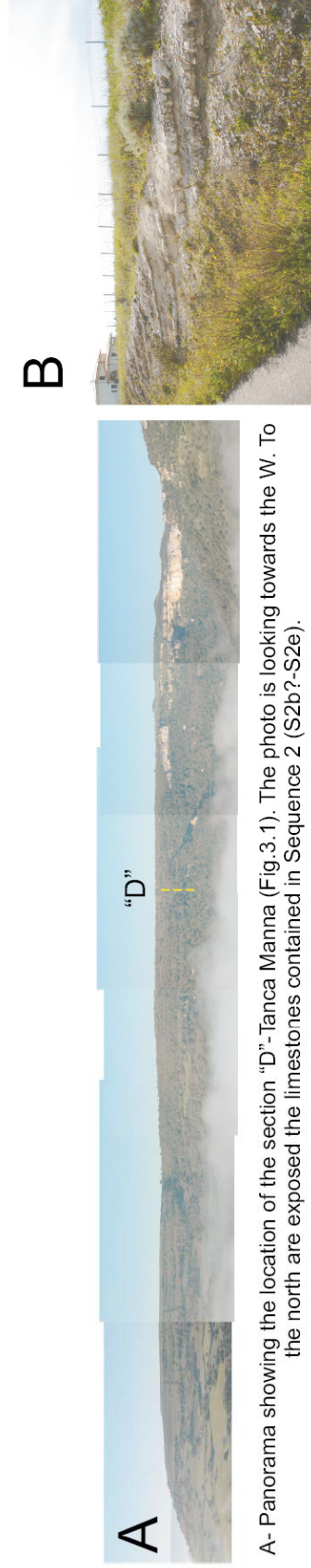
C- This figure shows part of the Transect called Sedini in Benisek et al. (in press) (Figure 3.1, 3.2, and 3.3). From this transect was studied a section measured in the outcrop named as "Sedini South" or section "F". The exact location of "F" is denoted in the figure "D" of this appendix.



D & E- Section "F". This section compiles exclusively the lower part of the Sedini Limestone Unit. It is only exposed the lower sequence 1 (S1a-b). Basically, the base (S1a) are floatstones to rudstones rich in red algal debris. Some bioturbation is found (E) The top (S1b) is characterize by finer grained limestones (bioclastic packstones and wackestones).

## APPENDIX 3.5

### Section "D"- Tanca Manna, Section "E"- Marls & "F"- Sedini South



A- Panorama showing the location of the section "D"-Tanca Manna (Fig.3.1). The photo is looking towards the W. To the north are exposed the limestones contained in Sequence 2 (S2b?-S2e).

B- This figure show the location of the section "E" or Marls. The road cut is located in the Sedini village (Fig.3.1)



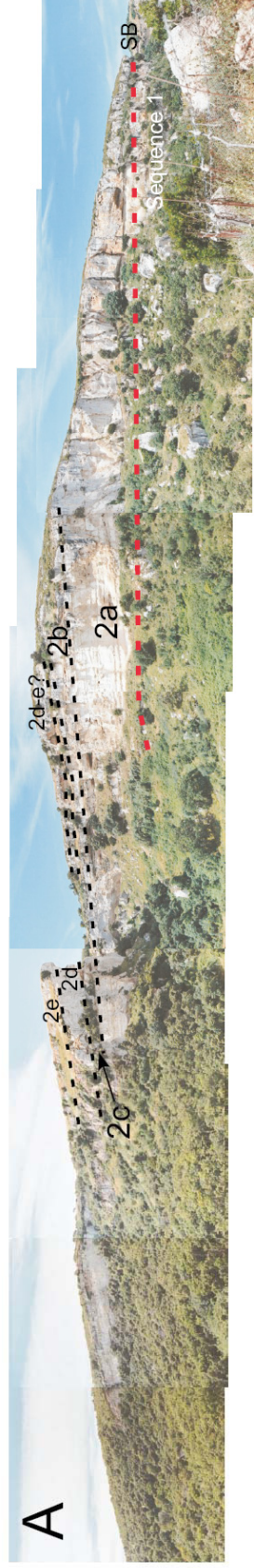
C- This figure shows part of the Transect called Sedini in Benisek et al. (in press) (Figure 3.1, 3.2, and 3.3). From this transect was studied a section measured in the outcrop named as "Sedini South" or section "F". The exact location of "F" is denoted in the figure "D" of this appendix.



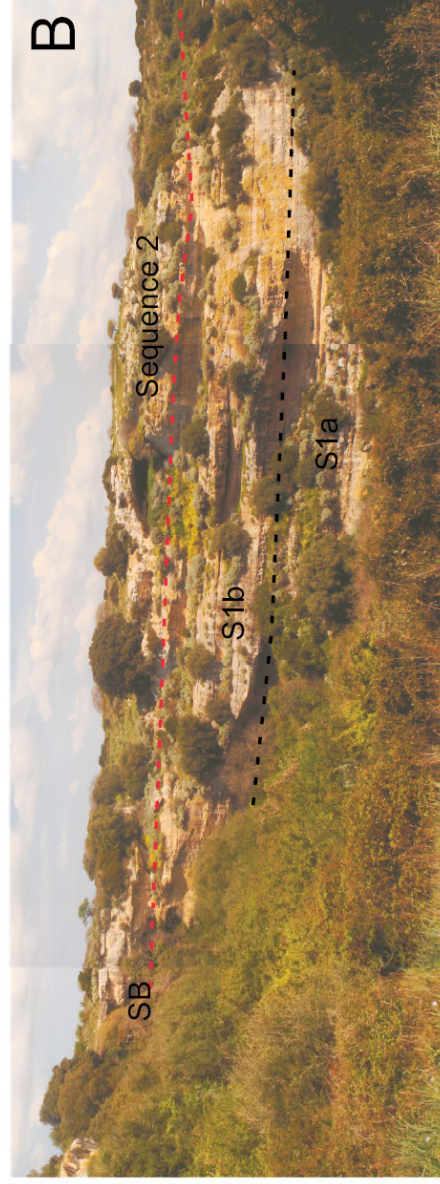
D & E- Section "F". This section comprises exclusively the lower part of the Sedini Limestone Unit. It is only exposed the lower sequence 1 (S1a-b). Basically, the base (S1a) are floatstones to rudstones rich in red algae debris. Some bioturbation is found (E) The top (S1b) is characterize by finer grained limestones (bioclastic packstones and wackestones).

## APPENDIX 3.6

### Transect Southern Ispilunca valley & Grotta Su Coloru



A- Panorama showing the Southern Ispilunca valley Transect (Fig.3.1). The photo is looking towards the W. In this outcrop the Sedini Limestone Unit is characterized by the upper Sequence 2 (2a-2e). Towards the N, the lower Sequence 1 outcrops; however is poorly exposed. In Benisek, Marcano et al. (in press) this transect is widely interpreted in terms of facies and lithology.



B- Panorama showing the Grotta Su Coloru Transect. The photo is looking towards the E. The access to this outcrop is highly restricted and poorly exposed. The lower part of the Sedini Limestone Unit is exposed. In Benisek, Marcano et al. (in press) this transect is widely interpreted in terms of facies and lithology. Benisek et al. (in press.) describes and interpret the sequence 1 (1a-b) and sequence 2 exposed in this location.

**APPENDIX  
CHAPTER 4**

# APPENDIX 4.1

## BIOTA DIVERSITY

The purpose of this appendix is to show the contrast of biota among the two sequences. The lower sequence 1 (ramp) is characterized by a heterozoan-dominated skeletal biotic association (e.g., bryozoans, red algae, bivalves, echinoids, barnacles), meanwhile the upper sequence 2 (platform) by a photozoan-dominated skeletal biotic association (e.g., corals).

Photographs of the biota diversity taken in the field and in thin sections are shown.

### Sequence 1/Ramp



Location: section sedini south-section "F". Detail of the floatstone to rudstone texture (Unit S1a) rich in red algal, echinoids and bivalve debris.



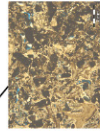
Detail of the basal contact of the Sequence 1 with the basal conglomerates. Complete and preserved echinoids can be found mixed with detrital carbonate and siliclastic material. Location: Sedini Transect (refer to Benisek, Marciano et al., in press).



Contact of the Sequence 1 with the basal conglomerates. Location: Sedini Transect (refer to Benisek, Marciano et al., in press).



Location: Northern Ispilunca valley (section S5, Unit S1a). Cross-bedded floatstones and rudstones. Biota is characterized by: large benthic foraminifers (left thin section photo); reworked echinoids, barnacles, bivalves, red algae, bryozoans, among others (right thin section photo).



Location: Northern Ispilunca valley. Detail of barnacles.

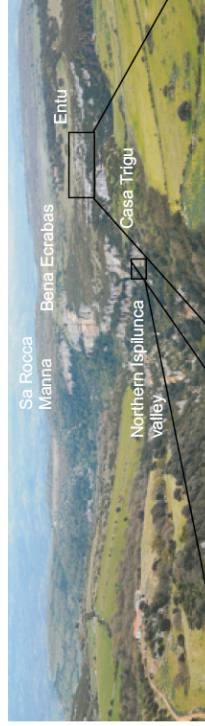


Location: section sedini south-section "F". Left photo shows bioturbation found at the unit S1a. Right photo shows the packstones-wackestones found at unit S1b.



Location: section sedini south-section "F". S1a/S1b boundary. This limit is found colonized by bivalves (oysters) and echinoids.

### Sequence 2/Platform



Location: Casa Trigu, Unit S2a-S2b. Red algal bindstones. Layers of red algae are found in combination with bivalves and echinoid spines (right photo) among others.



Location: Entu (south of Casa Trigu), Unit S2d-S2e?. Coral boundstones.



Location: Bena Ecrabas (north of Sa Rocca Manna). View from southern Ispilunca valley transect. Coral boundstones with at the base large and articulated oysters (right photo).



Sa Rocca Manna



Location: Transect Sa Rocca Manna, Unit S2e. Slope facies characterized by rhodoliths composed mainly by coralline red algae, bivalves, bryozoans, foraminifers, and echinoids.



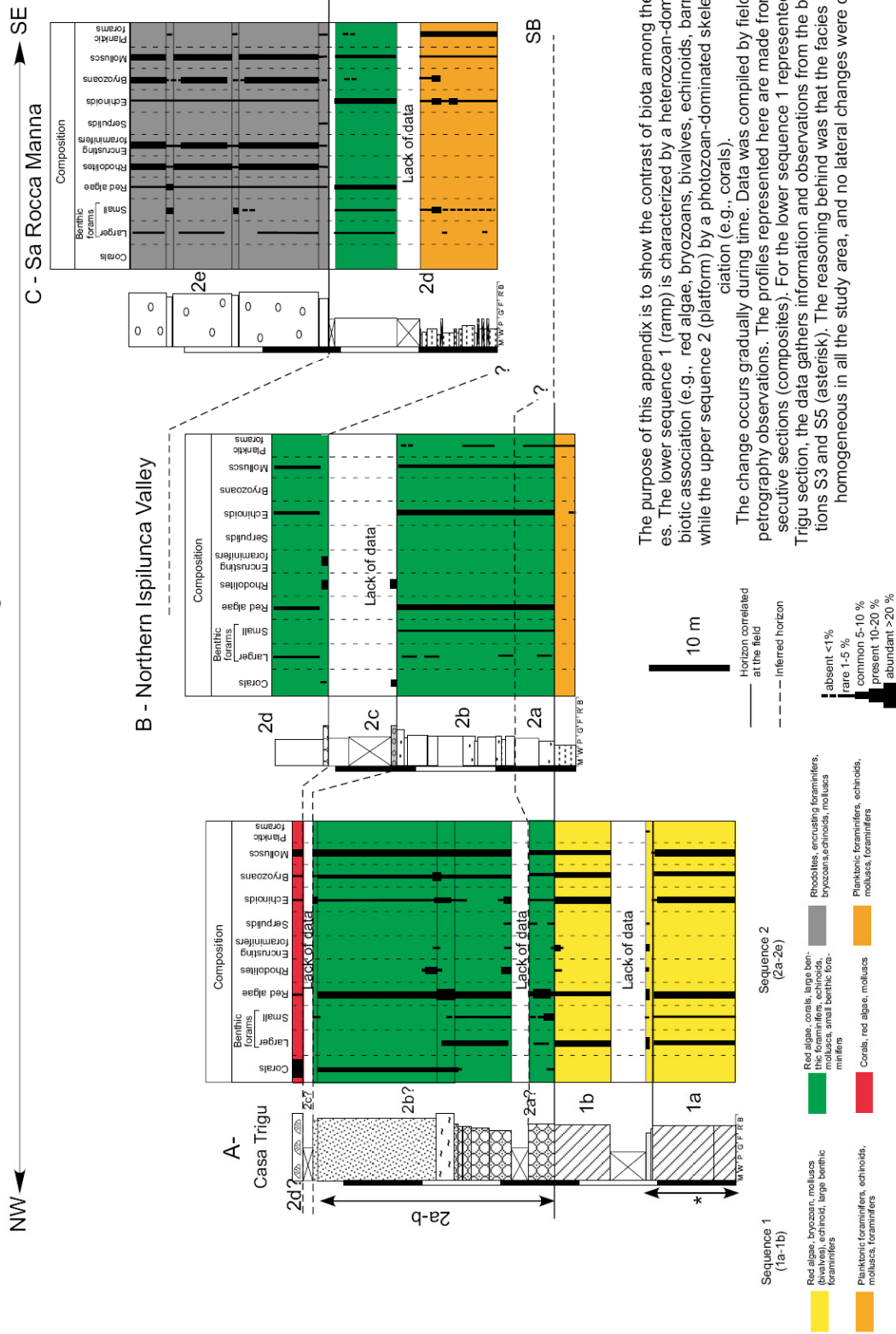
Location: south of Transect Sa Rocca Manna. View from southern Ispilunca valley transect. Packstones rich in echinoids.



Location: Bena Ecrabas (north of Sa Rocca Manna). View from southern Ispilunca valley transect. Coral boundstones with at the base large and articulated oysters (right photo).

# APPENDIX 4.2

## Vertical and lateral changes of the biotic associations



The purpose of this appendix is to show the contrast of biota among the two sequences. The lower sequence 1 (ramp) is characterized by a heterozoan-dominated skeletal biotic association (e.g., red algae, bryozoans, bivalves, echinoids, barnacles), meanwhile the upper sequence 2 (platform) by a photozoan-dominated skeletal biotic association (e.g., corals).

The change occurs gradually during time. Data was compiled by field and optical petrography observations. The profiles represented here are made from vertical consecutive sections (composites). For the lower sequence 1 represented at the Casa Trigu section, the data gathers information and observations from the base of the sections S3 and S5 (asterisk). The reasoning behind was that the facies is completely homogeneous in all the study area, and no lateral changes were observed.



# APPENDIX TABLES-CHAPTER 4

**Table 4.1. Facies and diagenetic features of Sequence 1**

Interpreted depositional setting	Transect	Seq.	Lithologies (Facies code)	Stratal patterns, structures and general attributes	Fossils (see Fig. 5, 6 and 7 for detailed distribution)	Early cements	General diagenetic features
Mid-ramp	Casa Trigu, Ispilunca valley	1a, 1b	Floatstones and rudstones	Large scale planar cross beds, with erosive top laps, 4-8 m thick  Highly fragmented and abraded bioclasts  Moderate sorting	Branching red algae (10-15 %) Bivalves (5-10 %) Large benthic foraminifers (5-10 %) ( <i>Amphistegina</i> , <i>Heterostegina</i> ) Small benthic foraminifers (< 5 %) Encrusting foraminifers (<5%) Barnacles (5-10 %) Reworked corals (< 5 %) Echinoids (5-10 %) Bryozoans (5-10 %)	Rare fibrous and bladed  Poor and fine micritic envelopes	Rare to common early cements  Syntaxial and blocky cements common to present  Biomolds (< 5 %)  Mechanical and chemical compaction
Mid-ramp to outer-ramp  low energy	Casa Trigu, Ispilunca Valley, Sedini south	1a	Floatstones and rudstones	< 8m thick, massive beds	Reworked bioclasts Serpulids	Rare early cements	Mechanical compaction  Scattered zoned dolomite crystals are partially and totally dissolved
Mid ramp	Casa Trigu, Ispilunca Valley	1a/1b	Floatstones	0.5-1.5 m thick, massive beds  Encrustation by red algae, encrusting foraminifers, nodular bryozoans  At Northern Ispilunca valley floatstones are rich in rhodolites	Large benthic foraminifers ( <i>Heterostegina</i> , <i>Amphistegina</i> ) are less fragmented than other facies  Encrusting biota as red algae (5-10 %), encrusting foraminifers (<5 %), bryozoans (< 5 %), and serpulids (1-3 %)	Rare fibrous cements  Common micritic cements	Mechanical compaction  Scattered zoned dolomite crystals are partially and total dissolved
Outer- (proximal) ramp	Ispilunca Valley, Sedini south	1b	Wackestones and Packstones	Parallel bedding, thickness < 1 m  Bioturbation	Echinoids (15-20 %) Bivalves (< 10 %) Serpulids (<5 %) Red algae (5-10 %)		Rare early cements  Some, zoned dolomite crystals are partially and total dissolved

**Table 4.2. Facies and diagenetic features of Sequence 2**

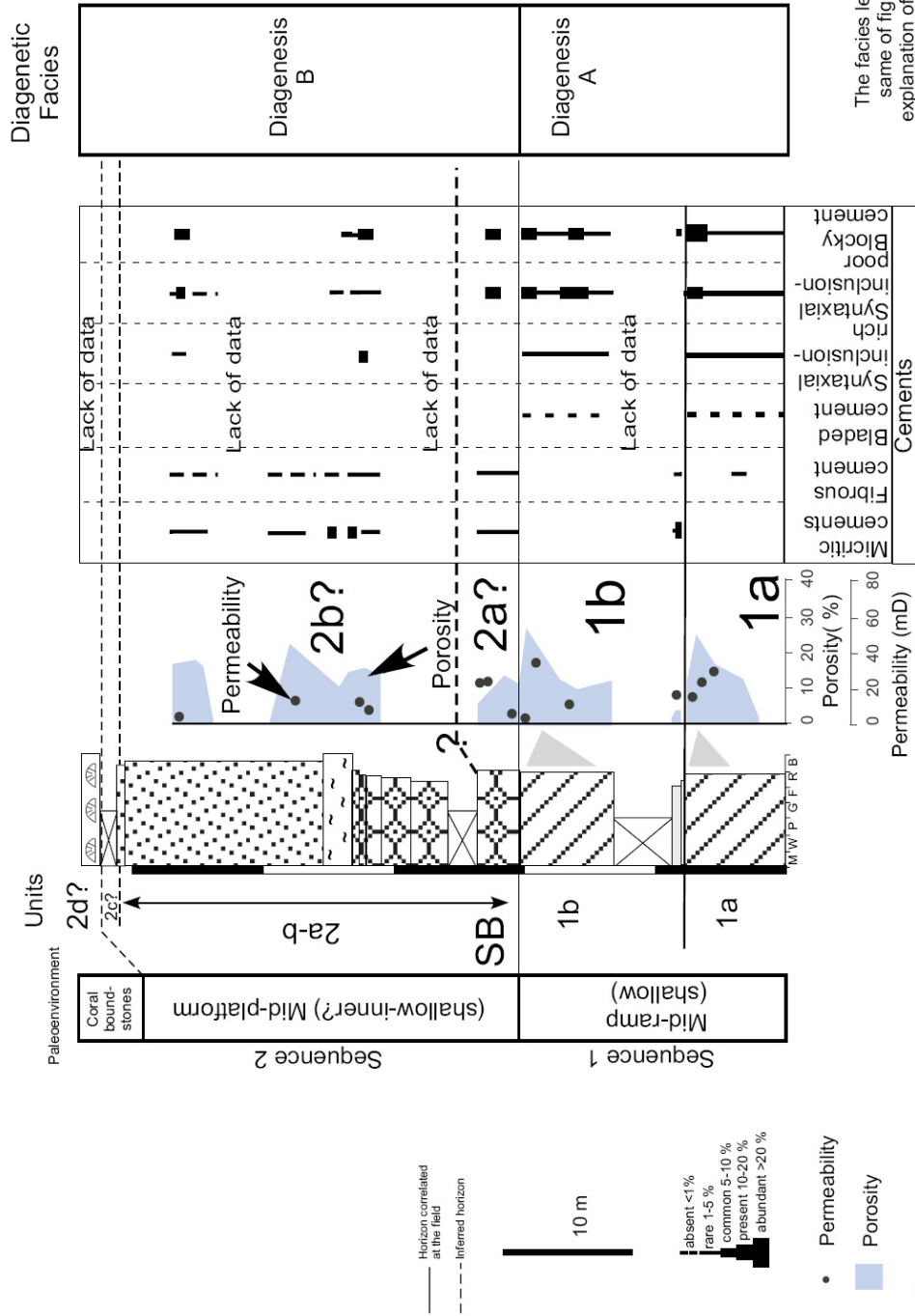
Interpreted depositional setting	Transect	Seq.	Lithologies (Facies code)	Stratal patterns, structures and general attributes	Fossils (see Fig. 5, 7A & 7B for detailed distribution)	Early cements	General diagenetic features
(Inner?) Mid-platform	Casa Trigu, Sa Rocca Manna	2a-e	Bindstones	< 4 m thick, lenses	Encrusting red algae (15-20 %) Bryozoan (5-10 %) Coral (10-15 %) Bivalve (5-10 %) Small benthic foraminifers (< 5 %) Barnacle (1-5 %)	Micritic cements (clotted micropeloidal and lacking internal structure)	Biomold (<5 %)
Platform top (reefer to Benisek et al. in press.)	Casa Trigu	2d?	Coral Boundstones	Up to <6 m thick	Coral (>30 %) Molluscs (10-15 %) Echinoid Nodular bryozoans Encrusting red algae	Lack of data	Lack of data
Mid-platform	Casa Trigu, Ispilunca, Sa Rocca Manna	2a-2d	Well to poor lithified floatstones to rudstones  (include Floatstones 2c described in Benisek et al., in press)	< 1 m- 2 m thick, single lenses Yellow to brown colour	Red algae (encrusting or reworked branches) (10-15 %) Coral fragments (1-5 %) Barnacles Mollusc (10-15 %) Bryozoan (5-10 %) Serpulid (< 1 %) Echinoid (5-10 %) Rhodolites Large benthic foraminifers	Micritic cements (micropeloidal and lacking internal structure),  Micritic envelopes	Rare to common early cements  Biomold (<5 %)
Mid-platform	Casa Trigu Sa Rocca Manna	2a-b	Rudstones to bindstones	Up to 8 m thick, lenses	At Casa Trigu: Coral (10-15 %) (mostly reworked) Mollusc (<10 %) Nodular bryozoans, Encrusting foraminifers Echinoid (1-5 %) Large benthic foraminifers Encrusting and braching red algae  At Sa Rocca Manna: Large benthic foraminifers (15-20 %) Red algae (10 %) Mollusc (< 10 %)	Micritic cements as clotted micropeloidal (> 15 %) (Casa Trigu)	Blocky cement (< 5 %).  Biomold (<5 %)
Mid-platform	Ispilunca, Sa Rocca Manna	2a-d	Wackestones, packstones and grainstones	Large and small scale trough cross-bedding yellow-white colours	Large benthic foraminifers ( <i>Amphistegina</i> , <i>Heterostegina</i> ) (<15 %) Molluscs (<15 %) Branching red algae (10-15 %) Reworked corals (1-5 %) Echinoid (5-10 %) Bryozoans (5-10 %) Small benthic foraminifers (< 10 %)	Fibrous and bladed cements  Micritic envelopes are common and well defined	Biomolds (>5 %)  Syntaxial and blocky cements

Slope	Sa Rocca Manna	2e	Floatstones and rudstones	Clinoforms	Rhodolites, encrusting foraminifers, encrusting bryozoans, molluscs, echinoids, benthic foraminifers		Mechanical and chemical compaction  Syntaxial and Blocky cement
Platform margin (edge)	Sa Rocca Manna	2e	Floatstones/ rudstones to bindstones	Clinoforms top set layers  (Detail information of clinoforms topsets in Benisiek et al, in press.)	Rhodolites, encrusting foraminifers, encrusting bryozoans, molluscs, echinoids Corals are present	Micritic cements	Mechanical compaction
Outer platform	Ispilunca, Sa Rocca Manna	S2	Wackestones and packstones	Brown to yellow- brown colour	Planktonic foraminifers (5-30 %) Small benthic foraminifers (5-10 %) Fragmented echinoids (1-10 %) Mollusc (1-15 %) Red algae (5-10 %) Bryozoan (1-5 %) Serpulid (1-5 %) Coral fragments (1-5 %)		Phosphate Glauconite  Biomolds filled by blocky cements

**APPENDIX  
TABLES-CHAPTER 5**

# APPENDIX 5.1

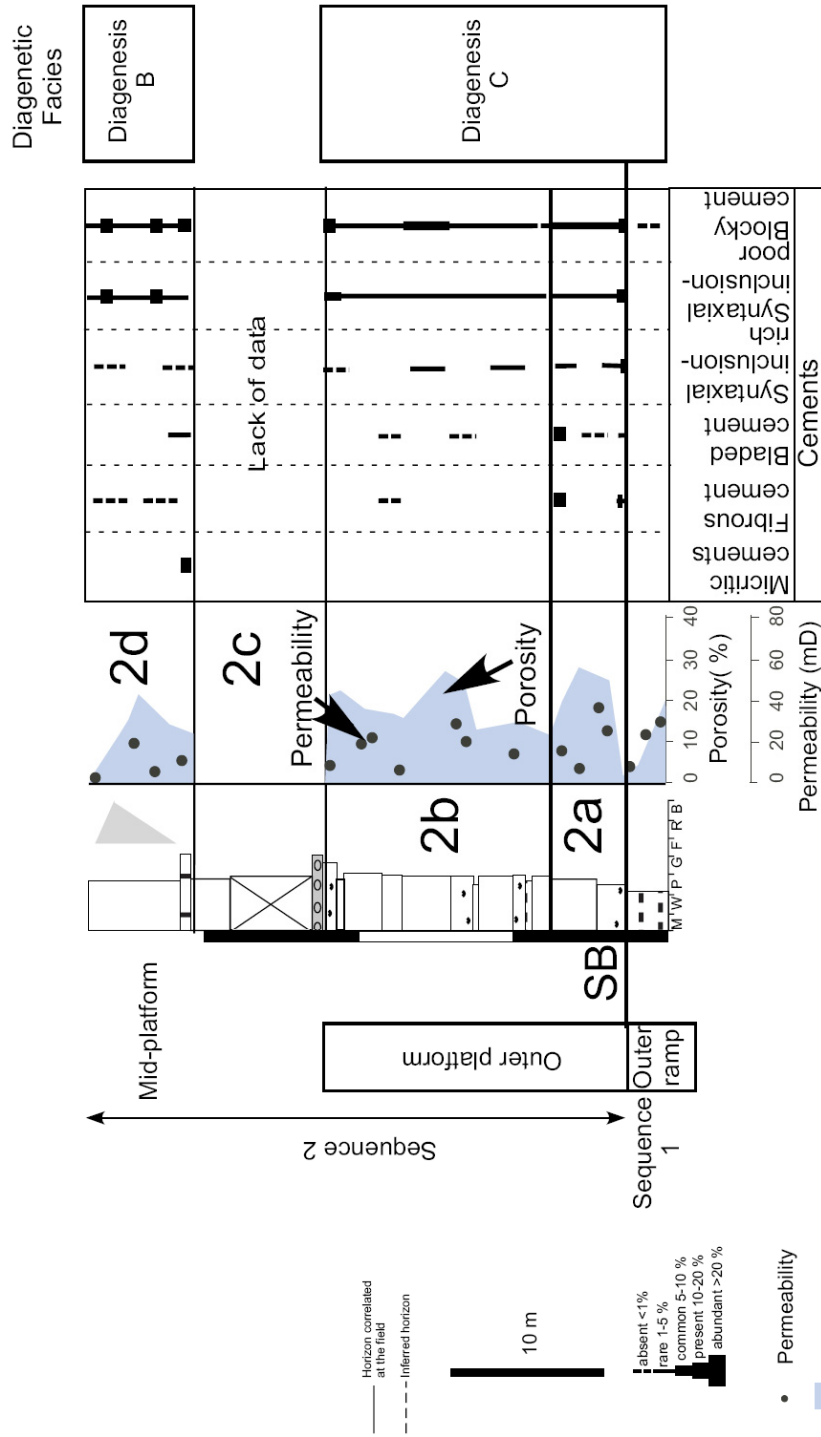
## Diagenesis A-Casa Trigu



The facies legend are the same of figure 5.3. The explanation of the diagenetic facies can be found in Chapter 5.

# APPENDIX 5.2

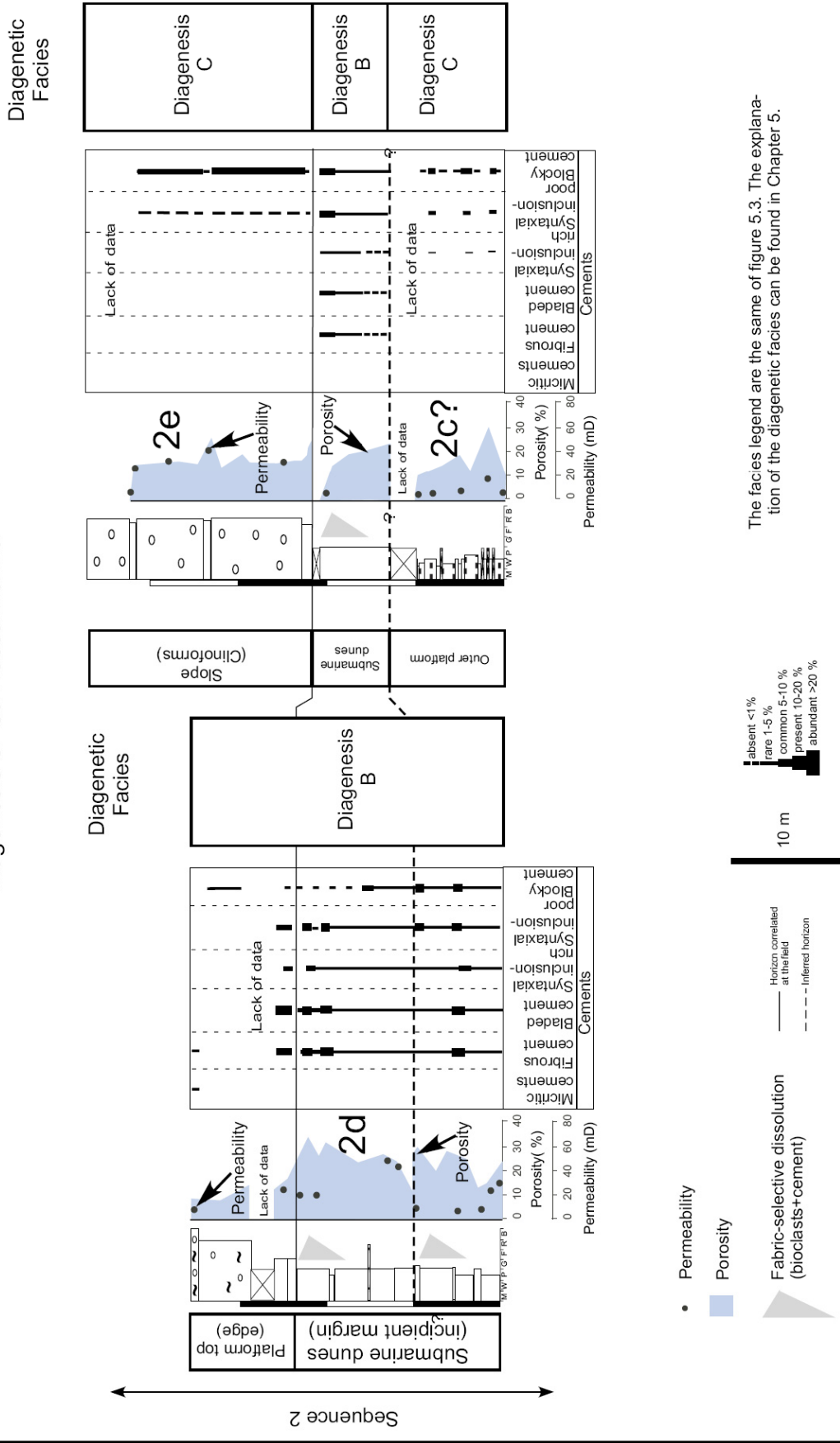
## Diagenesis B- Northern Ispilunca valley



The facies legend are the same of figure 5.3. The explanation of the diagenetic facies can be found in Chapter 5.

# APPENDIX 5.3

Diagenesis C- Sa Rocca Manna



The facies legend are the same of figure 5.3. The explanation of the diagenetic facies can be found in Chapter 5.

# APPENDIX 5.4

Diagenesis and stratigraphy: "Diagenetic Facies"

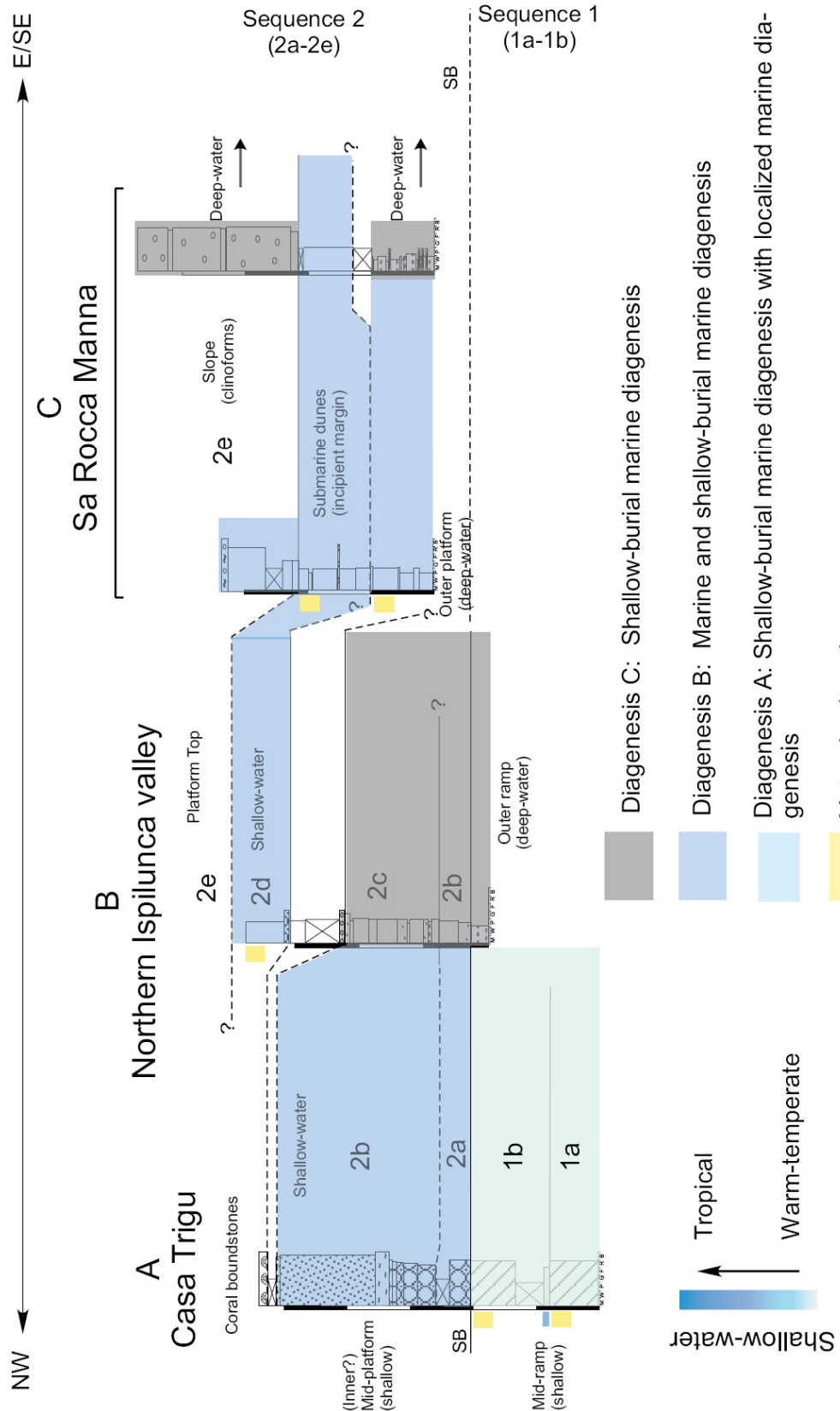




Table 5.1 Trace element values sequence 1

Element	Micrite			Fibrous			Bladed			Syntaxial inclusion rich					
	n	Mean	SD	Min	Max	n	Mean	SD	Min	Max	n	Mean	SD	Min	Max
Fe	9	328	324	0	1003	8	37	61	0	179	9	155	167	0	614
Mn	9	102	103	0	248	8	37	73	0	217	9	19	40	0	124
Mg	9	3571	1415	1466	5229	8	2668	1447	1206	5693	9	1183	259	615	1417
Sr	9	297	145	17	490	8	393	135	228	702	9	324	108	178	507
Ca	9	398652	9206	383208	409366	8	402792	7006	388411	411960	9	405946	14731	364483	412968
<b>Syntaxial inclusion poor</b>															
Element	n	Mean	SD	Min	Max	<b>Blocky calcite (bright orange)</b>			<b>Blocky calcite (dull)</b>						
Fe	13	115	149	0	443	5	152	144	0	365	34	995	431	0	2122
Mn	13	74	87	0	294	5	62	81	0	201	34	170	101	0	372
Mg	13	1107	441	398	2002	5	6785	2560	4397	10651	34	5525	5266	404	34262
Sr	13	265	210	0	702	5	397	101	245	516	34	743	150	262	820
Ca	13	408884	3374	403362	414955	5	378261	15129	356242	394986	34	386614	19146	310941	410645

Table 5.2 Trace element values sequence 2

Element	Micrite			Fibrous			Bladed			Syntaxial inclusion rich					
	n	Mean	SD	Min	Max	n	Mean	SD	Min	Max	n	Mean	SD	Min	Max
Fe	13	737	774	0	4431	2	93	93	0	187	7	131	161	0	435
Mn	13	83	73	0	217	2	0	0	0	0	7	11	18	0	46
Mg	13	3024	557	1858	4716	2	2554	323	2231	2877	7	2516	943	724	3878
Sr	13	459	132	169	972	2	478	114	364	592	7	556	217	245	913
Ca	13	403798	5156	387332	414540	2	399757	11482	388275	411238	7	384149	42676	289139	415348
<b>Syntaxial inclusion poor</b>															
Element	n	Mean	SD	Min	Max	<b>Blocky calcite (bright orange)</b>			<b>Blocky calcite (dull)</b>			<b>Blocky calcite (non-luminescent)</b>			
Fe	71	174	230	0	4043	5	421	362	0	863	12	4494	871	0	3972
Mn	71	59	76	0	98112	5	99	10	0	263	12	216	99	0	434
Mg	71	3095	652	51	16320	5	4982	1474	2370	6694	12	5184	1119	440	7074
Sr	71	316	204	0	803	5	480	331	211	1133	12	1185	235	169	1674
Ca	71	409619	3811	396623	418793	5	407363	4229	402583	413461	12	403030	3093	392606	402390
Fe	9	1759	2437	187	6980	9	102	159	0	403	9	3556	829	2509	5066
Mn	9	102	159	0	403	9	102	159	0	403	9	102	159	0	403
Mg	9	3556	829	2509	5066	9	3556	829	2509	5066	9	3556	829	2509	5066
Sr	9	421	160	135	685	9	421	160	135	685	9	421	160	135	685
Ca	9	405564	4013	399031	410181	9	405564	4013	399031	410181	9	405564	4013	399031	410181

**APPENDIX  
TABLES-CHAPTER 6**

Table 6.1. Section "D" (Tanca Manna/Q samples)

Sample	$\delta^{18}\text{O}$ Bulk rock (i) ‰ vs. PDB	$\delta^{13}\text{C}$ Bulk rock (i) ‰ vs. PDB	$\gamma$	$\Delta\sigma$	$\lambda$	$\Delta c$	$\delta^{18}\text{O}$ Bulk rock (f) ‰ vs. PDB	$\delta^{13}\text{C}$ Bulk rock (f) ‰ vs. PDB
Q-29	-2,56	0,04	-3,00	0,44	-2,00	2,04	-2,56	0,04
Q-28	-3,54	-0,54	-3,00	-0,54	-2,00	1,46	no data	-0,54
Q-27.6	-2,09	0,08	-3,00	0,91	-2,00	2,08	-2,09	0,08
Q-27.4	-1,86	-0,16	-3,00	1,14	-2,00	1,84	-1,86	-0,16
Q-27	-2,68	0,06	-3,00	0,32	-2,00	2,06	-2,68	0,06
Q-26.8	-1,39	0,61	-3,00	1,61	-2,00	2,61	-1,39	0,61
Q-26.6	-2,20	-0,26	-3,00	0,80	-2,00	1,74	-2,20	-0,26
Q-26	-2,72	0,26	-3,00	0,28	-2,00	2,26	-2,72	0,26
Q-25.8	-2,65	0,19	-3,00	0,35	-2,00	2,19	-2,65	0,19
Q-25.6	-1,96	0,46	-3,00	1,04	-2,00	2,46	-1,96	0,46
Q-25.4	-2,54	0,57	-3,00	0,46	-2,00	2,57	-2,54	0,57
Q-25	-2,11	0,71	-3,00	0,89	-2,00	2,71	-2,11	0,71
Q-24.8	-1,76	0,83	-3,00	1,24	-2,00	2,83	-1,76	0,83
Q-24.6	-1,96	0,53	-3,00	1,04	-2,00	2,53	-1,96	0,53
Q-24.4	-1,35	0,81	-3,00	1,65	-2,00	2,81	-1,35	0,81
Q-24.4	-1,49	0,65	-3,00	1,51	-2,00	2,65	-1,49	0,65
Q-24.2	-2,08	0,69	-3,00	0,92	-2,00	2,69	-2,08	0,69
Q-23.6	-1,93	0,58	-3,00	1,07	-2,00	2,58	-1,93	0,58
Q-23.6	-2,12	0,62	-3,00	0,88	-2,00	2,62	-2,12	0,62
Q-23.4	-1,60	0,83	-3,00	1,40	-2,00	2,83	-1,60	0,83
Q-23.2	-1,99	0,68	-3,00	1,01	-2,00	2,68	-1,99	0,68
Q-22.8	-2,31	0,55	-3,00	0,69	-2,00	2,55	-2,31	0,55
Q-22.4	-2,52	0,50	-3,00	0,48	-2,00	2,50	-2,52	0,50
Q-22.2	-2,37	0,59	-3,00	0,63	-2,00	2,59	-2,37	0,59
Q-22	-2,35	0,61	-3,00	0,65	-2,00	2,61	-2,35	0,61
Q-21.8	-2,82	0,64	-3,00	0,18	-2,00	2,64	-2,82	0,64
Q-21.6	-1,70	0,42	-3,00	1,30	-2,00	2,42	-1,70	0,42
Q-21.4	-2,43	0,39	-3,00	0,57	-2,00	2,39	-2,43	0,39
Q-21.2	-1,62	0,62	-3,00	1,38	-2,00	2,62	-1,62	0,62
Q-21	-1,81	0,46	-3,00	1,19	-2,00	2,46	-1,81	0,46
Q-20.6	-2,50	0,33	-3,00	0,50	-2,00	2,33	-2,50	0,33
Q-20.4	-1,81	0,67	-3,00	1,19	-2,00	2,67	-1,81	0,67
Q-20.2	-1,79	0,69	-3,00	1,21	-2,00	2,69	-1,79	0,69
Q-20	-1,63	0,43	-3,00	1,37	-2,00	2,43	-1,63	0,43
Q-19.6	-2,37	0,35	-3,00	0,63	-2,00	2,35	-2,37	0,35
Q-18.0	-1,80	0,59	-3,00	1,20	-2,00	2,59	-1,80	0,59
Q-17.7	-1,78	0,62	-3,00	1,22	-2,00	2,62	-1,78	0,62
Q-17.5	-1,84	0,49	-3,00	1,16	-2,00	2,49	-1,84	0,49
Q-17	-2,41	0,04	-3,00	0,59	-2,00	2,04	-2,41	0,04
Q-16.8	-2,47	0,25	-3,00	0,53	-2,00	2,25	-2,47	0,25
Q-16.6	-1,90	0,32	-3,00	1,10	-2,00	2,32	-1,90	0,32
Q-16.4	-2,19	0,35	-3,00	0,81	-2,00	2,35	-2,19	0,35
Q-16.2	-1,39	0,47	-3,00	1,61	-2,00	2,47	-1,39	0,47
Q-16.0	-1,40	0,64	-3,00	1,60	-2,00	2,64	-1,40	0,64
Q-15.8	-1,23	0,48	-3,00	1,77	-2,00	2,48	-1,23	0,48
Q-15.6	-2,28	0,41	-3,00	0,72	-2,00	2,41	-2,28	0,41
Q-15.4	-1,25	0,38	-3,00	1,75	-2,00	2,38	-1,25	0,38
Q-15.2	-2,47	0,57	-3,00	0,53	-2,00	2,57	-2,47	0,57
Q-15.0	-2,17	0,48	-3,00	0,83	-2,00	2,48	-2,17	0,48
Q-14.6	-2,17	0,53	-3,00	0,83	-2,00	2,53	-2,17	0,53
Q-14.4	-1,69	0,55	-3,00	1,31	-2,00	2,55	-1,69	0,55
Q-13.6	-1,47	0,66	-3,00	1,53	-2,00	2,66	-1,47	0,66
Q-13.4	-2,22	0,42	-3,00	0,78	-2,00	2,42	-2,22	0,42
Q-13.2	-2,45	0,68	-3,00	0,55	-2,00	2,68	-2,45	0,68
Q-12.4	-2,22	0,49	-3,00	0,78	-2,00	2,49	-2,22	0,49
Q-12.2	-1,60	0,34	-3,00	1,40	-2,00	2,34	-1,60	0,34
Q-11.4	-2,26	0,04	-3,00	0,74	-2,00	2,04	-2,26	0,04
Q-11.0	-2,46	0,50	-3,00	0,54	-2,00	2,50	-2,46	0,50
Q-10.8	-3,15	0,24	-3,00	-0,15	-2,00	2,24	no data	0,24
Q-10.6	-2,96	0,45	-3,00	0,04	-2,00	2,45	-2,96	0,45
Q-10.3	-2,17	0,54	-3,00	0,83	-2,00	2,54	-2,17	0,54
Q-10.0	-3,02	0,61	-3,00	-0,02	-2,00	2,61	no data	0,61

Cont. Table 6.1. Section "D" (Tanca Manna/Q samples)

Sample	$\delta^{18}\text{O}$ Bulk rock (i) ‰ vs. PDB	$\delta^{13}\text{C}$ Bulk rock (i) ‰ vs. PDB	$\gamma$	$\Delta\delta$	$\lambda$	$\Delta c$	$\delta^{18}\text{O}$ Bulk rock (f) ‰ vs. PDB	$\delta^{13}\text{C}$ Bulk rock (f) ‰ vs. PDB
Q-9.8	-2,48	0,52	-3,00	0,52	-2,00	2,52	-2,48	0,52
Q-9.6	-2,13	0,51	-3,00	0,87	-2,00	2,51	-2,13	0,51
Q-9.4	-2,83	0,52	-3,00	0,17	-2,00	2,52	-2,83	0,52
Q-9.0	-2,42	0,60	-3,00	0,58	-2,00	2,60	-2,42	0,60
Q-8.8	-2,31	0,56	-3,00	0,69	-2,00	2,56	-2,31	0,56
Q-8.6	-2,03	0,40	-3,00	0,97	-2,00	2,40	-2,03	0,40
Q-8.4	-1,65	0,16	-3,00	1,35	-2,00	2,16	-1,65	0,16
Q-8.0	-2,47	0,49	-3,00	0,53	-2,00	2,49	-2,47	0,49
Q-7.8	-3,54	0,44	-3,00	-0,54	-2,00	2,44	no data	0,44
Q-7.6	-3,05	0,41	-3,00	-0,05	-2,00	2,41	no data	0,41
Q-7.2	-2,92	0,69	-3,00	0,08	-2,00	2,69	-2,92	0,69
Q-6.9	-2,50	0,07	-3,00	0,50	-2,00	2,07	-2,50	0,07
Q-6.5	-3,03	0,61	-3,00	-0,03	-2,00	2,61	no data	0,61
Q-6.3	-2,70	0,24	-3,00	0,30	-2,00	2,24	-2,70	0,24
Q-5.9	-2,88	0,19	-3,00	0,12	-2,00	2,19	-2,88	0,19
Q-5.7	-2,17	0,58	-3,00	0,83	-2,00	2,58	-2,17	0,58
Q-5.5	-1,71	0,57	-3,00	1,29	-2,00	2,57	-1,71	0,57
Q-5.3	-1,80	0,45	-3,00	1,20	-2,00	2,45	-1,80	0,45
Q-4.7	-1,57	0,25	-3,00	1,43	-2,00	2,25	-1,57	0,25
Q-4.5	-2,30	0,19	-3,00	0,70	-2,00	2,19	-2,30	0,19
Q-4.2	-2,88	0,04	-3,00	0,12	-2,00	2,04	-2,88	0,04
Q-4.0	-2,63	-0,07	-3,00	0,37	-2,00	1,93	-2,63	-0,07
Q-3.7	-2,31	0,40	-3,00	0,69	-2,00	2,40	-2,31	0,40
Q-3.5	-2,77	-0,08	-3,00	0,23	-2,00	1,92	-2,77	-0,08
Q-2.9	-1,86	0,19	-3,00	1,14	-2,00	2,19	-1,86	0,19
Q-2.7	-2,26	0,24	-3,00	0,74	-2,00	2,24	-2,26	0,24
Q-2.5	-2,22	0,24	-3,00	0,78	-2,00	2,24	-2,22	0,24
Q-2.3	-3,27	0,33	-3,00	-0,27	-2,00	2,33	no data	0,33
Q-2.1	-3,64	0,27	-3,00	-0,64	-2,00	2,27	no data	0,27
Q-1.9	-3,90	0,36	-3,00	-0,90	-2,00	2,36	no data	0,36
Q-1.7	-3,32	0,04	-3,00	-0,32	-2,00	2,04	no data	0,04
Q-1.4	-2,45	0,53	-3,00	0,55	-2,00	2,53	-2,45	0,53
Q-1.2	-3,37	0,42	-3,00	-0,37	-2,00	2,42	no data	0,42
Q-1.0	-3,49	0,22	-3,00	-0,49	-2,00	2,22	no data	0,22
Q-0.8	-3,23	0,48	-3,00	-0,23	-2,00	2,48	no data	0,48
Q-0.6	-3,02	0,45	-3,00	-0,02	-2,00	2,45	no data	0,45
Q-0.4	-3,25	0,45	-3,00	-0,25	-2,00	2,45	no data	0,45
Q-0.2	-2,42	0,51	-3,00	0,58	-2,00	2,51	-2,42	0,51

Table 6.2. Section "E" (Marls/SM samples)

Sample	$\delta^{18}\text{O}$ Bulk rock (i) ‰ vs. PDB	$\delta^{13}\text{C}$ Bulk rock (i) ‰ vs. PDB	$\gamma$	$\Delta\alpha$	$\lambda$	$\Delta\epsilon$	$\delta^{18}\text{O}$ Bulk rock (f) ‰ vs. PDB	$\delta^{13}\text{C}$ Bulk rock (f) ‰ vs. PDB
SM-9.3	-3,50	-0,17	-3,00	-0,50	-2,00	1,83	no data	no data
SM-8.7	-2,76	0,42	-3,00	0,24	-2,00	2,42	-2,76	0,42
SM-8.1	-2,52	0,60	-3,00	0,48	-2,00	2,60	-2,52	0,60
SM-7.8	-2,80	0,84	-3,00	0,20	-2,00	2,84	-2,80	0,84
SM-7.5	-2,04	1,09	-3,00	0,96	-2,00	3,09	-2,04	1,09
SM-7.2	-3,55	0,62	-3,00	-0,55	-2,00	2,62	no data	no data
SM-6.9	-2,74	0,56	-3,00	0,26	-2,00	2,56	-2,74	0,56
SM-6.6	-2,44	0,27	-3,00	0,56	-2,00	2,27	-2,44	0,27
SM-6.3	-2,68	0,32	-3,00	0,32	-2,00	2,32	-2,68	0,32
SM-6.0	-2,70	0,76	-3,00	0,30	-2,00	2,76	-2,70	0,76
SM-5.7	-3,18	0,97	-3,00	-0,18	-2,00	2,97	no data	no data
SM-5.4	-2,59	0,74	-3,00	0,41	-2,00	2,74	-2,59	0,74
SM-5.1	-2,22	0,32	-3,00	0,78	-2,00	2,32	-2,22	0,32
SM-4.8	-3,01	0,34	-3,00	-0,01	-2,00	2,34	no data	no data
SM-4.5	-3,49	-0,44	-3,00	-0,49	-2,00	1,56	no data	no data
SM-4.2	-3,08	0,33	-3,00	-0,08	-2,00	2,33	no data	no data
SM-3.9	-2,73	0,86	-3,00	0,27	-2,00	2,86	-2,73	0,86
SM-3.6	-2,20	0,80	-3,00	0,80	-2,00	2,80	-2,20	0,80
SM-3.3	-2,70	0,79	-3,00	0,30	-2,00	2,79	-2,70	0,79
SM-3.0	-1,93	1,54	-3,00	1,07	-2,00	3,54	-1,93	1,54
SM-2.7	-1,97	1,11	-3,00	1,03	-2,00	3,11	-1,97	1,11
SM-2.4	-3,02	0,77	-3,00	-0,02	-2,00	2,77	no data	no data
SM-1.5	-2,91	0,73	-3,00	0,09	-2,00	2,73	-2,91	0,73
SM-1.2	-3,06	0,34	-3,00	-0,06	-2,00	2,34	no data	no data
SM-0.9	-2,41	0,82	-3,00	0,59	-2,00	2,82	-2,41	0,82
SM-0.3	-3,21	0,54	-3,00	-0,21	-2,00	2,54	no data	no data
SM-BASE	-2,32	0,95	-3,00	0,68	-2,00	2,95	-2,32	0,95

Table 6.3. Section "F" (Sedini South/S4ALDO samples)

Sample	$\delta^{18}\text{O}$ Bulk rock (i) ‰ vs. PDB	$\delta^{13}\text{C}$ Bulk rock (i) ‰ vs. PDB	$\gamma$	$\Delta\sigma$	$\lambda$	$\Delta c$	$\delta^{18}\text{O}$ Bulk rock (f) ‰ vs. PDB	$\delta^{13}\text{C}$ Bulk rock (f) ‰ vs. PDB
S4ALDO-14.5	-4,62	0,00	-3,00	-1,62	-2,00	2,00	no data	0,00
S4ALDO-14.0	-5,13	0,62	-3,00	-2,13	-2,00	2,62	no data	0,62
S4ALDO-13.5	-4,71	0,77	-3,00	-1,71	-2,00	2,77	no data	0,77
S4ALDO-12.9	-4,37	-0,29	-3,00	-1,37	-2,00	1,71	no data	-0,29
S4ALDO-12.6	-4,53	0,29	-3,00	-1,53	-2,00	2,29	no data	0,29
S4ALDO-12.3	-4,52	0,38	-3,00	-1,52	-2,00	2,38	no data	0,38
S4ALDO-12.00	-4,50	-0,23	-3,00	-1,50	-2,00	1,77	no data	-0,23
S4ALDO-11.6	-4,01	0,84	-3,00	-1,01	-2,00	2,84	no data	0,84
S4ALDO-11.3	-4,14	0,73	-3,00	-1,14	-2,00	2,73	no data	0,73
S4ALDO-10.8	-3,90	0,94	-3,00	-0,90	-2,00	2,94	no data	0,94
S4ALDO-10.4	-4,18	0,99	-3,00	-1,18	-2,00	2,99	no data	0,99
S4ALDO-10.00	-5,03	1,01	-3,00	-2,03	-2,00	3,01	no data	1,01
S4ALDO-9.70	-4,21	0,75	-3,00	-1,21	-2,00	2,75	no data	0,75
S4ALDO-9.00	-4,86	0,75	-3,00	-1,86	-2,00	2,75	no data	0,75
S4ALDO-8.35	-4,37	0,89	-3,00	-1,37	-2,00	2,89	no data	0,89
S4ALDO-8.05	-4,17	0,67	-3,00	-1,17	-2,00	2,67	no data	0,67
S4ALDO-7.75	-4,82	0,80	-3,00	-1,82	-2,00	2,80	no data	0,80
S4ALDO-7.3	-4,18	0,94	-3,00	-1,18	-2,00	2,94	no data	0,94
S4ALDO-7.00	-4,48	1,24	-3,00	-1,48	-2,00	3,24	no data	1,24
S4ALDO-6.25	-4,19	1,31	-3,00	-1,19	-2,00	3,31	no data	1,31
S4ALDO-5.95	-4,19	0,91	-3,00	-1,19	-2,00	2,91	no data	0,91
S4ALDO-5.55	-4,00	0,97	-3,00	-1,00	-2,00	2,97	no data	0,97
S4ALDO-4.9	-3,97	1,45	-3,00	-0,97	-2,00	3,45	no data	1,45
S4ALDO-4.45	-4,25	1,47	-3,00	-1,25	-2,00	3,47	no data	1,47
S4ALDO-4.0	-4,10	1,35	-3,00	-1,10	-2,00	3,35	no data	1,35
S4ALDO-3.7	-3,99	1,33	-3,00	-0,99	-2,00	3,33	no data	1,33
S4ALDO-3.4	-3,77	1,10	-3,00	-0,77	-2,00	3,10	no data	1,10
S4ALDO-3.25	-3,95	1,26	-3,00	-0,95	-2,00	3,26	no data	1,26

Table 6.4. Section "C" (Sa Rocca Manna/Section C1)

Sample	$\delta^{18}\text{O}$ Bulk rock (i) ‰ vs. PDB	$\delta^{13}\text{C}$ Bulk rock (i) ‰ vs. PDB	$\gamma$	$\Delta\alpha$	$\lambda$	$\Delta\epsilon$	$\delta^{18}\text{O}$ Bulk rock (f) ‰ vs. PDB	$\delta^{13}\text{C}$ Bulk rock (f) ‰ vs. PDB
VT5-3.0	-4,16	-1,16	-3,00	-1,16	-2,00	0,84	no data	-1,16
VT5-2.5	-4,99	-1,87	-3,00	-1,99	-2,00	0,13	no data	-1,87
VTCLINO-18	-4,72	-1,71	-3,00	-1,72	-2,00	0,29	no data	-1,71
VTCLINO-17	-4,37	-1,16	-3,00	-1,37	-2,00	0,84	no data	-1,16
VT4-2.5	-4,68	-1,67	-3,00	-1,68	-2,00	0,33	no data	-1,67
VT4-2.0	-3,29	-1,57	-3,00	-0,29	-2,00	0,43	no data	-1,57
VT4-1.2	-3,65	-0,30	-3,00	-0,65	-2,00	1,70	no data	-0,30
VT4-0.7	-2,60	-0,85	-3,00	0,40	-2,00	1,15	-2,60	-0,85
VTCLINO-8	-4,56	-1,08	-3,00	-1,56	-2,00	0,92	no data	-1,08
VTCLINO-6	-4,69	-1,43	-3,00	-1,69	-2,00	0,57	no data	-1,43
VTCLINO-3	-4,83	-1,87	-3,00	-1,83	-2,00	0,13	no data	-1,87
VTCLINO-2	-4,81	-1,23	-3,00	-1,81	-2,00	0,77	no data	-1,23
VTCLINO-1	-4,68	-1,28	-3,00	-1,68	-2,00	0,72	no data	-1,28
VT1-17.4	-4,61	-1,58	-3,00	-1,61	-2,00	0,42	no data	-1,58
H	-4,55	-1,45	-3,00	-1,55	-2,00	0,55	no data	-1,45
VT1-16.9	-3,81	-1,42	-3,00	-0,81	-2,00	0,58	no data	-1,42
VT1-16.4	-4,06	-2,71	-3,00	-1,06	-2,00	-0,71	no data	no data
VT1-15.9	-3,90	-1,83	-3,00	-0,90	-2,00	0,17	no data	-1,83
VT1-15.4	-3,26	-0,92	-3,00	-0,26	-2,00	1,08	no data	-0,92
VT1-14.9	-3,58	-0,50	-3,00	-0,58	-2,00	1,50	no data	-0,50
VT2-19	-4,76	-1,76	-3,00	-1,76	-2,00	0,24	no data	-1,76
VT2-18	-3,83	-1,65	-3,00	-0,83	-2,00	0,35	no data	-1,65
VT2-16	-3,08	-0,02	-3,00	-0,08	-2,00	1,98	no data	-0,02
VT2-9.77	-2,64	-0,13	-3,00	0,36	-2,00	1,87	-2,64	-0,13
VT2-9.37	-2,08	0,06	-3,00	0,92	-2,00	2,06	-2,08	0,06
VT2-8.45	-3,06	0,62	-3,00	-0,06	-2,00	2,62	no data	0,62
VT2-7.69	-2,37	0,56	-3,00	0,63	-2,00	2,56	-2,37	0,56
VT2-6.5	-2,64	0,47	-3,00	0,36	-2,00	2,47	-2,64	0,47
VT2-5.5	-1,72	0,86	-3,00	1,28	-2,00	2,86	-1,72	0,86
VT2-4.5	-3,44	0,22	-3,00	-0,44	-2,00	2,22	no data	0,22
VT2-3.56	-2,50	0,48	-3,00	0,50	-2,00	2,48	-2,50	0,48
VT2-3.56	-2,92	0,37	-3,00	0,08	-2,00	2,37	-2,92	0,37
VT2-3.06	-1,90	0,65	-3,00	1,10	-2,00	2,65	-1,90	0,65
VT2-2.56	-2,03	0,73	-3,00	0,97	-2,00	2,73	-2,03	0,73
VT2-2.06	-2,09	0,51	-3,00	0,91	-2,00	2,51	-2,09	0,51
VT2-1.64	-2,99	0,38	-3,00	0,01	-2,00	2,38	-2,99	0,38
VT2-1.3	-1,53	0,71	-3,00	1,47	-2,00	2,71	-1,53	0,71
VT2-1.08	-2,67	0,38	-3,00	0,33	-2,00	2,38	-2,67	0,38
VT2-0.5	-1,91	2,06	-3,00	1,09	-2,00	4,06	-1,91	2,06

Table 6.5. Section "C" (Sa Rocca Manna/Section VT7)

Sample	$\delta^{18}\text{O}$ Bulk rock (i) ‰ vs. PDB	$\delta^{13}\text{C}$ Bulk rock (i) ‰ vs. PDB	$\gamma$	$\Delta\alpha$	$\lambda$	$\Delta c$	$\delta^{18}\text{O}$ Bulk rock (f) ‰ vs. PDB	$\delta^{13}\text{C}$ Bulk rock (f) ‰ vs. PDB
VT7-TOP	-5,52	-2,52	-3,00	-2,52	-2,00	-0,52	no data	no data
VTCLINO-20	-5,12	-2,11	-3,00	-2,12	-2,00	-0,11	no data	no data
VTCLINO-21	-5,02	-1,98	-3,00	-2,02	-2,00	0,02	no data	-1,98
VTCLINO-22	-5,25	-1,89	-3,00	-2,25	-2,00	0,11	no data	-1,89
VT7-27	-4,97	-1,39	-3,00	-1,97	-2,00	0,61	no data	-1,39
VT7-26	-5,64	-1,69	-3,00	-2,64	-2,00	0,31	no data	-1,69
VT7-25.4	-6,03	-1,65	-3,00	-3,03	-2,00	0,35	no data	-1,65
VT7-25.1	-5,17	-1,05	-3,00	-2,17	-2,00	0,95	no data	-1,05
VT7-25	-5,67	-3,30	-3,00	-2,67	-2,00	-1,30	no data	no data
VT7-25	-5,68	-3,47	-3,00	-2,68	-2,00	-1,47	no data	no data
VT7-24	-5,43	-2,54	-3,00	-2,43	-2,00	-0,54	no data	no data
VT7-23.2	-4,75	-1,86	-3,00	-1,75	-2,00	0,14	no data	-1,86
VT7-23	-5,15	-1,37	-3,00	-2,15	-2,00	0,63	no data	-1,37
VT7-22.2	-5,22	-0,94	-3,00	-2,22	-2,00	1,06	no data	-0,94
VT7-21	-4,20	-0,46	-3,00	-1,20	-2,00	1,54	no data	-0,46
VT7-15.8	-4,01	-0,32	-3,00	-1,01	-2,00	1,68	no data	-0,32
VT7-15.5	-4,04	-0,59	-3,00	-1,04	-2,00	1,41	no data	-0,59
VT7-15.1	-4,12	-0,21	-3,00	-1,12	-2,00	1,79	no data	-0,21
VT7-15	-4,25	-0,70	-3,00	-1,25	-2,00	1,30	no data	-0,70
VT7-14.9	-4,26	-0,72	-3,00	-1,26	-2,00	1,28	no data	-0,72
VT7-14	-4,46	-1,44	-3,00	-1,46	-2,00	0,56	no data	-1,44
VT7-13	-4,27	-1,63	-3,00	-1,27	-2,00	0,37	no data	-1,63
VT7-13	-4,33	-1,55	-3,00	-1,33	-2,00	0,45	no data	-1,55
VT7-11.9	-4,57	-0,52	-3,00	-1,57	-2,00	1,48	no data	-0,52
VT7-10.7	-4,54	-0,70	-3,00	-1,54	-2,00	1,30	no data	-0,70
VT7-10.5	-4,27	-1,85	-3,00	-1,27	-2,00	0,15	no data	-1,85
VT7-10.4	-4,36	-2,49	-3,00	-1,36	-2,00	-0,49	no data	no data
VT7-8.8	-3,97	0,07	-3,00	-0,97	-2,00	2,07	no data	0,07
VT7-7.3	-4,59	-0,21	-3,00	-1,59	-2,00	1,79	no data	-0,21
VT7-6.2	-4,37	-2,53	-3,00	-1,37	-2,00	-0,53	no data	no data
VT7-6.0	-4,46	-0,39	-3,00	-1,46	-2,00	1,61	no data	-0,39
VT7-5.8	-4,03	-0,54	-3,00	-1,03	-2,00	1,46	no data	-0,54
VT7-5.2	-4,63	-0,56	-3,00	-1,63	-2,00	1,44	no data	-0,56
VT7-4.5	-4,61	-0,72	-3,00	-1,61	-2,00	1,28	no data	-0,72
VT7-4.0	-4,49	-0,24	-3,00	-1,49	-2,00	1,76	no data	-0,24
VT7-3.7	-5,06	-1,68	-3,00	-2,06	-2,00	0,32	no data	-1,68
VT7-3.1	-4,48	-1,98	-3,00	-1,48	-2,00	0,02	no data	-1,98
VT7-2.7	-3,93	-1,21	-3,00	-0,93	-2,00	0,79	no data	-1,21
VT7-1.5	-3,04	0,30	-3,00	-0,04	-2,00	2,30	no data	0,30



Table 6.6 Section "B" (Northern Ispilunca Valley)

Sample	$\delta^{18}\text{O}$ Bulk rock (i) ‰ vs. PDB	$\delta^{13}\text{C}$ Bulk rock (i) ‰ vs. PDB	$\gamma$	$\Delta\alpha$	$\lambda$	$\Delta c$	$\delta^{18}\text{O}$ Bulk rock (f) ‰ vs. PDB	$\delta^{13}\text{C}$ Bulk rock (f) ‰ vs. PDB
S8-9.9	-4,77	-1,02	-3,00	-1,77	-2,00	0,98	no data	-1,02
S8-9.5	-4,39	-1,02	-3,00	-1,39	-2,00	0,98	no data	-1,02
S8-9.0	-4,99	-0,61	-3,00	-1,99	-2,00	1,39	no data	-0,61
S8-8.0	-5,26	-0,58	-3,00	-2,26	-2,00	1,42	no data	-0,58
S8-7.5	-4,38	-0,72	-3,00	-1,38	-2,00	1,28	no data	-0,72
S8-7.0	-4,20	0,10	-3,00	-1,20	-2,00	2,10	no data	0,10
S8-6.5	-3,82	0,30	-3,00	-0,82	-2,00	2,30	no data	0,30
S8-6.0	-3,83	0,27	-3,00	-0,83	-2,00	2,27	no data	0,27
S8-5.5	-3,99	0,31	-3,00	-0,99	-2,00	2,31	no data	0,31
S8-5.0	-4,37	-0,47	-3,00	-1,37	-2,00	1,53	no data	-0,47
S8-4.5	-3,66	-0,13	-3,00	-0,66	-2,00	1,87	no data	-0,13
S8-4.0	-4,34	0,23	-3,00	-1,34	-2,00	2,23	no data	0,23
S8-3.5	-3,99	0,32	-3,00	-0,99	-2,00	2,32	no data	0,32
S8-3.0	-3,54	0,55	-3,00	-0,54	-2,00	2,55	no data	0,55
S8-2.5	-3,63	-0,03	-3,00	-0,63	-2,00	1,97	no data	-0,03
S8-2.0	-3,64	-0,16	-3,00	-0,64	-2,00	1,84	no data	-0,16
S8-1.5	-3,86	-0,08	-3,00	-0,86	-2,00	1,92	no data	-0,08
S8-1.0	-3,47	-0,04	-3,00	-0,47	-2,00	1,96	no data	-0,04
S8-0.5	-3,28	-0,28	-3,00	-0,28	-2,00	1,72	no data	-0,28
S8-0.3	-4,12	0,85	-3,00	-1,12	-2,00	2,85	no data	0,85
S7-14.5	-5,02	-0,85	-3,00	-2,02	-2,00	1,15	no data	-0,85
S7-14.4	-4,47	-1,81	-3,00	-1,47	-2,00	0,19	no data	-1,81
S7-14.0	-3,58	-0,75	-3,00	-0,58	-2,00	1,25	no data	-0,75
S7-13.5	-3,06	-0,90	-3,00	-0,06	-2,00	1,10	no data	-0,90
S7-13.0	-3,70	-1,98	-3,00	-0,70	-2,00	0,02	no data	-1,98
S7-12.8	-3,65	-0,16	-3,00	-0,65	-2,00	1,84	no data	-0,16
S7-12.5	-4,30	0,40	-3,00	-1,30	-2,00	2,40	no data	0,40
S7-12.0	-3,94	0,29	-3,00	-0,94	-2,00	2,29	no data	0,29
S7-11.5	-2,97	0,26	-3,00	0,03	-2,00	2,26	-2,97	0,26
S7-10.5	-4,10	0,09	-3,00	-1,10	-2,00	2,09	no data	0,09
S7-9.5	-3,93	-2,09	-3,00	-0,93	-2,00	-0,09	no data	-2,09
S7-9.0	-3,70	0,07	-3,00	-0,70	-2,00	2,07	no data	0,07
S7-8.5	-3,41	0,36	-3,00	-0,41	-2,00	2,36	no data	0,36
S7-8.0	-3,56	0,55	-3,00	-0,56	-2,00	2,55	no data	0,55
S7-7.9	-3,56	-0,34	-3,00	-0,56	-2,00	1,66	no data	-0,34
S7-7.5	-3,17	-0,78	-3,00	-0,17	-2,00	1,22	no data	-0,78
S7-7.0	-2,89	-0,15	-3,00	0,11	-2,00	1,85	-2,89	-0,15
S7-6.5	-3,42	-0,09	-3,00	-0,42	-2,00	1,91	no data	-0,09
S7-6.0	-2,51	0,03	-3,00	0,49	-2,00	2,03	-2,51	0,03
S7-5.5	-3,66	0,69	-3,00	-0,66	-2,00	2,69	no data	0,69
S7-5.0	-3,87	1,00	-3,00	-0,87	-2,00	3,00	no data	1,00
S7-4.7	-3,47	0,82	-3,00	-0,47	-2,00	2,82	no data	0,82
S7-4.5	-4,00	0,79	-3,00	-1,00	-2,00	2,79	no data	0,79
S7-4.0	-4,04	0,74	-3,00	-1,04	-2,00	2,74	no data	0,74
S7-3.0	-3,86	0,24	-3,00	-0,86	-2,00	2,24	no data	0,24
S7-2.0	-3,81	-0,23	-3,00	-0,81	-2,00	1,77	no data	-0,23
S7-1.0	-3,14	0,28	-3,00	-0,14	-2,00	2,28	no data	0,28
S7-0.5	-2,20	0,10	-3,00	0,80	-2,00	2,10	-2,20	0,10
S7-0.4	-3,16	0,10	-3,00	-0,16	-2,00	2,10	no data	0,10
S7-BASE	-2,67	0,18	-3,00	0,33	-2,00	2,18	-2,67	0,18
S6-4.5	-3,82	0,75	-3,00	-0,82	-2,00	2,75	no data	0,75
S6-4.0	-3,95	0,76	-3,00	-0,95	-2,00	2,76	no data	0,76
S6-3.5	-4,08	0,62	-3,00	-1,08	-2,00	2,62	no data	0,62
S6-3.0	-3,49	0,71	-3,00	-0,49	-2,00	2,71	no data	0,71

Cont. Table 6.6 Section "B" (Northern Ispilunca Valley)

Sample	$\delta^{18}\text{O}$ Bulk rock (i) ‰ vs. PDB	$\delta^{13}\text{C}$ Bulk rock (i) ‰ vs. PDB	$\gamma$	$\Delta\alpha$	$\lambda$	$\Delta c$	$\delta^{18}\text{O}$ Bulk rock (f) ‰ vs. PDB	$\delta^{13}\text{C}$ Bulk rock (f) ‰ vs. PDB
S6-2.5	-3,99	0,34	-3,00	-0,99	-2,00	2,34	no data	0,34
S6-2.0	-4,04	0,26	-3,00	-1,04	-2,00	2,26	no data	0,26
S6-1.5	-4,36	0,51	-3,00	-1,36	-2,00	2,51	no data	0,51
S6-1.0	-2,45	0,54	-3,00	0,55	-2,00	2,54	-2,45	0,54
S6-0.5	-2,56	0,42	-3,00	0,44	-2,00	2,42	-2,56	0,42
S6-BASE	-1,16	0,84	-3,00	1,84	-2,00	2,84	-1,16	0,84
S6-BASE	-1,62	0,00	-3,00	1,38	-2,00	2,00	-1,62	0,00
S6-BASE	-1,13	0,62	-3,00	1,87	-2,00	2,62	-1,13	0,62

Table 6.7. Section "A" (Casa Trigu)

Sample	$\delta^{18}\text{O}$ Bulk rock (i) ‰ vs. PDB	$\delta^{13}\text{C}$ Bulk rock (i) ‰ vs. PDB	$\gamma$	$\Delta\alpha$	$\lambda$	$\Delta c$	$\delta^{18}\text{O}$ Bulk rock (f) ‰ vs. PDB	$\delta^{13}\text{C}$ Bulk rock (f) ‰ vs. PDB
S2C-294.4	-5,52	-1,34	-3,00	-2,52	-2,00	0,66	no data	-1,34
S2C-36.7	-4,64	-1,27	-3,00	-1,64	-2,00	0,73	no data	-1,27
S2C-36.7	-4,70	-1,37	-3,00	-1,70	-2,00	0,63	no data	-1,37
S2B-31.5	-3,30	-2,33	-3,00	-0,30	-2,00	-0,33	no data	no data
S2B-30	-3,66	-2,27	-3,00	-0,66	-2,00	-0,27	no data	no data
S2C-26.2	-3,25	-2,35	-3,00	-0,25	-2,00	-0,35	no data	no data
S2B-25.8	-5,73	-2,10	-3,00	-2,73	-2,00	-0,10	no data	no data
S2C-25.1	-3,98	-1,73	-3,00	-0,98	-2,00	0,27	no data	-1,73
S2C-24.7	-5,14	-1,28	-3,00	-2,14	-2,00	0,72	no data	-1,28
S2C-24.2	-5,31	-1,15	-3,00	-2,31	-2,00	0,85	no data	-1,15
S2b-23	-5,53	-2,17	-3,00	-2,53	-2,00	-0,17	no data	no data
S2B-21.5	-5,08	-3,24	-3,00	-2,08	-2,00	-1,24	no data	no data
S2b-21.5	-5,30	-2,87	-3,00	-2,30	-2,00	-0,87	no data	no data
S2B-21	-3,50	-2,42	-3,00	-0,50	-2,00	-0,42	no data	no data
S2B-19	-5,26	-3,12	-3,00	-2,26	-2,00	-1,12	no data	no data
S2B-18	-5,80	-2,35	-3,00	-2,80	-2,00	-0,35	no data	no data
S2B-16	-5,54	-3,40	-3,00	-2,54	-2,00	-1,40	no data	no data
S3A-2.0	-3,17	-1,05	-3,00	-0,17	-2,00	0,95	no data	-1,05
S3A-0.5	-3,19	-0,04	-3,00	-0,19	-2,00	1,96	no data	-0,04
S3A-BASE	-1,89	0,66	-3,00	1,11	-2,00	2,66	-1,89	0,66
S5-4.0	-4,66	-1,20	-3,00	-1,66	-2,00	0,80	no data	-1,20
S5-3.5	-4,70	-1,19	-3,00	-1,70	-2,00	0,81	no data	-1,19
S5-3.0	-5,31	-0,85	-3,00	-2,31	-2,00	1,15	no data	-0,85
S5-2.0	-5,06	-0,95	-3,00	-2,06	-2,00	1,05	no data	-0,95
S5-1.6	-5,16	-0,86	-3,00	-2,16	-2,00	1,14	no data	-0,86
S5-1.2	-5,04	-1,09	-3,00	-2,04	-2,00	0,91	no data	-1,09
S5-0.8	-5,25	-0,92	-3,00	-2,25	-2,00	1,08	no data	-0,92
S5-0.4	-5,22	-0,61	-3,00	-2,22	-2,00	1,39	no data	-0,61
S5-BASE	-5,19	-0,47	-3,00	-2,19	-2,00	1,53	no data	-0,47

Table 6.8

Sample	$\delta^{18}\text{O}$ Bulk rock (f) ‰ vs. PDB	$\delta^{13}\text{C}$ Bulk rock (f) ‰ vs. PDB	$\sigma$ Value O	$\sigma$ Value C	$\Delta$ Value O	$\Delta$ Value C	Oxygen Peak ‰ vs. PDB	Carbon Peak ‰ vs. PDB
SM-3.0	-1,93	1,54	0,55	0,79	1,62	1,97	-1,93	1,54
Q-26.8	-1,39	0,61	0,75	0,20	2,50	1,15	-1,39	0,61
Q-24.4	-1,35	0,81	0,79	0,40	2,55	1,35	-1,35	0,81
Q-24.4	-1,49	0,65	0,66	0,24	2,41	1,19	-1,49	0,65
Q-23.4	-1,60	0,83	0,54	0,42	2,30	1,37	-1,60	0,83
Q-21.2	-1,62	0,62	0,52	0,21	2,27	1,16	-1,62	0,62
Q-16.2	-1,39	0,47	0,75	0,06	2,51	1,01	-1,39	0,47
Q-16.0	-1,40	0,64	0,74	0,23	2,50	1,18	-1,40	0,64
Q-15.8	-1,23	0,48	0,92	0,07	2,67	1,02	-1,23	0,48
Q-13.6	-1,47	0,66	0,67	0,24	2,43	1,20	-1,47	0,66
S4ALDO-4.9	no data	1,45	no data	0,62	no data	1,73	no data	1,45
S4ALDO-4.45	no data	1,47	no data	0,64	no data	1,76	no data	1,47
VT2-5.5	-1,72	0,86	0,59	1,37	1,27	2,73	-1,72	0,86
VT2-1.3	-1,53	0,71	0,78	1,22	1,47	2,58	-1,53	0,71
VT2-0.5	-1,91	2,06	0,40	2,57	1,09	3,93	-1,91	2,06
VT7-8.8	no data	0,07	no data	1,06	no data	2,05	no data	0,07
S8-0.3	no data	0,85	no data	0,84	no data	2,93	no data	0,85
S7-5.0	no data	1,00	no data	0,99	no data	3,09	no data	1,00
S6-BASE	-1,16	0,84	1,05	0,83	1,81	2,92	-1,16	0,84
S6-BASE	-1,13	0,62	1,08	0,61	1,84	2,70	-1,13	0,62
S3A-BASE	-1,89	0,66	0,00	1,59	0,00	2,40	-1,89	0,66